# Sustainable behaviour of buildings with steel-intensive façade systems

A Thesis Submitted to obtaining
the Scientific Title of PhD. in Engineering
from
Politehnica University Timișoara
in the Field of Civil Engineering
by

**Eng. Raluca Ioana LEGIAN**

| | |
|---|---|
| PhD Committee Chair: | Prof. Raul ZAHARIA, Ph.D. |
| PhD Supervisor: | Prof. Adrian Liviu CIUTINA, Ph.D. |
| Scientific Reviewers: | Prof. Dorina Nicolina ISOPESCU, Ph.D. |
| | Assoc.Prof. Ligia MOGA, Ph.D. |
| | Assoc.Prof. Adrian DOGARIU, Ph.D. |

Date of the PhD Thesis Defense: October 17, 2023

The Ph.D. thesis series of UPT are:

1. Automation
2. Chemistry
3. Energetics
4. Chemical Engineering
5. Civil Engineering
6. Electrical Engineering
7. Electronic Engineering and Telecommunications
8. Industrial Engineering
9. Mechanical Engineering
10. Computer Science and Information Technologies
11. Science and Material Engineering
12. Systems Engineering
13. Energy Engineering
14. Computers and Information Technology
15. Materials Engineering
16. Engineering and Management
17. Architecture
18. Civil Engineering and Installations
19. Electronics, Telecommunications

Politehnica University Timișoara, Romania, initiated the above series to disseminate the expertise, knowledge, and results of the research carried out within the doctoral school of the university. According to the Decision of the Executive Office of the University Senate No. 14/14.07.2006, the series includes the doctoral theses defended in the university since October 1, 2006.



Romania, 300223 Timișoara, Bd. Vasile Pârvan no. 2B
Tel./fax +40-(0)256 404677
e-mail: editura@upt.ro

# Foreword

This thesis has been elaborated during my activity in the Department of Steel Structures and Structural Mechanics (CMMC) of the Politehnica University Timişoara, Romania, the Research Institute for Renewable Energies (ICER) within Politehnica University of Timisoara and VTT – Tehnical Research Center of Finland. Research has been partially supported through the Research Project *Provisions for Greater Reuse of Steel Structures* (PROGRESS), funded by the European Commission's Research Fund for Coal and Steel, through the Research Project *Smart Buildings Adaptable to Climate Change Effects* (CIA_CLIM) funded by the Romanian Ministry of Research and Innovation, CCCDI – UEFISCDI within PNCDI III, and through the *Network of Excellence in applied research and innovation for doctoral and postdoctoral programmes / InoHubDoc*, project cofunded by the European Social Fund.

I would like to thank my thesis coordinator, Prof. Adrian Liviu Ciutina, for his support, kind guidance and patience throughout my research activity. Additionally, I want to extend my appreciation for his assistance and direction concerning laboratory work and as well, for his overall vision on various aspects surrounding the activity of a researcher shared with me. I would also like to thank him for involving me in the CIA-CLIM research project which cultivated my curiosity and interest in sustainability research domain.

In addition to guiding and nurturing my research activities, I express deep gratitude to Prof. Viorel Ungureanu for providing support and for sharing his knowledge and experience with me during my research work. I would also like to express my appreciation for including me in the PROGRESS research project, during which I was able to meet and work with distinguished researchers from all over Europe.

Sincerely thanks to Lect. Ioan Both for his help related to laboratory work, technical advice, and support during my research work. During the numerical analysis, great aid was received from my Ph.D. student colleagues Anna Ene and Daniel Luís Nunes, to whom I am deeply grateful for the unconditional help and shared friendship.

I would like to thank Prof. Aurel Stratan, Assoc.Prof. Adrian Dogariu, Lect. Andrei Crișan and Ph.D. student Dominiq Iakab for their observations and suggestions through the numerical investigations. I should also express gratitude to laboratory technician Ovidiu Abrudan for the help he showed during the experimental testing. Many thanks to Ionel Mărginean for the amity shown and help related to administrative aspects.

Heartfelt thanks to my husband and daughter for their support and especially patience that I received throughout the years of the PhD studies.

Timişoara, October 2023 ing. Raluca Ioana Legian

Recipients of dedication.

LEGIAN, Raluca Ioana

**Sustainable behaviour of buildings with steel-intensive façade systems**

**(Comportarea sustenabilă a clădirilor cu sisteme metalice de fațadă)**

PhD theses of UPT, Series X, No. YY, Editura Politehnica, 2023, 216 pages, 147 figures, 29 tables.

ISSN:
ISBN:

Keywords
steel-intensive façade systems, environmental impact, wind loads, vacuum chamber, life cycle assessment, reused components, liner trays, circular economy, industrial building, reused steel

Abstract
Global concerns about environmental sustainability have escalated in the last three decades, pressing industries to critically examine their practices and their contribution to the overall ecological footprint. The construction sector has become a significant contributor to environmental deterioration due to its extensive energy consumption, raw material extraction, and waste generation. The construction sector has the potential to reduce its environmental impact through two methods: reducing the embodied carbon footprint of buildings and reducing energy consumption during the construction use phase. The embodied carbon footprint of the building is related to the extraction of raw materials, the manufacture of building materials, the transportation of building materials, the energy used during the construction process, the energy consumption related to the demolition / deconstruction process, the transport of construction waste, the construction waste process, and disposal. The embodied carbon footprint can be decreased by the three R approaches – reduce, reuse, recycle and by using renewable construction materials. Emmissions related to energy consumed during the operational phase of buildings represent the preponderant share of emmissions associated with buildings reported throughout the life cycle of a construction. This highlights the urgent need to improve building performance, which is directly related to the performance of the construction envelope.
The thesis focusses on the evaluation of the behaviour of steel-intensive façade systems from a sustainable perspective. Among façade system solutions, steel liner tray claddings have emerged as a promising technology that has the potential to transform the industrial construction landscape. This research endeavour seeks to investigate the benefits, challenges, and broader implications of using steel liner trays as claddings in industrial halls. The research presented in the thesis investigated the structural behaviour of liner trays under the dynamic character of the loads induced by wind. The experimental investigations of the liner trays were carried out in a vacuum chamber, a pioneering experimental test accomplished in Romania on structural liner trays subjected to wind loads. Extensive experimental and numerical studies were used to obtain a deeper understanding of the dynamic effect of wind loads on the behaviour of the cladding system.
In the thesis was also presented the evaluation of the environmental impact of steel-intensive façade systems from a life-cycle perspective through a comparative life-cycle assessment (LCA) of various single-storey steel structures made of completely new materials, as well as structures made of reused elements. The analysis is also completed by a comparative LCA of industrial buildings that have envelopes consisting of liner tray cladding systems and sandwich panel cladding systems.

# Table of contents

# List of tables

# List of figures

# Notations, abbreviations, acronyms

*Notations*

| | |
|---|---|
| $b_u$ | overall width of the wide flange |
| $h_{u1,}$ $h_{u2}$ | intermediate stiffeners' height |
| $b_{f1}$, $b_{f2}$ | overal width of the narrow flanges |
| $h_1$, $h_2$ | Height of the webs of liner tray |
| c | overall width of the edge stiffener |
| $\dot{e}_{Le}$ | strain rate |
| t | steel thickness |
| $t_{cor}$ | steel core thickness without metallic coating |
| $t_{nom}$ | nominal steel sheet thickness after cold forming, including the mettalic coating |
| $t_{metallic\ coating}$: | thickness of the metallic coating |
| $M_{c,Rd}$ | buckling resistance moment of liner trays with wide flange under compression |
| $M_{b,Rd}$ | buckling resistance moment of liner trays with wide flange in tension |
| $h_{u1}$ | depth of the corrugation of the wide flange |
| $I_a$ | second moment of area of the wide flange, about its centroid |
| $s_1$ | longitudinal spacing of fasteners in the narrow flanges |
| $\overline{\lambda_p}$ | relative slenderness |
| $b_{eff}$ | effective width of the wide flange |
| $k_\sigma$ | buckling factor corresponding to the stress ratio and boundary conditions |
| ψ | stress ratio |
| ρ | reduction factor |
| $b_{e1}$, $b_{e2}$ | effective widths of wide flange under compression |
| $h_{eff}$ | effective width of the webs under bending |
| $b_{u,eff}$ | effective width of the wide flange |
| $\sigma_1$, $\sigma_2$ | stress |
| $f_y$ | yield strength |
| $f_{yb}$ | basic yield strength |
| $f_u$ | ultimate tensile strength |
| $s_1$ | longitudinal spacing of fasteners supplying lateral restraint to the narrow flanges |
| $\beta_b$ | correlation factor |
| L | length of the liner tray |
| $I_{y,eff}$ | effective second moment of area of the effective cross-section of a liner tray with the wide flange under compression or in tension, about the y-y axis |

| | |
|---|---|
| $z_c$: | distance from the effective centroidal axis to the system line of the compressed flange |
| $z_t$: | distance from the effective centroidal axis to the system line of the flange in tension |
| $W_{eff,y}$ | effective section modulus of the cross-section for only bending about the y - y axis; |
| $A_{s1}$, $A_{s2}$ | effective cross-sectional area of the edge stiffeners |
| $I_{s1}$, $I_{s2}$ | effective second moment of area of the stiffener, taken as that of its effective area As about the centroidal axis a - a of its effective cross-section |
| $\sigma_{cr,s1}$ | elastic critical buckling stress for stiffener of the narrow flange $b_{pf1}$ |
| $\sigma_{cr,s2}$ | elastic critical buckling stress for stiffener of the narrow flange $b_{pf1}$ |
| $L_e$ | the distance between adjacent points of zero bending moment |
| k | stiffness of the liner trays |
| $w_e$ | maximum unfactored wind pressure value |
| RP1, RP2 | reference points |
| σ | axial/normal stress |
| E | elastic modulus (Young's modulus) |
| ε | axial/normal strain |
| $\sigma_{cr,d}$ | elastic critical distortional buckling stress |
| $e_{0,global}$ | global equivalent imperfection |
| $e_{o,local}$ | local buckling imperfection |
| $e_{o,dist}$ | distorsional buckling imperfection |
| $\delta_{max}$: | maximum deflection at the mid-span of the liner tray for a simply supported beam |

*Abbreviations*

| | |
|---|---|
| GHG | Greenhouse gas emissions |
| LCA | Life Cycle Assessment |
| $CO_2$ | Carbon dioxide |
| $CO_2$ | Equivalent carbon dioxide |
| WEB | projections of greenhouse gas emissions marked considering existing measures |
| WAM | projections of greenhouse gas emissions marked considering additional measures |
| EN | The European Standard |
| ELISSA mock-up | a modular lightweight steel system developed during the ELISSA European FP7 project (Energy Efficient LIghtweight-Sustainable-SAfe-Steel Construction) |
| DLCA | Dynamic Life Cycle Assessment |
| PET | Polyethylene terephthalate |

| | |
|---|---|
| PIR | Polyisocyanurate |
| LSF | Light steel frame |
| EPS | Expanded polystyrene |
| MW | Mineral wool |
| XPS | Extruded polystyrene |
| CDW | Construction and demolition waste |
| SSB | Single-storey steel building |
| DfD | Design for Deconstruction |
| GD+Z | Dipped, galvanized with a zinc coating |
| ST | Nominal values according to the provisions of the material standard EN 10346 |
| NOM | nominal value |
| EXP | value determined experimentally |
| SEM | Scanning Electron Microscopy |
| EDX | Energy Dispersive X-ray Spectroscopy |
| LT-SO-P-P | **L**iner **T**ray – **S**imple **O**pened – **P**ressure - **P**inned |
| LT-SO-P | **L**iner **T**ray – **S**imple **O**pened – **P**ressure |
| LT-SO-S | **L**iner **T**ray – **S**imple **O**pened – **S**uction |
| LT-SC-P | **L**iner **T**ray – **S**imple **C**losed – **P**ressure |
| LT-SC-S | **L**iner **T**ray – **S**imple **C**losed – **S**uction |
| LT-RO-P | **L**iner **T**ray – **R**estrained **O**pened – **P**ressure |
| LT-RO-S | **L**iner **T**ray – **R**estrained **O**pened – **S**uction |
| LT-RC-P | **L**iner **T**ray – **R**estrained **C**losed – **P**ressure |
| LT-RC-S | **L**iner **T**ray – **R**estrained **C**losed – **S**uction |
| LVDT | Linear Variable Differential Transformer |
| ULS | Ultimate Limit State |
| SLS | Serviceability Limit State |
| FEM | Finite Element Method |
| SSD | Scalar stiffness degradation |
| DOF | Degree of Freedom |
| CUFSM | Constrained and Unconstrained Finite Strip Method |
| $F_{max\_exp}$ | equivalent of maximum load value recorded immediately before failure in the experimental investigations |
| EPD | Environmental Product Declaration |

*Acronyms*

| | |
|---|---|
| SCSS | Standing Committee on Structural Safety |
| NEPA | National Environmental Policy Act of 1969 |
| EN | European Standards |
| UN | United Nations |
| SDG | Sustainable Development Goal |
| UNFCCC | United Nations Framework Convention on Climate Change |
| UNCED | United Nations Conference on Environment and Development |

| | |
|---|---|
| NASA | The National Aeronautics and Space Administration civil space program |
| GISS | Goddard Institute for Space Studies |
| EU | European Union |
| EC | European Commission |
| ETS | Emissions Trading System |
| CBAM | Carbon Border Adjustment Mechanism |
| ISO | International Standards Organisation |
| ECCS | European Convention on Constructional Steelwork |
| PROGRESS | Provisions for Greater Reuse of Steel Structures |
| GRISPE | Guidelines and recommendations for Integrating Specific Profiled Steels sheets in the Eurocodes - project |
| GRISPE PLUS | Valorisation of Knowledge for Specific Profiled Steel Sheets - project |
| RFCS | Research Fund for Coal and Steel |
| UPT-CEMSIG | The Research Center for Mechanics of Materials and Structural Safety within Politehnica University of Timisoara |
| UPT-ICER | The Research Institute for Renewable Energies within Politehnica University of Timisoara |
| CEN | European Committee for Standardization |

# REZUMAT

Preocupările globale cu privire la impactul asupra mediului și consecințele acestuia au crescut în ultimele trei decenii, presând industriile să-și examineze critic practicile și contribuția lor la amprenta ecologică generală. Sectorul construcțiilor a devenit un contribuitor semnificativ la deteriorarea mediului din cauza consumului extins de energie, extracției și prelucrării de materii prime, precum și generării de deșeuri. Sectorul construcțiilor are potențialul de a-și reduce impactul asupra mediului prin două metode: prin reducerea amprentei de carbon încorporate clădirilor și prin reducerea consumului de energie în faza de utilizare a clădirilor. Amprenta de carbon încorporată clădirii este cauzată de extracția materiilor prime, fabricarea materialelor de construcții, transportul materialelor de construcții, energia utilizată în timpul procesului de construcție, consumul de energie aferent procesului de demolare/dezasamblare, transportul de deșeuri din construcții, procesul de sortare a deșeurilor din construcții și eliminarea acestora. Amprenta de carbon încorporată clădirilor poate fi redusă prin cele trei abordări R – reducerea, reutilizarea, reciclarea materialor de construcții și prin utilizarea unor materiale de construcții din surse regenerabile. Emisiile legate de energia consumată în faza de exploatare a clădirilor reprezintă ponderea cea mai mare a emisiilor asociate clădirilor raportate pe parcursul ciclului de viață al unei construcții. Acest lucru evidențiază nevoia urgentă de îmbunătățire a performanței clădirilor pe durata lor de viață, performanță care este direct legată de performanța anvelopei construcțiilor.

Teza de doctorat se concentrează pe evaluarea comportării sistemelor metalice de fațadă dintr-o perspectivă durabilă. Printre soluțiile de sisteme de fațadă, fațadele pe bază de casete structurale din oțel au apărut ca o tehnologie promițătoare, care are potențialul de a transforma peisajul construcțiilor industriale. Cercetarea desfășurată și prezentată în teză, a urmărit să investigheze beneficiile, provocările și implicațiile mai largi ale utilizării casetelor structurale din oțel ca sistem de fațadă în halele industriale. Cercetarea prezentată în teză a investigat comportamentul structural al casetelor din oțel sub caracterul dinamic al încărcării induse de vânt. Încercările experimentale ale casetelor structurale au fost efectuate într-o cameră de vacuum, un test experimental de pionierat realizat în România pentru casete structurale supuse solicitărilor din vânt. Au fost realizate studii experimentale și numerice ample pentru a obține o înțelegere mai profundă a efectului dinamic al încărcărilor din vânt asupra comportamentului sistemului metalic de fațadă.

În teză a fost prezentată și evaluarea impactului asupra mediului al sistemelor metalice de fațadă din perspectiva evaluării pe ciclul de viață, printr-o evaluare comparativă a diferitelor structuri industriale din oțel, realizate din materiale complet noi, precum și structuri realizate din elemente reutilizate. Rezultatele cercetării prezentate in teză sunt, de asemenea, completate de o analiză comparativă pe ciclu de viață al clădirilor industriale care au fațade din sisteme bazate pe casete structurale și fațade din sisteme bazate panouri sandwich.

# SUMMARY

Global concerns about environmental sustainability have escalated in the last three decades, pressing industries to critically examine their practices and their contribution to the overall ecological footprint. The construction sector has become a significant contributor to environmental deterioration due to its extensive energy consumption, raw material extraction, and waste generation. The construction sector has the potential to reduce its environmental impact through two methods: reducing the embodied carbon footprint of buildings and reducing energy consumption during the construction use phase. The embodied carbon footprint of the building is related to the extraction of raw materials, the manufacture of building materials, the transportation of building materials, the energy used during the construction process, the energy consumption related to the demolition / deconstruction process, the transport of construction waste, the construction waste process, and disposal. The embodied carbon footprint can be decreased by the three R approaches – reduce, reuse, recycle and by using renewable construction materials. Emmissions related to energy consumed during the operational phase of buildings represent the preponderant share of emmissions associated with buildings reported throughout the life cycle of a construction. This highlights the urgent need to improve building performance, which is directly related to the performance of the construction envelope.

The thesis focusses on the evaluation of the behaviour of steel-intensive façade systems from a sustainable perspective. Among façade system solutions, steel liner tray claddings have emerged as a promising technology that has the potential to transform the industrial construction landscape. This research endeavour seeks to investigate the benefits, challenges, and broader implications of using steel liner trays as claddings in industrial halls. The research presented in the thesis investigated the structural behaviour of liner trays under the dynamic character of the loads induced by wind. The experimental investigations of the liner trays were carried out in a vacuum chamber, a pioneering experimental test accomplished in Romania on structural liner trays subjected to wind loads. Extensive experimental and numerical studies were used to obtain a deeper understanding of the dynamic effect of wind loads on the behaviour of the cladding system.

In the thesis was also presented the evaluation of the environmental impact of steel-intensive façade systems from a life-cycle perspective through a comparative life-cycle assessment (LCA) of various single-storey steel structures made of completely new materials, as well as structures made of reused elements. The analysis is also completed by a comparative LCA of industrial buildings that have envelopes consisting of liner tray cladding systems and sandwich panel cladding systems.

# 1 Introduction

## 1.1 Motivation

In recent years, global concerns about environmental sustainability have escalated, prompting industries to critically examine their practices and their contribution to the overall ecological footprint. The construction sector has become a significant contributor to environmental degradation due to its extensive energy consumption, raw material extraction, and waste generation. Greenhouse gas (GHG) emissions within the construction sector could be mitigated by addressing two major pathways. The first path is to reduce the embodied carbon footprint of the building accountable for extraction of raw materials, manufacturing of building materials, transportation of building materials, energy consumption related to the construction process, energy consumption related to the demolition/deconstruction process, transport of construction waste, construction waste process, and disposal. The second path to diminishing the environmental impact of the construction sector is to reduce energy consumption during the use phase of constructions, since during the operational life span of buildings, the most significant share of emmissions associated with buildings is recorded as these emmissions are related to energy consumption.

In general, the industrial buildings have a shorter lifespan (commonlly 20-25 years, after which these buildings are usually replaced due to a change in demand) than other types of structures (50-100 years), leading to a higher ratio of embodied carbon to operational carbon compared to longer-lasting structures. This emphasises the importance of assessing the impact of materials and construction processes, as the proportion of embodied carbon emissions might be relatively higher. Therefore, this study seeks to delve into the environmental implications of industrial halls, aiming to provide comprehensive insights that drive the transition towards more sustainable construction practices.

Assessing the environmental impact of buildings requires a comprehensive life-cycle perspective. This includes not only the embodied carbon associated with materials manufacturing, transportation, and construction, as well as emissions related to the demolition, deconstruction, waste process, and disposal of the building materials, but also operational energy. A thorough life cycle assessment of industrial halls can highlight hotspots of environmental impact and offer insights into low-carbon alternatives, which is why the research presented in this thesis includes a comparative life cycle assessment (LCA) of various single-storey steel structures made of completely new materials, as well as structures made of reused elements for the entire structure, for components, or just for some individual members of the structure.

As the construction industry is witnessing a growing interest in sustainable materials and principles of circular economy, exploring façade systems, recycled content, and reusable envelope components can not only enhance the environmental profile of industrial hall envelopes but also stimulate innovation within the sector. The longevity and structural integrity of industrial halls are essential factors in ensuring

their long-term functionality and minimising maintenance requirements. In the last decade, in the industrial hall and warehouse sector, approximately half of the structures were covered with sandwich panels and 50% with built-up systems with two skins [1]. Steel liner trays, known for their durability and resistance to various environmental factors, have the potential to extend the service life of industrial halls. In light of the 'Alert' entitled 'Effects of scale' [2], issued in 2018 by the United Kingdom Standing Committee on Structural Safety (SCOSS), it is most likely that façade systems made of built-in cladding systems, such as liner tray cladding systems, will face an increase in demand compared to sandwich panels envelope solutions.

Among façade system solutions, steel liner tray claddings have emerged as a promising technology that has the potential to transform the industrial construction landscape. This research endeavour seeks to investigate the benefits, challenges, and broader implications of using steel liner trays as claddings in industrial halls. By examining the performance of steel liner trays under different conditions, this research can contribute to a more comprehensive understanding of their durability and reliability. Liner trays have traditionally been designed as structures with a single span. In such scenarios, the bending moment that causes sagging is typically the most critical in design, and the bending moment resistance becomes particularly critical, especially when the structure is subjected to significant wind loads [3]. For this reason, the research presented in this thesis investigated the structural behaviour of liner trays subjected to realistic wind loads. Few researchers have addressed the problem of the dynamic character of the loads induced by wind to liner trays, thus the experimental investigations of the behaviour of liner trays were carried out in a vacuum chamber. This ensured a more natural way of wind loading, but in fully controlled testing conditions, resulting in a deeper understanding of the dynamic effect of wind loads on cladding system behaviour. The study of liner tray wall cladding system subjected to wind loads through a vacuum chamber proved to be worthwhile, as it was the first of its kind conducted in Romania.

The urgency of addressing environmental challenges requires interdisciplinary research efforts that can contribute to sustainable practices across all sectors. Thus this study aims to fill the existing research gap by comprehensively analysing the environmental impact of industrial halls and the structural behaviour of liner trays cladding systems, an envelope widely spread through industrial steel structures. Through a combination of life cycle assessments, exploration of sustainable materials, circular economy approach of end-of-life buildings, and structural behaviour of steel-intensive façade systems, this research can guide the industry towards more responsible construction practices. By focussing on industrial hall envelopes, we not only address a crucial aspect of the construction sector, but also pave the way for a more sustainable future.

As industries grapple with their role in environmental preservation, this research offers an opportunity to drive positive change within the construction sector, mitigate environmental impacts, and contribute to a greener and more sustainable global landscape.

## 1.2 Objectives

The main purpose of the thesis was to evaluate the behaviour of steel-intensive façade systems from a sustainable perspective. Two main objectives and several derived secondary objectives emerged upon:

- The evaluation of the environmental impact of steel-intensive façade systems from a life-cycle perspective:
  - obtain a comparative life cycle assessment of various single-storey steel structures made of completely new materials, as well as structures made of reused elements. The analysis include benefits and loads beyond the building's life cycle stage to have an overall understanding; of the environmental impact of buildings with relatively short life span.
  - acquire a comparative LCA of industrial buildings that have envelopes consisting of liner tray cladding systems and sandwich panel cladding system;
- the achievement of a deeper understanding in the structural behaviour of liner trays under the dynamic effect of wind loads:
  - to achieve reliable experimental outcomes through a comprehensive experimental framework involving relevant experimental specimens and test setup. The design and instrumentation of the tests should offer valuable understanding of the performance of liner trays subjected to wind loads;
  - to determine the buckling moment resistance of liner trays subjected to wind pressure and wind suction according to the standards in use and compare it to the results of the experimental investigations;
  - to provide accurate and calibrated numerical models of liner trays subjected to pressure and suction;
  - to perform FEM parametric studies with the aim of acquiring reliable data on the influence of parameters such as thickness, height, and length on the behaviour of specimens.

## 1.3 Thesis outline

**Chapter 1: Introduction**

The research subject was introduced, highlighting the scope and objectives of the thesis. In addition, an overview of the thesis structure was provided.

**Chapter 2: State of knowledge**

The second chapter presents the state-of-the-art on legislative proposals, frameworks, and principles for climate action that has an impact on the construction sector, as well as the environmental impact of the construction sector. The state of knowledge also provides insight into the structural behaviour of the liner trays subjected to wind loads. In this chapter, the advantages of experimental tests on wind loads conducted through a vacuum chamber are outlined.

**Chapter 3: Experimental investigation of liner trays subjected to wind loads**

The third chapter presents a calculation of the design values of liner trays in wall claddings subjected to horizontal loads following the procedure recommended by European Standards (EN). Furthermore, the experimental investigation on liner trays subjected to wind loads was presented. Different test configurations of liner trays (simple liner trays with and without outer cladding, restrained liner trays with and without outer cladding) were tested, in a vacuum chamber, to establish their ultimate moment resistance under real conditions of service. The test results were split into two groups based on the type of wind loading, namely, pressure and suction. Within each group, the test results were described, observing the location and nature of the failure zones. The results of the experimental tests were compared to the design values obtained following the procedure recommended by EN.

**Chapter 4: Numerical investigations on liner trays**

Chapter four presents the results of two sets of numerical simulations performed: (1) two models calibrated in order to replicate the experimental behaviour of liner trays in the post-test finite element analysis: one model that simulates the behaviour of simple-opened liner trays subjected to wind pressure and another model that reflects the behaviour of simple-opened liner trays subjected to wind suction; (2) study of the influence of parameters such as thickness, web height, and static scheme / liner tray length in liner trays subjected to pressure and suction.

**Chapter 5: Environmental impact of buildings with steel-intensive façade systems**

Starting from an optimal design case of a single-storey industrial hall considering a new steel structure with new materials, in Chapter 5 a comparative life cycle assessment of further design possibilities for the same steel building using reclaimed elements is presented. The structural feasibility and the environmental benefits of a construction strategy based on the circular economy approach were shown. In addition, a comparative life cycle assessment of industrial buildings with envelopes consisting of liner tray cladding systems and sandwich panel cladding systems is presented.

**Chapter 6: Conclusions of PhD study. Contributions of the author. Future research**

The final chapter provides an overview of the conclusions drawn from the PhD study, highlights the main contributions made by the author, discusses the dissemination of results, and outlines future research activities.

**Annex**

Within the annex, additional information is provided regarding the specifics of liner tray specimens following experimental tests.

# 2 State of knowledge

## 2.1 Introduction

Sustainability refers to the capacity to uphold or facilitate a process consistently over time. This principle is commonly divided into three fundamental dimensions: economic, environmental, and social. The evolution of sustainability has been shaped by various government decisions and initiatives aimed at addressing environmental concerns, promoting economic development, and ensuring social well-being. So far, not just governments but also businesses have pledged to pursue sustainable objectives, with a focus on the conservation and responsible use of natural resources, reducing pollution and waste, promoting biodiversity and ecosystem health, or promoting social equity.

In an era defined by environmental concerns and resource scarcity, the construction industry faces the imperative to shift toward sustainable practises. This transformation is not only a response to global challenges, but also a proactive approach to ensure a harmonious coexistence between built environments and the natural world. At the forefront of this evolution are sustainable buildings, which strive to minimise their ecological footprint while maximising their functionality, comfort, and aesthetic appeal. Central to the realisation of sustainable buildings are innovative façade systems, particularly those that harness the strength and versatility of steel to create high-performance, environmentally conscious structures. As the world grapples with the impacts of climate change, resource depletion, and urbanisation, the imperative for sustainable construction becomes evident.

## 2.2 Background

### 2.2.1 The international dimension

The demand for an 'economic development that may have benefits for current and future generations without harming the planet's resources or biological organisms' [4] defined as sustainable development appeared first in 1969 in the law that constituted the *National Environmental Policy Act of 1969* (the NEPA) under the auspices of the Environmental Protection Agency in the United States.

In 1983, the World Commission on Environment and Development was established by the United Nations (UN) with the purpose to study the connection between economic development, ecological health, and social equity. Later, in 1987, the famous *Brundtland Report* [5] produced by several countries for the UN introduced the concept of sustainability, as we understand it today, and described how it could be achieved. In the same year, governments collaborated to address the depletion of the ozone layer by adopting the *Montreal Protocol* [6]. This agreement showcased global cooperation to phase out ozone-depleting substances, highlighting the potential for collective action on environmental issues. The United Nations has since adopted the *Sustainable Development Goals* (SDGs), a set of 17 goals aimed at addressing

global challenges, including poverty, inequality, climate change, and environmental degradation [7].

On 9 May 1992 the *United Nations Framework Convention on Climate Change* (UNFCCC) was established, an international environmental convention signed by 154 states at the United Nations Conference on Environment and Development (UNCED), also known as the *Earth Summit*. The UNFCCC sets out the basic legal framework and principles for international climate action, acknowledges the vulnerability of all countries to the effects of climate change, and calls for special efforts to alleviate the consequences [8]. The Convention recognises the importance of sustainable development and the need to address climate change in the context of broader environmental and socio-economic concerns.

Extending the UNFCCC, in 1997 the *Kyoto Protocol* was signed. The *Kyoto Protocol* marked a significant milestone in climate change mitigation. It sets binding targets for developed countries to reduce greenhouse gas emissions. Although not without challenges, this agreement highlighted the role of international agreements in addressing global environmental challenges [9].

Building on the *Kyoto Protocol*, in 2015 the *Paris Agreement was followed,* an international treaty adopted by 196 parties at the United Nations Climate Change Conference in Paris, France. The agreement emphasised collective efforts to limit global warming, with countries committing to substantially reduce global greenhouse gas emissions in an effort to limit the increase in global temperature in this century to 2 degrees Celsius above preindustrial levels, while pursuing the means to limit the increase to 1.5°C [10]. The agreement highlighted the importance of individual countries' commitments toward a common goal. According to NASA's Goddard Institute for Space Studies (GISS), in 2017, the warming caused by human activities reached approximately 1 ° C above the levels existing before the industrial era (see Figure 2.1), while in 2022, the warming reached 1.1°C above preindustrial levels.

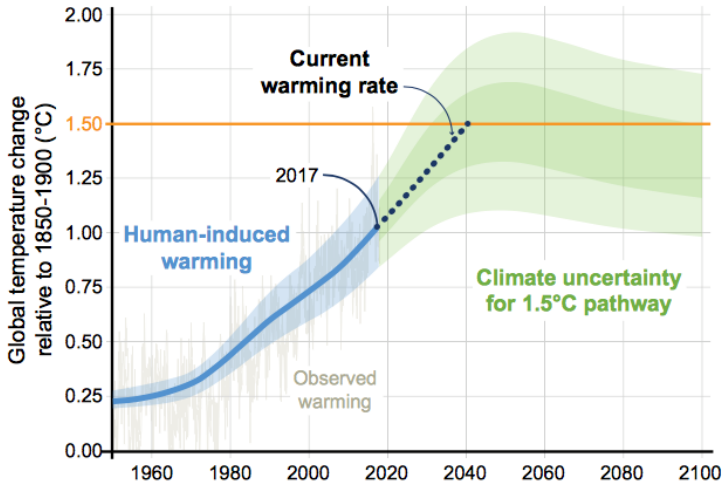


Figure 2.1 Global temperature change relative to 1850-1900 [11]

If the current pace persists, Earth's average temperatures are projected to surpass the 1.5-degree Celsius mark by approximately 2040 [11]. In the European region, an even more ambitous agreement was gratified in 2019: the European Union's *Green Deal* aims to make Europe the world's first climate-neutral continent by 2050 [12]. The *Green Deal* encompasses various strategies for a growth strategy to transition the EU economy to a sustainable economic model, resulting in a cleaner environment, more affordable energy, smarter transport, new jobs, and overall better quality of life. The plan has the overarching objective of reviewing each existing law on its climate merits and introducing new legislation on the circular economy, building renovation, biodiversity, farming and innovation.

After the European promise of achieving carbon neutrality by 2050, China, the world's largest emitter of greenhouse gases, announced in 2020 its intention to become climate neutral by 2060 [13]. This pledge signifies a major shift toward sustainability and has the potential to reshape global climate efforts, underscoring the nation's recognition of the urgent need to address climate change.

Endorsing agreements and setting goals will not be sufficient to adress the global climate change caused by the increased industrialization, urbanization, and energy consumption over the past few decades. The success of these commitments will depend on comprehensive policy frameworks, technological innovations, and international collaboration. During the year 2021, building energy codes were in place in 40% of worldwide countries (79 out of 196), either as obligatory requirements for certain segments of their building stock or as part of a voluntary framework. However, only 26% of countries had made these codes mandatory for the entire spectrum of their building sector [14].

### 2.2.2 The european context

The European Union (EU) has been a proactive advocate for sustainability and has established various agreements and policies to address environmental challenges, promote renewable energy, and combat climate change. Based on the commitment made by embracing the *Paris Agreement* [10] and the *European Green Deal* [12], to reduce its greenhouse gas emissions by at least 40% by 2030 compared to 1990 levels and to become the world's first climate-neutral continent by 2050, respectively, the EU settled *2030 climate and energy framework.* This framework sets binding targets for member states to collectively achieve a 40% reduction in greenhouse gas emissions, a 32% share of renewable energy consumption (ratified by the *Renewable Energy Directive*), and a 32.5% improvement in energy efficiency (endorsed by the *Energy Efficiency Directive*) by 2030, compared to 1990 levels. Other key european agreements and policies include the *Circular Economy Action Plan* adopted in 2020 (this Plan aims to transition the EU to a circular economy model, where resources are used efficiently and waste is minimised, while outlines initiatives to promote sustainable product design, reduce waste generation, and encourage recycling and resource recovery [15]), the *Emissions Trading System,* EU ETS (a flagship policy tool to reduce greenhouse gas emissions, operating on a cap-and-trade principle, setting

a limit on total emissions from certain sectors, including energy production, energy-intensive industries, civil aviation and certain parts of the chemical and steel industries; EU ETS permits the trading of emission allowances to incentivise emission reductions [16]), the *Biodiversity Strategy* (this strategy aims to protect and restore ecosystems, stop the loss of biodiversity, and support nature-based solutions, including goals such as designating protected areas, reducing pollution, and promoting sustainable agriculture and forestry practises [17]) and the *Single-Use Plastics Directive* - this directive addresses the issue of plastic pollution by banning certain single-use plastic products, implementing extended producer responsibility schemes, and promoting alternative solutions [18].

The EU's most recent step towards strengthening its position as a global climate leader is introducing on 14 July 2021 a package of legislative proposals named *Fit for 55* as part of the *European Green Deal*. The name "Fit for 55" reflects the aim of reducing the EU's greenhouse gas emissions by at least 55% by 2030 compared to 1990 levels. In July 2023, the European Council adopted the *Fit for 55* package and its rules will become law in the European Union after publication in the official journal of the EU. The package includes a wide spectrum of new legislative proposals and updates to existing policies (see Figure 2.2) in a range of policy areas and economic sectors, to ensure that they are in line with the EU's updated climate targets. Some key components of the *Fit for 55* package include:

- Revised *Emission Trading System* (ETS): The EU ETS, a cornerstone of the package, aims to expand and strengthen the carbon market. It includes measures such as extending the ETS to new sectors and implementing a more ambitious reduction trajectory for emissions covered under the system
- *Renewable Energy Directive*: The package aims to raise the share of renewable energy in the EU energy mix to 40% by 2030. This involves setting more ambitious national targets for renewable energy generation and expanding the scope of renewable energy use
- *Energy Efficiency Directive*: The *Fit for 55* package aims to increase energy efficiency by setting more stringent requirements for energy savings, both in sectors covered by the ETS and in other sectors
- *Carbon Border Adjustment Mechanism* (CBAM): The CBAM is a proposal to impose a carbon border tax on imports of certain goods to prevent "carbon leakage" and ensure a level playing field for industries subject to emission reduction requirements
- *Revised Energy Taxation Directive*: The package includes a revision of the *Energy Taxation Directive*, which sets the framework for taxing energy products and electricity; the goal is to align taxation with energy and climate objectives
- *Sustainable Transport Initiatives*: The package includes measures to promote cleaner and more sustainable transportation, including stricter emissions standards for vehicles, incentives for electric vehicles, and support for the development of charging infrastructure.

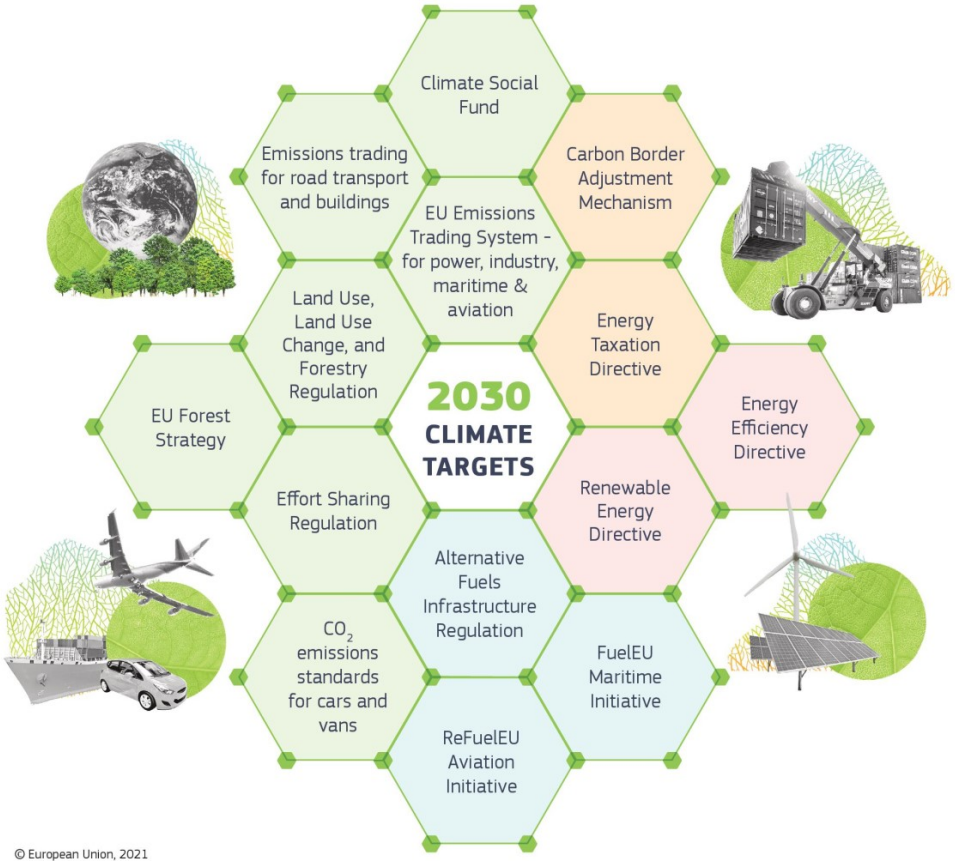


Figure 2.2 Directives and regulations within *Fit for 55* package (figure courtesy of [19])

Another key regulation targeted by the *Fit for 55* package was *The Effort Sharing Regulation* [17], which assigns individual national targets to each EU member state, aiming to achieve a reduction in greenhouse gas emissions by 2030. It addresses sectors that include agriculture, domestic transport (excluding aviation), small industry, buildings, and waste. The combined emissions governed by this Regulation represent nearly 60% of the total domestic emissions of the EU [21]. Originally approved in 2018, the Regulation underwent revisions in 2023. Through these updated national targets, member states will collaboratively contribute to an EU-wide emission reduction of 40% from 2005 levels within the Effort Sharing sectors. Table 2.1 shows the annual targets for greenhouse gas emissions (GHG) required for each EU member state. The targets were established primarily based on relative wealth of the member state (the gross domestic product per capita), which means that rich countries have higher responsibility than countries with a less developed economy. Through these updated national targets, each country must achieve a reduction of GHG emissions with 8-12% more than the initial target set in 2018.

Table 2.1 Member State GHG emission reductions by 2030 in comparison to their 2005 levels determined according to Article 4(3) of the Effort Sharing Regulation [20]

| Country | Old targets (set in 2018) | New targets (since 2023) | Country | Old targets (set in 2018) | New targets (since 2023) |
|---|---|---|---|---|---|
| Belgium | -35 % | -47 % | Lithuania | -9 % | -21 % |
| Bulgaria | -0 % | -10 % | Luxembourg | -40 % | -50 % |
| Czechia | -14 % | -26 % | Hungary | -7 % | -18,7 % |
| Denmark | -39 % | -50 % | Malta | -19 % | -19 % |
| Germany | -38 % | -50 % | Netherlands | -36 % | -48 % |
| Estonia | -13 % | -24 % | Austria | -36 % | -48 % |
| Ireland | -30 % | -42 % | Poland | -7 % | -17,7 % |
| Greece | -16 % | -22,7 % | Portugal | -17 % | -28,7 % |
| Spain | -26 % | -37,7 % | Romania | -2 % | -12,7 % |
| France | -37 % | -47,5 % | Slovenia | -15 % | -27 % |
| Croatia | -7 % | -16,7 % | Slovakia | -12 % | -22,7 % |
| Italy | -33 % | -43,7 % | Finland | -39 % | -50 % |
| Cyprus | -24 % | -32 % | Sweden | -40 % | -50 % |
| Latvia | -6 % | -17 % | | | |

## 2.3 Environmental impact of the construction sector

The construction sector plays an important role in causing environmental degradation through its processes, such as energy consumption, waste generation, and the release of greenhouse gases [22]. Understanding the multifaceted factors involved is essential to address the intricate environmental impact that derives from construction activities.

### 2.3.1 Emissions

According to the *2022 Global Buildings Climate Tracker* and the *United Nations Environment Programme, the* construction sector and buildings are off track to achieve decarbonisation by 2050 [23], [24]. The report shows a negative trend in the decarbonisation of the buildings sector, achieving higher emissions since 2020. During 2021, the $CO_2$ emissions linked to the operational energy of the buildings sector reached a record-breaking 10 gigatons of $CO_2$, marking a rise that exceeds the 2020 levels by approximately 5%, and the prepandemic peak of 2019, by 2%. Within the same time frame, operational energy demand within buildings reached an unprecedented 135 exajoules, demonstrating an increase of about 4% from the previous year, and significantly eclipsed the previous peak in 2019 by more than 3% [14]. This implies that on a worldwide scale, the building and construction sector is responsible for around 37% of $CO_2$ emissions derived from energy use and industrial processes [14]. Figure 2.3 shows the global share of operational and process-related $CO_2$ emissions for the year 2021 accounted for buildings and the construction sector. The total share of the sector is 37% of the $CO_2$ emissions recorded in 2021. Within these emissions, the manufacture of building materials and products such as concrete,

steel, bricks, and glass is accounted for 9% of total $CO_2$ emissions recorded worldwide in 2021.

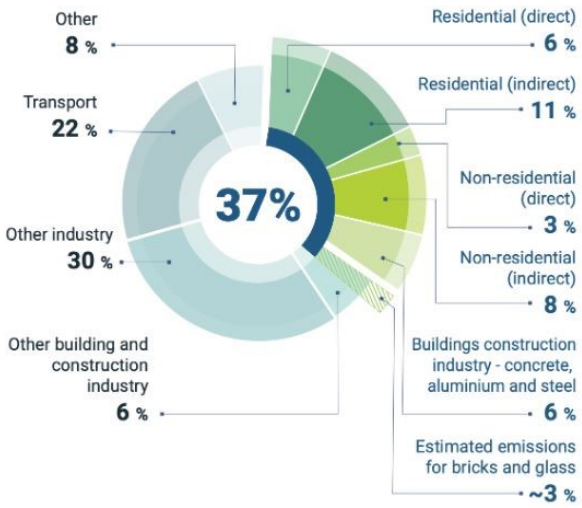


Figure 2.3 Global share of operational and process-related $CO_2$ emissions for buildings and construction, in 2021 (figure courtesy of [14])

The same rising trend since 2020 in the GHG emissions related to the buildings sector is recorded at the regional level, in the EU. Within the European Union, buildings also account for more than a third of the greenhouse gas emissions. The imperative to diminish these emissions is a critical requirement to realise climate neutrality by the year 2050. Figure 2.4 presents the GHG emissions trends under the scope of the *Effort Sharing Regulation*, for EU-27, for each non-ETS sector. In the figure, projections of GHG emissions are also marked considering existing measures (WEM) and additional measures (WAM) scenarios while showing the clear ascendent trend of emissions to all sectors, including the construction sector, since 2020.

Reducing GHG emissions in buildings and construction sector may be achieved through implementation of several key startegies:

- a holistic approach in building design: embodying a holistic approach in building design, which encompasses interdisciplinary analysis and multi-object optimisation, and places significant importance on technology and operational life of buildings, leads to the ability to find optimal solutions of a sustainable approach in construction projects [25], [26], [24].
- efficiency in material design: by prioritising material efficiency in the construction of buildings and infrastructure, one can achieve substantial emissions reduction. Eliminating material waste during the design phase has the potential to result in a 18% decrease in greenhouse gas emissions from 2017 to 2050 [25].
- reuse of building materials and components: reusing building materials and components plays a significant role in lessening the need for new

resources and diminishing emissions related to the extraction of raw materials, transport, and production processes. Although reused construction materials might not immediately fulfill the entire demand of new building projects, integrating highly reusable materials, such as structural steel, from previous use-phases can substantially aid in cutting down emissions [29], [30], [31], [32]

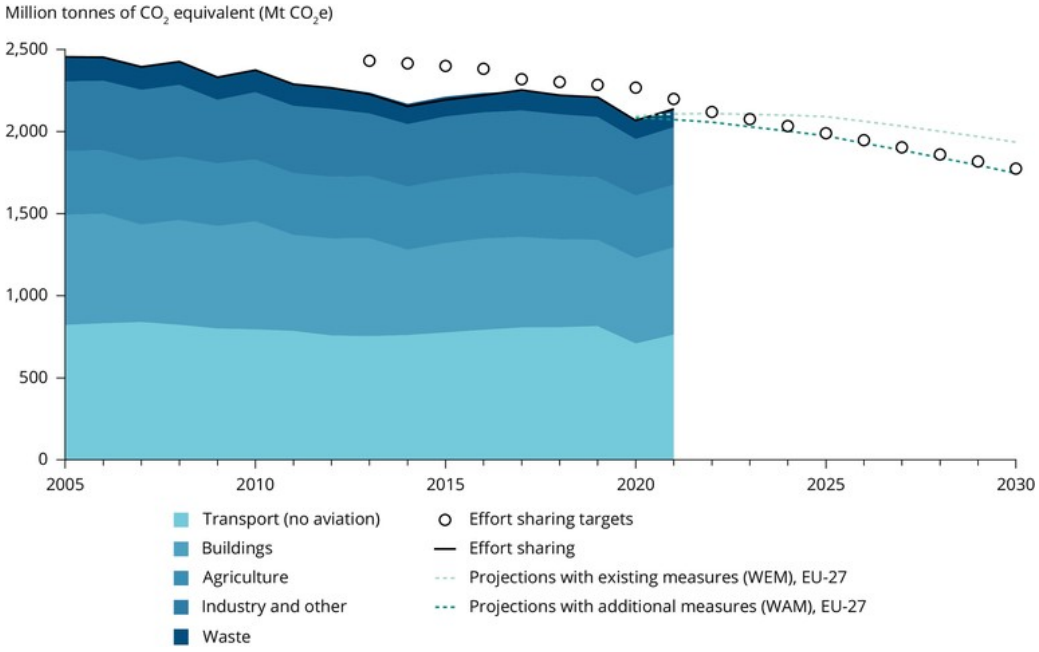


Figure 2.4 GHG emissions trends and projections under the scope of the *Effort Sharing Regulation*, EU-27, with existing (WEM) and with additional measures (WAM) scenarios (figure courtesy of European Environment Agency (EEA) [33])

- Reduce transportation distances: by diminishing the distances covered by construction materials and equipment, emissions can be effectively decreased. Establishing facilities close to construction sites for equipment and materials storage can play a key role in mitigating the emissions associated with transportation [30], [34]
- extending the lifespan of current buildings: extending the utilisation of existing structures can result in the reduction of emissions. This can be achieved by retrofitting and repurposing existing building stock, optimising energy efficiency, and adopting sustainable measures [35], [36], [34]..
- diminishing the carbon impact of construction materials: emissions reduction of construction materials can be achieved through using renewable and recycled materials, through reuse of construction materials and components, through using alternative materials with lower

emissions and adopting sustainable manufacturing processes [38], [39], [40]
- reducing energy consumption: the construction sector is a significant consumer of energy, with activities that require energy for heating, cooling, lighting and the operation of equipment; improved energy-efficient façades and increased end-use savings would lead to lower GHG emissions related to energy consumption [38], [25], [41]
- reducing waste generation from construction materials: reducing GHG emissions in the construction sector by addressing waste from construction materials may be achieved through recycling materials and reusing components at the end of buildings' lifespan, through design for deconstruction, upcycling materials for second lifespan, and using prefabricated construction elements [30], [31], [42], [43], [44].

Adopting the legislative proposals from the *Fit for 55* package as law in UE will enforce applying several above-mentioned strategies to UE country members. Some of the compulsory changes affecting construction sector are:
- as of 2028, new buildings owned by public bodies and as of 2030, all new buildings will have to be *zero-emission*
- as of 2030, it will be mandatory for all new buildings to have *energy performance certificates*
- by 2033, all existing residential buildings will have to be at least *D energy performance class level* and by 2040, all existing residential buildings will have to be at the level fixed by each country to ensure reaching zero-emission building stock in 2050
- as of 2027, all new public and non-residential buildings that have a useful floor area above 250 $m^2$ must have *solar energy installations*; for existing public and non-residential buildings undergoing through renovation this rule is in force starting as of 2028, while for all new residential buildings, as of 2030 solar energy installations will be mandatory [45].

### 2.3.2 Energy Consumption

As in the case of greenhouse gas emissions derived from the construction sector, energy consumption related to the construction sector and buildings has also increased since 2020 [39], [24]. During 2021, operational energy demand within buildings reached an unprecedented 135 exajoules, demonstrating an escalation of approximately 4% from the previous year, and significantly eclipsed the previous peak in 2019 by more than 3% [14]. This means that globally, the building and construction sector are responsible for approximately over 34% of energy demand [14] – see Figure 2.5.

Despite the fact that investments in building energy efficiency increased by 16% in 2021 (documented mainly in EU countries, the USA, Canada and Japan), the

growth in floor space exceeded efficiency efforts [39] and a significant share of the world's energy consumption is attributed to commercial and residential buildings [14].

The same upward trend since 2020 in the GHG emissions related to the building sector is recorded at the regional level, in the EU. An even more severe condition than in the global context was recorded for the building sector in the EU where buildings account for 40% of final energy consumption [22], confirming that greater energy efficiency along with reduced energy consumption is necessary to achieve the goal of climate neutrality by 2050.

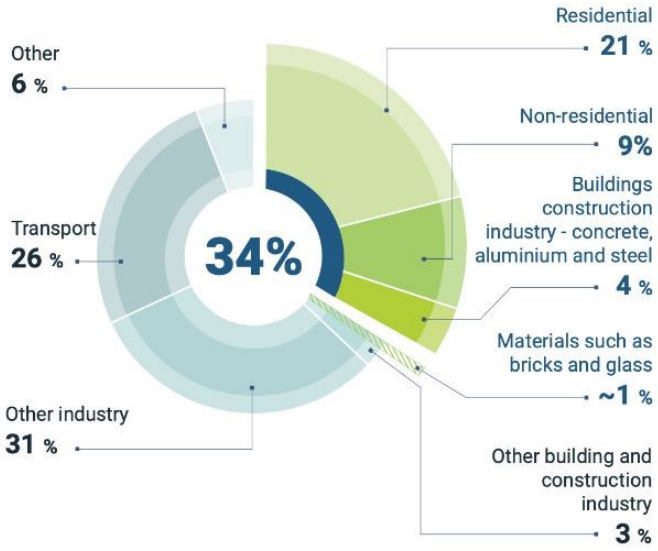


Figure 2.5 Global share of final energy demand for buildings and construction in 2021 (figure courtesy of [14])

There is considerable potential for energy preservation in buildings through renovation and retrofitting projects. The revised Energy Performance of Buildings Directive [46] requires EU member states to establish minimum energy efficiency criteria for both new constructions and certain renovated buildings by 2030 [47]. According to [19] 75% of the existing buildings in UE are inefficient in terms of energy and will require energy-efficiency renovation on a large scale. By 2030, at the European Union level, the goal is to achieve a significant decrease of -11.7% in final energy consumption compared to projections for energy consumption made in 2020. On average, the European Union has realised a reduction of 29%, by 2023 (relative to 2030 forecasts made in 2007). The existing reduction targets (previous to targets adopted through the revision of *Fit for 55* package in 2023) stand at -32.5% for both primary (total demand for energy) and final consumption (the energy consumed by end users). However, the new policy requires a more ambitious target of -40.6% target for primary consumption (as an indicative target) and a mandatory target of -38% for final consumption [48].

Under the updated regulations, member states will be required to incrementally increase their energy savings between 2024 and 2030. Overall energy savings emerging from end-use applications will contribute, on average, 1.49% of total consumption each year, progressively reaching 1.9% by 2030 [48].

The improvement of global energy efficiency and sustainability in buildings can be achieved by reducing energy losses through the building envelope, with façade systems playing an essential role. With the European Union adopting energy-saving regulations and actively pursuing its goals to reduce greenhouse gas emissions, the importance of façade systems has grown. Façade systems serve as the exterior shell of the building, acting as a barrier between indoor and outdoor environments. They have a profound influence on building energy consumption by affecting heat transfer. Façade designs incorporate insulation, thermal breaks, and advanced glazing to reduce heat loss during winter and prevent heat gain in summer. This enhances the building's energy efficiency, lowers the need for mechanical heating and cooling, and ultimately diminishes the overall carbon footprint.

#### *2.3.2.1 Advances in knowledge in the environmental impact of façade systems*

Extensive research has been conducted throughout the life cycle of the construction sector to assess green and sustainable methods and practises, due to their major contributions towards environmental impacts and energy consumption. Life cycle assessment (LCA) is recognised as a highly comprehensive tool for evaluating and predicting the environmental consequences of a process or a product [49], [47], and is the accepted method worldwide used for this purpose. The general framework for LCA is established by ISO 14040 - *Environmental management. Life cycle assessment. Principles and framework* [51] and ISO 14044 - *Environmental management. Life cycle assessment. Requirements and guidelines* [52], both of which possess general applicability. Additionally, CEN/TC 350 has issued standards specifically addressing the evaluation of sustainability for construction projects: EN 15643 - *Sustainability of construction works. Framework for assessment of buildings and civil engineering works* [53], EN 15804 - *Sustainability of construction works. Environmental product declarations. Core rules for the product category of construction products* [54], and EN 15978 - *Sustainability of construction works. Assessment of environmental performance of buildings. Calculation method* [55]. These standards focus on the evaluation of the built environment and embrace a life-cycle approach, aligning with the fundamental framework set forth by the ISO standards. The LCA proves to be instrumental in assisting the decision-making process when choosing a building structure or construction system. This is achieved by identifying the key advantages and drawbacks of competing systems throughout their entire lifespan [56]. In fact, the most pronounced influence on the life cycle performance of buildings is the initial phases of building design, during which decisive choices are made, as postulated by Gervásio et al. [57]. Current research outcomes from studies examining the life cycle of buildings have generated notable changes in

the construction sector, guiding efforts toward emissions reduction and improved energy efficiency [58], [59].

The façade, which constitutes the outer walls of a structure, represents one of the most significant building elements and represents the component that plays a crucial role in the transfer of heat between the interior and exterior environments [60], [61]. Specifically, it accounts for a considerable portion of thermal transmittance, approximately 20% to 30%, influencing a significant portion of total energy consumption in a building [62]. Research studies showed that for a building façade, in order to meet sustainability performance criteria, the selection of relevant façade materials is equally important for cladding elements [63], [64] and thermal insulation.

For cladding materials, along with a high recyclability / reuse attribute [65], [29], which represents the environmental component of the sustainable concept, producing a unique appearance for the building [66] is also a requirement with regard to the social component of the sustainable concept. Given that construction projects vary greatly in terms of their characteristics, location, and intended use, compiling an exhaustive catalogue of potential requirements for cladding materials proves unfeasible. However, the subsequent enumeration aims to emphasise the foremost and pivotal demands in this context: protection from external environmental conditions, cladding must withstand outer loads, thermal performance, fireproof performance, acoustic performance, aesthetic appearance, durability, material and installation costs, maintenance requirements, recyclability / reusability [66]. Therefore, the choice of façade cladding material constitutes a significant decision that involves multiple criteria, as it affects the building's appearance, cost of the project, the duration of the construction, and the overall sustainability of the building [60].

The last decade has witnessed an increase in research articles based on the life-cycle assessment (LCA) comparison of different façade systems. Taborianski and Prado [67] have reported that within their study exploring various façade alternatives, structural glazing coupled with uncolored glass demonstrated the highest $CO_2$ emissions, while brickwork and mortar façade systems exhibited the lowest. Kim [68] has pointed out that transparent composite façade systems entail substantially diminished environmental impacts compared to glass curtain wall systems. Further studies by Ottele et al. [69] reported that the potential energy savings of green façade systems is relatively double that of a conventional European brick façade, for a building in the Mediterranean climate. Han et al. [70] have demonstrated that when gauged in terms of environmental efficacy, decorative ceramic façades exhibit superiority over commonly employed curtain wall materials such as glass, marble, and aluminium.

Likewise, plenty of similar comparative life cycle analyses has been carried out by numerous researchers [71], [72], [73], [74] encompassing varying categories of exterior walls. Pulselli et al. [75] showed the environmental implications of three distinct exterior wall systems: an insulated wall enhanced with external cork cover, a traditional air-cavity wall, and a ventilated wall that incorporates external brick panels affixed to extruded frames. Their study underscored the influence of external climatic

conditions on the relative performance of these systems [75]. Iuorio et al. demonstrated that quantifying the sustainability of a structural system is crucial to reduce impacts. Their research illustrates that meticulous material selection aimed at withholding both operational energy and embodied carbon accentuates the significant role of the structural system in LCA impacts. In their study, an innovative modular lightweight steel system (named the ELISSA mock-up) and their research results showed that when comparing one square metre of the ELISSA mock-up wall with a conventional reinforced masonry wall, the environmental impacts of the former are considerably reduced compared to the latter [44]. Kahhat et al. stated a comprehensive comparison of various external wall systems for a single-storey residential building. They emphasised that the selection of an optimal wall system should be based on the environmental effects of the overall life cycle, rather than focussing solely on individual phase impacts [76].

The literature categorises thermal insulation materials into various types, primarily falling within two main categories as shown in Figure 2.6: inorganic and organic, aligned with the source of their raw materials. Each of these two primary categories is further subdivided into natural and synthetic insulation materials, based on their production processes. Additionally, there exist composite products and emerging technology materials that continually undergo refinement and advancement [77].

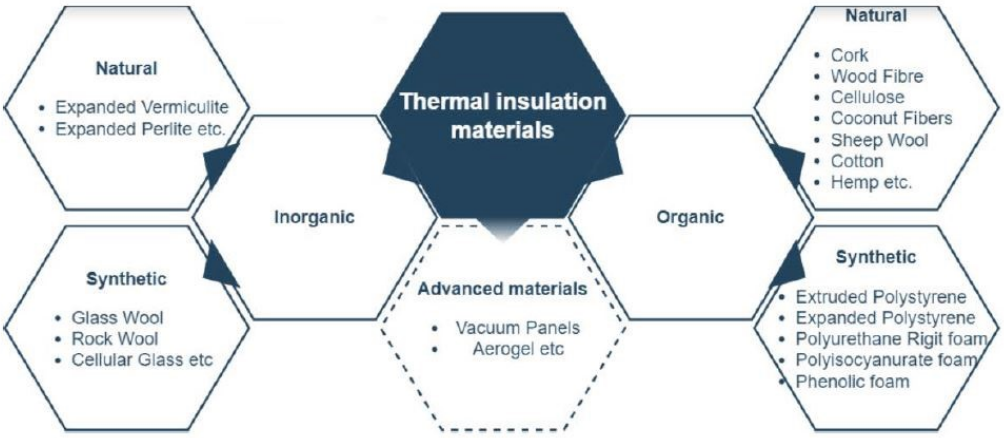


Figure 2.6 Classification of thermal insulation materials [38]

Different insulation materials that allow an adequate thermal performance of walls, dealing with various thicknesses of the insulation layers, have also been extensively researched in recent decades. From advanced materials such as aerogel (that can have 2 to 2.5 times lower thermal conductivity than mineral wool insulation [78], [79]), vacuum insulation panels (that can have 5-8 times higher thermal resistance than conventional thermal insulation materials [77], but are fragile, expensive and prone to thermal bridging effect [81]), to more sustainable thermal insulation materials such as thermal insulator obtained from recycled glass waste

(that under specific circumstances, may yield favourable environmental impacts, considering the mitigation of resource depletion from non-abundant materials and fossil fuels, alongside the supplementary advantages deriving from glass recycling [82]), or thermal insulation wadding made from post-consumer PET bottles (that has similar environmental impacts in an LCA with mineral wool insulation [38]), and up to conventional thermal insulation materials such as mineral wool and polyisocyanurate insulation (PIR) [65], or renewable materials such as cellulose, cork (cellulose together cork have clearly lower global warming potential impacts when compared to conventional insulation materials [83], [84]) and hemp (that acquire a potentially negative GWP impact due to the interaction of sequestration and $CO_2$ absorption through lime-based binders [85], [86], [87]) were investigated.

Through a parametric investigation conducted by Gervásio et al. [88] involving a light steel frame residential structure (LSF) located in Portugal, various insulation levels were examined. The primary objective was to evaluate the equilibrium between energy efficiency and embodied energy throughout the life cycle of buildings. The outcomes of this study led to the determination that, within the typical climatic conditions of southern Europe, substantial improvements in the thermal efficiency of residential buildings can be achieved by increasing the insulation level of the vulnerable elements of the building envelope. Importantly, this can be accomplished without acquiring a notable increase in the overall embodied energy of the building [88].

Füchsl et al. conclude in a critical review of the LCA of thermal insulation materials that improvements are required in the production processes of conventional inorganic materials and that the environmental impacts of organic non-renewable materials can be diminished through sustainable sources of raw materials. Insulation materials derived from renewable resources, such as hemp, cellulose, or wood fibre, exhibit considerable potential for improvement. By changing additives and binders toward more sustainable alternatives, these insulation materials could see substantial improvements in their environmental impact [89]. However, mineral wool (MW), glass wool, expanded polystyrene insulation (EPS), extruded polystyrene insulation (XPS) and rigid polyurethane foam (PUR) are the dominant insulation materials in the market, accounting for 90 % of the market [87]. Therefore, in this thesis, the environmental impact assessment investigated in steel-intensive façade systems considered mineral wool as thermal insulation material.

Current concerns related to environmental, energy, economic, and social sustainability underscore the need for more adjustable buildings [56], especially for industrial buildings [30], [31], and steel-intensive façade systems can offer valuable contributions in this domain [90], [30]. Gosling et al. [91] analysed the notion of building adaptability and presented a conceptual framework that systematically explains adaptability within the construction industry. A 'designed for flexibility' should not only apply to structures, but also to the envelope of the buildings. O'Grady et al. show that building renovation can be achieved by disassembling approximately 83% of walls and ceilings during the operational phase [92], therefore, steel-intensive façade systems are preferred in a sustainable design solution for buildings that

considers both energy efficiency performance and embodied energy of building materials [90], [93].

#### *2.3.2.2 Research gaps in environmental impact of façade systems*

Despite recent progress in research, considerable voids remain in our understanding of the environmental impacts derived from construction activities. An important gap emerges from the scarcity of data on the environmental impacts of construction activities within developing nations.

The lack of standardisation in the methods used to assess the environmental impacts of construction activities, as a generic and standard system boundary for the construction stage, represents another distinct gap.

Furthermore, more research is needed for environmental impacts linked to construction activities beyond the production phase, extending to aspects like building construction, building utilisation, and maintenance [50], [59].

There is also a need for long-term comprehensive studies that evaluate the actual environmental performance of façade systems over their lifespan; this includes monitoring energy consumption, occupant satisfaction, and material durability [94].

With the increasing impacts of climate change, there is a need to develop façade systems that can adapt to changing environmental conditions; Research should focus on innovative solutions that improve resilience and minimise the environmental impact of façades in the face of climate change [95].

Also in light of climate change and occupancy behaviour, a gap identified in the current state of the art is to improve the assessment of the operational phase in LCA studies by contributing to the dynamic LCA (DLCA) framework [96]. DLCA considers dynamic factors in the life cycle of buildings, such as technological progress, variation in occupancy behaviour [97], changes in the external system of the building like changes in energy-mix production, climate conditions, and changes in climate regulations [96].

The circular economy approach, which focusses on reducing waste and promoting resource efficiency, needs to be further integrated into façade design and construction practises; this involves exploring strategies for material reuse, recycling and end-of-life management [29], [30], [98].

### 2.3.3 Waste

The European Union waste management policies aim to decrease waste generation and enhance resource utilisation efficiency. These policies focus on addressing the potential of waste-derived resources to the fullest extent, thereby reducing the environmental impact of waste. The Waste Framework Directive 98/2008/EC [99] advocates for a waste hierarchy that prioritises prevention, followed by reuse and recycling, with disposal as the last resort (presented in Figure 2.7).


Figure 2.7 Waste hierarchy according to Waste Framework Directive [100]

Given that construction and demolition waste (CDW) constitutes more than a third of the total waste output in the EU [101], reaching a 37.5% in 2020 a 37.5% (as shown in Figure 2.8), it has emerged as a crucial waste stream. This situation places considerable demand on the sector to significantly increase the recycling, reuse, and other forms of material recovery from CDW. Amplifying the recovery of materials from CDW not only promises an economy characterised by resource efficiency and competitiveness but also addresses the issue of high greenhouse gas emissions (GHGs) originating from the construction sector.

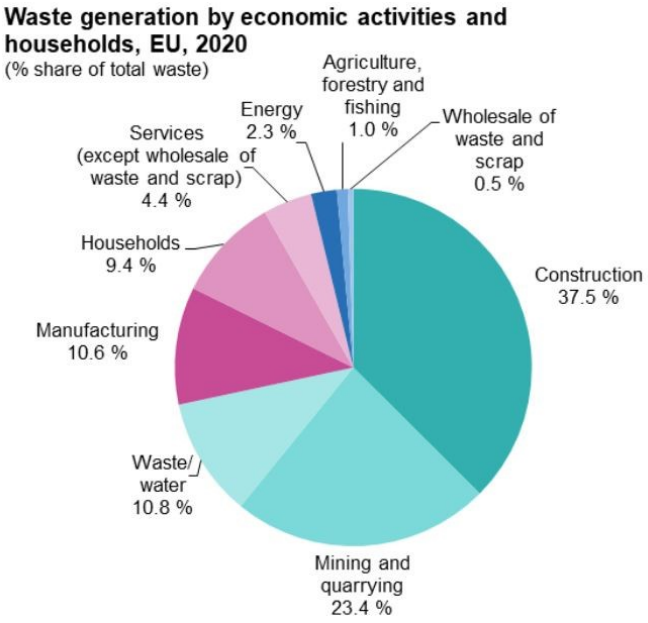


Figure 2.8 EU Waste generation by economic activities and households in 2020 (Source: Eurostat – online data code: env_wasgen [101])

The concept of reusing building components originates from older periods when the availability of construction materials was limited and their production was a slow, labour-intensive, and costly endeavour. Over time, this practise gradually became less feasible due to the widespread mass production of building materials and the demand for high levels of structural safety, material quality, and health and safety aspects of demolition and deconstruction processes. Striking a balance between adhering to these modern standards and promoting environmentally efficient material circulation has emerged as a notable challenge within the research community in the last decade. This challenge has also gained importance among contractors in the construction industry, who now need to transition from traditional demolition practises to more intricate deconstruction processes. This shift is crucial to preserve the value of building elements. Consequently, the reuse of building components is a central aspect of international efforts to develop a circular economy within the construction sector [31].

Reusing building materials and components from existing structures can significantly reduce the demand for new materials [30], [31], [42], [43], [44]. This includes elements such as doors, windows, fixtures, and structural components that can be refurbished and incorporated into new construction projects. The implementation of efficient waste management strategies at construction sites facilitates the separation and recycling of construction materials. These include primarily concrete, steel, glass, wood, ceramic, asphalt, and plastics, all of which can undergo processing and conversion into new construction materials or alternative products.

In the context of the circular economy, the World Steel Association [102] has stressed the substantial benefits offered by the steel industry compared to alternative materials. These advantages arise from practises centred on reduction, reuse, remanufacturing, and recycling. Within the construction sector, steel exhibits remarkable potential to improve resource efficiency due to its substantial capacity for reuse, in addition to recycling. In the domain of steel construction, single-storey steel buildings (SSBs) have a significant market share. Furthermore, the structural components found in SSBs frequently feature extended spans and relatively simple configurations, and they are frequently left exposed and accessible at safe working heights. As a result, SSBs present the highest degree of potential for reutilization [29], [32].

#### *2.3.3.1 Knowledge advances*

Assessing the environmental impact and financial expenses associated with the reuse of construction and demolition waste and striving to maximise the efficient use of high-quality construction waste require a comprehensive consideration of the interaction between economic and environmental factors [103].

Reuse refers to the practice of using a discarded item for its intended initial purpose in its original state or with minor modifications. Recycling is the process of collecting, processing, and transforming used or discarded materials into new products or raw materials. A process in between the two (reuse and recycle) is

refurbishment: it typically involves repairing or replacing worn or outdated components, and improving the overall appearance and performance of the item. When products and their components retain their functionality for a prolonged period, it results in reduced energy consumption, decreased utilisation of material resources, and the generation of less waste compared to recycling, which primarily addresses the materials themselves [104]. This approach contributes significantly to environmental sustainability. Figure 2.9 shows the different paths a component takes when involved in a reuse, remanufacture, or recycling process.

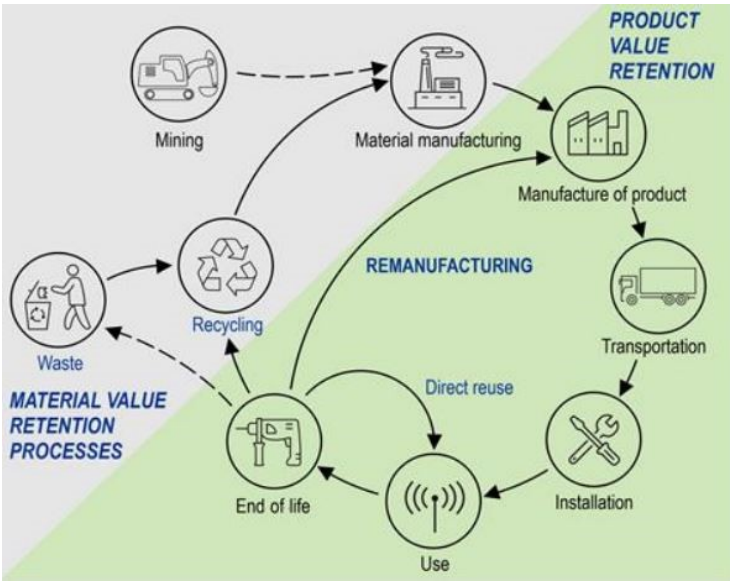


Figure 2.9 Reuse, remanufacture and recycling processes in a circular economy (Source: European Topic Centre Waste and Materials in a Green Economy (2021) [104])

In a study by Di Maria et al. [105], LCA methodologies were used to analyse four distinct scenarios for the end-of-life of CDW in Belgium. The findings of this study underscored that increasing the recycling of high-quality CDW has the potential to substantially reduce the environmental impact of the entire system. Llatas et al. [106], in a study that evaluated the potential environmental benefits of the waste management hierarchy using LCA, found that CDW can be reduced by up to 57% when using prevention programmes compared to non-prevention programmes.

There were several successful reuse projects in Europe [107] that demonstrated that structural steel reuse is possible and represents a viable solution in the construction sector, producing considerable benefits in terms of carbon emissions savings, time savings, or cost savings. The buildings which are most suitable to reuse projects (not only through components but also as a whole) are steel structures. The sustainable asset of steel is that it is characterised by durability and capacity for repeated reuse and recycling, without losing its properties [26]. Building with reclaimed elements requires additional involvement in deconstruction, reconditioning (e.g. sandblasting, coating steel elements) and transport, which can

create a burden on environmental impact but, at the same time, prevents the burdens of the impact caused by the production of new structural elements that demand material sourcing and energy-intensive fabrication processes [34].

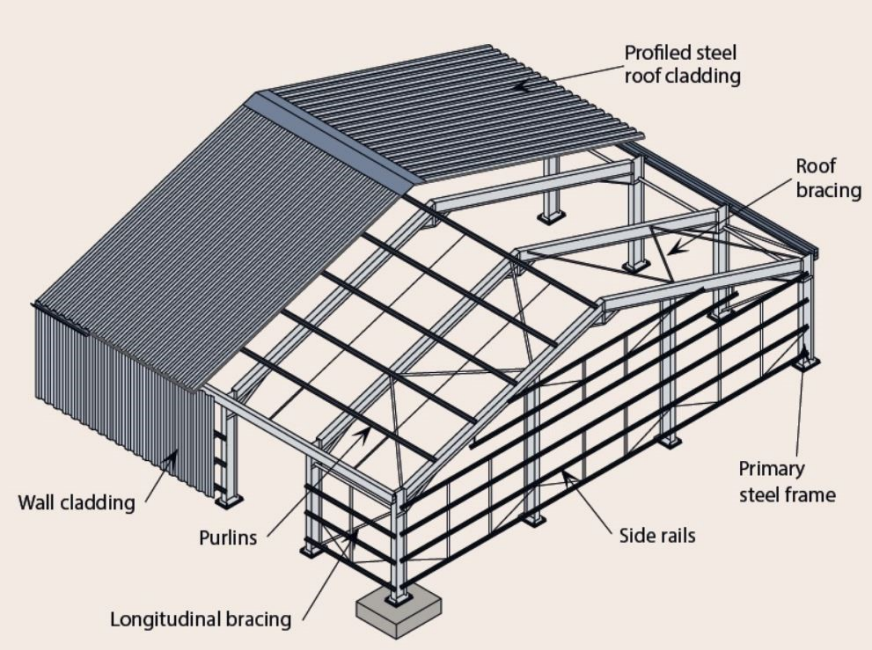


Figure 2.10 Arrangement of a typical single-storey building (figure courtesy of [108])

The existing building stock lacks designs that lessen deconstruction, making the process of material recovery for end-of-life reuse complex and challenging. Vares et al. [32] showed that the net benefits in the case of reused steel structures (when the reuse of frames, rails, purlins and envelope is considered) are more than three times higher than in the case when steel structures are demolished and recycled.

Hradil et al. [29] developed a method to predict the reusability of building components and structures as a whole through a pilot study of three different single-storey steel buildings. The study aimed to generate a single reusability indicator for the entire end-of-life scenario and showed that the current value of steelwork eligible for reuse ranges between 1.5% and 7% of its initial cost. Consequently, a larger perspective can be ensured when assessing the economic feasibility of the investment. This could include considerations beyond the steelwork, stressing the importance of considering the potential for reusing the building envelope, as well as other structural elements.

The market for the reuse of steel structures remains relatively limited, although there exists substantial potential for its expansion. Reuse can involve an entire structure or its individual components such as frames, beams, columns, purlins, and cladding systems. In order to facilitate future reuse, the European Commission through the European Convention on Constructional Steelwork (ECCS) and the

Research Fund for Coal and Steel underwent a project to develop methods, systems, and protocols for the reuse of various components of steel-framed single-storey buildings [109]. The project addressed the dual aspects of deconstructing and reusing existing buildings, as well as developing strategies for designing, constructing and documenting new buildings to enhance their potential for future reuse. It was addressed to primary structures (frames), secondary structures, and the incorporation of multi-material hybrid components within the building envelope.

#### *2.3.3.2 Gaps in building's circularity*

Even with increasing recognition of circular economy methodologies such as building deconstruction and reuse [30], [31], [42], [43], [44], a standardised approach to assess the potential for reusing building materials remains absent [110]. By creating an index to quantify the circularity of a building [106] not only will this gap be filled, but will also enable practitioners to make informed decisions aimed at mitigating the environmental impact associated with buildings [92].

Extensive exploration of the literature has revealed various obstacles impeding the adoption of Design for Deconstruction (DfD) principles and the practice of reuse. Given that DfD is likely to introduce higher initial construction costs, while the associated benefits may materialise in the distant future (at the end of the construction), this equation might not be readily attractive to investors, particularly when the timing of the deconstruction remains uncertain [31]. To effectively constrain investors, designers, and builders to consider DfD during the building design stage, enticement is essential. One potential avenue involves strengthening legislation, which could create a framework that encourages greater consideration of deconstruction. Subsequently, such measures would facilitate more viable prospects for reusing building components [31].

Another gap revealed in the literature is that of re-certification: CE markings and Declarations of Performance are needed for reused components [32]. Building components intended for reuse must adhere to predetermined quality standards. The testing of reused building components should ideally be cost-efficient, and in certain instances, the need for testing could be omitted if the component's quality can be assured through alternative means. Moreover, a shift in customer perceptions is essential, moving from an inclination to disregard reclaimed building components to embracing their acceptance [31], [42].

However, the extent of the use of LCA in the context of building material reuse holds the promise of better understanding the actual environmental impacts and benefits associated with this practice. The LCA results can contribute to the development of regulations and standards that incentivise and reward sustainable practises such as material reuse, and they can uncover opportunities for innovation in material reuse techniques, contributing to the advancement of sustainable construction practices.

## 2.4 Steel-Intensive Façade Systems

Currently, a large number of façade systems are available to facilitate the creation of sustainable building designs. The primary obstacles facing façade designers involve the exploration of new technologies and efficient sustainable systems that achieve superior structural and sustainable performance, while maintaining a visually pleasing aesthetic [94].

One of the earliest strategies for achieving the sustainability of building façades involves the reduction of both the overall mass and the orientation of main façades [111]. Until today, various approaches have been adopted to minimise the energy demands of building systems [94], [112], [113] such as harnessing solar and wind energy [114], [115], favour natural ventilation [116], optimise daylight utilisation [117], [118], integrate vegetation with façades [119], [120] or use smart and adaptive devices [26], [121], [122]. Furthermore, technological advances (wireless sensors, smart actuators, adjustable overhangs, thermoelectric modules, self-loading frameworks) and smart materials (solar controll glass, reflective coatings, phase change materials) are used to ensure thermal efficiency, reduce interior cooling loads, improve energy efficiency, and adjust climatic factors such as light, temperature, and humidity in interior spaces in real time [94]. However, façade technology could present a higher sensitivity to deterioration compared to conventional materials, thus increasing maintenance and replacement expenses over time [123]. The incorporation of intricate systems such as lighting and shading can also present difficulties linked to high construction costs and the utilisation of costly materials [122], [124].

A steel-intensive façade system is a building envelope that prominently features steel elements as a primary structural component and as an aesthetic component. Traditionally used in agricultural and industrial construction, in last decades steel-intensive façade systems have faced a growing demand in retail, commercial, and educational buildings [94]. Whether in the form of built-up wall steel insulated panel cladding systems (Figure 2.11-left), sandwich panel wall system (Figure 2.11-middle) or liner-tray wall system (Figure 2.11-right), or in the form of single skin façade panels (Figure 2.12) and modular cassettes (Figure 2.13), steel-intensive façade systems reached increasing interest in the construction sector due to their strength, flexibility, and recyclability characteristics, emerging as a particularly inviting path to achieve sustainability goals.


Figure 2.11 Built-up wall system (left), sandwich panel wall system (middle) and liner tray wall system (right) [31]

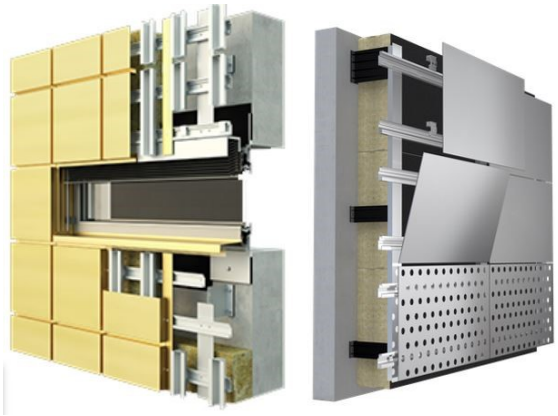

Figure 2.12 Single skin façade panels [125], [126]

Figure 2.13 Modular façade system [127]

Among the key ways in which steel-intensive façade systems contribute to sustainability are:

- Energy Efficiency: Steel-intensive façade systems can improve the energy efficiency of buildings by reducing heat loss and gain, thereby reducing energy consumption and associated greenhouse gas emissions

- Durability: Steel is a durable material that can withstand harsh environmental conditions, reducing the need for frequent repairs and replacements. In addition, it can withstand high loads and stresses, making it ideal for use in façade systems
- Circular Economy: The reuse and recycling of steel components in façade systems align with the principles of the circular economy, promoting a more sustainable and efficient approach to resource management. Furthermore, the versatility and recyclability of steel contribute to the reduction of material waste and the extension of a building's life cycle
- Aesthetics: Steel-intensive façade systems offer a wide range of aesthetic options, allowing architects and engineers to create intricate designs that enhance the aesthetic appeal of a building, maximise daylight penetration, and optimise thermal insulation.

### 2.4.1 Liner tray wall systems

According to the International Association for Lightweight Metal Building Envelopes in the Recommendations for the Selection of Corrosion Protection Systems, the life-span of industrial buildings is generally 20-25 years. After this extent of time, these buildings are usually replaced due to a change in demand, business growth, technological efficiency improvements, changing regulations, market demand, contract manufacturing, etc. This would lead to a burden from a sustainable perspective, as a shorter life span of buildings brings a higher ratio of embodied carbon structures (the total amount of energy used for the extraction of raw materials, manufacturing, transportation, construction, use, and eventual disposal or recycling of product) to operational carbon, compared to longer-lasting structures (other types of structure than industrial buildings that usually have a life span of 50-100 years). The growing demand for sustainable construction practices presents opportunities for manufacturers and suppliers of façade cladding systems to position their products as environmentally responsible solutions.

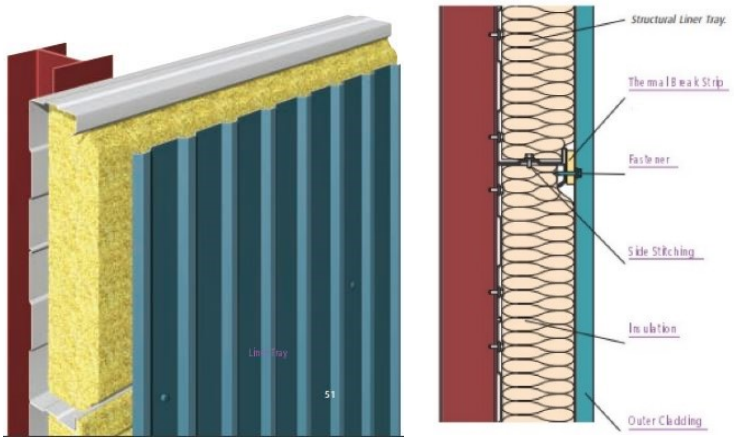


Figure 2.14 Typical liner tray wall system [128]

In the last decade, in the industrial halls and warehouse sector, approximately half of the structures were covered with sandwich panels and 50% with built-up systems with two skins [1]. In light of the 'Alert' entitled 'Effects of scale' [2], issued in 2018 by the United Kingdom Standing Committee on Structural Safety (SCOSS) regarding the behaviour of the cladding systems to wind loads in structures with heights to eaves of 20 metres or more [1], it is most likely that façade systems made of built-in cladding systems, such as liner tray cladding systems, will face an increase in demand compared to sandwich panels envelope solutions. From this perspective, in this study, a liner tray cladding system (presented in Figure 2.14) was studied, providing a comprehensive understanding of its environmental impact and structural behaviour.

Liner trays are lightweight thin-walled metal components (see Figure 2.15) with a material thickness of 0.75–1.50 mm. They can be used horizontally, forming the inner layer of the walls (presented in Figure 2.14), in which case they are termed "structural liner trays" or vertically, forming the outer layer of the walls (presented in Figure 2.16), in which case they are termed "cassettes". The cassette-formed cladding system has been pioneered in France, under the name 'CIBBAP' by the company 'Produits Acier Batiment' (PAB) [129].

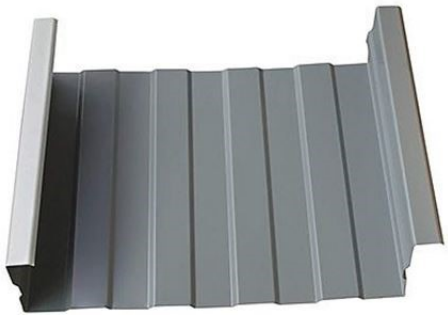

Figure 2.15 Typical liner tray

When liner trays span horizontally between the main structural columns, there is no need for additional secondary cladding rails. This achievement is made possible due to the substantial depth of the liner tray profile and the inherent bending stiffness that resulting from it. As a consequence of this design, the absence of supplementary steel framework offers distinct benefits, particularly with regard to the efficiency and cost-effectiveness of the construction process, as well as the installation tolerances.

In a wall cladding system, liner trays are used as an inner shell of a double-shell wall system (see Figure 2.14), while connected to corrugated steel sheets or trapezoidal profiles, which function as an outer shell. The outer shell provides weather protection, while the liner trays have a supporting function, as they effectively resist perpendicular uniformly distributed wind loads, and additionally they serve the purpose of establishing a skin-diaphragm effect, which bear horizontal loads (wind or earthquake). These systems are conventionally constructed using a specified quantity of horizontally aligned and interconnected liner trays that are positioned adjacently.

The sinusoidal or trapezoidal sheeting is installed perpendicularly to the direction of the liner tray, featuring vertical corrugations. This assembly creates a rigid metallic cellular structure that essentially forms the exterior cladding of the building [130]. The interior space of this cellular structure is filled with thermal insulation material, contributing to improved energy efficiency and thermal performance.

The joining system provides a high degree of tightness preventing from collecting water in between, ensures a quick and easy installation which leads to reduced time and cost of assembly, and has a low own weight but a high bearing capacity. This research contributes to informed decision making, better construction practices, and the broader sustainability goals of the construction industry.

#### *2.4.1.1 Advances in knowledge of steel liner trays*

The steel grades used for the design of liner trays and profiled sheets are prescribed by Eurocode EN1993-1-3 [131]. Steel sheets are generally galvanised as prescribed in EN10346 [132] to avoid corrosion and increase durability. The continuous hot-dip zinc galvanised strip steel is designated S220GD+Z, S250GD+Z, S280GD+Z, S320GD+Z, S350GD+Z or S550GD+Z, which means that the basic yield strength changes from 220 to 550 N/mm$^2$ and there is a minimum G275 coating. The normal thickness of the zinc coating is 0.04 mm (275 g/m$^2$). The zinc coating and the paint coating applied on the liner trays lead to excellent durability.

Three primary load systems are relevant to cassette walls: axial compression, effected by the above floors, bending, caused by wind pressure/ suction, and shear determined by wind or earthquake-induced diaphragm action [133].

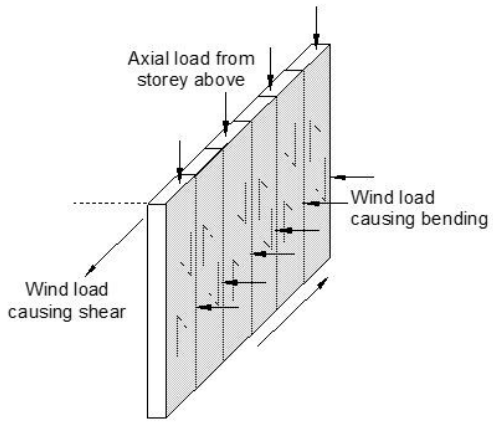


Figure 2.16 Loading cases for vertically spanning liner trays walls – casettes [134]

Liner trays have traditionally been designed as structures with a single span. In such scenarios, the bending moment that causes sagging is typically the most critical in design, whereas the vertical shear forces and the lateral forces in the supports can often be ignored. The bending moment resistance becomes particularly critical, especially when the structure is subjected to significant wind loads [3].

In the case of liner trays with two or more spans, the design calculations have to consider both web crippling at support areas and shear strength of the web. The resistance of the liner trays in this case is provided by the hogging moment and local transverse forces.

### 2.4.1.1.1 Design procedures

The behaviour of structural liner tray sections was first investigated by Baehre and Buca [135] in Karlsruhe, Germany, in 1986. The behaviour of liner trays was studied under three primary loading conditions: axial compression, shear, and bending. The methodology developed by Baehre, as documented in [135], [136], [137], and [138], was further enriched by research carried out by Davies at the University of Manchester, detailed in [139], [140], [141], [136], and [137]. The results of these experimental and theoretical studies have formed the basis of the design procedure outlined in Eurocode EN 1993-1-3 [131]. The range of validity on geometric parameters within this design process was established due to the constraints imposed by the tests conducted by Baehre, and is presented in Figure 2.17.

Since the clauses EN1993-1-3:2006 explicitly demand the stabilising impact of the second metal layer, it is essential to reevaluate their suitability for cassette wall construction scenarios where this second skin is unlikely to exist (or could potentially be substituted with a significantly weaker material) [133] or for liner tray wall systems where the longitudinal spacing of fasteners supplying lateral restraint to the narrow flanges, $s_1$, is greater than 1000mm [143].

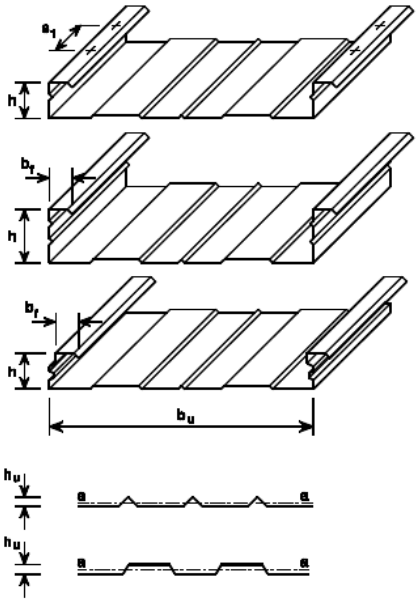


| | | | | |
|---|---|---|---|---|
| 0,75 mm | ≤ | $t_{nom}$ | ≤ | 1,5 mm |
| 30 mm | ≤ | $b_f$ | ≤ | 60 mm |
| 60 mm | ≤ | $h$ | ≤ | 200 mm |
| 300 mm | ≤ | $b_u$ | ≤ | 600 mm |
| | | $I_a / b_u$ | ≤ | 10 mm$^4$/mm |
| | | $s_1$ | ≤ | 1000 mm |

Figure 2.17 Typical geometry for liner trays (left) and range of validity for design procedures acc. to EN 1993-1-3 [131]

There is great variability in the comparison between test results and theory in the case of cold-formed sections in bending, primarily due to the phenomenon of "flange curling" (the tendency of the wide flange of liner trays to curl towards its neutral axis – see Figure 2.18). The test results are likely to produce significantly higher bending strength than the calculations [133].

According to EN 1993-1-3 [131] the moment resistance $M_{c,Rd}$ of a liner tray can be obtained considering two cases of the behaviour of liner tray, depending on the direction of the load applied to the liner tray: (1) bending with the wide flange under compression and (2) bending with the wide flange in tension. The calculation of the moment resistance $M_{c,Rd}$ of the liner trays following the procedures stated by EN 1993-1-3 is contingent to (I) the geometrical properties of the liner trays being within the range of validity and (II) the depth, $h_u$, of the corrugations of the wide flange not exceeding h/8 (h represents the overall depth of the liner tray (see Figure 2.17).

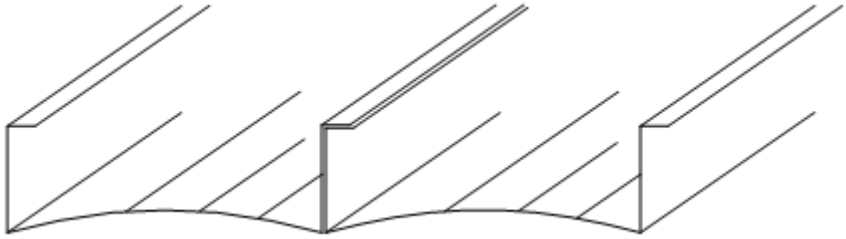

Figure 2.18 Flange curling in liner trays [133]

When calculating the moment resistance of a liner tray with its wide flange in compression (behaviour occurred in liner tray wall cladding systems subjected to wind suction), according to EN 1993-1-3 in force provisions, a step-by-step procedure must be followed (as presented in Figure 2.19):

- Step 1: The effective areas of all compression elements of the cross-section is determined based on values of the stress ratio $\psi = \sigma_2 / \sigma_1$ obtained using the effective widths of the compression flanges but the gross areas of the webs
- Step 2: The centroid of the effective cross section is located, after then, the moment resistance $M_{c,Rd}$ is obtained from:

$$M_{c,Rd} = \frac{0.8 \cdot W_{eff,min} \cdot f_{y,b}}{\gamma_{M0}} \tag{2.1}$$

Where,

$$W_{eff,min} = \min\left(\frac{I_{y,eff}}{z_c}, \frac{I_{y,eff}}{z_t}\right) \tag{2.2}$$

and:

$I_{y,eff}$: -the effective second moment of area of the effective cross-section of the liner tray with the wide flange under compression about the y-y axis

$z_c$: -the distance from the effective centroidal axis to the system line of the compressed wide flange (see Figure 2.19)

$z_t$: -the distance from the effective centroidal axis to the system line of the narrow flange in tension (see Figure 2.19).

In this case, of liner trays with the wide flange in compression, the primary factor influencing bending behaviour is the local buckling of the wide flange. However, when the wide flange is in compression, it undergoes flange curling, which interacts with local buckling. A rigorous address to this interaction is not prescribed in EN1993-1-3:2006. Instead, the standard recommends that the advantageous impact of intermediate stiffeners should be disregarded, and a conventional effective width procedure should be employed. This procedure is adjusted by increasing the material factor material factor of $\gamma_M$ from 1.0 to 1.25, in order to account for the added uncertainty introduced by flange curvature [133].

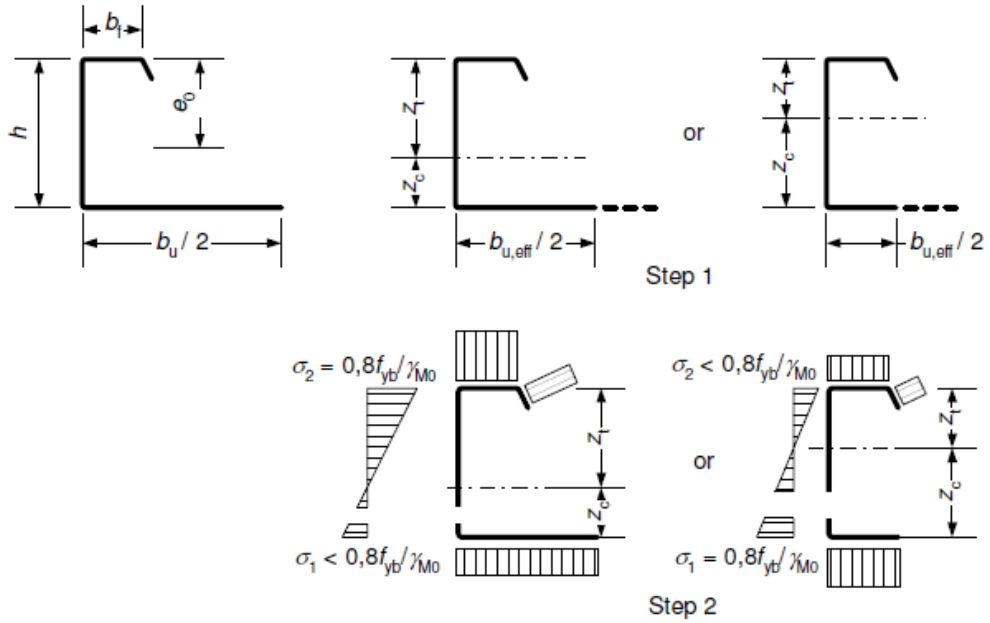


Figure 2.19 Determination of the moment resistance of a liner tray with its wide flange in compression according to EN 1993-1-3:2006 [131]

Since the narrow flanges and the edge stiffeners are subjected to tension, they do not buckle and the absence or presence of the second skin has no impact, as there is no impact either of the longitudinal spacing of the fasteners that supply the lateral restraint to the narrow flanges, $s_1$.

A step-by-step procedure must also be followed when calculating the moment resistance of a liner tray with its wide flange in tension (behaviour occurred in liner

tray wall cladding systems subjected to wind pressure) according to the EN 1993-1-3 [131] provisions (as presented in Figure 2.20). The steps are the following:

- Step 1: The centroid of the cross section is found
- Step 2: The effective width of the wide flange $b_{u,eff}$ allowing for possible flange curling is obtained from:

$$b_{u,eff} = \frac{53.3 \cdot 10^{10} \cdot e_0^2 \cdot t^3 \cdot t_{eq}}{h \cdot L \cdot b_u^3} \tag{2.3}$$

where:

$e_0$: -the distance from the centroidal axis of the gross cross-section to the centroidal axis of the narrow flanges

t: -thickness of the wide web

$t_{eq}$: -the equivalent thickness of the wide flange - see eq. (2.4)

h: -the overall depth of the liner tray

L: -the span of the liner tray

$b_u$: -the overall width of the wide flange

$$t_{eq} = (\frac{12 \cdot I_a}{b_u})^{\frac{1}{3}} \tag{2.4}$$

where:

$I_a$: -the second moment of area of the wide flange, about its centroid

- Step 3: The effective areas of all compression elements of the cross section are determined based on values of the stress ratio $\psi = \sigma_2 / \sigma_1$ obtained using the effective widths of the compressed part in flanges but the gross areas of the webs
- Step 4: The centroid of the effective cross section is located, and after that, the buckling resistance moment $M_{b,Rd}$ is obtained from:

$$M_{b,Rd} = \frac{0.8 \cdot \beta_b \cdot W_{eff,min} \cdot f_{y,b}}{\gamma_{M0}} \tag{2.5}$$

where:

$\beta_b$: -the correlation factor; $\beta_b$= 1.0 for $s_1 \leq 300$ mm and $\beta_b$= 1.15-$s_1$/2000 for 300 mm ≤ $s_1$ ≤ 1000 mm where $s_1$ is the longitudinal spacing of fasteners supplying lateral restraint to the narrow flanges

and,

$$W_{eff,min} = \min (\frac{I_{y,eff}}{z_c}, \frac{I_{y,eff}}{z_t}) \tag{2.6}$$

where:

$I_{y,eff}$: -the effective second moment of area of the effective cross-section of a liner tray with the wide flange in tension, about the y-y axis

$z_c$: -the distance from the effective centroidal axis to the system line of the narrow flange under compression (see Figure 2.20)

$z_t$: -the distance from the effective centroidal axis to the system line of the wide flange in tension (see Figure 2.20)

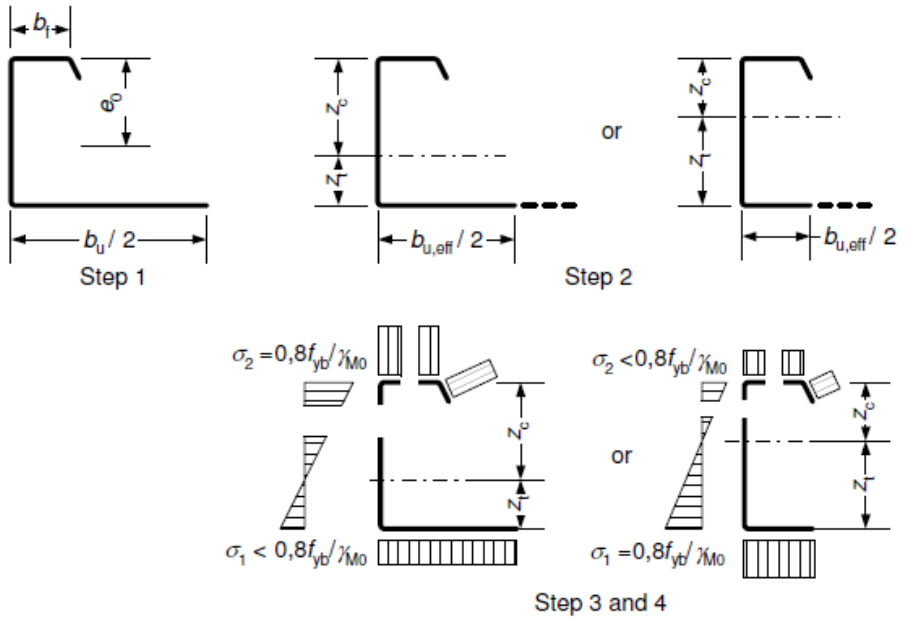


Figure 2.20 Determination of the moment resistance of a liner tray with its wide flange in tension according to EN 1993-1-3:2006 [131]

As shown in the step-by-step procedure, the EN 1993-1-3 standard provides for the calculation of the bending moment of liner trays with narrow flanges under compression (wide flange in tension), a fixing distance $s_1$ only up to 1000 mm ($s_1$ is the longitudinal spacing of fasteners supplying lateral restraint to the narrow flanges – see Figure 2.17-left). For distances larger than 1000 mm, the EN 1993-1-3 standard does not provide a procedure for the calculation of the moment resistance of a liner tray. According to [144], a calculation method that improves the coefficient $\beta_b$ (the influence of $s_1$) and extends the application range of this coefficient for distances greater than 1000 mm was established, but the calculation model has not yet been transferred to the European Codification.

The shear lag effects do not need to be considered if $L/b_{u,eff} \geq 25$. Otherwise, a reduced value of ρ should be determined according to [131].

### 2.4.1.1.2 Analytical developments

Extensive experimental studies have been conducted according to EN 1993-1-3:2010 on the load bearing capacity of liner trays within the range of the European

RFCS Research Project GRISPE (Guidelines and recommendations for Integrating Specific Profiled Steels sheets in the Eurocodes) and GRISPE PLUS (valorisation of Knowledge for Specific Profiled Steel Sheets) [145]. These investigations have led to the development of practical calculation approaches derived from existing methodologies and regulations. Regarding the liner trays, the purpose of the research was to develop a new method of design by calculation, the method being considered for inclusion in the Eurocodes [144]. Up to the moment of writing this thesis, EN 1993-1-3 was not yet updated, but the new calculation methods proposed in the research project were included in the FprEN 1993-1-3 as submitted to Formal Vote [146].

The experimental programme involving liner trays of the GRISPE project aimed to improve and broaden the design methodology outlined in Eurocode EN 1993-1-3. This enhancement focused particularly on improving the lateral stabilisation of the narrow flanges, whose stability is determined by the coefficient $\beta_b$, which is influenced by the spacing of the fastenings or spacers in the outward cladding (referred to as $s_1$). The results of the research study presented that the impact of the fixing distance $s_1$ on the bending moment is consistent across different sheet thicknesses. However, the height of the liner tray emerged as a more significant factor in the results presented within the project. In instances where higher liner trays were used, the reduction in the bending moment with increasing fixing distance was more pronounced. On the basis of these findings, a design method resulted which relies on establishing the buckling load for the compressed flange of the liner tray. The fixed points within this system are represented by the spacers, while the lateral buckling of the flange was evaluated using the Mandell formula by treating the beam as having a horizontal lateral spring, thus deriving a new expression for the coefficient $\beta_b$. This expresion is rooted in the ratio between the reference buckling load calculated for $s_1$ within the range specified by EN 1993-1-3 and the scenario where $s_1 > 1$m for the specific case under consideration [143]. For the purpose of optimising the computation, the effective cross-sectional area of the compressed flange is determined by iterative steps. This involves recalculating the critical buckling stress by successive iterations. To facilitate these computations using the mechanical and geometrical attributes of the compressed flange, an Excel software tool was developed as an outcome of the research project.

#### 2.4.1.1.3 Experimental investigations of liner trays subjected to bending moment

Alternatively to the design procedures for structural liner trays prescribed by EN 1993-1-3, the moment resistance of a liner trays can be determined by testing, as long as precautions are taken to ensure that the testing equipment does not influence the local behaviour of the liner trays, as outlined in Annex A of EN 1993-1-3:2006 [131]. Several research studies [130], [142], [147], [148], [149], [150] were conducted on the behaviour of structural liner trays under wind loads determined by experimental and numerical investigations. However, these investigations were conducted by apllying steel or timber cross beams arranged in such a way as to approximate uniformly distributed loading and the dynamic effect of the wind load

could not be reviewed. In [130], Georgescu et al. presented an experimental arrangement to simulate the behaviour to wind loads of the liner tray, consisting of an assembly of three adjacent liner trays. The authors concluded that certain crucial elements within the analysed experimental arrangement, particularly the fastening components, play a vital role in defining and establishing accurate boundary conditions within the experimental setup. This precision is necessary to effectively simulate real-world conditions with the required level of accuracy, emphasising that evaluation of the variation in wind pressure or suction around buildings perimeter, which depends on the wind direction, clearly illustrates the dual scenario for each liner tray: either subjected to pressure or exposed to suction forces. In [149] Georgescu et al. confirmed the conservative nature of the current code model by conducting experimental research and numerical analysis on the strength of liner trays subjected to wind loads on building cladding. Voutay studied in [151] the behaviour of wide flanges in compression with and without intermediate stiffeners. He concluded that when intermediate stiffeners are introduced in the wide flange of the liner trays, the ultimate load capacity is significantly increased but in the same time the number of buckling modes is also increased, leading to a more complex behaviour of liner trays and leading to interactive buckling between the modes. In [152], Wiegand conducted extensive research on the influence of changed wind load assumptions on liner tray wall systems and on the influence of the stiffening of liner trays using sandwich panels to determine to what extent an outer shell made of a sandwich panel can provide stability to the narrow flanges of the liner trays against lateral deflection. Georgescu et al. showed in [147] and [148] that when trying to assess the resistance of liner trays through experimental investigations, precise constructional details become a significant factor, introducing rather intricate challenges in establishing an experiment that faithfully replicates real-world conditions. Therefore, testing a single-liner tray requires the accurate emulation of genuine boundary conditions.

#### *2.4.1.2 Novelty of Testing Liner Trays to Wind Actions in a Vacuum Chamber*

The interaction between building components and wind loads is a critical consideration in structural engineering. Liner trays play a significant role in the external cladding of modern buildings, contributing both to aesthetics and structural integrity. However, the behaviour of liner trays under wind actions remains a complex and evolving field of study. This thesis aims to explore the novelty and importance of testing liner trays to wind action within a vacuum chamber, providing insight into the potential benefits and advancements that such an approach offers.

Liner trays, as lightweight cladding components, have gained popularity due to their ease of installation, cost-effectiveness, and versatility in architectural design. However, the effects of wind actions on liner trays have traditionally been studied through mechanical tests (by steel or timber cross beams arranged to approximate uniformly distributed loading) computational simulations, and field observations. This thesis proposes an approach to studying the wind behaviour of liner trays by conducting tests within a vacuum chamber. This novel approach is conducted for the first time in Romania within the research body. The vacuum chamber offers a

controlled environment that eliminates the influence of external factors such as air density variations and interference from nearby structures. This controlled setting provides a unique opportunity to isolate the wind-induced forces and vibrations acting on the liner trays, allowing for more accurate and focused observations.

Historically, research on wind effects in construction has focused on full-scale building tests, wind tunnel experiments, and computational simulations of fluid dynamics. These methods, while valuable, have limitations in replicating the real-world behaviour of cladding components under wind actions. Wind tunnel tests, for example, are subject to scale effects and boundary conditions that may not accurately represent the complexities of actual buildings. The vacuum chamber approach builds on these traditional methods by creating a controlled environment in which the air pressure can be adjusted to simulate different wind scenarios. This approach has been successfully employed in aerospace and automotive engineering to study aerodynamics and structural responses, and its application to the field of construction offers a new dimension of investigation.

The utilisation of a vacuum chamber for testing liner trays to wind action offers several notable benefits:

- Isolation of Wind Effects: by removing the influence of air density variations and other atmospheric factors, the vacuum chamber enables a more accurate study of the pure wind-induced effects on the liner trays
- Controlled Testing Conditions: the ability to control wind speeds, pressure differentials, and other parameters allows for systematic and repeatable experiments that can be precisely tailored to specific scenarios
- Reduction of External Factors: vacuum chamber testing eliminates the impact of neighbouring structures, terrain effects, and turbulence, which can complicate wind tunnel tests conducted in open environments
- Innovation and Advancement: the vacuum chamber approach introduces a novel methodology to the field of construction engineering, potentially leading to innovative design solutions and a deeper understanding of cladding system behavior.

## 2.5 Concluding remarks

In a time marked by environmental considerations and limited resources, the construction sector is compelled to transition to sustainable approaches, as it is a major contributor to the environmental impact. Over the past five years, approximately 40% of countries around the world have introduced building energy codes. These codes have been implemented either as mandatory standards for specific segments of building stock or within a voluntary framework. In July 2023, at the european level it was addopted a package of legislative proposals named Fit for 55 which aims to diminish the EU's greenhouse gas emissions by at least 55% by 2030 compared to 1990 levels. The legislative package includes new and revised directives, such as the Emission Trading System, Renewable Energy Directive, Energy

Efficiency Directive, or Waste Framework Directive, with a direct impact in the construction sector.

Due to the fact that a significant share of the world's energy consumption is attributed to commercial and residential buildings, and with the European Union adopting energy-saving regulations and actively pursuing its goals of reducing greenhouse gas emissions, the importance of building envelopes and façade systems has grown. Technological advances and the wide range of materials have led to a wide spectrum of façade systems. From the sustainable perspective, steel-intensive façade systems represent a valuable solution with respect to energy-efficiency performance, embodied energy of building materials, reuse, and recycling high potential.

In recent decades, steel-intensive façade systems have attracted increasing interest in the construction sector, particularly in retail, commercial, and educational buildings. Liner tray cladding systems are especially valued due to distinct benefits they offer, such as enhanced load-bearing capacity and stability, speed of installation, reduced maintenance, aesthetic versatility, cost efficiency, and sustainability.

For structural liner trays with a single span, the bending moment that causes sagging is typically the most critical in design, while vertical shear forces and lateral forces on supports may be, in most cases, ignored. The bending moment resistance becomes particularly critical, especially when the structure is subjected to significant wind loads. Liner trays tested to wind loads in a more natural way of loading but in fully controlled testing conditions should be conducted in order to have a deeper understanding of cladding system behaviour. In this context, the study of liner trays cladding system subjected to wind loads through a vacuum chamber is worthwhile, contributing to a higher comprehension of the dynamic effect of wind loads on these envelope solutions.

The use of a vacuum chamber to study the wind behaviour of the liner trays presents a novel and innovative approach that has the potential to revolutionise the field of construction engineering. By providing a controlled environment, this approach allows a deeper understanding of the dynamic interactions between the wind and the cladding components. The benefits of accurate data collection, isolation of wind effects, and innovative design insights make vacuum chamber testing a promising avenue for advancing the science of wind-resistant building envelopes.

As research and experimentation in this area continues to evolve, vacuum chamber testing may become standard practise in the evaluation and design of liner trays and other cladding components. This advancement could lead to more resilient and reliable building façades that can withstand the challenges posed by dynamic wind actions.

# 3 Experimental investigation of liner trays subjected to wind loads

The experimental program consists of the empirical study of multiple liner trays, subjected to bending resulting from wind pressure and wind suction.

## 3.1 Introduction

Liner trays are subjected to three primary load combinations: axial load, shear and bending [134], [153]. The axial compression occurs from the storeys above, the shear emerge from wind-induced diaphragm action, while the bending about the minor axis develops from wind pressure or suction [134]. In the experimental program presented in this work, the liner trays subjected to bending due to wind pressure and suction were studied, through the medium of a vacuum chamber.

According to the EN 1993-1-3 standard [131], the design of a liner tray subjected to bending due to wind pressure (in which the wide flange is in tension and the narrow flanges are under compression) should consider the flange curling of the wide flange which is under tension, the local buckling of the web and narrow flanges, the distortional buckling of the narrow flanges along with the edge stiffener assemblies, and the effects of shear lag. Further, the design of a liner tray subjected to bending due to wind suction (in which the wide flange is under compression and the narrow flanges are in tension) should consider the local buckling of the wide flange (the narrow flange and edge stiffener assemblies are in tension and do not buckle). No specifications are mentioned in the standard for the influence of the wide flange curling subjected to local buckling and compression.

The experimental program was carried out on nine liner tray specimens supplied by a European provider acting on the Romanian market [154]. A typical liner tray section has one wide flange ($b_u$) with intermediate stiffeners ($h_{u1}$) two narrow flanges ($b_{f1}$, $b_{f2}$), two webs ($h_1$, $h_2$) with intermediate stiffeners ($h_{u2}$), and two edge stiffeners (c). Figure 3.1 shows the typical cross-section geometry of the liner trays used in this experimental program.

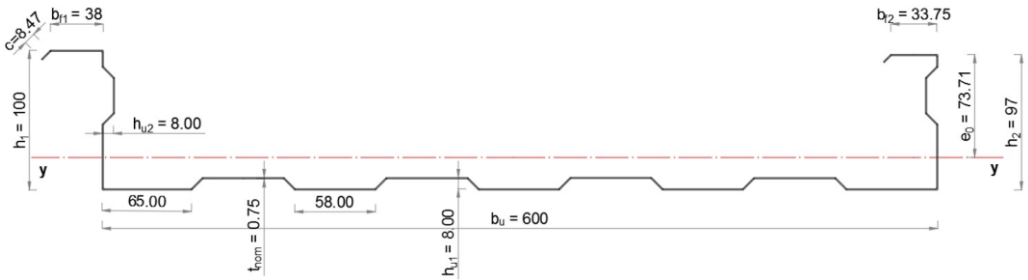


Figure 3.1 Geometry of the liner tray used in the experimental program

## 3.2 Geometric Characteristics of Liner Trays

### 3.2.1 Determination of the moment resistance of a liner tray according to the European Standard EN 1993-1-3:2007

The statical scheme of the liner trays studied in the experimental program represents a simply supported beam (one span of 4000 mm – see Figure 3.2). For the determination of the moment resistance of the liner tray according to the European Standard EN 1993-1-3-2007, the analytical calculations were performed with the use of Mathcad 14.0 [155], while the AutoCAD software [156] was used to calculate the effective section properties of the element.

The underlying principle of the method considers that the wide flange, without stiffeners, doesn't fully contribute to bending effectiveness, whether it's under tension or compression, therefore, the section is analyzed considering only the effective flange instead of the complete wide flange. At the same time, the effective area of the narrow flanges, stiffeners and webs must be determined when these elements are in compression. The estimation of this effective part of the elements depends on the stress sign.

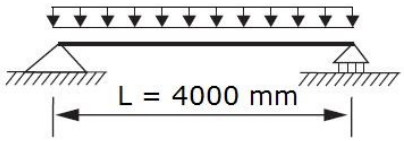


Figure 3.2 Statical scheme of the liner trays

#### *3.2.1.1 Determination of the design thickness of the liner tray*

According to [131], equation (3.3c), the thickness of the liner tray considered for the calculations is:

$$t = t_{cor} = t_{nom} - t_{metallic\ coating} = 0.75 - 0.04 = 0.71\ mm, \tag{3.1}$$

where:

t: – the steel thickness

$t_{cor}$: – the steel core thickness without metallic coating

$t_{nom}$: – the nominal steel sheet thickness after cold forming, including the mettalic coating; tnom = 0.75 mm

$t_{metallic\ coating}$: – the thickness of the metallic coating; for the zinc coating used for the liner trays, Z275, $t_{metallic\ coating}$ = 0.04 mm

#### *3.2.1.2 Verification of the validity of the calculation procedure according to Eurocode 3 - Part 1.3.*

The guidelines provided in SR-EN 1993-1-3 can be applied for cross sections that fall within specific dimensions range. Table 10.6 in [131] specifies a range of

validity for geometrical characteristics of the liner trays in order to determine the moment resistance, $M_{c,Rd}$, of the liner trays using the procedure described in section 10.2.2. Aside from these geometrical characteristics, the condition also requires that the depth of the corrugation of the wide flange, $h_{u1}$, does not exceed h/8 (where h represents the overall depth of the liner tray). Table 3.1 shows the dimensions and the geometric configuration of the liner trays used in the experimental program in comparison with the range of validity specified by the EN 1993-1-3.

Table 3.1 Dimensions and geometric proportions of elements of the cross-section of the liner tray

| Dimensions and geometric proportions of elements of cross-section (see Figure 3.1) | Range of validity as in Tab. 10.6 in [131] |
|---|---|
| $t_{nom}$ = 0.75 mm | 0.75mm ≤ $t_{nom}$ ≤ 1.5mm |
| $b_{f1}$ = 38 mm | 30 mm ≤ $b_f$ ≤ 60 mm |
| $b_{f2}$ = 33.75 mm | 30 mm ≤ $b_f$ ≤ 60 mm |
| $h_1$ = 100 mm | 60 mm ≤ h ≤ 200 mm |
| $h_2$ = 97 mm | 60 mm ≤ h ≤ 200 mm |
| $b_u$ = 600 mm | 300 mm ≤ $b_u$ ≤ 600 mm |
| $I_a$/ $b_u$ = 6443 mm$^4$ / 600 mm<br>$I_a$/ $b_u$ = 10.73 mm$^4$ / mm (see Figure 3.3) | $I_a$/ $b_u$ ≤ 10 mm$^4$ / mm |
| $s_1$ = 500 mm | $s_1$ ≤ 1000 mm |
| $h_{U1}$ = 8 mm | $h_1$ / 8 = 100 mm/8 =12.5 mm<br>$h_2$ / 8 = 97 mm/8 =12.12 mm |

where:

$I_a$: - the second moment of area of the wide flange, about its centroid (determined with the use of AutoCAD [156]); $I_a$ = 6443 mm$^4$

$s_1$: - the longitudinal spacing of fasteners in the narrow flanges

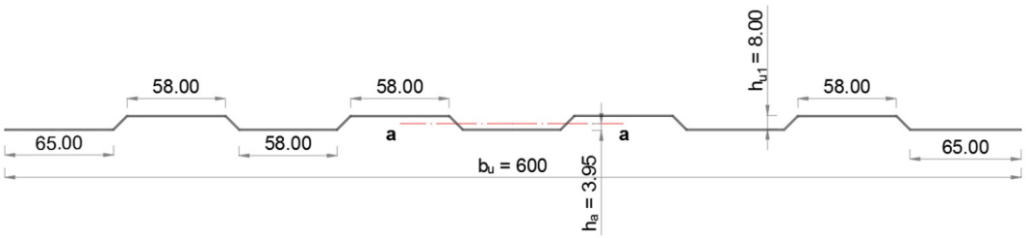


Figure 3.3 Geometry of the wide flange of the liner tray

To ensure adequate stiffness and prevent the primary buckling of the stiffener itself, EN 1993-1-3 [131] require the dimensions of the stiffener to be constrained within the range shown in Table 3.2:

Table 3.2 Ratios of the stiffeners' sizes

| Element of cross-section | Geometric proportions (see Figure 3.1) | Sizes of stiffeners as in eq. (5.2a) in [131] |
|---|---|---|
| edge stiffener, $c_1$ | $c_1 / b_{f1}$ = 8.78 mm / 38 mm<br>$c_1 / b_{f1}$ = 0.231 | 0.2 <c/b < 0.6 |
| edge stiffener, $c_2$ | $c_2 / b_{f2}$ = 8.62 mm/33.75 mm<br>$c_2 / b_{f2}$ = 0.255 | 0.2 <c/b < 0.6 |

### *3.2.1.3 Determination of the effective characteristics of the liner tray cross-section in the case of a wide flange under compression*

#### 3.2.1.3.1 Determination of the effective width $b_{eff}$ of the wide flange under compression

According to paragraph 4.4(2) in [157], the relative slenderness, $\overline{\lambda_p}$, is computed by:

$$\overline{\lambda_p} = \frac{\overline{b}/t}{28.4 \cdot \varepsilon \cdot \sqrt{k_\sigma}} = \frac{598.5/0.71}{28.4 \cdot 0.7308 \cdot \sqrt{4}} = 20.31, \tag{3.2}$$

where:

$\overline{b}$: $\overline{b} = b_{pu}$ = 598.5 mm (see Figure 3.4)

t: -thickness of the wide flange; t = 0.71 mm (see eq. (3.1))

$k_\sigma$: -the buckling factor corresponding to the stress ratio ψ and boundary conditions; $k_\sigma$=4 (Tabel 4.1 in [157], as for uniform compression in the flange)

$$\varepsilon = \sqrt{\frac{235}{f_{yb}}} = \sqrt{\frac{235}{441.2}} = 0.7298, \tag{3.3}$$

where:

$f_{y,b}$: $f_{y,b}$= 441.2 N/mm$^2$ (according to tensile tests of the material – see sect. 3.5.1)

The relative slenderness, $\overline{\lambda_p}$ >0.673, therefore the reduction factor, ρ, of effective width according to (4.2) in [157] is:

$$\rho = \frac{\overline{\lambda_p} - 0.055 \cdot (3+\psi)}{\overline{\lambda_p}^2} = \frac{20.31 - 0.055 \cdot (3+1)}{20.31^2} = 0.0487 \leq 1.0, \tag{3.4}$$

where:

ψ: -the stress ratio determined in accordance with 4.4(3) from [8]

ψ = 1 (the entire wide flange is subjected to compression, therefore ψ = $\sigma_2/\sigma_1$ = 1)

$$\overline{\lambda_p} = 20.31 > 0.5+\sqrt{0.085 - 0.055\psi} = 0.5+\sqrt{0.085 - 0.055 \cdot 1.0} = 0.6732 \quad (3.5)$$

The effective width, $b_{u,eff}$ of the wide flange, $b_u$ may be determined according to Table 4.1 in [157] as:

$$b_{u,eff} = \rho \cdot \overline{b} = 0.0487 \cdot 598.5 = 29.15 \text{ mm} \quad (3.6)$$

where:

$\overline{b}$: $\overline{b} = b_{pu} = 598.5$ mm (see Figure 3.4)

ρ: $\rho = 0.0487$ (see eq. (3.4))

The effective widths, $b_{e1}$ and $b_{e2}$, shown in Figure 3.4 were determined according to Table 4.1 in [157]:

$$b_{e1} = b_{e2} = 0.5 \cdot b_{u,eff} = 0.5 \cdot 29.15 = 14.57 \text{ mm} \quad (3.7)$$

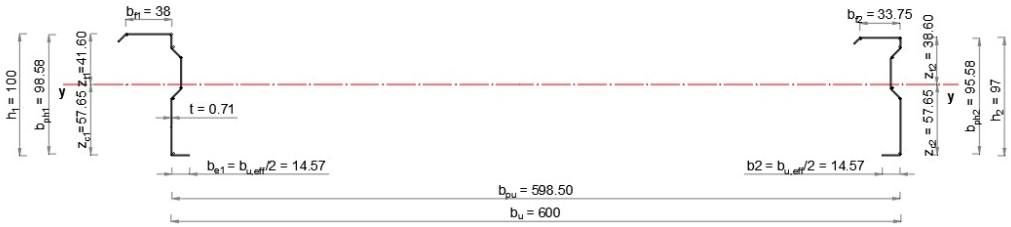


Figure 3.4 Effective cross-section of the wide flange under compression and the entire cross sections of the webs

### 3.2.1.3.2 Determination of the effective width $h_{eff}$ of the webs under bending

For web $h_1$:

According to 4.4(2), eq. (4.2) in [157], the relative slenderness, $\overline{\lambda_p}$, is:

$$\overline{\lambda_p} = \frac{\overline{b}/t}{28.4 \cdot \varepsilon \cdot \sqrt{k_\sigma}} = \frac{98.58/0.71}{28.4 \cdot 0.7298 \cdot \sqrt{17.44}} = 1.601, \quad (3.8)$$

where:

$\overline{b}$: $\overline{b} = b_{ph1} = 98.58$ mm (see Figure 3.4)

t: -thickness of the wide web; t = 0.71 mm (see eq. (3.1))

$k_\sigma$: -the buckling factor for web_1 corresponding to the stress ratio ψ and boundary conditions, according to (Tabel 4.1 in [157]); $k_\sigma$=17.44 (see eq. (3.3))

ε: ε = 0.7298 mm (see eq. (3.3))

As, -1<ψ<0 (see eq. (3.10), according to Tabel 4.1 in [157], $k_\sigma$ may be determined as follows:

$$k_\sigma = 7.81 - 6.29 \cdot \psi + 9.78 \cdot \psi^2 = 7.81 - 6.29 \cdot (-0.721) + 9.78 \cdot (-0.721)^2 = 17.44 \quad (3.9)$$

where:

ψ: -the stress ratio; ψ = -0.7216 (see eq.(3.10))

$$\psi = \frac{\sigma_2}{\sigma_1} = \frac{z_{t1}}{z_{c1}} = -\frac{41.60}{57.65} = -0.721 \quad (3.10)$$

The relative slenderness, $\overline{\lambda_p}$ >0.673, therefore the reduction factor, ρ, of effective width according to (4.2) in [157] is:

$$\rho = \frac{\overline{\lambda_p} - 0.055 \cdot (3+\psi)}{\overline{\lambda_p}^2} = \frac{1.60 - 0.055 \cdot (3 - 0.721)}{1.60^2} = 0.575 \leq 1.0, \quad (3.11)$$

The effective width of the web with $h_1$ = 100 mm, $h_{eff,1}$, shown in Figure 3.5 were determined according to Table 4.1 in [157]:

$$h_{eff,1} = \rho \cdot b_{c,1} = 0.575 \cdot 57.65 = 33.17 \text{ mm} \quad (3.12)$$

where:

$b$: $b = b_{c,1} = z_{c,1}$ = 57.65 mm (see Figure 3.4)

ρ: $\rho$= 0.5754 (see eq.(3.11))

The values of the effective widths of the web with $h_1$ = 100 mm, $h_{e1}$ and $h_{e2}$, shown in Figure 3.5 were determined, according to Table 4.1 in [157], as follows:

$$h_{e1} = 0.4 \cdot h_{eff,1} = 0.4 \cdot 33.17 = 13.26 \text{ mm} \quad (3.13)$$

$$h_{e2} = 0.6 \cdot h_{eff,1} = 0.6 \cdot 33.17 = 19.90 \text{ mm} \quad (3.14)$$

For web $h_2$:

According to 4.4(2), eq. (4.2) in [157], the relative slenderness, $\overline{\lambda_p}$, is:

$$\overline{\lambda_p} = \frac{\overline{b}/_t}{28.4\cdot\varepsilon\cdot\sqrt{k_\sigma}} = \frac{95.58/_{0.71}}{28.4\cdot 0.7298\cdot\sqrt{16.40}} = 1.601, \quad (3.15)$$

where:

$\overline{b}$: $\overline{b}$ = $b_{ph2}$ = 95.58 mm (see Figure 3.4)

t: -thickness of the wide web; t = 0.71 mm (see eq. (3.1))

$k_\sigma$: -the buckling factor for web_2 corresponding to the stress ratio ψ and boundary conditions, according to (Tabel 4.1 in [157]); $k_\sigma$=16.40 (see eq. (3.16))

ε: ε = 0.7298 mm (see eq. (3.3))

As, -1<ψ<0 (see eq. (3.17), according to Tabel 4.1 in [157], $k_\sigma$ may be determined as follows:

$$k_\sigma = 7.81 - 6.29\cdot\psi + 9.78\cdot\psi^2 = 7.81 - 6.29\cdot(-0.669) + 9.78\cdot(-0.669)^2 = 16.40 \quad (3.16)$$

where:

ψ: -the stress ratio; ψ = -0.6696 (see eq.(3.17))

$$\psi = \frac{\sigma_2}{\sigma_1} = \frac{z_{t2}}{z_{c2}} = -\frac{38.60}{57.65} = -0.6696 \quad (3.17)$$

The relative slenderness, $\overline{\lambda_p}$=1.6013 >0.673, therefore the reduction factor, ρ, of effective width according to (4.2) in [157] is:

$$\rho = \frac{\overline{\lambda_p} - 0.055\cdot(3+\psi)}{\overline{\lambda_p}^2} = \frac{1.60 - 0.055\cdot(3-0.669)}{1.60^2} = 0.574 \le 1.0, \quad (3.18)$$

The effective width of the web with $h_2$ = 97 mm, $h_{eff,2}$, shown in Figure 3.5 were determined according to Table 4.1 in [157]:

$$h_{eff,2} = \rho\cdot b_{c,2} = 0.574\cdot 57.65 = 33.11 \text{ mm} \quad (3.19)$$

where:

$b$: $b$ = $b_{c,2}$ = 57.65 mm (see Figure 3.4)

ρ: $\rho$= 0.574 (see eq.(3.18))

The values of the effective widths of the web with $h_2$ = 97 mm, $h_{e1}$ and $h_{e2}$, shown in Figure 3.5 were determined, according to Table 4.1 in [157], as follows:

$$h_{e1} = 0.4\cdot h_{eff,2} = 0.4\cdot 33.11 = 13.24 \text{ mm} \quad (3.20)$$

$$h_{e2} = 0.6 \cdot h_{eff,2} = 0.6 \cdot 33.11 = 19.87 \text{ mm} \tag{3.21}$$

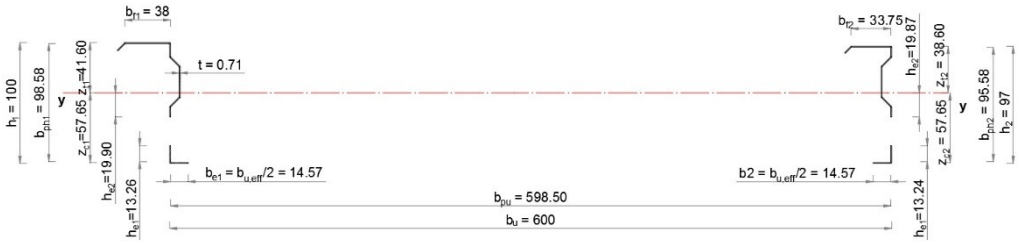


Figure 3.5 Effective cross-section of a 600/100 liner tray with the wide flange under compression

3.2.1.3.3 The effects of shear lag

According to EN 1993-1-3 section 10.2.2.2 (2) in [131], the effects of shear lag may be neglected here because,

$$\rho = \frac{L}{b_{u,eff}} = \frac{4000}{29.15} = 137.20 > 25, \tag{3.22}$$

where:

$L$: -the length of the liner tray; $L$ = 4000 mm

$b_{u,eff}$: -the effective width of the wide flange under compression; (see eq. (3.6))

### *3.2.1.4 Determination of the moment resistance of a liner tray cross-section with its wide flange under compression*

According to art. 10.2.2.1 in [131], the moment resistance $M_{c,Rd}$ of liner trays with wide flange in compression may be obtained as follows:

$$M_{c,Rd} = \frac{0.8 \cdot W_{eff,min} \cdot f_{y,b}}{\gamma_{M0}} = \frac{0.8 \cdot 4335.09 \cdot 441.2}{1.00} = 1.53 \text{ kNm}, \tag{3.23}$$

where:

$W_{eff,min}$: $W_{eff,min}$= 4335.09 mm$^3$ (see eq. (3.24));

$f_{y,b}$: $f_{y,b}$= 441.2 N/mm$^2$ (according to tensile tests of the material – see sect. 3.5.1)

$\gamma_{M0}$: $\gamma_{M0}$ = 1.00 (art. 2.(3) in [131]).

$$W_{eff,min} = \min\left(\frac{I_{y,eff}}{z_c}, \frac{I_{y,eff}}{z_t}\right) = \min\left(\frac{249918}{57.65}, \frac{249918}{41.60}\right) = 4335.09 \text{ mm}^3, \tag{3.24}$$

where:

$I_{y,eff}$: -the effective second moment of area of the effective cross-section of a 600/100 liner tray with the wide flange under compression (see Figure 3.5) about the y-y axis
$I_{y,eff}$ = 249918.15 mm$^4$ (calculated on the effective cross-section by the use of the AutoCAD tool [156])

$z_c$: -the distance from the effective centroidal axis to the system line of the compression wide flange (see Figure 3.4)
$z_c$ = max($z_{c1}$, $z_{c2}$) = 57.65 mm

$z_t$: -the distance from the effective centroidal axis to the system line of the narrow flange in tension (see Figure 3.4)
$z_t$ = max($z_{t1}$, $z_{t2}$) = max(41.60, 38.60) = 41.60 mm

### *3.2.1.5 Determination of the effective characteristics of the liner tray cross-section in the case of a wide flange under tension*

In the case of liner trays with the wide flange under tension (liner trays subjected to wind pressure), the maximum positive bending moment is typically restricted by the ultimate compression forces of the small flanges. In general, to prevent lateral buckling, the compressed flanges are stabilized through connections between the liner tray and outer cladding. The buckling length of the compressed flange, and consequently the ultimate compression forces of the small flanges, are determined by the fixing distance, denoted as $s_1$. As a result, the ultimate bending moment can be considered roughly proportional to the compression resistance of the small flanges [144].

#### 3.2.1.5.1 Determination of the effective width $b_{eff}$ of the wide flange under tension

According to 10.2.2.2 (1), eq. (10.20) in [131], the effective width of the wide flange under tension, $b_{u,eff}$, allowing for possible flange curling, is:

$$b_{u,eff} = \frac{53.3\cdot10^{10}\cdot e_0^2\cdot t^3\cdot t_{eq}}{h\cdot L\cdot b_u^3} = \frac{53.3\cdot10^{10}\cdot 72.60^2\cdot 0.71^3\cdot 5.05}{100\cdot 4000\cdot 600^3} = 58.78 \text{ mm}, \quad (3.25)$$

where:

$e_0$: -the distance from the centroidal axis of the gross cross-section to the centroidal axis of the narrow flanges
$e_0$:= 72.60 mm (see Figure 3.1)

t: -thickness of the wide web; t = 0.71 mm (see eq. (3.1))

$t_{eq}$: -the equivalent thickness of the wide flange, $t_{eq}$=5.05 mm (see eq. (3.26))

h: -the overall depth of the liner tray; h = 100 mm (see Figure 3.1);

L: -the span of the liner tray; L = 4000 mm

$b_u$: -the overall width of the wide flange; $b_u$ = 600 mm (see Figure 3.1)

$$t_{eq} = (\frac{12 \cdot I_a}{b_u})^{\frac{1}{3}} = (\frac{12 \cdot 6443}{600})^{\frac{1}{3}} = 5.05 \text{ mm}, \tag{3.26}$$

where:

$I_a$: -the second moment of area of the wide flange, about its centroid (determined with the use of AutoCAD [156]); $I_a$ = 6443 mm$^4$

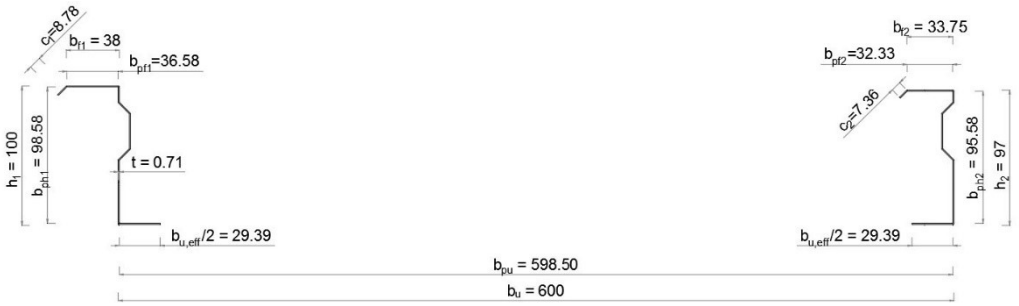


Figure 3.6 Effective width of the wide flange in tension of the liner tray

### 3.2.1.5.2 Determination of the effective width, $b_{eff}$, of the narrow flanges under compression

For the narrow flange, $b_{f1}$:

According to 4.4(2), eq. (4.2) in [157], the relative slenderness, $\overline{\lambda_p}$, is:

$$\overline{\lambda_p} = \frac{\overline{b}/t}{28.4 \cdot \varepsilon \cdot \sqrt{k_\sigma}} = \frac{36.58/0.71}{28.4 \cdot 0.7298 \cdot \sqrt{4}} = 1.24 > 0.673, \tag{3.27}$$

where:

$\overline{b}$: $\overline{b}$ = $b_{pf1}$ = 36.58 mm (see Figure 3.6)

t: -thickness of the narrow flange; t = 0.71 mm (see eq. (3.1))

$k_\sigma$: -the buckling factor for flange_1 corresponding to the stress ratio ψ and boundary conditions, according to Tabel 4.1 in [157]; $k_\sigma$=4 (uniform compression in the narrow flange)

ε: ε = 0.7298 mm (see eq. (3.3))

The relative slenderness, $\overline{\lambda_p}$ >0.673, therefore the reduction factor, ρ, of effective width according to (4.2) in [157] is:

$$\rho = \frac{\overline{\lambda_p} - 0.055 \cdot (3+\psi)}{\overline{\lambda_p}^2} = \frac{1.24 - 0.055 \cdot (3+1)}{1.24^2} = 0.6622 \leq 1.0, \tag{3.28}$$

where:

ψ: -the stress ratio determined in accordance with 4.4(3) from [8];

ψ = 1 (the entire narrow flange is subjected to compression, therefore ψ = $\sigma_2/\sigma_1$ = 1)

$$\overline{\lambda_p} = 1.24 > 0.5+\sqrt{0.085 - 0.055\psi} = 0.5+\sqrt{0.085 - 0.055 \cdot 1.0} = 0.6732 \quad (3.29)$$

The effective width, $b_{1,eff}$ of the narrow flange, $b_{f1}$ may be determined according to Table 4.1 in [157] as:

$$b_{1,eff} = \rho \cdot \overline{b} = 0.6622 \cdot 36.58 = 24.22 \text{ mm} \quad (3.30)$$

where:

$\overline{b}$: $\overline{b} = b_{pf1}$ = 36.58 mm (see Figure 3.6)

ρ: $\rho$= 0.6622 (see eq.(3.28))

The effective widths, $b_{1,e1}$ and $b_{1,e2}$, shown in Figure 3.8 were determined according to Table 4.1 in [157]:

$$b_{1,e1} = b_{1,e2} = 0.5 \cdot b_{1,eff} = 0.5 \cdot 24.22 = 12.11 \text{ mm} \quad (3.31)$$

For the narrow flange, $b_{f2}$:

According to 4.4(2), eq. (4.2) in [157], the relative slenderness, $\overline{\lambda_p}$, is:

$$\overline{\lambda_p} = \frac{\overline{b}/t}{28.4 \cdot \varepsilon \cdot \sqrt{k_\sigma}} = \frac{32.33/0.71}{28.4 \cdot 0.729 \cdot \sqrt{4}} = 1.098 > 0.673, \quad (3.32)$$

where:

$\overline{b}$: $\overline{b} = b_{pf2}$ = 32.33 mm (see Figure 3.6)

t: -thickness of the narrow flange; t = 0.71 mm (see eq. (3.1))

$k_\sigma$: -the buckling factor for flange_2 corresponding to the stress ratio ψ and boundary conditions, according to (Tabel 4.1 in [157]); $k_\sigma$=4 (uniform compression in the narrow flange)

ε: ε = 0.729 mm (see eq. (3.3))

The relative slenderness, $\overline{\lambda_p}$ >0.673, therefore the reduction factor, ρ, of effective width according to (4.2) in [157] is:

$$\rho = \frac{\overline{\lambda_p} - 0.055 \cdot (3+\psi)}{\overline{\lambda_p}^2} = \frac{1.098 - 0.055 \cdot (3+1)}{1.098^2} = 0.728 \leq 1.0, \quad (3.33)$$

where:

ψ: -the stress ratio determined in accordance with 4.4(3) from [8];

ψ = 1 (the entire narrow flange is subjected to compression, therefore ψ = $\sigma_2/\sigma_1$ = 1)

$$\overline{\lambda_p} = 1.098 > 0.5+\sqrt{0.085 - 0.055\psi} = 0.5+\sqrt{0.085 - 0.055 \cdot 1.0} = 0.6732 \quad (3.34)$$

The effective width, $b_{2,eff}$ of the narrow flange, $b_{f2}$ may be determined according to Table 4.1 in [157] as:

$$b_{2,eff} = \rho \cdot \overline{b} = 0.728 \cdot 32.33 = 23.53 \text{ mm} \quad (3.35)$$

where:

$\overline{b}$: $\overline{b} = b_{pf2} = 32.33$ mm (see Figure 3.6)

ρ: $\rho = 0.728$ (see eq. (3.33))

The effective widths, $b_{2,e1}$ and $b_{2,e2}$, shown in Figure 3.9, were determined according to Table 4.1 in [157]:

$$b_{2,e1} = b_{2,e2} = 0.5 \cdot b_{2,eff} = 0.5 \cdot 23.53 = 11.76 \text{ mm} \quad (3.36)$$

### 3.2.1.5.3 Determination of the effective width of the edge stiffener of the narrow flange under compression

When determining the cross-section of an edge stiffener of the narrow flange under compression, it should be considered to include the effective segments of the stiffener itself, represented by element c, as depicted in Figure 3.7, plus the adjacent effective portion of the plane element $b_p$ [131].

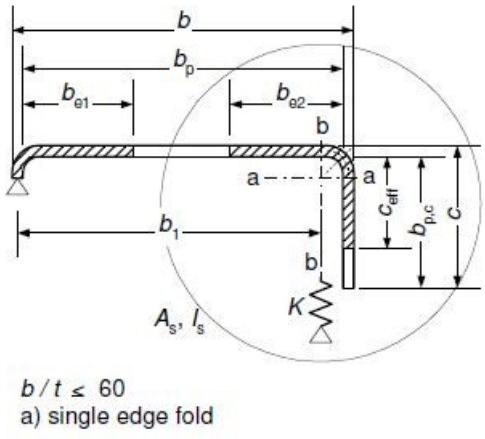


Figure 3.7 Edge stiffener widths [131]

After obtaining the initial effective cross-section for the stiffener using effective widths determined by assuming that the stiffener gives full restraint, the reduction factor for flexural buckling of the stiffener (distortional buckling) must be determined, allowing for the effects of the continuous spring restraint [131]. The standard EN 1993-1-3:2007 states that optionally, the reduction factor for buckling of the stiffener may be iterated to refine its value.

For the edge stiffener, $c_1$:

For a single-edge fold stiffener, the initial values of the effective width, $c_{eff}$, according to (5.13a) in [131] is:

$$c_{1,eff} = \rho \cdot b_{p,c1} = 0.921 \cdot 8.78 = 8.08 \text{ mm} \tag{3.37}$$

where:

$b_{p,c1}$: $b_{p,c1} = c_1 = 8.78$ mm (see Figure 3.6)

ρ: $\rho = 0.921$ (see eq. (3.40))

According to 4.4(2), eq. (4.3) in [157], the relative slenderness, $\overline{\lambda_p}$, is:

$$\overline{\lambda_p} = \frac{\overline{b}/t}{28.4 \cdot \varepsilon \cdot \sqrt{k_\sigma}} = \frac{8.47/0.71}{28.4 \cdot 0.729 \cdot \sqrt{0.5}} = 0.843 > 0.748, \tag{3.38}$$

where:

$\overline{b}$: $\overline{b} = b_{p,c1} = 8.78$ mm (see Figure 3.6)

t: -thickness of the stiffener; t = 0.71 mm (see eq. (3.1))

$k_\sigma$: -the local buckling factor for stiffener_1 according to eq. (5.13b) in [131]) and eq. (3.39); $k_\sigma = 0.5$

ε: ε = 0.729 mm (see eq. (3.3))

The local buckling factor for stiffener $c_1$:

$$\frac{b_{p,c}}{b_p} = \frac{8.78}{36.58} = 0.24 < 0.35, \text{ therefore, } k_\sigma = 0.5 \tag{3.39}$$

where:

$b_{p,c}$: $b_{p,c} = b_{p,c1} = 8.78$ mm (see Figure 3.6)

$b_p$: $b_{pf1} = 36.58$ mm (see Figure 3.6)

The relative slenderness, $\overline{\lambda_p} > 0.748$, therefore the reduction factor, ρ, of effective width according to (4.3) in [157] is:

$$\rho = \frac{\overline{\lambda_p} - 0.188}{\overline{\lambda_p}^2} = \frac{0.843 - 0.188}{0.843^2} = 0.9211 \leq 1.0, \tag{3.40}$$

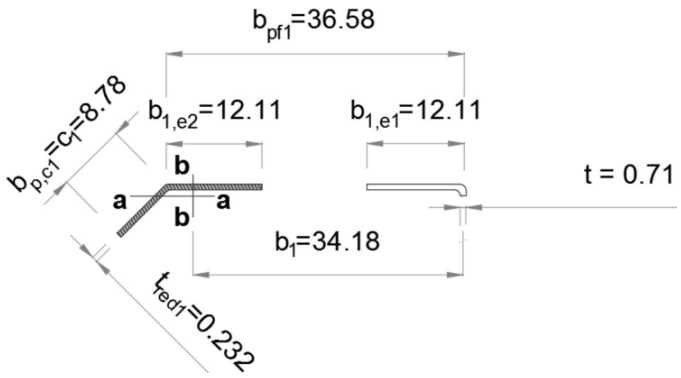


Figure 3.8 The edge stiffener of the compressed narrow flange $b_{f1}$ of the 600/100 liner tray

For the edge stiffener, $c_2$:

The analytical calculations for the edge stiffener, $c_2$, were performed in the same manner as for $c_1$: for a single edge fold stiffener, the initial values of the effective width, $c_{2,eff}$, according to (5.13a) in [131] is:

$$c_{2,eff} = \rho \cdot b_{p,c2} = 1 \cdot 7.36 = 7.36 \text{ mm} \tag{3.41}$$

where:

$b_{p,c2}$: $b_{p,c2} = c_2 = 7.36$ mm (see Figure 3.6)

ρ: $\rho = 1$ (see eq. (3.44))

According to 4.4(2), eq. (4.3) in [157], the relative slenderness, $\overline{\lambda_p}$, is:

$$\overline{\lambda_p} = \frac{\overline{b}/t}{28.4 \cdot \varepsilon \cdot \sqrt{k_\sigma}} = \frac{7.36/0.71}{28.4 \cdot 0.729 \cdot \sqrt{0.5}} = 0.707 < 0.748, \tag{3.42}$$

where:

$\overline{b}$: $\overline{b} = b_{p,c2} = 7.36$ mm (see Figure 3.6)

t: -thickness of the stiffener; t = 0.71 mm (see eq. (3.1))

$k_\sigma$: -the local buckling factor for stiffener_2 according to eq. (5.13b) in [131]) and eq. (3.39); $k_\sigma = 0.5$

ε: ε = 0.729 mm (see eq. (3.3))

The local buckling factor for stiffener $c_1$:

$$\frac{b_{p,c}}{b_p} = \frac{7.36}{32.33} = 0.227 < 0.35, \text{ therefore, } k_\sigma = 0.5 \tag{3.43}$$

where:

$b_{p,c}$: $b_{p,c} = b_{p,c2} = 7.36$ mm (see Figure 3.6)

$b_p$: $b_p = b_{pf2} = 32.33$ mm (see Figure 3.6)

The relative slenderness, $\overline{\lambda_p}$ < 0.748, therefore the reduction factor, ρ, of effective width according to (4.3) in [157] is:

$$\rho = 1 \tag{3.44}$$

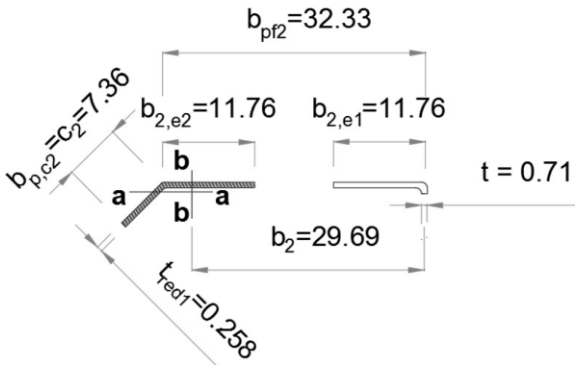


Figure 3.9 The edge stiffener of the compressed narrow flange $b_{f2}$ of the 600/100 liner tray

The effective cross-sectional area of the edge stiffeners was determined according to 5.5.3.2(6), eq. (5.14a) in [131] as follows:

$$A_{s1} = t(b_{1,e2} + c_{eff,1}) = 0.71 \cdot (12.11+8.08) = 14.33 \text{ mm}^2 \tag{3.45}$$

where:

t: -thickness of the stiffener; t = 0.71 mm (see eq. (3.1))

$b_{1,e2}$: $b_{1,e2}$ = 12.11 mm (see eq. (3.31))

$c_{1,eff}$ $c_{1,eff}$ = 8.08 mm (see eq.(3.37))

$$A_{s2} = t(b_{2,e2} + c_{eff,2}) = 0.71 \cdot (11.76+7.36) = 13.57 \text{ mm}^2 \tag{3.46}$$

where:

t: -thickness of the stiffener; t = 0.71 mm (see eq. (3.1))

$b_{2,e2}$: $b_{2,e2}$ = 11.76 mm (see eq. (3.36))

$c_{2,eff}$ $c_{2,eff}$ = 7.36 mm (see eq. (3.41))

The effective second moment of area of the stiffener, taken as that of its effective area $A_s$ about the centroidal axis a - a of its effective cross-section (see Figure 3.8 and Figure 3.9) was determined with the use of AutoCAD tool [156]:

$$I_{s1} = 38.7 \text{ mm}^4 \tag{3.47}$$

$$I_{s2} = 34.2 \text{ mm}^4 \tag{3.48}$$

The reduction factor, $\chi_d$, for the distortional buckling resistance of the stiffener of the narrow flange $b_{pf1}$ was obtained from the relative slenderness, $\overline{\lambda_d}$, according to 5.5.3.1(7) in [131] as follows:

$$\overline{\lambda_d} = \sqrt{\frac{f_{yb}}{\sigma_{cr,s1}}} = \sqrt{\frac{441.2}{109.03}} = 2.01, \tag{3.49}$$

where:

$\overline{\lambda_d}$: –the relative slenderness;

$f_{yb}$: -basic yield strength; $f_{yb}$ = 441.2 N/mm$^2$ (according to tensile tests of the material – see sect. 3.5.1)

$\sigma_{cr,s1}$: -the elastic critical buckling stress for stiffener of the narrow flange $b_{pf1}$ according with eq. (5.15) in [131]) and eq.(3.50); $\sigma_{cr,s1}$=109.03 N/mm$^2$

The elastic critical buckling stress for the edge stiffener of the narrow flange $b_{pf1}$ is:

$$\sigma_{cr,s1} = \frac{2\cdot\sqrt{K\cdot E\cdot I_{s1}}}{A_{s1}} = \frac{2\cdot\sqrt{0.075\cdot 2.1\cdot 10^5\cdot 38.7}}{14.33} = 109.03 \text{ N/mm}^2, \tag{3.50}$$

where:

K: –is the spring stiffness for displacement, per unit length; according to eq. (5.9) in [131]) and eq. (3.51); K =0.075 N/mm$^2$)

E: -elastic modulus; E=210000 N/mm$^2$

$I_{s1}$: -effective second moment of area of the stiffener (see eq.(3.47)); $I_{s1}$=38.7 mm$^4$

$A_{s1}$: -effective cross-sectional area of the edge stiffener (see eq.(3.45)); $A_{s1}$=14.33 mm$^4$

According to 5.5.3.1(2) in [131] the spring stiffness of an edge stiffener should be determined by applying a unit load per unit length u as illustrated in Figure 3.10.

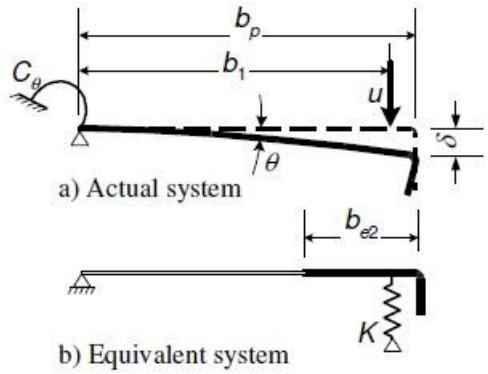


Figure 3.10 Determination of spring stiffener [131]

The spring stiffener for the edge stiffener of the narrow flange $b_{pf1}$ is:

$$K = \frac{u}{\delta} = \frac{1}{13.316} = 0.075 \text{ N/mm}^2 \tag{3.51}$$

where:

u: -the unit load applied per unit length; u=1

$\delta$: -the deflection of the stiffener due to the unit load u acting in the centroid ($b_1$) of the effective part of the cross-section - see eq. (5.10a) in [131] and eq. (3.52); $\delta$=13.316 mm

The deflection, $\delta$, of an edge stiffener should be obtained, according to 5.5.3.1(4) in [131] from:

$$\delta = \theta \cdot b_p + \frac{u \cdot b_p^3}{3} \cdot \frac{12 \cdot (1-\nu^2)}{E \cdot t^3} = 0.251 \cdot 34.18 + \frac{1 \cdot 34.18^3}{3} \cdot \frac{12 \cdot (1-0.3^2)}{2.1 \cdot 10^5 \cdot 0.71^3} \tag{3.52}$$

$\delta$ =13.31 mm

where:

$b_p$: –the distance from the web-to-flange junction to the gravity center of the effective area of the edge stiffener (including effective part $b_{e2}$ of the flange) of the narrow flange $b_{pf1}$ (see Figure 3.8); $b_p = b_1$ = 34.18 mm)

u: -the unit load applied per unit length; u=1

$\nu$: -the Poisson's ratio, $\nu$ = 0.3

E: -the elastic modulus; E=210000 N/mm$^2$

t: -thickness of the stiffener; t = 0.71 mm (see eq. (3.1))

and:

$$\theta = \frac{u \cdot b_f}{C_\theta} = \frac{1 \cdot 36.58}{209.46} = 0.174, \tag{3.53}$$

where:

$b_p$: $b_p$= $b_{pf1}$ = 36.58 mm (see Figure 3.6)

$C_\theta$: -the rotational spring stiffnesses; $C_\theta$=209.46 (see eq (3.54))

$$C_\theta = \frac{E \cdot t^3}{4 \cdot (1-\nu^2) \cdot h} = \frac{2.5 \cdot 10^5 \cdot 0.71^3}{4 \cdot (1-0.3^2) \cdot 98.58} = 209.46, \tag{3.54}$$

where:

E: -the elastic modulus; E=210000 N/mm$^2$

t: -thickness of the stiffener; t = 0.71 mm (see eq. (3.1))

$\nu$: -the Poisson's ratio, $\nu$ = 0.3

h: $h = b_{ph1}$ = 98.58 mm (see Figure 3.4)

As $\overline{\lambda_d}$ = 2.01 > 1.38, the reduction factor, $\chi_d$, for the distortional buckling resistance of the stiffener of the narrow flange $b_{pf1}$, according to (5.12c) in [131] is:

$$\chi_d = \frac{0.66}{\overline{\lambda_d}} = \frac{0.66}{2.01} = 0.328 < 1, \tag{3.55}$$

The reduced thickness $t_{red1}$ of the edge stiffener in the compressed flange $b_{f1}$ is:

$$t_{red1} = \chi_d \cdot t = 0.328 \cdot 0.71 = 0.232 \text{ mm} \tag{3.56}$$

The analytical calculations for narrow flange $b_{f2}$ (see Figure 3.9) were performed in the same manner as for narrow flange $b_{f1}$. The reduction factor, $\chi_d$, for the distortional buckling resistance of the stiffener of the narrow flange $b_{pf2}$ was obtained from the relative slenderness, $\overline{\lambda_d}$, according with 5.5.3.1(7) in [131] as follows:

$$\overline{\lambda_d} = \sqrt{\frac{f_{yb}}{\sigma_{cr,s2}}} = \sqrt{\frac{441.2}{133.69}} = 1.81, \tag{3.57}$$

where:

$\overline{\lambda_d}$: –the relative slenderness

$f_{yb}$: -basic yield strength; $f_{yb}$ = 441.2 N/mm$^2$; (according to tensile tests of the material – see sect. 3.5.1)

$\sigma_{cr,s2}$: -the elastic critical buckling stress for stiffener of the narrow flange $b_{pf1}$ according with eq. (5.15) in [131]) and eq.(3.58)(3.50)

$\sigma_{cr,s1}$=133.69 N/mm$^2$

The elastic critical buckling stress for the edge stiffener of the narrow flange $b_{pf1}$ is:

$$\sigma_{cr,s2} = \frac{2\cdot\sqrt{K\cdot E\cdot I_{s2}}}{A_{s2}} = \frac{2\cdot\sqrt{0.1146\cdot 2.1\cdot 10^5\cdot 34.2}}{13.57} = 133.69 \text{ N/mm}^2, \quad (3.58)$$

where:

K: –is the spring stiffness for displacement, per unit length; according to eq. (5.9) in [131]) and eq. (3.59)(3.51); K =0.1146 N/mm$^2$)

E: -elastic modulus; E=210000 N/mm$^2$

$I_{s2}$: -effective second moment of area of the stiffener - see eq.(3.48),(3.47); $I_{s2}$=34.2 mm$^4$

$A_{s2}$: -effective cross-sectional area of the edge stiffener - see eq. (3.46); $A_{s2}$=13.57 mm$^4$

The spring stiffener for the edge stiffener of the narrow flange $b_{pf2}$ is:

$$K = \frac{u}{\delta} = \frac{1}{8.7283} = 0.1146 \text{ N/mm}^2 \quad (3.59)$$

where:

u: -the unit load applied per unit length; u=1

$\delta$: -the deflection of the stiffener due to the unit load u acting in the centroid ($b_2$) of the effective part of the cross-section - see eq. (5.10a) in [131] and eq. (3.60)(3.52); $\delta$=8.7283 mm

The deflection, $\delta$, of the edge stiffener was obtained, according to 5.5.3.1(4) in [131] from:

$$\delta = \theta\cdot b_p + \frac{u\cdot b_p^3}{3}\cdot\frac{12\cdot(1-\nu^2)}{E\cdot t^3} = 0.149\cdot 29.69 + \frac{1\cdot 29.69^3}{3}\cdot\frac{12\cdot(1-0.3^2)}{2.1\cdot 10^5\cdot 0.71^3} \quad (3.60)$$

$\delta$ =8.7283 mm

where:

$b_p$: –the distance from the web-to-flange junction to the gravity center of the effective area of the edge stiffener (including effective part $b_{2,e2}$ of the flange) of the narrow flange $b_{pf2}$ - see Figure 3.9 $b_p = b_2$ = 29.69 mm)

u: -the unit load applied per unit length; u=1

$\nu$: -the Poisson's ratio, $\nu$ = 0.3

E: -the elastic modulus; E=210000 N/mm$^2$

t: -thickness of the stiffener; t = 0.71 mm - see eq. (3.1)

and:

$$\theta = \frac{u \cdot b_f}{C_\theta} = \frac{1 \cdot 29.69}{216.03} = 0.1497, \tag{3.61}$$

where:

$b_p$: $b_p$= $b_{pf2}$ = 29.69 mm (see Figure 3.9)

$C_\theta$: -the rotational spring stiffnesses; $C_\theta$=209.46 - see eq. (3.62)

$$C_\theta = \frac{E \cdot t^3}{4 \cdot (1-\nu^2) \cdot h} = \frac{2.1 \cdot 10^5 \cdot 0.71^3}{4 \cdot (1-0.3^2) \cdot 95.58} = 216.03, \tag{3.62}$$

where:

E: -the elastic modulus; E=210000 N/mm$^2$

t: -thickness of the stiffener; t = 0.71 mm (see eq. (3.1))

$\nu$: -the Poisson's ratio, $\nu$ = 0.3

h: $h = b_{ph2}$ = 95.58 mm (see Figure 3.4)

As $\overline{\lambda_d}$ = 1.81 > 1.38, the reduction factor, $\chi_d$, for the distortional buckling resistance of the stiffener of the narrow flange $b_{pf2}$, according to (5.12c) in [131] is:

$$\chi_d = \frac{0.66}{\overline{\lambda_d}} = \frac{0.66}{1.81} = 0.363 < 1, \tag{3.63}$$

The reduced thickness $t_{red2}$ of the edge stiffener in the compressed flange $b_{f2}$ is:

$$t_{red2} = \chi_d \cdot t = 0.363 \cdot 0.71 = 0.258 \text{ mm} \tag{3.64}$$

After refining the value of $\chi_d$ by iteration until $\chi_{d,n} \approx \chi_{d,(n-1)}$, according to 5.5.3.2(9) in [131] (see Figure 3.11), the adopted values for the effective cross-section of the narrow flanges under compression (see Figure 3.12) are:

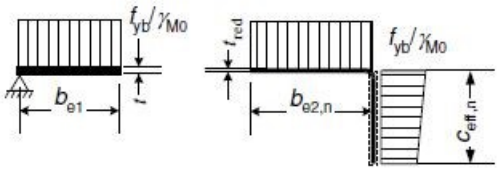


Figure 3.11 Effective cross-section of the narrow flange and stiffener after iteration [131]

For the edge stiffener, $c_1$:

$$\chi_{d,n} = 0.297 \tag{3.65}$$

$$t_{red1} = \chi_{d,n} \cdot t = 0.297 \cdot 0.71 = 0.210 \text{ mm} \quad (3.66)$$

$$c_{1,eff} = 8.08 \text{ mm} \quad (3.67)$$

$$b_{1,e2} = 12.11 \text{ mm} \quad (3.68)$$

For the edge stiffener, $c_2$:

$$\chi_{d,n} = 0.341 \quad (3.69)$$

$$t_{red2} = \chi_{d,n} \cdot t = 0.341 \cdot 0.71 = 0.242 \text{ mm} \quad (3.70)$$

$$c_{2,eff} = 7.36 \text{ mm} \quad (3.71)$$

$$b_{2,e2} = 11.76 \text{ mm} \quad (3.72)$$

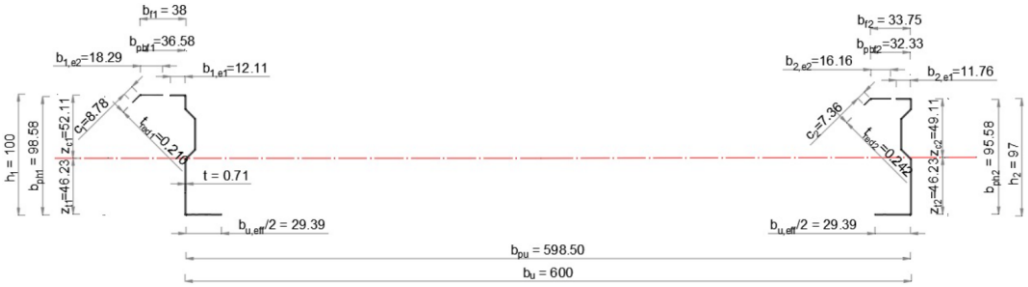


Figure 3.12 Effective cross-section of the liner tray with narrow flanges under compression and the entire cross-section of the webs

### 3.2.1.5.4 Determination of the effective depth, $h_{eff,}$ of the webs under bending

For web $h_1$:

According to 4.4(2), eq. (4.2) in [157], the relative slenderness, $\overline{\lambda_p}$, is:

$$\overline{\lambda_p} = \frac{\overline{b}/t}{28.4 \cdot \varepsilon \cdot \sqrt{k_\sigma}} = \frac{98.58/0.71}{28.4 \cdot 0.729 \cdot \sqrt{21.08}} = 1.45, \quad (3.73)$$

where:

$\overline{b}$: $\overline{b}$ = $b_{ph1}$ = 98.58 mm (see Figure 3.4)

t: -thickness of the wide web; t = 0.71 mm - see eq. (3.1)

$k_\sigma$: -the buckling factor for the web with $h_1$ = 100 mm, corresponding to the stress ratio ψ and boundary conditions, according to (Tabel 4.1 in [157]); $k_\sigma$=21.08 - see eq. (3.74)

ε: ε = 0.729 mm - see eq. (3.3)

As, -1<ψ<0 - see eq. (3.75), according to Tabel 4.1 in [157], $k_\sigma$ may be determined:

$$k_\sigma = 7.81 - 6.29 \cdot \psi + 9.78 \cdot \psi^2 = 7.81 - 6.29 \cdot (-0.921) + 9.78 \cdot (-0.921)^2 = 21.90 \quad (3.74)$$

where:

$$\psi = \frac{\sigma_2}{\sigma_1} = \frac{z_{t1}}{z_{c1}} = -\frac{46.23}{52.11} = -0.887 \quad (3.75)$$

The relative slenderness, $\overline{\lambda_p}$ >0.673, therefore the reduction factor, ρ, of effective width according to (4.2) in [157] is:

$$\rho = \frac{\overline{\lambda_p} - 0.055 \cdot (3+\psi)}{\overline{\lambda_p}^2} = \frac{1.45 - 0.055 \cdot (3-0.887)}{1.45^2} = 0.631 \le 1.0, \quad (3.76)$$

The effective width of the web with $h_1$ = 100 mm, $h_{eff,1}$, was determined according to Table 4.1 in [157]:

$$h_{eff,1} = \rho \cdot b_{c,1} = 0.631 \cdot 52.11 = 32.87 \text{ mm} \quad (3.77)$$

where:

$b_{c,1}$: $b_{c,1} = z_{c1}$ = 52.11 mm (see Figure 3.12)

ρ: $\rho$= 0.631 - see eq. (3.76)

The values of the effective widths of the web with $h_1$ = 100 mm, $h_{1,e1}$ and $h_{1,e2}$, shown in Figure 3.13 were determined, according to Table 4.1 in [157], as follows:

$$h_{1,e1} = 0.4 \cdot h_{eff,1} = 0.4 \cdot 32.87 = 13.15 \text{ mm} \quad (3.78)$$

$$h_{1,e2} = 0.6 \cdot h_{eff,1} = 0.6 \cdot 32.87 = 19.72 \text{ mm} \quad (3.79)$$

For web $h_2$:

According to 4.4(2), eq. (4.2) in [157], the relative slenderness, $\overline{\lambda_p}$, is:

$$\overline{\lambda_p} = \frac{\overline{b}/_t}{28.4 \cdot \varepsilon \cdot \sqrt{k_\sigma}} = \frac{95.58/_{0.71}}{28.4 \cdot 0.729 \cdot \sqrt{22.39}} = 1.37, \quad (3.80)$$

where:

$\overline{b}$: $\overline{b}$ = $b_{ph2}$ = 95.58 mm (see Figure 3.4)

t: -thickness of the wide web; t = 0.71 mm - see eq. (3.1)

$k_\sigma$: -the buckling factor for the web with $h_2$ = 97 mm corresponding to the stress ratio ψ and boundary conditions, according to (Tabel 4.1 in [157]); $k_\sigma$=22.39 - see eq.(3.81)

ε: ε = 0.729 mm - see eq. (3.3)

As, -1<ψ<0 - see eq.(3.82), according to Tabel 4.1 in [157], $k_\sigma$ may be determined as follows:

$$k_\sigma = 7.81 - 6.29 \cdot \psi + 9.78 \cdot \psi^2 = 7.81 - 6.29 \cdot (-0.941) + 9.78 \cdot (-0.941)^2 = 22.39 \quad (3.81)$$

where:

ψ: -the stress ratio; ψ = -0.941 (see eq.(3.82))

$$\psi = \frac{\sigma_2}{\sigma_1} = \frac{z_{t2}}{z_{c2}} = -\frac{46.23}{49.11} = -0.941 \quad (3.82)$$

The relative slenderness, $\overline{\lambda_p}$=1.37 >0.673, therefore the reduction factor, ρ, of effective width according to (4.2) in [157] is:

$$\rho = \frac{\overline{\lambda_p} - 0.055 \cdot (3+\psi)}{\overline{\lambda_p}^2} = \frac{1.37 - 0.055 \cdot (3-0.941)}{1.37^2} = 0.668 \leq 1.0, \quad (3.83)$$

The effective width of the web with $h_2$ = 97 mm, $h_{eff,2}$, was determined according to Table 4.1 in [157]:

$$h_{eff,2} = \rho \cdot b_{c,2} = 0.668 \cdot 49.11 = 32.83 \text{ mm} \quad (3.84)$$

where:

$b_{c,2}$: $b_{c,2}$ = $z_{c2}$ = 49.11 mm (see Figure 3.4)

ρ: $\rho$= 0.668 (see eq.(3.83))

The values of the effective widths of the web with $h_2$ = 97 mm, $h_{2,e1}$ and $h_{2,e2}$, shown in Figure 3.13 were determined, according to Table 4.1 in [157], as follows:

$$h_{2,e1} = 0.4 \cdot h_{eff,2} = 0.4 \cdot 32.83 = 13.13 \text{ mm} \quad (3.85)$$

$$h_{2,e2} = 0.6 \cdot h_{eff,2} = 0.6 \cdot 32.83 = 19.69 \text{ mm} \quad (3.86)$$

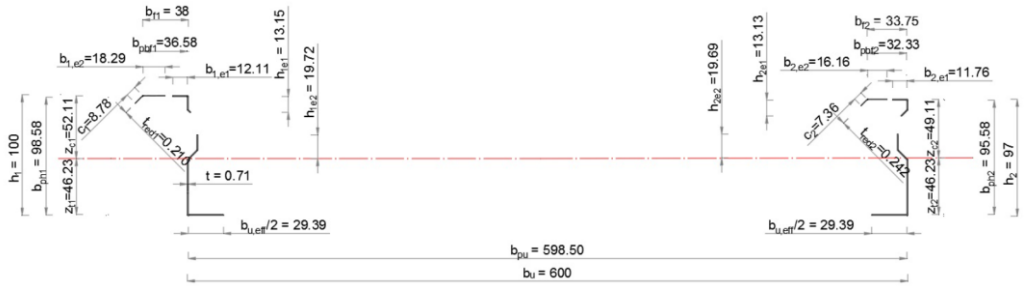


Figure 3.13 Effective cross-section of a 600/100 liner tray with the wide flange in tension

### 3.2.1.5.5 The effects of shear lag

According to EN 1993-1-3 art. 10.2.2.2 (2) in [131], the effects of shear lag may be neglected here because,

$$\rho = \frac{L}{b_{u,eff}} = \frac{4000}{58.78} = 68.04 > 25, \quad (3.87)$$

where:

$L$: -the length of the liner tray; $L$ = 4000 mm

$b_{u,eff}$: -the effective width of the wide flange in tension; $b_{u,eff}$ = 58.78 mm -see eq.(3.25), because $b_{u,eff,shear\_lag}$ = 289.57 mm - see eq. (3.88) is greater than the effective width of the wide flange in tension

According to 3.2 in [157], the effective width $b_{eff}$ for shear lag should be determined as follows:

$$b_{u,eff,shear\_lag} = \beta \cdot b_0 = 0.9653 \cdot 300 = 289.57 \text{ mm}, \quad (3.88)$$

where:

$\beta$: -the effective width factor for sagging bending; $\beta$ = 0.965 - see eq.(3.89)

$b_0$: -half the width of an internal element; $b_0 = b_u / 2$ = 300 mm

As 0.02≤ k=0.075 ≤0.70 (according to Table 3.1 in [157]), the effective width factor for sagging bending was determined as follows:

$$\beta = \frac{1}{1+6.4 \cdot k^2} = \frac{1}{1+6.4 \cdot 0.075^2} = 0.9653, \quad (3.89)$$

where:

$$k = \frac{a_0 \cdot b_0}{L_e} = \frac{1 \cdot 1}{4000} = 0.075, \tag{3.90}$$

where:

$a_0$: $a_0$ = 1 for plate elements without longitudinal stiffeners

$b_0$: -half the width of an internal element; $b_0$ = 300 mm

$L_e$: -the distance between adjacent points of zero bending moment; $L_e$ = L = 4000 mm

As the effective width resulting from plate buckling $b_{u,eff}$ = 58.78 mm (see eq.(3.25)) is smaller than the effective width for shear lag under elastic conditions $b_{u,eff,shear\_lag}$ = 289.57 mm - see eq. (3.88), the effective width used in the calculations was $b_{u,eff}$ =58.78 mm, conducting to the conclusion that in this case the effects of shear lag can be neglected.

### *3.2.1.6 Determination of the moment resistance of a liner tray cross-section with the wide flange in tension*

According to section 10.2.2.2 in [131], the moment resistance $M_{b,Rd}$ of liner trays with wide flange in tension is reduced by a reduction coefficient that takes into account the effect of the fixing distance of fasteners supplying lateral restraint to the narrow flanges.

$$\beta_b = 1.15 - \frac{s_1}{2000}, \tag{3.91}$$

where:

$s_1$: -the longitudinal spacing of fasteners supplying lateral restraint to the narrow flanges (see Figure 3.19-c)

The reduction coefficient, $\beta_b$, considers the influence of the fixing distance $s_1$ at distances exceeding 300 mm. When the fixing distance falls below 300 mm, there is no need in reducing the bending moment. However, the current design guideline for the fixing distance is rather conservative and restricts it to a maximum of $s_1$ = 1000 mm, which is now inadequate to meet the growing architectural and thermal demands [144].

The moment resistance $M_{b,Rd}$ may be obtained as follows:

$$M_{b,Rd} = \frac{0.8 \cdot \beta_b \cdot W_{eff,min} \cdot f_{y,b}}{\gamma_{M0}} = \frac{0.8 \cdot 0.9 \cdot 4918.89 \cdot 441.2}{1.00} = 1.56 \text{ kNm}, \tag{3.92}$$

where:

$\beta_b$: -the correlation factor; $\beta_b$= 0.9 for $s_1$ = 500 mm, where $s_1$ is the longitudinal spacing of fasteners supplying lateral restraint to the narrow flanges

$W_{eff,min}$: $W_{eff,min}$= 4918.89 mm$^3$ - see eq. (3.93)

$f_{y,b}$: $f_{y,b}$= 441.2 N/mm$^2$; (according to tensile tests of the material – see sect. 3.5.1)

$\gamma_{M0}$: $\gamma_{M0}$ = 1.00 (section 2.(3) in [131])

$$W_{eff,min} = \min\left(\frac{I_{y,eff}}{z_c}, \frac{I_{y,eff}}{z_t}\right) = \min\left(\frac{256323}{52.11}, \frac{256323}{46.23}\right) = 4918.89 \text{ mm}^3, \quad (3.93)$$

where:

$I_{y,eff}$: -the effective second moment of area of the effective cross-section of a 600/100 liner tray with the wide flange in tension (see Figure 3.13) about the y-y axis
$I_{y,eff}$ = 256323.62 mm$^4$ (determined with the use of the AutoCAD tool [156])

$z_c$: -the distance from the effective centroidal axis to the system line of the narrow flange under compression (see Figure 3.13)
$z_c = \max(z_{c1}, z_{c2}) = \max(52.11, 49.11) = 52.11$ mm

$z_t$: -the distance from the effective centroidal axis to the system line of the wide flange in tension (see Figure 3.13)
$z_t = \max(z_{t1}, z_{t2}) = 46.23$ mm

### 3.2.2 Design by code vs. experimental investigations of structural behaviour of liner trays

Alternatively to the design procedures for structural liner trays prescribed by EN 1993-1-3, the moment resistance of a liner trays can be determined by testing, as long as precautions are taken to ensure that the testing equipment does not influence the local behaviour of the liner trays, as outlined in Annex A of EN 1993-1-3:2006 [131]. Several research studies [130], [142], [147], [148], [149], [150] were conducted on the behaviour of structural liner trays under wind loads determined by experimental and numerical investigations showing the conservative character of the design procedures provided by the standard in force. However, these experimental investigations were carried out by apllying steel or timber cross beams arranged in such a way as to approximate uniformly distributed loading (Eurocode EN 1993-1-3 [131], Section A2, presents the test procedures for profiled sheets, including for liner trays, stating that the 'loading may be applied through air bags or in a vacuum chamber or by steel or timber cross beams"). Therefore, the dynamic effect of wind load could not be reviewed in these experimental investigations. To simulate uniformly distributed loads (corresponding to wind suction and wind pressure loads) in order to investigate the behaviour of the liner trays to bending along with the dynamic effect of wind loads, experimental tests on liner trays were carried out in a vacuum chamber. Different configurations of liner tray specimens (simple liner trays and restrained liner trays, with or without cladding), in order to establish the lower limit of their bending moment capacity. When the results of the experimental specimens are compared to the design values obtained following the procedure recommended by EN, a more

exhaustive overview of the conservative design approach of the standard may be seen.

## 3.3 Tested specimens and experimental setup

### 3.3.1 Experimental program of liner trays

The tested liner tray specimens manufactured by a European provider acting on the Romanian market [4] consist of steel sheeting according to EN 10346:2015 [132], formed into liner trays and trapezoidal sheets. All the tested liner trays have a height of 100 mm, a width of 600 mm, a gross thickness of 0.75 mm, and an S280GD steel grade (according to EN 10346:2015). The cross-section geometry of the liner trays is shown in Figure 3.14.

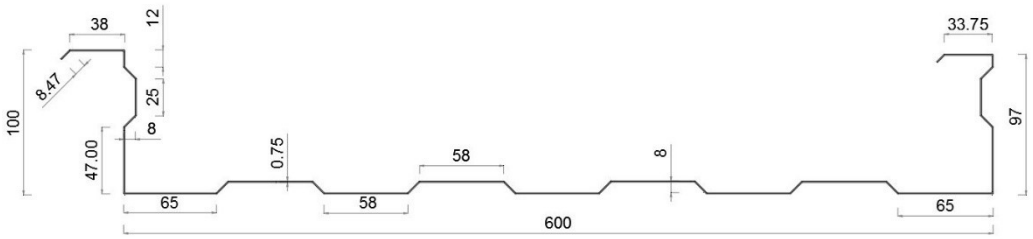


Figure 3.14 Liner tray 100 x 600 / 0.75 mm cross-section

Due to the constraints of the available laboratory testing rig (specifically, the dimensions of the vacuum chamber), an experimental test setup with a span of 4.0 m was chosen, following a simply supported static scheme, as presented in Figure 3.2.

To establish the lower limit of the bending moment capacity of the liner trays, tests were performed using simple liner trays without any outer cladding. In this scenario, the stabilizing effect of the outer cladding was absent and the compressed narrow flanges of the liner trays were solely supported against lateral buckling by the lateral bending stiffness of the liner trays' webs and not by any external restraining outer cladding. Considering this static scheme, the buckling length of the small flanges was equal to the span length.

In practice, the outward cladding works as a compression flange (in wind suction) or as a tension flange (in wind pressure) of the overall cross-section and the load-bearing behaviour is expected to be more favourable for liner trays closed with corrugated steel sheet than in the case of simple liner trays without cladding. In order to get the direct contribution to the limit of the bending moment capacity of the liner trays of the outer shell of a liner tray wall system (the outer shell consisting in the corrugated steel sheets fixed with the upper flange of the liner trays), aside from the tests of pure liner trays, the experimental program included tests with outer cladding (see Figure 3.15).

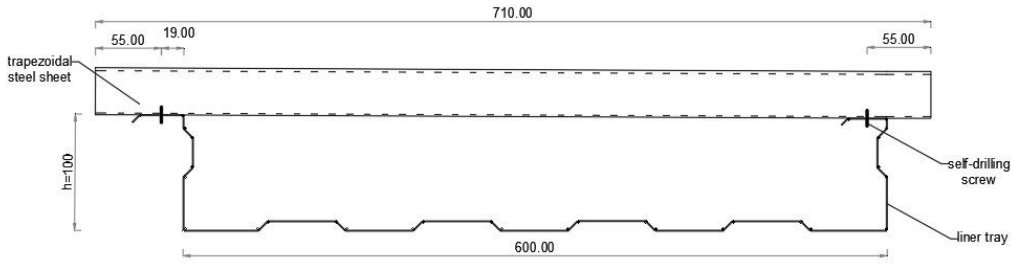


Figure 3.15 Cross-section of the experimental setup of a simple liner tray tested with outer cladding

In practice, a liner tray wall system consists of several liner trays used as an inner shell of a double shell wall system (see Figure 2.14), while connected to corrugated steel sheets or to trapezoidal profiles. Therefore, the experimental program included also tests on liner trays consisting in a complete liner tray along with two half liner trays, (which are fixed in the webs and hereafter referred to as "restrained liner trays") and a trapezoidal steel-sheet perpendicular to the liner tray fixed with the upper flange of the liner tray, as presented in Figure 3.16. This setup was tested to establish the limit of the bending moment capacity of the liner trays to wind pressure and suction, in cases closest to practical conditions. It is worth to mention that the current study does not focus on the strong diaphragm effect that occurs within the plane of liner tray cladding systems. This investigation exclusively concerns the perpendicular loads acting on the cladding.

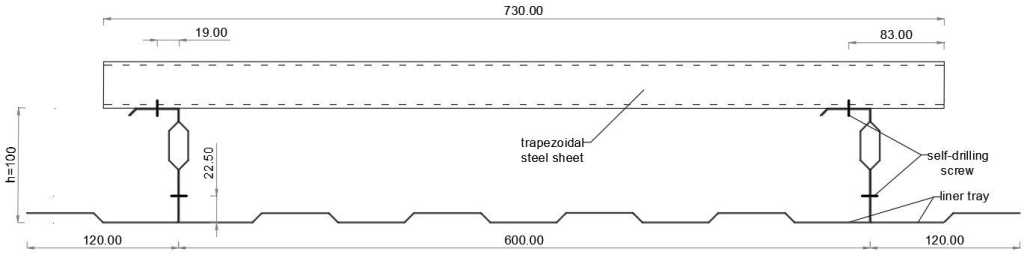


Figure 3.16 Cross-section of experimental setup resembling the double-shell wall system (restrained liner trays with outer cladding)

The tests performed are all described by the labels and characteristics listed in Table 3.3. All specimens had a length of 4.0m and were simply supported. Additionally, tensile tests according to EN 6892-1:2009 [158] on samples extracted from the sheeting were performed to determine the material properties.

Table 3.3 Experimental program of liner trays

| Test name | Type of setup | Outer cladding presence | Type of test |
|---|---|---|---|
| LT-SO-P-P | simple liner tray - pinned | no | wind pressure |
| LT-SO-P | simple liner tray | | wind pressure |
| LT-SO-S | | | wind suction |
| LT-SC-S | | yes | wind suction |
| LT-SC-P | | | wind pressure |
| LT-RO-S | restrained liner tray | no | wind suction |
| LT-RO-P | | | wind pressure |
| LT-RC-S | | yes | wind suction |
| LT-RC-P | | | wind pressure |

#### *3.3.1.1 Simple-opened liner trays*

The experimental program on simple-open liner trays concerns three specimen typologies:

- LT-SO-P: simply supported, subjected to wind pressure
- LT-SO-P-P: simple-open liner trays, pinned at one end and simply supported at the other, subjected to wind pressure (Figure 3.17-b)
- LT-SO-S: simple-open liner trays, simply supported, subjected to wind suction (Figure 3.17-a).

The experimental setup assumes a 4000 mm inter-axial span of the liner trays and a support overhang of 50 mm.

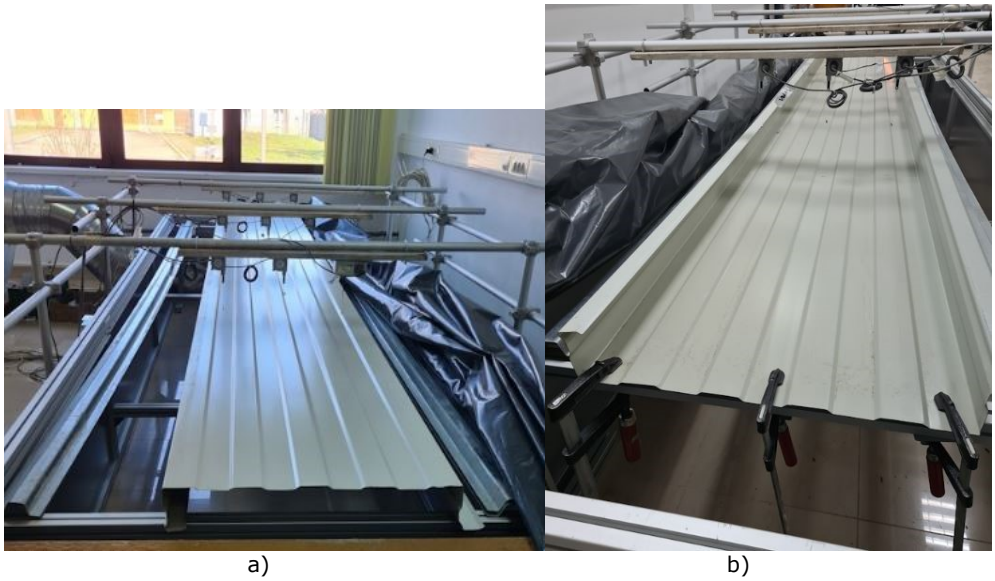

a) b)

Figure 3.17 Simple-opened liner tray specimens prepared for wind tests: a) LT-SO-S and b) LT-SO-P-P

### *3.3.1.2 Simple-closed liner trays*

The simple-closed liner trays refer to simple liner trays with outer cladding:

- LT-SC-S: simple-closed liner trays subjected to wind suction (Figure 3.30-a)
- LT-SC-P: simple-closed liner trays, subjected to wind pressure (Figure 3.18-b).

The statical scheme of the experimental setup represents a simply supported beam with one span of 4000 mm and a support overhang of 50 mm. The 35x212x0.5 mm trapezoidal steel-sheet (presented in Figure 3.19-a and Figure 3.19-b), perpendicular to the liner trays, was fixed with the upper flange, by self-drilling screws, at spacing $s_1$ = 500 mm (see Figure 3.19-c).

a) b)

Figure 3.18 Simple-closed liner tray specimens prepared for wind tests: a) LT-SC-S and b) LT-SC-P

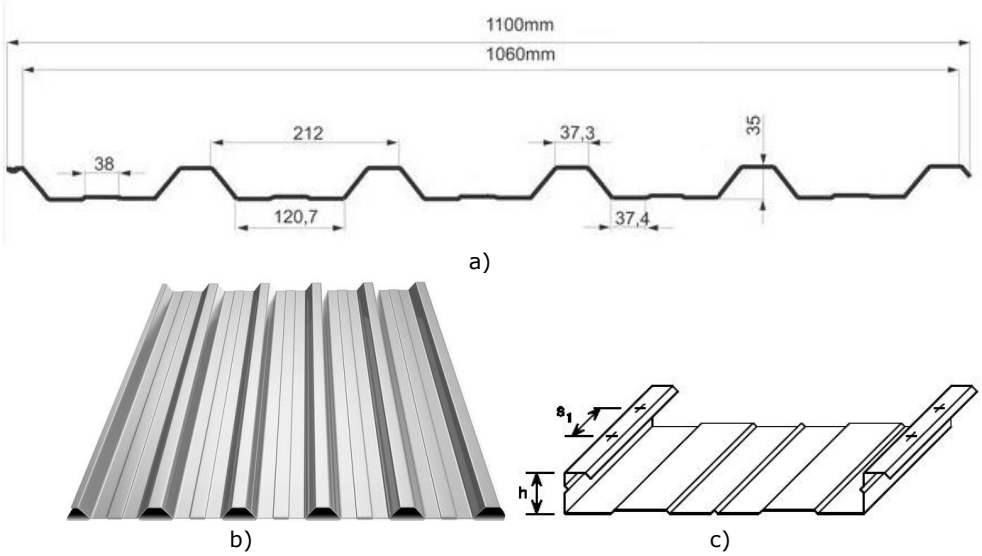


a) b) c)

Figure 3.19 Trapezoidal steel-sheet used in tests a) Cross-section geometry; b) View of the trapezoidal steel-sheet c) Distance $s_1$ = 500 mm in liner trays [131]

During the first test on liner trays subjected to wind suction, it was observed that the wide flange gained a strong deformation in the support area of the specimen (see Figure 3.20). Under real conditions of service, this flange deformation in the support area of the liner trays could not occur due to the connection between the liner tray and the columns (through self-drilling screws), thus timber blocks (visible in Figure 3.18 a) and b)) with the dimension of 45x10x10 cm were inserted between the wide flange of the liner trays and the support. As the length of the timber blocks was smaller than the width of the liner trays, having the timber blocks inserted in the support area of the liner trays did not affect the possible lateral-torsional buckling of the webs in the area. This helped the model to reproduce the real behaviour of the liner trays and reaching realistic failure modes. Therefore, the timber blocks inserted inside the cross-section of the liner trays in the support area were adopted in all the experimental tests to wind suction. This solution is in accordance with testing procedures on liner trays agreed by EN 1993-1-3 Annex A2.1(3).

Figure 3.20 Video caption of the strong deformation of the wide flange in the support area, during the first test of liner trays subjected to wind suction

### *3.3.1.3 Restrained-opened liner trays*

The restrained-opened liner trays refer to test arrangements of liner trays consisting of one simple liner tray and two adjacent half-liner trays, with overlapping webs (which doubles the webb thickness, as is the case under real conditions of service), without outer cladding:

- LT-RO-S: restrained-opened liner trays subjected to wind suction (Figure 3.21-a)
- LT-RO-P: restrained-opened liner trays, subjected to wind pressure (Figure 3.21-b).

The statical scheme of the experimental rig represents a simply supported beam with one 4000 mm span and a support overhang of 50 mm. The width of the remaining wide flange of each "half"-liner tray was 120 mm.

The restrained-opened liner trays had the statical scheme of a simply supported beam with one span of 4000 mm and a support overhang of 50 mm. The width of the remaining wide flange of each "half"-liner tray was 120 mm.

The webs of the adjacent liner trays were connected by self-drilling screws every 250 mm, while the overlapped upper flanges were fixed every 500 mm, as presented in Figure 3.22.

A timber block was placed at each end of the liner tray in the support area, in case of tests of liner trays subjected to wind suction, to prevent the wide flange from curling in the support area.

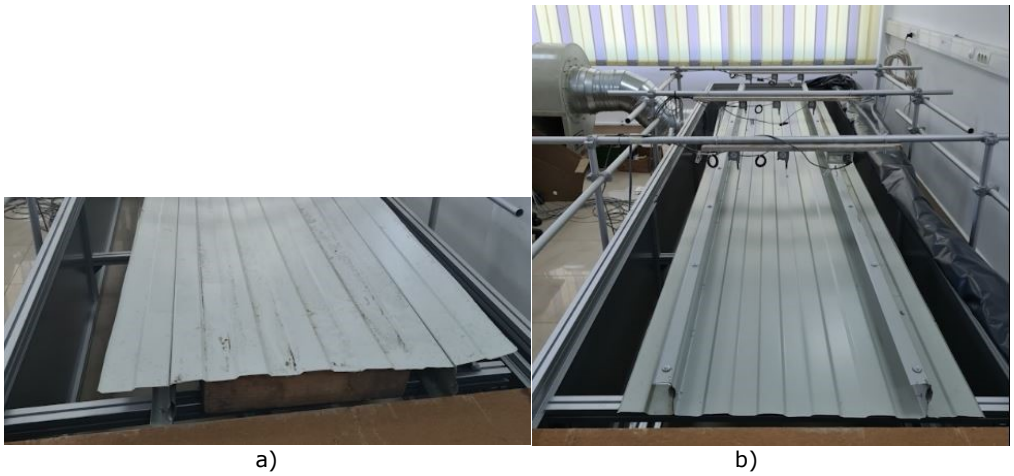

a) b)

Figure 3.21 Restrained-opened liner tray specimens prepared for wind tests: a) LT-RO-S and b) LT-RO-P

Figure 3.22 Restrained-opened liner trays prepared for wind tests: a) LT-RO-S and b) LT-RO-P

#### *3.3.1.4 Restrained-closed liner trays*

The restrained-closed liner trays regard the same experimental setup parameters as restrained-opened liner trays but considering the outer cladding. This series includes two specimens:

- LT-RC-S: restrained-closed liner trays subjected to wind suction (Figure 3.23-a)
- LT-RC-P: restrained-closed liner trays subjected to wind pressure (Figure 3.23-b).

The statical scheme of the experimental setup represents a simply supported beam with one 4000 mm span and a support overhang of 50 mm. The trapezoidal steel-sheet, perpendicular to the liner trays, was fixed with the upper flange, at the same distance as in previous study cases: $s_1$ = 500 mm.

a) b)

Figure 3.23 Restrained-closed liner tray specimens prepared for wind tests: a) LT-RC-S and b) LT-RC-P

### 3.3.2 Experimental setup and loading protocol

To achieve realistic results in strength testing, it is essential that the boundary conditions of the tested specimen accurately replicate the observed constructional details [3].

Eurocode EN 1993-1-3 section A2 presents the test procedures for profiled sheets with the specification that "similar test procedures based on the same principles may also be used for liner trays" [131]. To simulate uniformly distributed loads (corresponding to wind suction and wind pressure loads) the experimental tests were carried out in a vacuum chamber. The test load is administered using air pressure and the mode to apply the test load conforms with the Eurocode EN 1993-1-3 standard.

The tests were performed using calibrated testing machines of the UPT-ICER laboratory [159]. The experimental setup consisted of a vacuum chamber formed by a rigid 5.9m x 1.3m with a 0.6m height enclosure – presented in Figure 3.24-a) and b)), from which air is removed by a vacuum pump – presented in Figure 3.24-c), connected to a pressure transmitter i.e. a differential pressure sensor with display, operating in the range of 0 to 4.000 Pa – see Figure 3.25. A 0.20 mm thick polyethylene foil fixed between rubber seals secured the differential pressure between

the vacuum chamber and the ambient environment. A quasi-static load was considered for the test with a pressure rate of 1.8 $s^{-1}$.

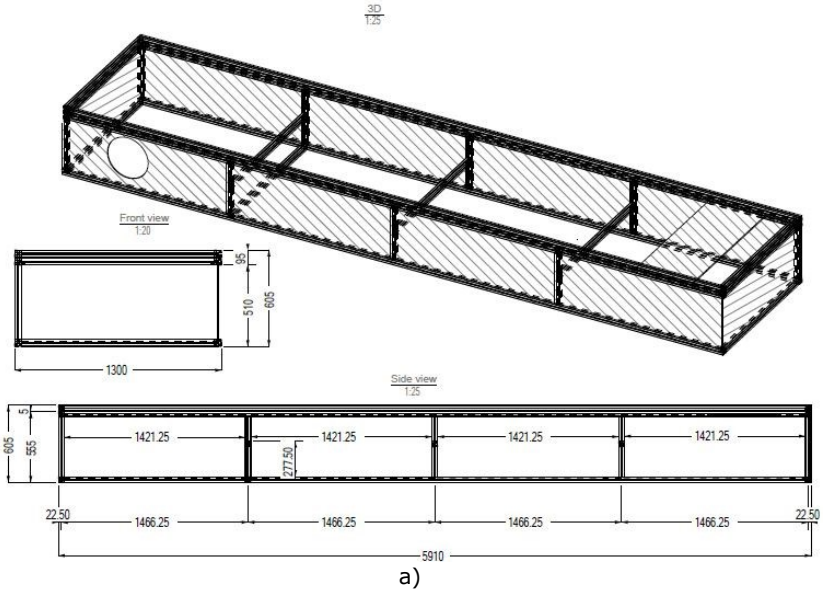


a)

b) c)

Figure 3.24 The experimental setup for liner trays tests: a) the vacuum chamber – graphic view; b) laboratory setup of the vacuum chamber; c) the vacuum pump [160]

The experimental setup also included computer-aided acquisition and post-processing of results. The test specimens were subjected to a monotonic uniformly distributed air suction loading. The ultimate bending moment was determined by load tests with single-span liner trays. To control and verify the imposed load, the air pressure was measured.

The experimental setup involved as well, nine displacement transducers (LVDT) to measure the gap at the initial and ultimate state. The transducers were

placed, as shown in Figure 3.26, in 3 lines by 3 rows, at the mid-span of the liner trays in the transverse and longitudinal direction, at 200 mm left and right from the midspan, in transverse direction, and at 1000 mm left and right from the midspan, in longitudinal direction. Thus, a grid of 9 measurement points was formed, aiming at observing the deformed shapes of the specimens during loading.


Figure 3.25 Differential pressure transmitter connected to the vacuum chamber [161]

As the experimental program aimed to study both loading situations of liner trays – pressure and suction, and as the vacuum chamber allows only air suction during testing, the liner trays were alternatively reversed in order to consider pressure and suction of the liner trays.

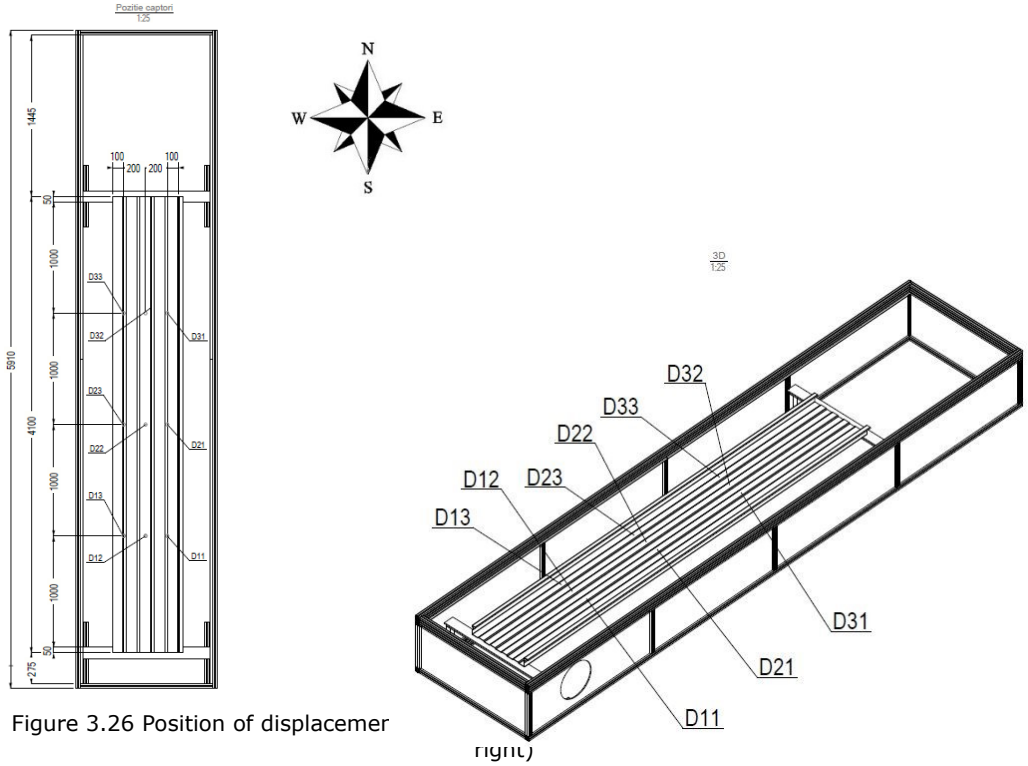


Figure 3.26 Position of displacemer

right)

## 3.4 Wind load tests

An accurate understanding of all constructional details and real loading conditions is crucial for creating a precise experimental model while testing elements and observing their failure behaviour. The adjacent liner trays, which are connected along the longitudinal joint and overlap, collaborate with double-thickness webs. Additionally, the trapezoidal sheet's axial stiffness, spanning across the narrow flanges of the liner trays, which are connected by fasteners, prevents lateral deflection, torsion, or distortion of the cross-section in the event of a collapse [10]. As a result, primarily local failure modes are expected both in practical scenarios and in the experimental model of this study.

The results of the tests considered the maximum value of the loading applied to the specimen coincident with the last recorded value immediately prior to failure, as appointed in EN 1993-1-3, Annex A2.1.(8) [131]. The flexural stiffness is determined from a plot of the load-deflection behaviour, according to A2.2(4) in EN 1993-1-3 [131].

Two calculation scenarios were taken into account for dimensioning at the Ultimate Limit State (ULS). In the first scenario, the calculations considered the pressure load brought by the wind, while in the second scenario, they accounted for the suction load caused by the wind. For the dimensioning at Serviceability Limit State (SLS), the admissible limit values for the deflections were taken into account, the test results being compared with the limit load corresponding to a maximum deflection allowed by L/300 (kN/m$^2$).

### 3.4.1 Experimental results of liner trays subjected to wind pressure

When subjected to wind pressure, liner trays have the wide flange in tension while the narrow flanges are under compression. The failure of specimens presented, in general, a non-symmetrical pattern, showing the influence of non-symmetric cross-section which is specific to liner trays. The non-symmetrical failure pattern had more pronounced collapse effects on one lateral side.

The measured displacements and loads were post-interpreted as load-deflection curves.

#### *3.4.1.1 Simple-opened liner trays*

The load-displacement curve of the simple-opened liner tray subjected to wind pressure is showed in Figure 3.27. The displacement value represents the average values recorded by the three transducers placed at the mid-span of the liner tray (transducers D2.1, D2.2, and D2.3 represented in Figure 3.26). The maximum pressure value recorded immediately before failure was 1087.25 Pa. The displacement value recorded immediately before failure was 35.93 mm.

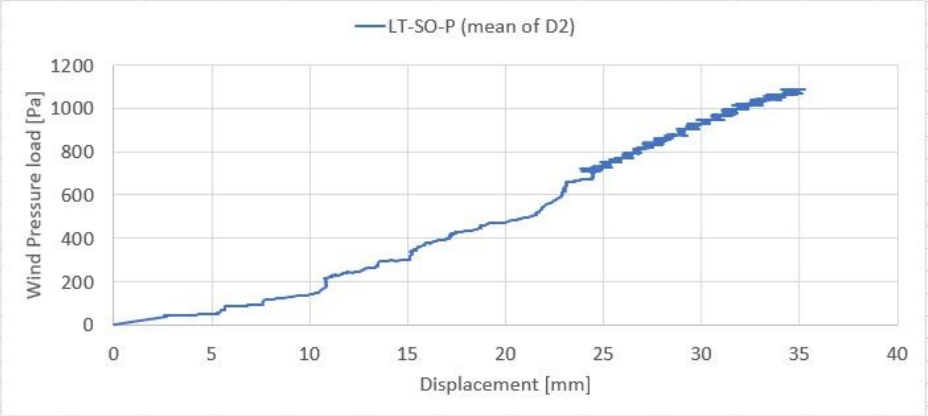


Figure 3.27 Load-displacement curve of the LT-SO-P specimens

Displacements of the liner tray measured during the test to wind pressure are illustrated in Figure 3.28. The displacements were measured continuously by nine displacement transducers (as presented in section 3.3.2 of this paper and Figure 3.26) and they were measured on the wide flange. The graphics show the displacements recorded at $0.3 \cdot P_{max,}$ (where $P_{max,}$ is the maximum pressure applied on the specimen, equal to the last recorded value immediately before failure), at $0.7 \cdot P_{max,}$ and the displacement recorded at $P_{max}$, in both transverse and longitudinal directions. The non-symmetrical pattern in the behaviour of the liner tray can be seen in the mid-span transverse displacement figure promptly from the $0.3 \cdot P_{max}$ load: the tests revealed a smaller displacement in the cross-section of the liner trays closer to the webs than at the mid-span, and, in the same time, the values of displacements are different on the sides, emphasizing the non-symmetrical pattern in the behaviour of the specimens. The mid-span longitudinal displacement chart shows that the displacements at the distance from the support of 1m and 3m (1m distance - symmetrical from the mid-span) are similar and they represent 85% of the value of the displacement recorded at the mid-span of the liner tray. These results validate the parabola-shaped deformed model of the liner tray. It is worth mentioned that the displacements at $P_{max}$, showed by the mid-span longitudinal displacement chart, are double as values than the displacements at $0.3 \cdot P_{max}$.

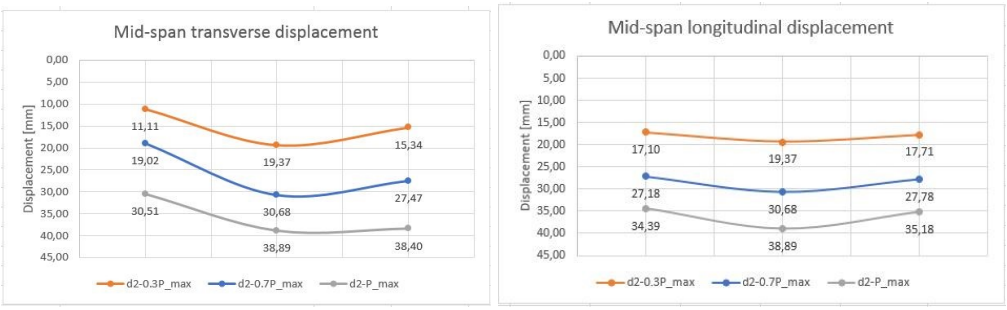


Figure 3.28 Displacements of the LT-SO-P liner tray during the test

In the case of testing wind pressure on simple-opened liner trays (LT-SO-P) the failure was determined by the local buckling of the compressed narrow flange combined with distortion of the web, as presented in Figure 3.29 and Figure 3.30. The failure occurred at the mid-span of the liner tray and had a non-symmetrical pattern.

Figure 3.29 LT-SO-P specimen after failure: local buckling of the wide flange in the support area (left); typical non-symmetric failure at mid-span (right)

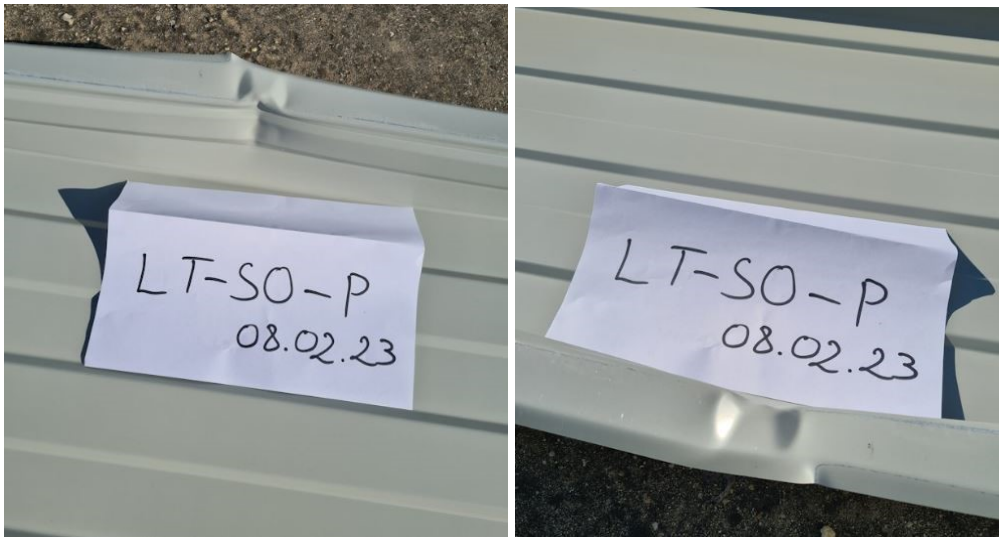


Figure 3.30 Detail of the failure zone; interaction between local buckling and distortional buckling

### *3.4.1.2 Simple-opened liner trays with one pinned support*

Figure 3.31 shows the load-displacement curve of the LT-S-O-P-P liner tray. The maximum load value recorded immediately before failure was 1135.84 Pa, while the displacement value recorded immediately before failure was 34.78 mm, computed as average values recorded by the LVDT transducers placed at the mid-span of the liner tray.

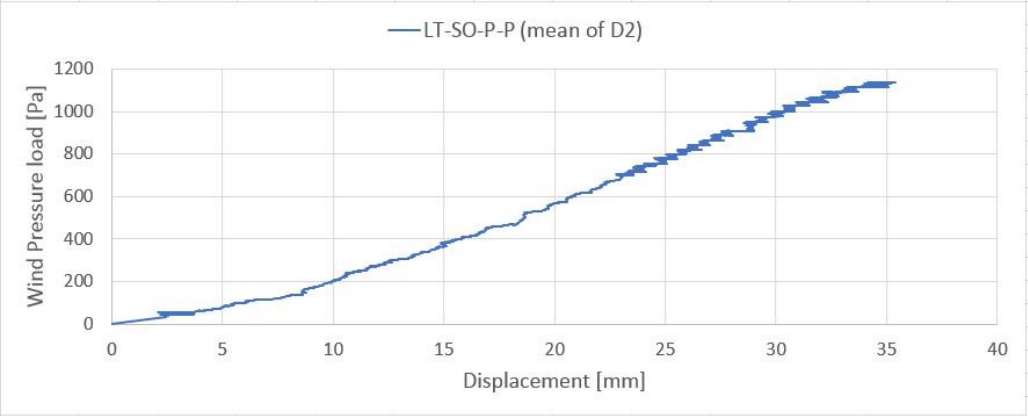


Figure 3.31 Load-displacement curve of the LT-SO-P-P liner tray

Displacements of the LT-SO-P-P liner tray measured during the test to wind pressure are illustrated in Figure 3.32. From Figure 3.28 and Figure 3.32, it may be observed that displacements of the liner trays subjected to wind pressure when the liner trays were simply supported at both ends (LT-SO-P) and when one end of the liner tray was pinned (LT-SO-P-P) are similar as nature and as value, thus similar conclusions could be drawn.

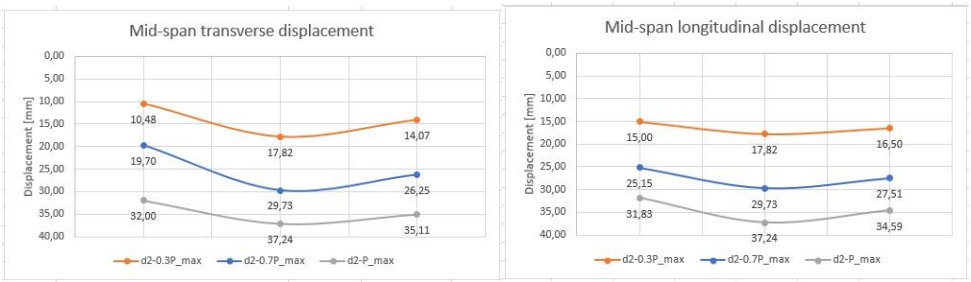


Figure 3.32 Deformations of the LT-SO-P-P liner tray during the test

The pinned simple-opened liner tray tested to wind pressure (LT-SO-P-P) had the same experimental setup as the simple-opened liner tray (LT-SO-P), apart from the pinned support at one end of the liner tray. In this case, as well as in the case of LT-SO-P, the failure was determined by the local buckling of the compressed narrow flange combined with the distortion of the web, as presented in Figure 3.33 and Figure 3.34. The failure occurred in the same web+narrow flange in both cases, even though

the liner trays were placed reversed with respect to the air suction duct, emphasizing the influence of the non-symmetrical cross-section of the liner tray in its behaviour.

Figure 3.33 LT-SO-P-P liner tray specimen after failure: showing typical non-symmetric failure at mid-span

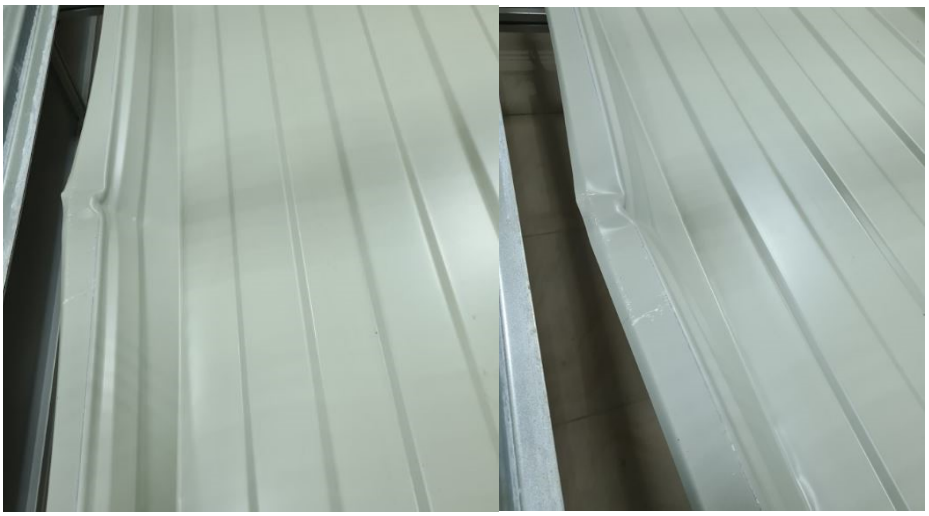

Figure 3.34 Detail of the failure zone; interaction between local buckling of the narrow flange and distortional buckling of the web

Figure 3.35 shows a comparison between the load-displacement curves of the LT-SO-P and LT-S-O-P-P liner trays. They show similar behaviour in terms of resistance and stiffness, with differences smaller than 5% (see Table 3.4):

- $P_{max\_LT\text{-}SO\text{-}P} / P_{max\_LT\text{-}SO\text{-}P\text{-}P} = 0.957$
- $S_{LT\text{-}SO\text{-}P} / S_{LT\text{-}SO\text{-}P} = 41.63 / 40.9 = 1.01$

These considerations allowed the continuity of the testing of the other specimens in the simply supported beam statical scheme.

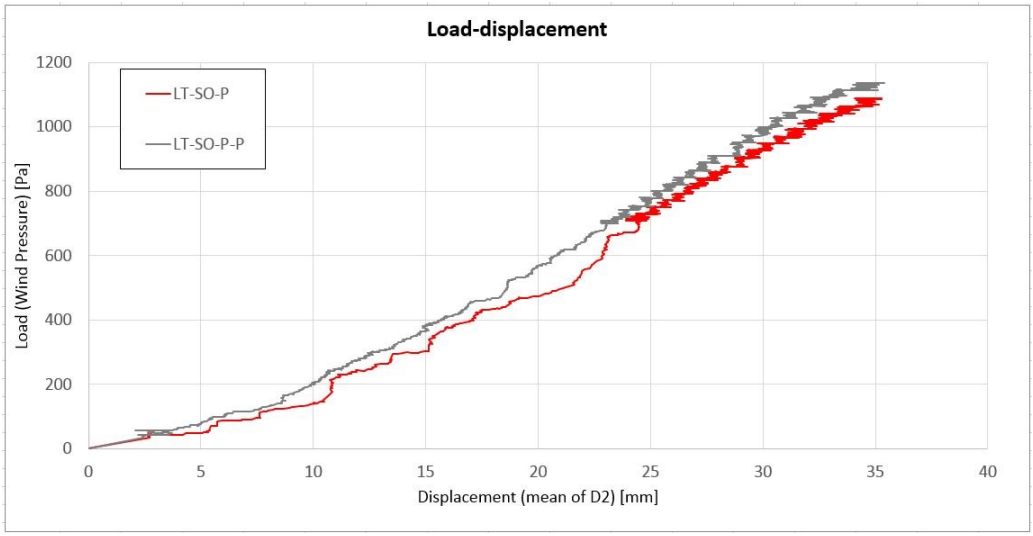


Figure 3.35 Load-displacement results comparison between LT-SO-P and LT-SO-P-P liner trays

### *3.4.1.3 Simple-closed liner trays*

Figure 3.36 shows the pressure - displacement (mean values recorded for LVDTs D2.1, D2.2, and D2.3) curve of the simple-closed liner tray subjected to wind pressure. The maximum pressure value recorded was 1462.61 Pa. The failure displacement was 52.21 mm (equivalent to L/77).

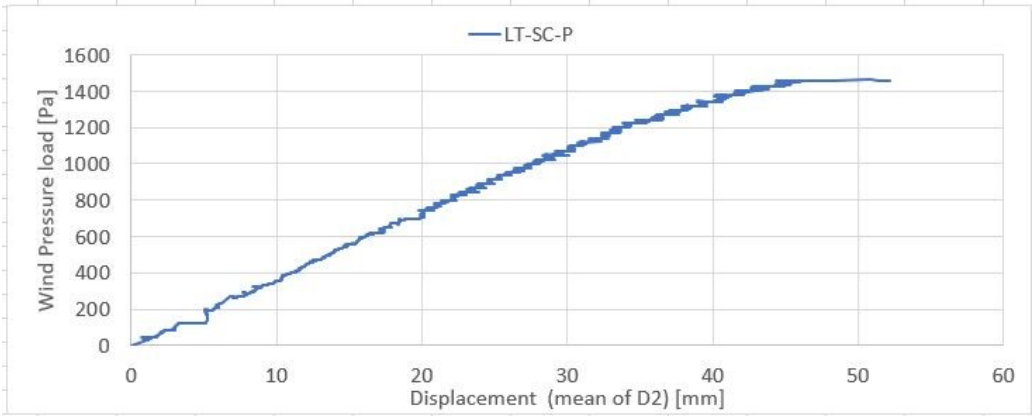


Figure 3.36 Load-displacement curve of the LT-SC-P liner tray

Displacements of the LT-SC-P liner tray measured during the test to wind pressure are illustrated in Figure 3.37. From the recordings of the mid-span transverse LVDTs, it may be observed that the LT-SC-P liner tray had similar deflections in the cross-section up to the moment the loading pressure reached $0.7 \cdot P_{max}$ value. It was only before failure when, west side of the wide flange started

to have a small difference (4 mm difference) compared to the east side of the wide flange (across the mid-span in the longitudinal direction).

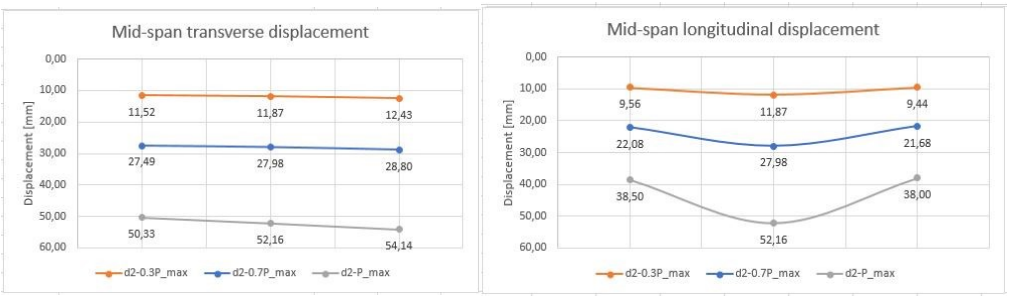


Figure 3.37 Displacements of the LT-SC-P liner tray during the test

In the case of testing wind pressure on simple-closed liner trays (LT-SC-P) the failure occurred by local buckling of the upper flange combined with the local buckling and distortion of the webs, as presented in Figure 3.38 and Figure 3.39. The failure occurred at the mid-span of the liner tray, right near the fixation of the upper flange. Also, a flange curling may be identified in the wide flange of the liner tray (see Figure 3.39-right).

Figure 3.38 LT-SC-P liner tray specimen after failure: showing failure at mid-span

Figure 3.39 Detail of the failure zone on both sides of the liner tray: interaction between local+distortional buckling of the narrow flange and local+distortional buckling of the websRestrained-opened liner trays

### *3.4.1.4 Restrained-opened liner trays*

Figure 3.40 shows the load-displacement curve of the restrained-opened liner tray subjected to wind pressure. The maximum load value recorded immediately before failure was 2331.60 Pa, significantly higher (more than 2.2 times higher) than the maximum load recorded in simple-opened liner trays. The displacement value (displacement transducers in the transverse direction) recorded immediately before failure was 64.35 mm (L/62), almost double than the average values recorded by the transducers of the LT-SO-P liner tray.

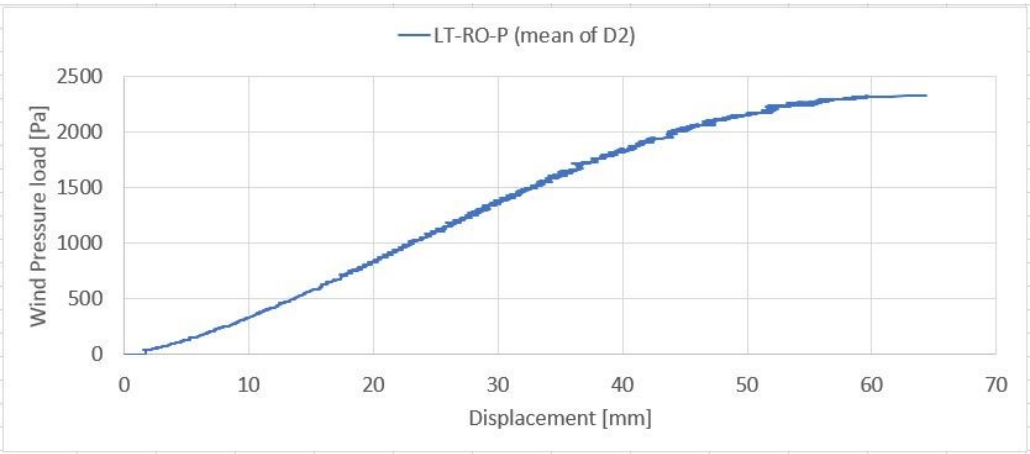


Figure 3.40 Load-displacement curve of the LT-SC-P liner tray

Displacements of the LT-RO-P cross-section at the mid-span of the liner tray measured during the test are illustrated in Figure 3.41. The transducer recordings show that the LT-RO-P liner tray had a non-symmetrical deflection behaviour in the cross-section up to a pressure load of 0.7·Pmax. Before failure the deflections of the cross-section of the liner tray (mid-span transverse displacement - Figure 3.41-left) reached similar values.

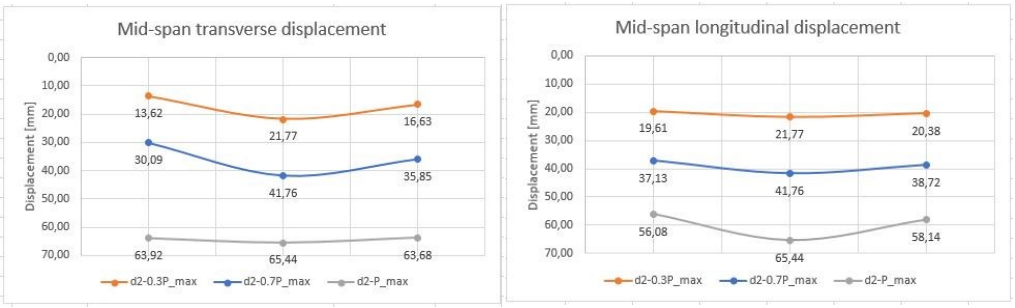


Figure 3.41 Deformations of the LT-RO-P liner tray during the test

In the case of testing wind pressure on restrained-opened liner trays (LT-RO-P) the failure occurred by local buckling of the upper flange along with web crippling. The local buckling and distortion of the webs, as well as the local buckling and distortion of the narrow flanges, are shown in Figure 3.42 and Figure 3.43. The failure occurred at the mid-span of the liner tray, close to the fixation of the upper flange. At the same time, a flange curling occurred in the wide flange of the liner tray.


Figure 3.42 LT-RO-P liner tray after failure: showing failure at mid-span

Figure 3.43 Detail of the failure zone of the liner tray: interaction between local+distortional buckling of the narrow flange and local+distortional buckling of the webs

### *3.4.1.5 Restrained-closed liner trays*

Figure 3.44 shows the load-displacement curve of the restrained-closed liner tray subjected to wind pressure. The maximum load value recorded before failure was 2416.07 Pa, slightly higher (3.5% higher) than the maximum load recorded in restrained-opened liner trays, showing that the contribution of the outer cladding in the global behaviour of restrained liner tray is negligible. The mid-span displacement value recorded immediately before failure was 66.36 mm (L/60), value which is similar to the value recorded in case of the LT-RO-P specimen (64.35 mm).

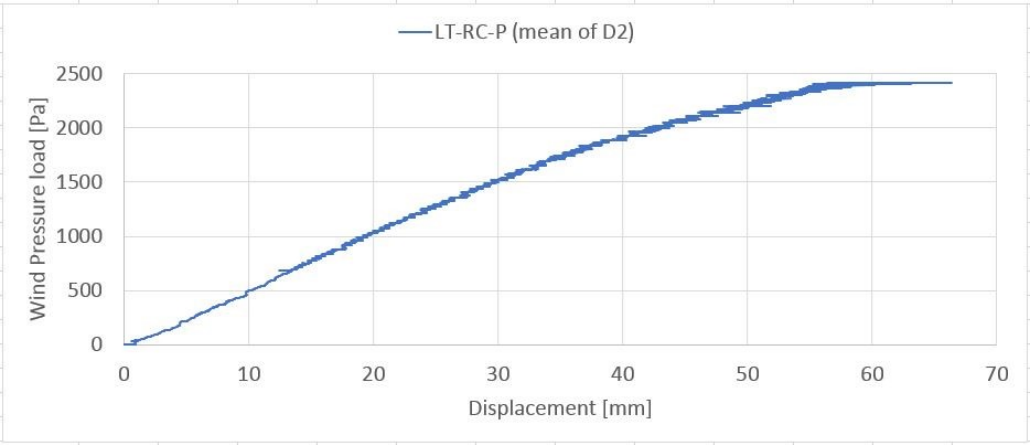


Figure 3.44 Load-displacement curve of the LT-RC-P specimen

Displacements of the LT-RC-P cross-section at the mid-span of the liner tray measured during the test are illustrated in Figure 3.45. From the recordings of the displacement sensors, it may be observed that the LT-RC-P liner tray had a symmetrical deflection behaviour in the cross-section up to the moment the loading pressure reached $0.7 \cdot P_{max}$ value, similar to the behaviour of LT-SC-P liner tray. Immediately before failure, the deflections of the cross-section of the liner tray (mid-span transverse displacement - Figure 3.45-left) reached a linear difference of about 8 mm between $D_{21}$ (east) and $D_{23}$ (west) positions - see the position of the displacement transducers in Figure 3.26.

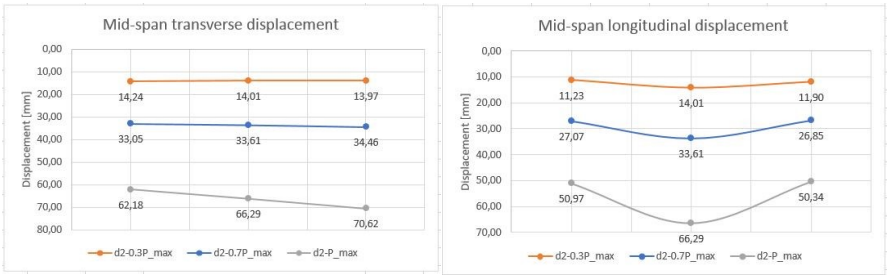


Figure 3.45 Deformations of the LT-RC-P liner tray during the test: mid-span transverse displacement (left) and mid-span longitudinal displacement (right)

The restrained-closed liner trays (LT-RC-P) were tested on wind pressure and due to their configuration represent the most appropriate to real conditions of service. The failure of the tested setup, also due to local buckling, was observed at the level of the compression web zone and connected narrow flange. A web crippling appeared at the mid-span of the liner tray, causing the final failure (see Figure 3.46 and Figure 3.47-left). Also, local buckling of the wide flange in the support area was visible, as shown in Figure 3.47-right.

Figure 3.46 LT-RC-P liner tray specimen after failure: showing failure at mid-span

Figure 3.47 Detail of the failure zone of the liner tray: web crippling (left) and wide flange local buckling in the support area (right)

### 3.4.2 Experimental results of liner trays subjected to wind suction

When subjected to wind suction, liner trays have the wide flange under compression and narrow flanges in tension. The failure of specimens presents, in general, a non-symmetrical pattern, similar to the case of the liner trays subjected to wind pressure, definitely showing the influence of the non-symmetric cross-section of the liner trays. The non-symmetrical failure pattern had more pronounced collapse effects on one lateral side, also similar to the wind pressure case, but higher deformability was observed for wind suction tests on the liner tray than in the liner trays tested for wind pressure. The failure pattern occurred near the compressed fibber of the section, namely the upper part of the liner tray (in the wind suction tests the tray sections were practically rotated by 180 degrees).

#### *3.4.2.1 Simple-opened liner trays*

Figure 3.48 shows the load-displacement curve of the simple-opened liner tray subjected to wind suction, considering the average values recorded by the three wire displacement transducers placed at the mid-span of the liner tray (captors D2.1, D2.2, and D2.3). The maximum load value recorded immediately before failure was 1044.27 Pa (smaller by 4% than in the case of the same setup tested to wind pressure – see section 3.4.1.1). The displacement value recorded immediately before failure was 104.75 mm, three times higher than in the case of the simple-opened liner tray subjected to wind suction.

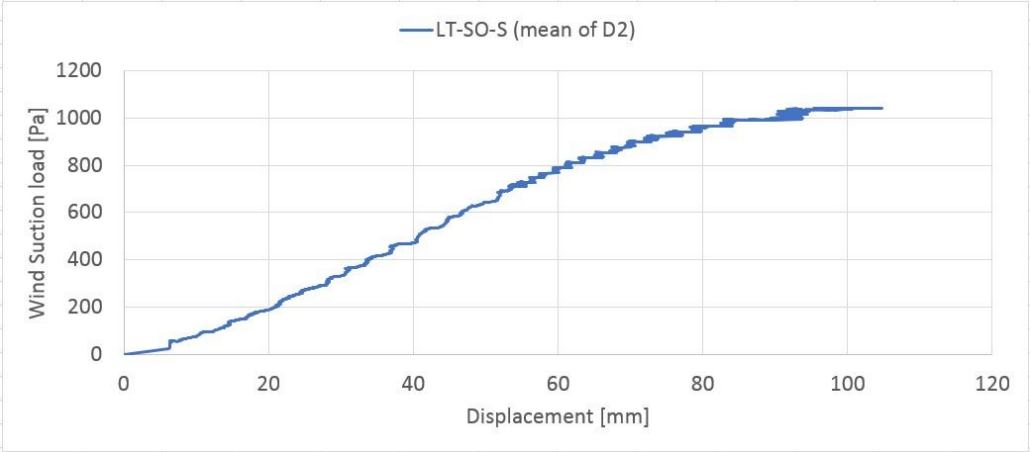


Figure 3.48 Load-displacement curve of the LT-SO-S specimen

Displacements of the liner tray measured during the test to wind pressure are illustrated in Figure 3.49. In the same way as in previous study cases, the displacements were monitored continuously by nine wire displacement transducers (detailed in section 3.3.2 and Figure 3.36) located on the upper part of the wide flange. The graphics show the displacements recorded at $0.3 \cdot P_{max}$, at $0.7 \cdot P_{max}$, and at $P_{max}$, the last recorded value immediately before failure, in both transverse and longitudinal directions. The non-symmetrical pattern in the behaviour of the liner tray can be clearly seen in the mid-span transverse displacement figure (presented in Figure 3.49-left): the deformations were almost symmetrical on both sides (east and west) until before the pressure reached $P_{max}$, when the west side of the specimen gained a significant deformation. It was due to the local buckling of the western side of the wide flange in compression that the failure occurred. Displacements in the longitudinal direction were relatively symmetric, the specimen having a parabolic shape deformation up to the failure moment.

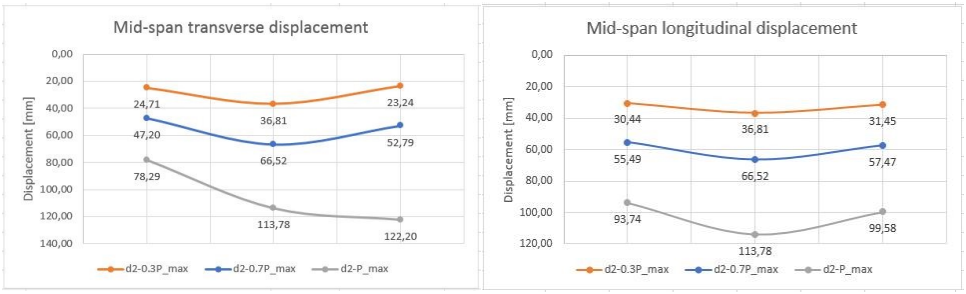


Figure 3.49 Deformations of the LT-SO-S liner tray during the test: mid-span transverse displacement (left) and mid-span longitudinal displacement (right)

In the case of testing wind suction on simple-opened liner trays (LT-SO-S) the failure was determined by the local buckling of the compressed wide flange combined with local buckling of the compressed area of the web, as presented in Figure 3.50 and Figure 3.51. The failure occurred at the mid-span of the liner tray and had a non-symmetrical pattern, as in the case of the simple-opened liner trays subjected to wind pressure.

Figure 3.50 LT-SO-S specimen after failure: typical non-symmetric failure at mid-span


Figure 3.51 Detail of the failure zone: local buckling of the area under compression

### *3.4.2.2 Simple-closed liner trays*

Figure 3.52 shows the load-displacement curve of the simple-closed liner tray subjected to wind suction. The maximum load value recorded immediately before failure was 1379.57 Pa (smaller than in the case of the same setup tested to wind pressure – see section 3.4.1.3, where the failure occurred immediately after a pressure of 1462.61 Pa was recorded in the vacuum chamber). The displacement value recorded immediately before failure was 111.21 mm, two times higher than in LT-SC-P case. Interestingly, there is also an unexpected increase of the stiffness when the pressure reached 600 Pa (about half of the maximum pressure value recorded before failure).

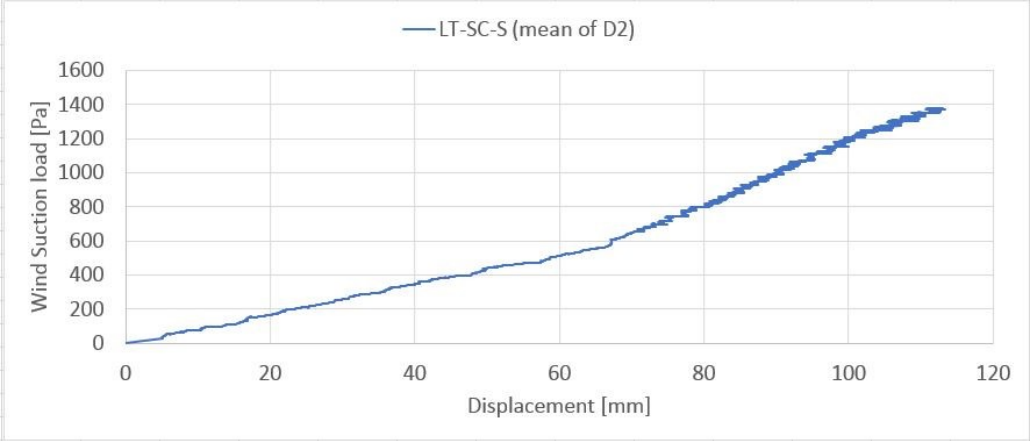


Figure 3.52 Load-displacement curve of the LT-SC-S liner tray

The displacements of the LT-SC-S liner tray measured during the test to wind pressure are illustrated in Figure 3.53. From the recordings of the mid-span transverse displacement sensors, it may be observed that the LT-SC-S liner tray had similar deflections, on both western and eastern sides, in the cross-section up to the moment the loading pressure reached 0.3·Pmax value, after when the non-symmetrical behaviour started to strengthen. Compared to LT-SC-P specimen, in this case (simple-closed liner tray subjected to suction), the mid-span displacements, in both transverse and longitudinal directions are 2 to 3 times higher, while the maximum load pressure recorded similar values in both cases.

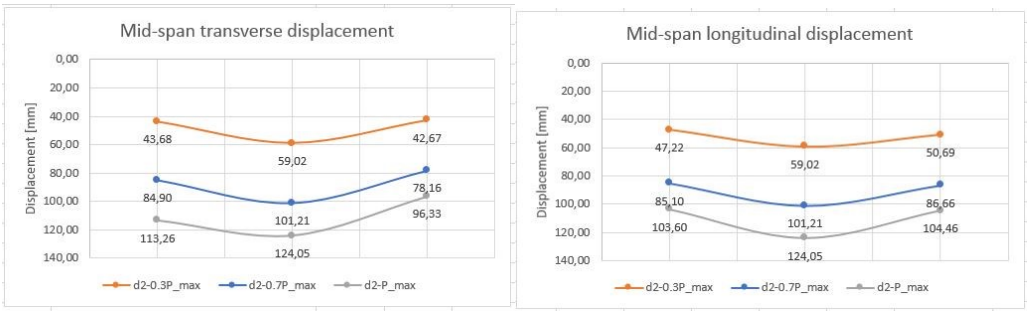


Figure 3.53 Deformations of the LT-SC-S specimen during the test: mid-span transverse displacement (left) and mid-span longitudinal displacement (right)

In the case of testing wind suction on simple-closed liner trays (LT-SC-S) the failure occurred by local buckling of the wide flange interacting with distortional and local buckling of the web, as presented in Figure 3.54 and Figure 3.55.


Figure 3.54 LT-SC-S liner tray specimen after failure: typical non-symmetric failure at mid-span

Figure 3.55 Detail of the failure zone of the liner tray: local buckling of the wide flange interacting with local+distortional buckling of the web (left) and flattening of the corrugated steel sheet in the support area (right)

The failure occurred at the mid-span of the liner tray, close to the fixation of the corrugated steel sheet with the upper flange. Also, a flattening of the corrugated steel sheet may be identified in the support area (see Figure 3.55-right).

### *3.4.2.3 Restrained-opened liner trays*

Figure 3.56 shows the load-displacement curve of the restrained-opened liner tray subjected to wind suction. The maximum load value recorded immediately before failure was 2585.06 Pa, significantly higher (almost two times higher) than the maximum load recorded in simple-opened liner trays, and with 10% higher than in the case of LT-RO-P liner trays. The average displacement value of the mid-span displacement transducers recorded immediately before failure was 107.27 mm, similar to the average values recorded by the displacement sensors of the LT-SO-S specimen (104.75 mm), but significantly higher than the average values recorded for the LT-RO-P specimen (64.35 mm).

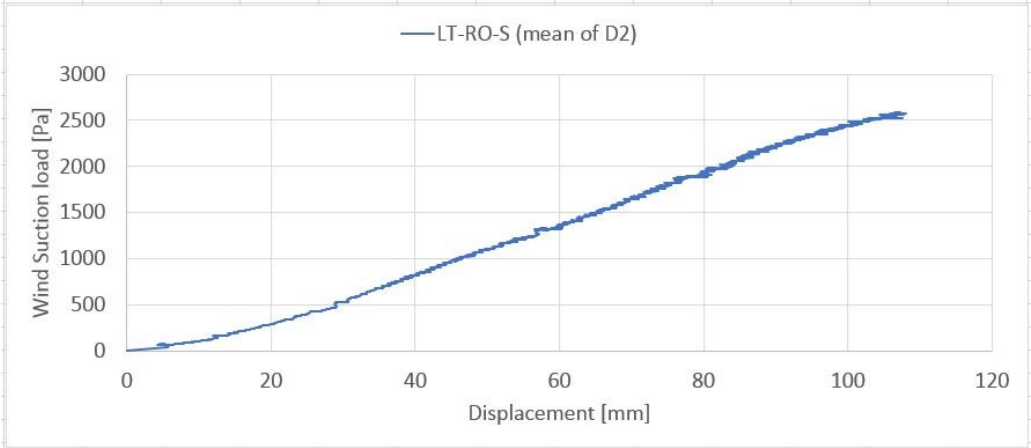


Figure 3.56 Load-displacement curve of the LT-RO-S specimen

The displacements of the LT-RO-S cross-section at the mid-span of the liner tray measured during the test are illustrated in Figure 3.57. From the recordings of the displacement transducers, it may be observed that the LT-RO-S specimen had a non-symmetrical deflection behaviour in the cross-section, in contrast to the LT-RO-P liner tray where before failure, the deflections of the cross-section of the liner tray (mid-span transverse displacement - Figure 3.52-left) recorded similar values.

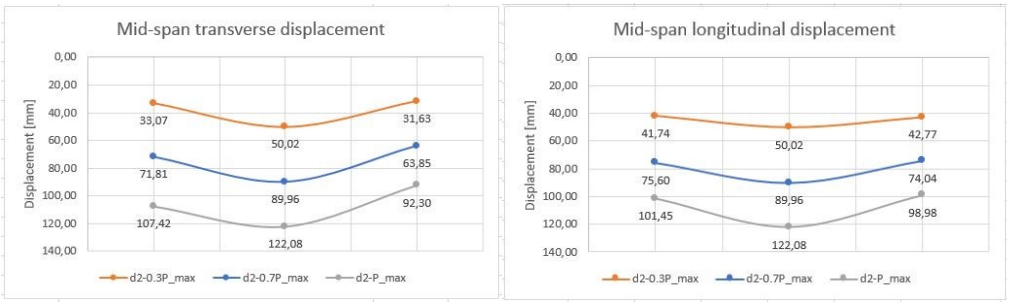


Figure 3.57 Deformations of the LT-RO-S liner tray during the test: mid-span transverse displacement (left) and mid-span longitudinal displacement (right)

In the case of testing wind suction on restrained-opened liner trays (LT-RO-S specimen) the failure occurred by local buckling of the wide flange along with local buckling and distortion of the web. General view and details of the failure zone of the liner tray are shown in Figure 3.58 and Figure 3.59. The failure occurred at the mid-span of the liner tray, presenting a typical non-symmetric behaviour in the cross-section.


Figure 3.58 LT-RO-S specimen after failure: typical non-symmetric failure at mid-span

Figure 3.59 Detail of the failure zone of the liner tray: interaction between local+distortional buckling of the web and local buckling of the wide flange

### *3.4.2.4 Restrained-closed liner trays*

Figure 3.60 shows the load-displacement curve of the restrained-closed liner tray subjected to wind suction. The failure load was 2219.11 Pa, smaller (with 15% smaller) than the maximum load recorded in the case of restrained-opened liner trays (2585.06 Pa) subjected to wind suction, showing one more time that the contribution

of the outer cladding in the global behaviour of restrained liner tray is negligible. The displacement value recorded immediately before failure was 87.61 mm, also smaller than the values recorded in the case of the LT-RO-S liner tray (107.27 mm).

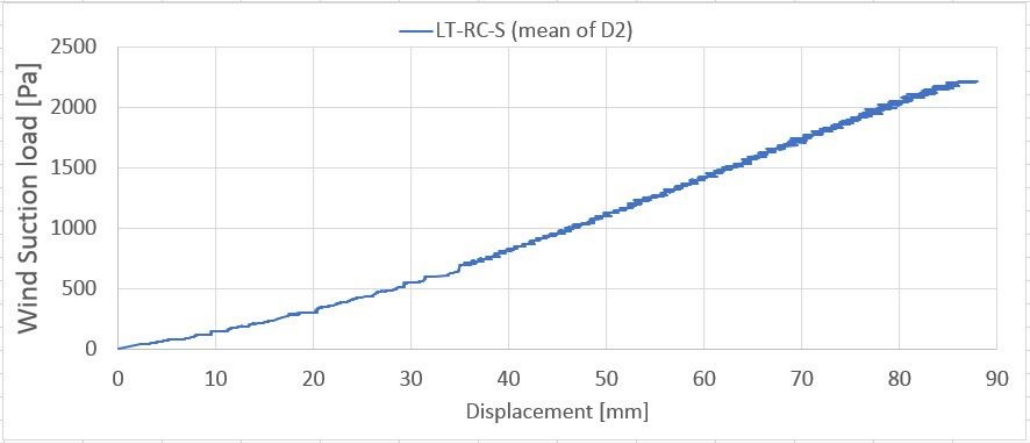


Figure 3.60 Load-displacement curve of the LT-RC-S liner tray

Displacements of the LT-RC-S cross-section at the mid-span of the liner tray measured during the test are illustrated in Figure 3.61 for both transverse and longitudinal directions. From the recordings of the displacement sensors, it may be observed that the LT-RC-S liner tray had a non-symmetrical deflection behaviour in the cross-section, similar to the behaviour of all liner trays tested to wind suction.

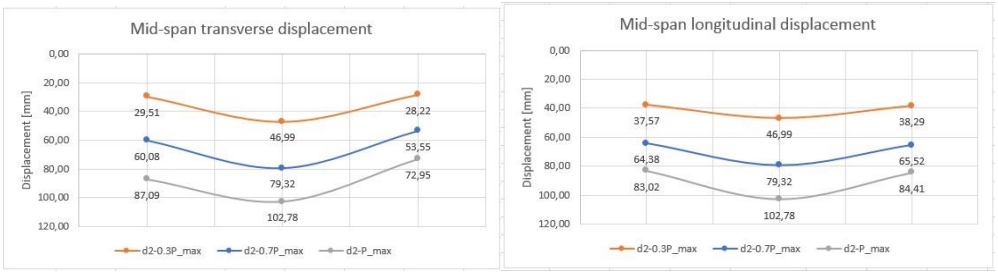


Figure 3.61 Deformations of the LT-RC-S specimen during the test: mid-span transverse displacement (left) and mid-span longitudinal displacement (right)

The restrained-closed specimen tested on wind suction (LT-RC-S) was the most appropriate setup tested for the real conditions of service. The failure of the specimen was due to the local buckling of the wide flange and local buckling of the compression web zone (Figure 3.62). A web crippling appeared at the mid-span of the liner tray (see Figure 3.63-right), similar to the other specimens subjected to suction.


Figure 3.62 LT-RC-S specimen failure at mid-span

Figure 3.63 Detail of the failure zone of the liner tray: interaction between local+distortional buckling of the wide flange and web crippling

### 3.4.3 Comparison of experimental results

Supplementary photos of the tested liner trays and failure details may be seen in Annex Annex A1.

Figure 3.64 and Figure 3.65 show the comparison of the load-displacement curves as resulted from the experimental investigation of liner tray specimens subjected to wind pressure and wind suction, respectively.

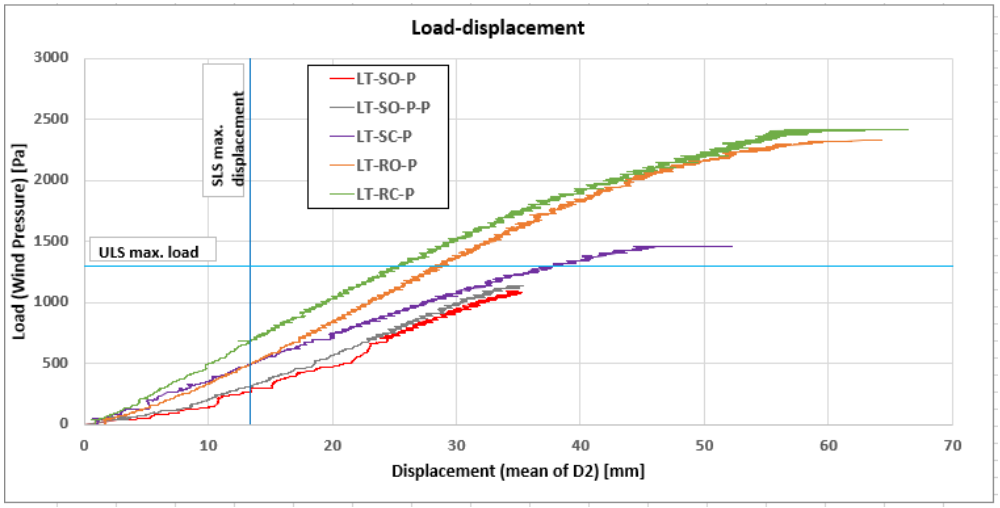


Figure 3.64 Load-displacement chart for tested liner trays subjected to wind pressure (wide flange in tension)

On the chart, the maximum allowed deflection at the serviceability limit state (SLS: L/300) and the maximum allowed pressure at the ultimate limit state (ULS) were indicated. These markings highlight the rather conservative design approaches recommended by [131], with design load values within the safe range.

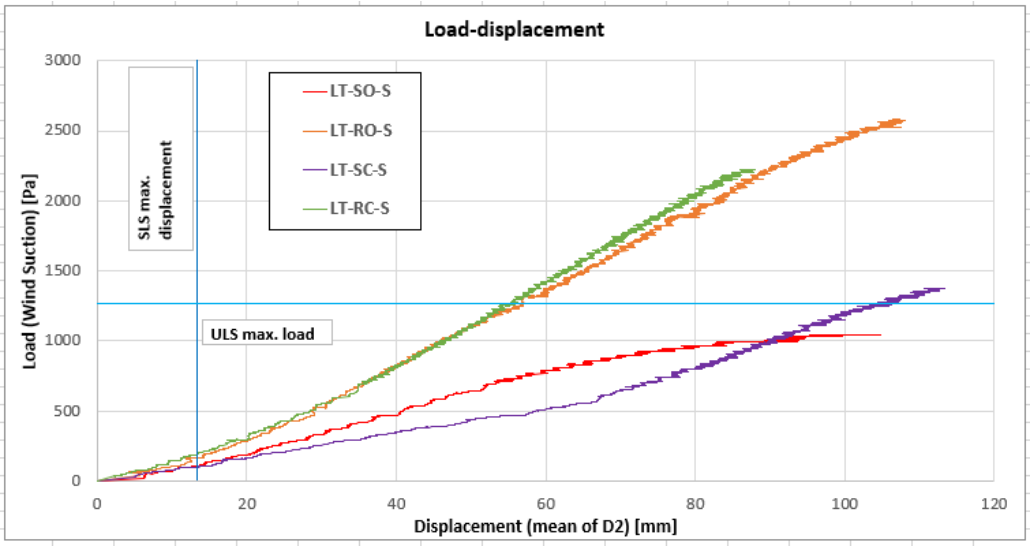


Figure 3.65 Load-displacement chart for tested liner trays subjected to wind suction (wide flange under compression)

Figure 3.64 and Figure 3.65 reveal that the SLS criterion is definite in the elastic zone of the tested liner trays. Moreover, the restrained liner trays reach more

than double load bearing resistances (in both cases – pressure and suction tests), when compared to simple liner trays.

From Figure 3.64 and Figure 3.65 it can be seen that the ULS criterion is not reached for simple opened liner trays. However, this is not the case for a liner tray configuration under real service conditions, because these elements do not work independently in a liner tray cladding system.

Table 3.4 shows a comparison between results recorded during the experimental investigation of liner trays subjected to wind loads (uniform pressure) and the design load values (see section 3.2.1 of this paper) of the liner trays, including the maximum allowed ULS pressure, according to [131].

The values for $P_{code}$ shown in Table 3.4 were determined as follows:

$$P_{code} = \frac{8 \cdot M_{Rd}}{b_u \cdot L^2}, \tag{3.94}$$

where:

$M_{Rd}$: - the moment resistance of a liner tray: $M_{b,Rd}$ for liner trays with wide flange in tension – see eq. (3.92) or $M_{c,Rd}$ for liner trays with wide flange under compression – see eq. (3.23)

$b_u$: - the width of the wide flange of the liner trays; $b_u$ = 600 mm (see Figure 3.3)

$L$: - the length of the liner trays between supports; L = 4000 mm (see Figure 3.2)

Table 3.4 Comparison between design values acc. to [131] and experimental values

| Specimen | Design load, $P_{code}$ [kN/m$^2$] | Allowed SLS deflection L/300 [mm] | Ultimate load $P_{exp}$ [kN/m$^2$] | Ultimate deflection [mm] | Strength ratio ($P_{exp}/P_{code}$) |
|---|---|---|---|---|---|
| LT-SO-P | - | 13.33 | 1.087 | 35.93 | - |
| LT-SO-PP | - | | 1.135 | 34.78 | - |
| LT-SC-P | 1.302 | | 1.462 | 52.21 | 1.12 |
| LT-RO-P | | | 2.331 | 64.35 | 1.79 |
| LT-RC-P | | | 2.416 | 66.36 | 1.85 |
| LT-SO-S | 1.266 | | 1.044 | 104.75 | 0.82 |
| LT-SC-S | | | 1.379 | 111.21 | 1.08 |
| LT-RO-S | | | 2.585 | 107.27 | 2.04 |
| LT-RC-S | | | 2.219 | 87.61 | 1.75 |

In Table 3.4 the design pressure load, $P_{code}$, is missing for single-opened liner trays (LT-SO-P) and pinned single-opened liner trays (LT-SO-P-P) subjected to wind pressure because the standard EN 1993-1-3 provides for the calculation of the bending moment of liner trays with narrow flanges under compression, a fixing

distance $s_1$ only up to 1000 mm ($s_1$ is the longitudinal spacing of fasteners supplying lateral restraint to the narrow flanges – see Figure 3.19-c) and Section 3.2.1.6 of this thesis). For distances larger than 1000 mm, the EN 1993-1-3 standard does not provide a procedure for the calculation of the moment resistance of a liner tray. According to [144], a calculation method that improves the coefficient $\beta_b$ (the influence of $s_1$) and extends the application range of this coefficient for distances greater than 1000 mm was established, but the calculation model has not yet been transferred to the European Codification. In the experimental tests, the LT-SO-P and LT-SO-P-P liner trays did not have the narrow flanges stabilised against lateral buckling by connections, therefore in these cases, $s_1$ would be equal to the distance between the supports of the liner trays (4000mm), a distance larger than the allowed distance accepted by the EN 1993-1-3 standard's procedures. In these two tests $P_{exp}$ did not exceed the design load ($P_{code}$), showing that the ultimate positive bending moment of the tested liner trays subjected to wind pressure (generally determined by the ultimate compression forces of the narrow flanges) is smaller than the moment resistance determined according to EN 1993-1-3 standard (see Section 3.2.1.6 of this thesis) for the fixing distance of the connections between the liner tray and the outer cladding $s_1$ = 500 mm. Yet again, this configuration does not represent a configuration under real service conditions, as in a liner tray cladding system the liner trays are restrained by outer sheeting and they are also connected together, having a double-web system and forming a rigid metallic cellular structure. At the same time, the EN 1993-1-3 standard does not provide a different design procedure for the calculation of the moment resistance for restrained liner trays.

Table 3.4 shows that $P_{exp}$ values for restrained specimens (the test configuration which is the closest to the real conditions of service) are up to 1.85 times higher than $P_{code}$ in both cases (tests to wind pressure and tests to wind suction), which concludes that the current design rule in determining the bending moment capacity of liner trays according to EN 1993-1-3 [131] is rather conservative (indicated as well by the large values obtained for the experimental per design strength ratio: i.e. $P_{exp}$ / $P_{code}$ = 1.75,…,2.04).

As can be seen in Table 3.4, the maximum load value recorded immediately before failure was generally higher in cases of liner tray specimens subjected to wind pressure (wide flange in tension) but with values close to each other for the same test configuration (i.e., LT-SC-P compared to LT-SC-S). In terms of ultimate deflections, when subjected to wind suction all specimens recorded significantly higher displacement values in comparison with the same setups subjected to wind pressure.

Table 3.5 presents a comparison between stiffness within design values determined according to EN 1993-1-3 [130] and stiffness established through experimental tests.

The values for stiffness established through experimental tests were determined as follows:

$$S_{exp} = \frac{0.7 \cdot P_{max} - 0.3 \cdot P_{max}}{\delta_{0.7 \cdot P_{max}} - \delta_{0.3 \cdot P_{max}}}, \tag{3.95}$$

where:

$P_{max}$: the maximum load value recorded immediately before failure

$\delta_{0.7 \cdot P_{max}}$: the average cross-section deflection at the mid-span of the liner tray when the value of $0.7 \cdot P_{max}$ was reached

$\delta_{0.3 \cdot P_{max}}$: the average cross-section deflection at the mid-span of the liner tray when the value of $0.3 \cdot P_{max}$ was reached.

The values for stiffness within design values determined according to EN 1993-1-3 [130] were calculated as follows:

$$S_{code} = \frac{q}{\delta_{max}} = \frac{P_{code} \cdot b_u}{\frac{5}{384} \cdot \frac{q \cdot L^4}{E \cdot I_{y,eff}}}, \tag{3.96}$$

where:

$P_{code}$: maximum allowed ULS pressure, according to [131]; see eq. (3.94)

$\delta_{max}$: maximum deflection at the mid-span of the liner tray for the value $P_{code}$, for a simply supported beam

E: elastic modulus; E=210000 N/mm$^2$

$b_u$: the width of the wide flange of the liner trays; $b_u$ = 600 mm (see Figure 3.3)

$I_{y,eff}$: the effective second moment of area of the effective cross-section of a 600/100 liner tray with the wide flange in tension (see Figure 3.13) about the y-y axis; $I_{y,eff}$ = 256323.62 mm$^4$ (determined with the use of the AutoCAD tool [156])

Table 3.5 Comparison between stiffness within design values acc. to [131] and experimental values

| Specimen | Design load, $P_{code}$ [kN/m$^2$] | Stiffness, by code $S_{code}$ [Pa/mm] | Stiffness, by experimental tests $S_{exp}$ [Pa/mm] | Strength ratio ($S_{exp}/S_{code}$) |
|---|---|---|---|---|
| LT-SO-P | - | 26.24 | 41.63 | 1.58 |
| LT-SO-PP | - | | 40.90 | 1.56 |
| LT-SC-P | 1.300 | | 36.23 | 1.38 |
| LT-RO-P | | | 50.26 | 1.91 |
| LT-RC-P | | | 49.23 | 1.87 |
| LT-SO-S | 1.275 | 26.91 | 15.27 | 0.56 |
| LT-SC-S | | | 13.92 | 0.51 |
| LT-RO-S | | | 27.95 | 1.03 |
| LT-RC-S | | | 30.18 | 1.12 |

When subjected to wind suction all tested specimens presented a smaller stiffness in comparison with the same setups subjected to wind pressure. However, when comparing the stiffness of the simple liner trays (with or without cladding), it can be seen an increase in stiffness of 20-50% for specimens subjected to wind pressure, while in the stiffness of the restrained liner trays (with or without cladding) occured an increase of 80-135%. The stiffness of specimens having the same configuration but with/without trapezoidal steel sheet are similar, showing once again that the outer cladding does not bring a significant role in the stiffness of the liner trays. Thus contribution to the load-bearing behaviour is principally made by the stiffeners of the narrow flanges.

When comparing stiffness established through experimental tests ($k_{exp}$) with the stiffness within design values determined according to EN 1993-1-3 [130] ($k_{code}$) it can be seen that for liner trays subjected to wind pressure, $k_{exp}$ exceeds $k_{code}$ with 58-87%. In the case of the liner trays subjected to wind suction, $k_{exp}$ is below values of $k_{code}$ for simple liner trays, and exceeds $k_{code}$ for restrained liner trays with 3-12%.

In order to correlate the acquired experimental results with real loading conditions, a comparison was made between peak values of pressure/suction on walls of an industrial hall and the obtained experimental values of restrained liner trays with outer cladding, as presented in Table 3.6.

Table 3.6 Comparison between peak values of pressure/suction acc. to [147] and experimental values of restrained liner trays

| Peak value of pressure / suction | $w_e$ (max) [kN/m$^2$] | Ultimate limit state (ULS) $w_{ULS}=1.5\cdot w_e$ | Ultimate load $P_{exp}$ [kN/m$^2$] |
|---|---|---|---|
| Pressure on the gable wall | +0.630 (zone D) | +0.945 | 2.416 |
| Pressure on the longitudinal wall | +0.630 (zone D) | +0.945 | |
| Suction on the gable wall | -1.080 (zone A) | -1.620 | 2.219 |
| Suction on longitudinal wall | -1.080 (zone A) | -1.620 | |

According to [147], for an industrial building located in Timisoara (Romania) with a length of 40 m, a span of 20 m, eaves height of 6 m, and ridge height of 7 m, considering an IIIrd category ground (suburban zone) and class III of importance for the construction, at the ultimate limit state (ULS) the peak values reach 0.945 kN/m$^2$ in wind pressure and 1.620 kN/m$^2$ in wind pressure (the maximum unfactored pressure values, $w_e$, determined for transversal and longitudinal wind load were multiplied with the afferent ULS partial safety factor). By examining Table 3.6, once again the conservative character of the present code model is proved, the code wind values being smaller than the experimental ones (0.538% in pressure, 0.570% in

suction). However, it should be noted that the critical condition is considered for suction rather than for pressure.

## 3.5 Material tests

In order to provide mechanical properties of the steel sheet used to manufacture the liner trays, a set of experimental tensile tests on steel coupons were carried out. The scope was to assess the material characteristics as yield stress, ultimate strength, and ductility of the investigated steel, as well as the actual thickness of the sheet used in the design and further numerical analyses.

The specimens were produced and provided in a single delivery. The results indicate that all the specimens exhibit similar properties. As a result, the overall mean values are considered representative for these specimens.

### 3.5.1 Tensile tests

Uniaxial tensile tests were performed according to SR EN ISO 6892-1:2019 provisions [158] in the UPT-CEMSIG laboratory [162]. These tests were carried out using the Zwick Z010 AllRoundLine universal testing machine (Figure 3.66) which has a maximum capacity of 10 kN and includes computer-aided control, acquisition and post-processing of the results. The coupon specimens were subjected to a monotonic tensile load according to Method A (strain rate-based tensile testing) stipulated in the ISO 6892-1:2016 code [158]. During the determination of the upper yield strength and the proof strength properties, the strain rate was kept in the range 2: $\dot{e}_{Le}$ = 0,00025 $s^{-1}$, with a relative tolerance of ±20 %, throughout the test.

Figure 3.66 Illustration of tensile testing machine

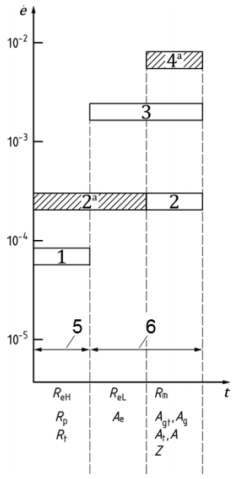


Figure 3.67 Method A - Test rate based on strain rate [158]

For these tests, three rectangular steel coupons with dimensions of 12.5x120 mm (Figure 3.68), were considered. The dimensions of the specimens were designed

considering the capacity of the test machine (10 kN). The specimens were extracted parallel to the rolling direction (longitudinal direction) from the wide flange of the liner trays.


Figure 3.68 Tensile test steel specimen

The main mechanical characteristics of the steel specimens obtained as a result of the monotonic tensile tests are summarized in Table 3.7. The tensile test results showed values of yield stress which substantially exceed the minimum values specified in the corresponding material standard; all the values of yield stress were 57% higher than the nominal values (an increase about 160-161 N/mm$^2$).

Table 3.7 Mechanical properties of the steel used for liner trays

| **Specimen** | **$f_y$ *(N/mm²)*** | | **$f_u$ *(N/mm²)*** | | **A *(%)*** | |
|---|---|---|---|---|---|---|
| | *EXP* | *ST* | *EXP* | *ST* | *EXP* | *ST* |
| T1 | 441,7 | 280 (min.) | 499,8 | 360 (min.) | 27,7 | 18 (min.) |
| T2 | 440,5 | | 495,8 | | 28,9 | |
| T3 | 441,4 | | 494,0 | | 26,0 | |
| ST – nominal values according to the provisions of the material standard EN 10346:2015 [132]<br>EXP – values determined experimentally, as results of monotonic tensile tests | | | | | | |

The results of the experimental monotonic tensile tests on steel sheet coupons, presented in terms of stress-strain diagram are shown in Figure 3.69. During tensile tests, due to grip slippage within the elastic range of the stress-strain behaviour, as well as some specific strain measurement errors, experimentally obtained stiffness is significantly lower than the nominal steel stiffness equal to 210 Mpa. To rule out this measurement inaccuracy, within further numerical simulations, the elastic stiffness was adjusted to comply with nominal elastic modulus.

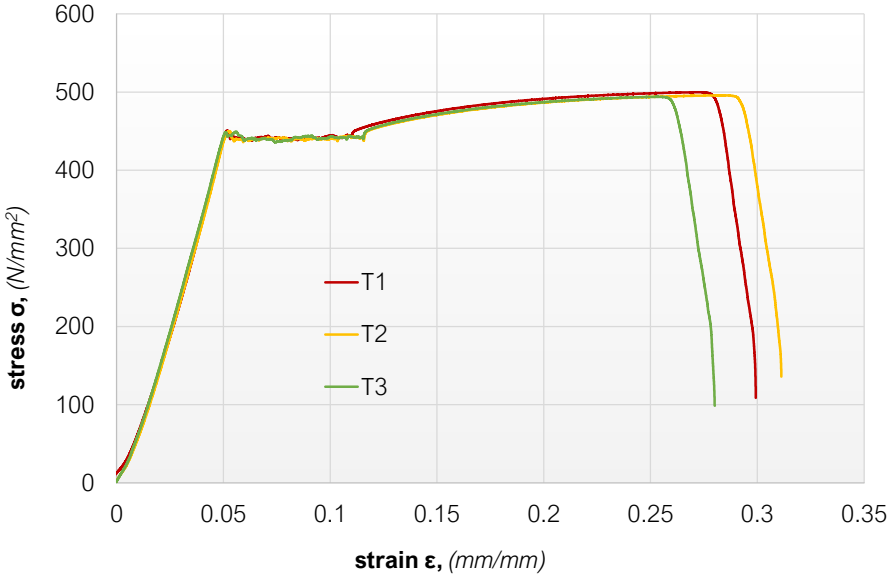


Figure 3.69 Experimental stress-strain diagrams for steel specimens subjected to monotonic tensile test

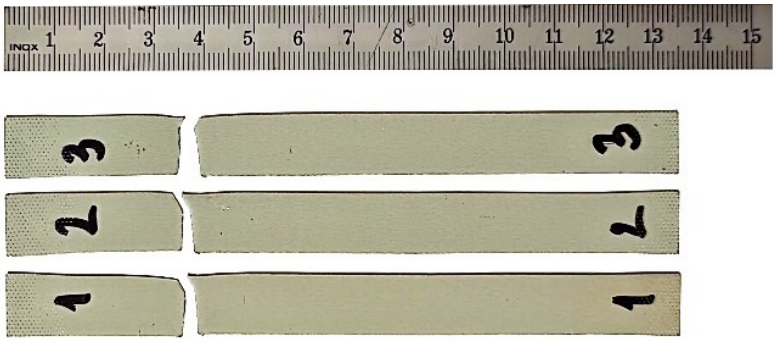

Figure 3.70 Tensile test steel specimens after failure

As can be observed both from the stress-strain diagrams (Figure 3.69) and from the image of the tested specimens after failure (Figure 3.70), due to the geometrical parameters of the specimens and the low sheet thickness, the necking phenomenon is almost absent for these steel coupons, and the fracture occurs immediately after reaching the ultimate proof strength. From this point of view, the after-necking behaviour of tested steel specimens resemble the behavior of high-strength steel. This resemblance is further indicated by the observation of high yield strength values, approximately around 440 MPa.

### 3.5.2 Nominal thickness measurement

In order to determine the nominal thickness of the steel sheet, measurements of steel specimens cut off from liner trays were performed using both electronic digital micrometere calliper measurements and scanning electron microscope measurements. The measurements were conducted in the UPT-ICER (Research Institute for Renewable Energies) laboratory [159].

For the measurements in which the electronic digital micrometre caliper was used, the paint coating was chemically removed before measurements. Figure 3.71 shows the steel sample before and after removing the paint coating. The results of the measurements showed values between 0.74 mm and 0.76 mm for steel thickness. Table 3.8 shows the result of the electronic digital micrometre calliper measurements of the specimens.

Table 3.8 Nominal thickness of steel liner trays

| | T1 | T2 | T3 | T4 | T5 | T6 | AVERAGE |
|---|---|---|---|---|---|---|---|
| Thickness [mm] | 0.75 | | | | | | |
| Actual thickness [mm] | 0,75 | 0,75 | 0,76 | 0,74 | 0,75 | 0,74 | 0,748 |

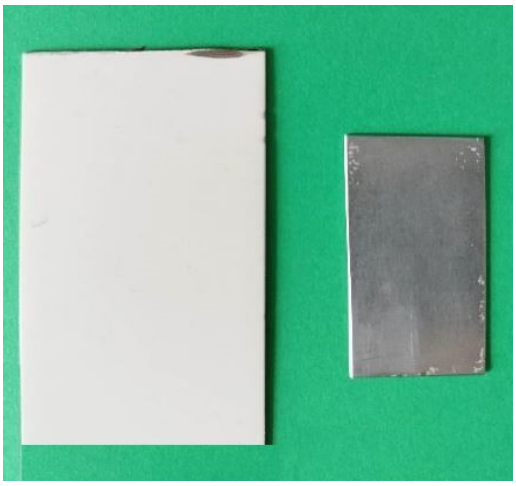

Figure 3.71 Steel sample before (left) and after (right) removing the paint coating

Additional measurements were carried out through an electron microscopy analysis. Scanning Electron Microscopy (SEM) is a test process that scans a sample (solid inorganic materials) with an electron beam to produce a high-magnified image for analysis being very effective in microanalysis and failure analysis, generating precise measures and high-resolution images. In Figure 3.72 it can be seen the steel

specimens before SEM analysis and photo-examples of thickness measurements during the SEM test.

Table 3.9 shows the scanning electron microscope test results of the specimens.

Table 3.9 Steel thickness of liner trays through SEM testing

| Specimen | Measured thickness [mm] | Average thickness [mm] |
|---|---|---|
| T1 | 0,7360 | 0,7334 |
| T2 | 0,7349 | |
| T3 | 0,7313 | |
| T4 | 0,7319 | |
| T5 | 0,7337 | |
| T6 | 0,7306 | |
| T7 | 0,7304 | |
| T8 | 0,7382 | |

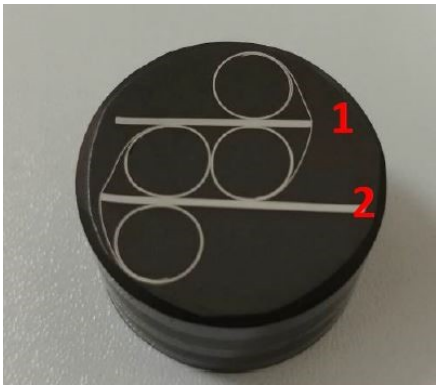


a)

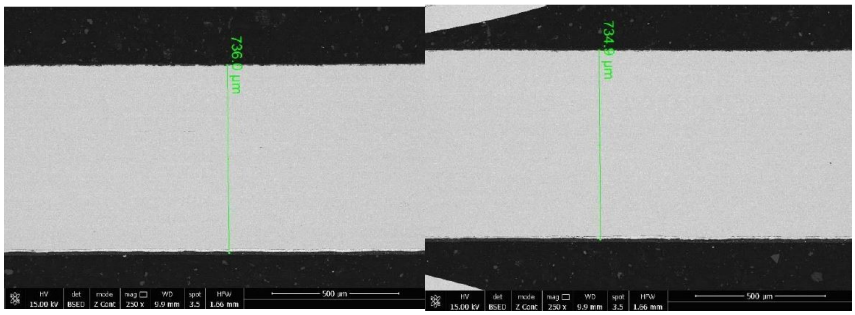

b)

Figure 3.72 SEM analysis: a) steel specimens b) example of high-resolution image and measurement during tests

The average measured thickness of the steel in the tested liner trays ($t_{average}$ = 0.7334 mm) was higher than the thickness considered by the EN 1993-1-3 standard [131], t=0.71 mm (see eq. (3.1)). Further measurements and tests were performed to obtain the thickness and the composition of the coating. Using Energy Dispersive X-ray Spectroscopy (EDX), it was determined the composition of the thin films of the coating, which is presented in Figure 3.73, while the coating thickness values were above 20 μm.

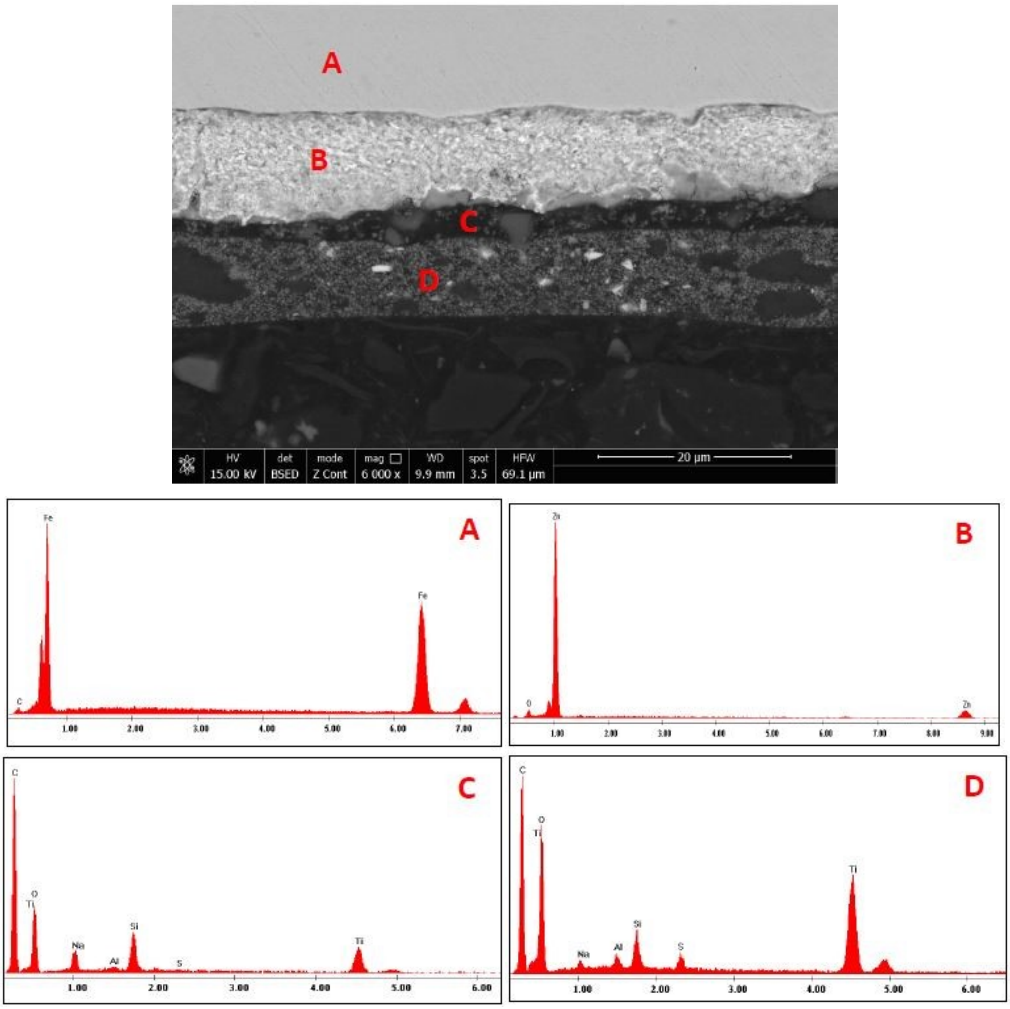


Figure 3.73 Composition and measurements of the material sample of the liner tray: A – Steel, B - Zinc, C and D – Carbon mostly, along with Titanium, Sodium, Silicon and Aluminium

## 3.6 Concluding remarks

An experimental investigation on liner trays with different test configurations subjected to wind loads was presented. To establish the lower limit of the bending moment capacity of the liner trays, tests were performed using simple liner trays without any outer cladding. Furthermore, with regard to getting the direct contribution to the limit of the bending moment capacity of the outer shell in a liner tray wall system, apart from the tests of pure liner trays, the experimental program included tests with outer cladding. Moreover, as in practice, a liner tray wall system consists of several liner trays used as an inner shell of a double shell wall system, restrained liner trays with and without outer cladding were tested to establish the ultimate moment resistance of a liner tray wall system under real conditions of service.

An accurate understanding of all constructional details and real loading conditions is crucial for creating a precise experimental model while testing elements and observing their failure behavior. The test results were categorized into two groups based on the type of wind loading, namely pressure and suction. Within each group, test results are described, observing the location and nature of failure zones.

The adjacent liner trays, which are connected along the longitudinal joint and overlap, collaborate with double-thickness webs. Additionally, the trapezoidal sheet's axial stiffness, spanning across the narrow flanges of the liner trays, which are connected by fasteners, prevents lateral deflection, torsion, or distortion of the cross-section in the event of a collapse [10]. As a result, primarily local failure modes were expected both in practical scenarios and in the experimental model of this study.

The ultimate load values showed that when subjected to wind pressure, it is not the cladding that has a paramount role in the load-bearing behaviour of a liner tray double-shell wall system, but the fasteners in the narrow flanges of the liner trays. At the same time, in the case of both types of wind loading, the double wall thickness of the restrained liner tray leads to a significantly increased load-bearing limit of the liner trays.

Comparing the results of the experimental specimens to the design values obtained following the procedure recommended by EN, the conservative design approach of the Standard, with design load values well within the safe range, was presented.

To demonstrate the efficiency of various options of liner trays, numerical investigations were performed following EN 1993-1-14:2022 [163]. The boundary conditions and outcomes of these simulations are detailed in the next chapter of the thesis.

# 4 Numerical investigation on liner trays

## 4.1 Introduction

The post-test finite element analysis on liner trays is a two-task purpose: (i) to calibrate the experimental behaviour of liner trays and (ii) to allow the assessment of certain parameters influence on liner trays subjected to real loading conditions. Therefore, as a first step, an accurate material model should be calibrated for further simulations of the liner tray model. The calibrated numerical model can be employed in further finite element (FE) parametric study, using Abaqus package software [164]. Thus, the main objective of this chapter is to provide accurate numerical models of liner trays subjected to pressure and suction, and reliable data on the influence of parameters such as thickness, height, and length on the behaviour of specimens.

## 4.2 Constitutive model of steel

### 4.2.1 Calibration of tensile response of steel material based on coupon tests

The accuracy of numerical simulations on liner trays depends on the reliability of the steel constitutive models. For the calibration of the material model were used the results obtained from the tensile tests described in section 3.5 and the mechanical properties of steel used in FEM numerical simulations is further described in Table 4.1. from section 4.2.2. One stress-strain curve was selected that considers the mean mechanical properties of the three steel specimens tested as input data set to define the characteristics of the numerical model, as presented in Figure 4.1.

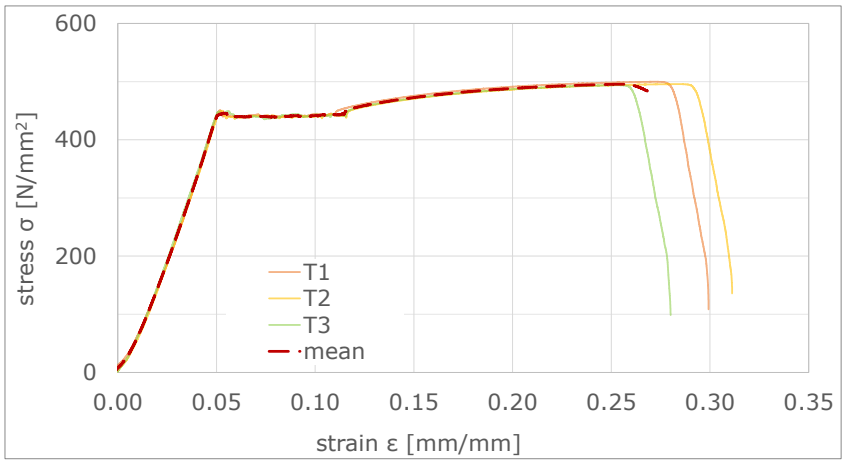


Figure 4.1 Mean Stress-strain curve obtained on tensile response of coupon tests

In the next step, a simplified engineering model was developed, considering experimental yield and proof strengths, and adjusting the elastic zone to comply with the nominal value of Young's modulus (210 MPa). The relationship between the yield strain and the fracture strain was kept according to the experimental results. The engineering stress-strain curve in this case consists of three distinct ranges, as follows:

1) $f < f_y$: elastic range, characterised by Hooke's law $\sigma = E \cdot \varepsilon$, which represents a linear behaviour;
2) $f = f_y$: yield plateau for which the behaviour of the material is characterised by constant stress;
3) $f_y \leq f \leq f_u$: strain hardening zone, which is described using a polynomial relationship, up to the necking.

The adjusted engineering stress-strain curve, which accounts for the nominal elastic modulus and the main mechanical characteristics obtained from the experimental tests, is presented in Figure 4.2. The simplified engineering model also reduces computational time due to a small amount of input values.

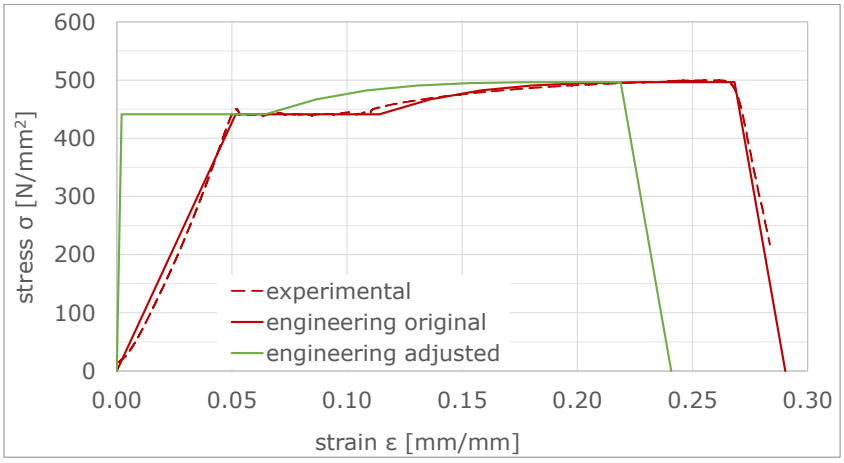


Figure 4.2 Adjusted experimental stress-strain diagram of the investigated steel

### 4.2.2 Calibration procedure of steel behaviour based on tensile tests

During conventional tensile testing, two parameters are generally measured: applied tension force and gauge length. The resulting engineering stress-strain curve does not account for any cross-sectional area changes. As described in [165], due to instantaneous variation of the cross-section area of the specimen subjected to tensile loading, the material seems to soften, while it actually hardens. Therefore, the material curve that considers the necking of the specimen and could be used for further numerical purposes is known as the true stress-strain curve. This curve coincides with the engineering curve up to the yield point. For the range $0 \leq f \leq f_u$,

the conversion of the engineering stress-strain to true (Cauchy) stress and logarithmic plastic strain should be accomplished using the following relationships [157]:

$$\sigma_{true} = \sigma_{engineering} \cdot (1 + \varepsilon_{engineering}) \quad (4.1)$$

$$\varepsilon_{true} = \ln(1 + \varepsilon_{engineering}) \quad (4.2)$$

The after-necking region of the strain-stress curve would be converted to true by means of a set of predictions of trial points (on the hardening part) using the extrapolation method [166]. As the engineering stress-strain curve reveals the failure of the specimen forthwith the reaching ultimate strength, the whole calibration procedure was limited to the application of the above relationships. Additionally, another assumption was adopted about material damage: material failure was explicitly characterised by defining the slope of almost vertical post-fracture curve (Figure 4.4).

Table 4.1 reveals the mean mechanical properties of steel from tensile tests, with adjusted elastic modulus, used for numerical material simulations.

Table 4.1 Mechanical properties of steel used in FEM numerical simulations

| **Mechanical property** | **Engineering value** | **True value** |
|---|---|---|
| Yield strength | $\mathbf{f_y}$ = 441,2 N/mm$^2$ | $\boldsymbol{\sigma_y}$ = $f_y(1+e_y)$ = 442,2 N/mm$^2$ |
| Yield strain | $\mathbf{e_y}$ = 0,0021 mm/mm | $\boldsymbol{\varepsilon_y}$ = $\ln(1+e_y)$ = 0,0021 mm/mm |
| End of yield plateau | $\mathbf{e_{sh}}$ = 0,0645 mm/mm | $\boldsymbol{\varepsilon_{sh}}$ = $\ln(1+e_{sh})$=0,0645 mm/mm |
| Ultimate strength | $\mathbf{f_u}$ = 496,5 N/mm$^2$ | $\boldsymbol{\sigma_u}$ = $f_u(1+e_u)$ = 605,2 N/mm$^2$ |
| Ultimate strain | $\mathbf{e_u}$ = 0,218 mm/mm | $\boldsymbol{\varepsilon_u}$ = $\ln(1+e_u)$ = 0,198 mm/mm |
| Rupture strength | $\mathbf{f_r}$ = 493,8 N/mm$^2$ | $\boldsymbol{\sigma_r}$ = $f_r(1+e_r)$ = 601,8 N/mm$^2$ |
| Rupture strain | $\mathbf{e_r}$ = 0,226 mm/mm | $\boldsymbol{\varepsilon_r}$ = $\ln(1+e_r)$ = 0,204 mm/mm |

In order to validate the material model calibration, a numerical simulation of the tensile test of the steel sheet specimens was performed, using Abaqus software package [164]. The specimen subjected to monotonic, quasi-static tensile loading, was modelled with 4-node shell finite elements with reduced integration (S4R). The material was defined through several characteristics, such as: density, Young's Modulus, Poisson's ratio and true stress-strain curve. Between the specimen ends and Reference Points RP1 and RP2, two corresponding *Coupling, Structural distributing* constraints were defined. The RP2 reference point was fully restrained, while an axial displacement was imposed to RP1 reference point as *Boundary Condition*, as shown in Figure 4.3. The model was meshed using *quad, structured*, 2×2 finite elements.

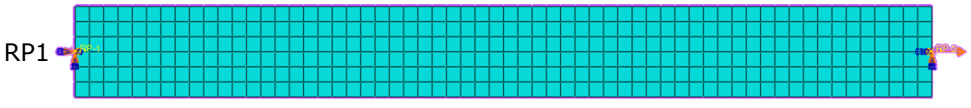


Figure 4.3 FEM model of the steel specimen subjected to tensile loading

The whole analysis was performed by means of Dynamic, Implicit solver. In order to capture the material fracture, the *Field Output* – STATUS (some failure and plasticity models, VUMAT) and SDEG (Scalar stiffness degradation) options were activated, as well as *Element deletion* option in *Mesh* Module.

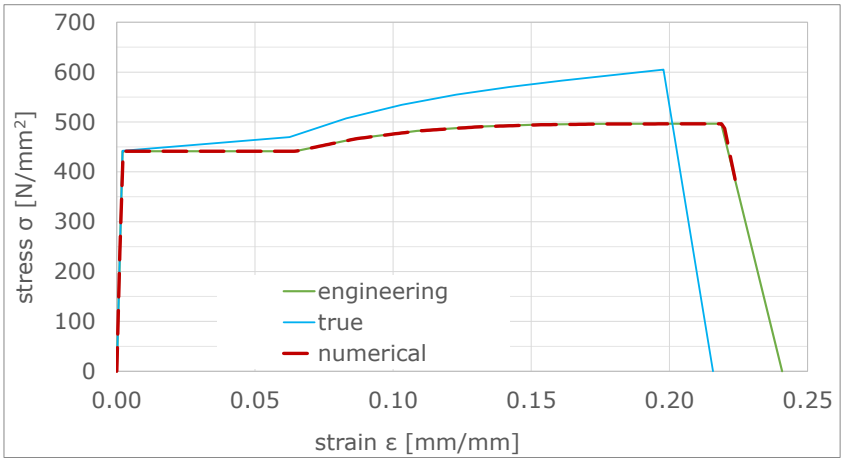


Figure 4.4 Calibration of the true stress-strain material model

Figure 4.4 reveals the output stress-strain curve obtained after the numerical simulation of the steel specimen subjected to quasi-static tensile loading. It can be observed that using the true stress-strain values as input data for the FEM model, the resulted behaviour recreates the engineering (simplified experimental) curve with a high level of accuracy. It worth noting that within the experimental test, the plastic strain distribution determined a non-symmetrical failure pattern. This phenomenon also occurs explicitly within numerical analysis, the comparison between after-fracture experimental and numerical specimens being presented in Figure 4.5.

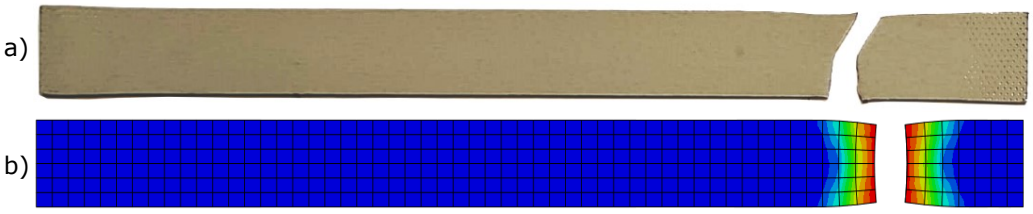


Figure 4.5 Post-test deformed experimental specimen (a) and plastic strain distribution on the deformed shape of the material FEM model (b)

Considering the results presented above in terms of the stress-strain relationship and the deformed shape of specimens subjected to tensile testing, it can be concluded that the material model obtained by means of the described calibration procedure is validated. A very good correlation between engineering and numerical

stress-strain diagrams reflects the high reliability of the constitutive model of steel, which can be used for developing FEM models of liner trays.

## 4.3 Finite element analysis of liner trays with the wide flange in tension

Considering that one of the main objectives of this study is the investigation of different features on the liner trays behaviour, it is crucially important to develop a reliable Finite Element (FE) model of liner trays, based on real material properties, real geometry, and loading conditions similar to those recorded in experimental tests. Thus, the accurate calibration of the numerical models of the liner trays is essential for further assessment.

### 4.3.1 Calibration of the FE model of liner trays

#### *4.3.1.1 Model description*

The finite element model of the liner trays subjected to equivalent wind pressure was created by means of the Abaqus software package [164]. As a first step, a *.dxf scheme of the cross-sectional shape was imported into the model, to act as the *Sketch* for *Shell extrude* feature (Figure 4.6). The part was assigned a *Homogeneous Shell* section, with a thickness equal to 0,7334 mm (according to measurements presented in Sect. 3.5.2). The mechanical properties of the steel material used are the true stress-strain values from the material model calibrated as explained in the previous section (Sect. 4.2).

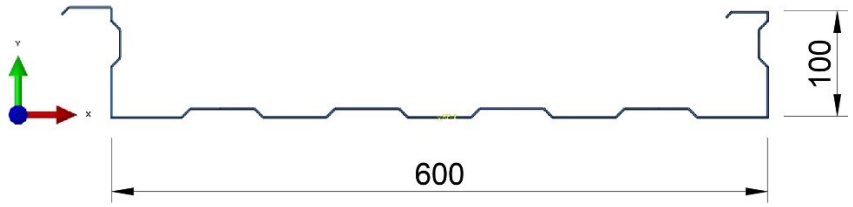


Figure 4.6 Cross-section sketch of the liner tray, imported in Abaqus CAE

The liner tray was modelled using 4-node doubly curved thin shell finite elements, with reduced integration, hourglass control, and finite membrane strains – S4R. This type of finite element, by addressing the issue as a surface problem, allows significantly reducing computational time compared with solid elements. This *shell* model allows being meshed into 10×10 mm finite elements, the bending effect being ensured as rotational DOF according to Kirchoff theory [167]. While neglecting what happens in the thickness of the element, it still provides highly accurate results in terms of surface stress or strain, and it is an appropriate model for such thin structures as liner trays.

### *4.3.1.2 Boundary conditions and applied loads*

In order to reproduce experimental boundary conditions, two node regions at the bottom of the longitudinal stiffeners were selected to act as supports (Figure 4.7). Additionally, two *Reference Points* at the ends of the liner tray were defined: RP-1 and RP-2. To each of these points, a *Kinematic Coupling* was assigned, with all 6 constrained degrees of freedom. In the next step, to each of the constraint it was imposed a *Boundary Condition*, which is detailed in Figure 4.7.

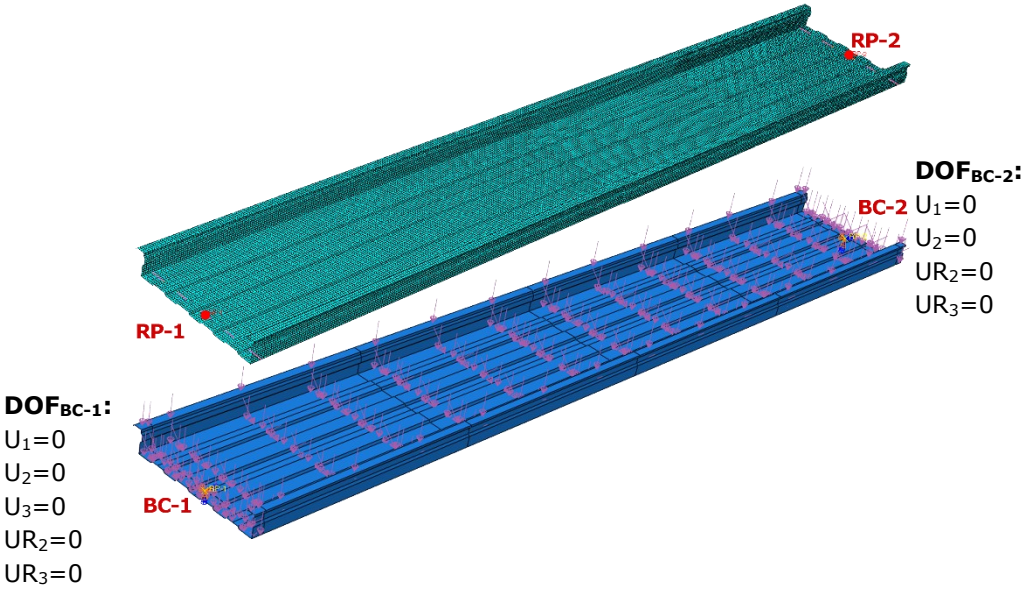


Figure 4.7 3D FEM model for liner trays, with constraints, boundary conditions and loads

The pressure load was applied as increasing uniform *pressure* on the wide and narrow flange surfaces, to ensure similarity to the experimental loading conditions. On the basis of the recorded experimental values for pressure, in the numerical model the maximum magnitude of the pressure was set to 0,001087 N/mm$^2$ (1087 Pa).

### *4.3.1.3 Equivalent geometrical imperfections*

As the liner tray are thin-walled steel members with a reduced thickness in comparison with their width/length, they are highly prone to imperfections. Thus, in the FE model of the analysed liner trays imperfections should also be included. According to [163], "for FE analysis of cold-formed structures covered by EN 1993-1-3 where imperfections are modelled, all imperfections should be modelled with equivalent geometric imperfections", which means that both the geometrical imperfections and the residual stresses should be considered. Geometric imperfections denote the modification of a structural element from its ideal geometric form and may be the result of the manufacturing process, shipping and storage, as well as the construction process [168]. Imperfections of a component may include bending, warping, and torsion, along with local deviations (dents and regular sways

of the steel plate) [169]. Residual stresses can be represented through a stress distribution originating from the manufacturing process.

According to [163] Section 5.5, when using both geometric imperfections and residual stresses, all geometric imperfections and residual stresses must be introduced simultaneously into the model. The same standard provides that for cold-formed elements covered by EN 1993-1-3, when integrating local and/or distortional buckling modes with the global mode, the suggested magnitude for the global equivalent imperfection is L/1000, with L representing the member's length (see 5.5(4) in [163], therefore in the case of the tested liner trays is obtained:

$$e_{0,global} = \frac{L}{1000} = \frac{4000}{1000} = 4 \text{ mm}, \tag{4.3}$$

The magnitude of the equivalent geometric imperfection of the outstand elements for cold-formed structures when considering local buckling, $e_{o,local}$, was determined according to Table 5.6 and Table 5.7 in [163] as:

$$e_{0,local} = \frac{b}{125} = \frac{100}{125} = 0.8 \text{ mm}, \tag{4.4}$$

where:

b: - the height of the liner tray; b = 100 mm (see Figure 3.1 and Figure 4.8)

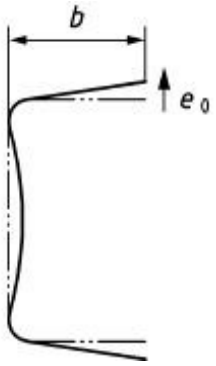


Figure 4.8 Equivalent geometric imperfections for local buckling of outstand elements for cold-formed structures [163]

The magnitude of the equivalent geometric imperfection of outstand elements for cold-formed structures when considering distortional buckling, $e_{o,dist}$ (see Figure 4.9), was determined according to Table 5.6, Table 5.7 and eq. (5.17) in [16] as:

$$e_{0,dist} = 0.3 \cdot t \cdot \sqrt{\frac{f_{yb}}{\sigma_{cr,d}}} = 0.3 \cdot 0.7334 \cdot \sqrt{\frac{440}{40}} = 0.729 \text{ mm}, \tag{4.5}$$

where:

t: -the thickness of the sheet; $t$ = 0.7334 mm; (according to measurements presented in Sect. 3.5.2)

$f_{yb}$: -the basic yield strength; $f_{yb}$ = 440 N/mm$^2$ (according to measurements presented in Sect.3.5.1)

$\sigma_{cr,d}$: -the elastic critical distortional buckling stress; $\sigma_{cr,d}$ = 40 N/mm$^2$ (see Figure 4.10)

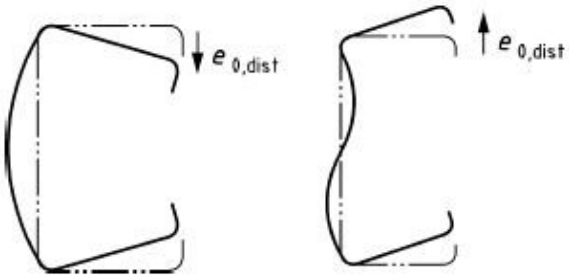


Figure 4.9 Equivalent geometric imperfections for local buckling of outstand elements for cold-formed structures [163]

The critical loads were calculated through the finite strip method, and further adopted into the design standard's equations. The elastic critical distortional buckling stress, $\sigma_{cr,d}$, was determined through a cross-section elastic buckling analysis using CUFSM finite strip analysis software [170]. When subjected to pressure (wide flange in tension) the liner tray with the cross-section described in section 3.2 and Figure 3.1 lead to an elastic critical distortional buckling stress of 40 N/mm$^2$ (see Figure 4.10).

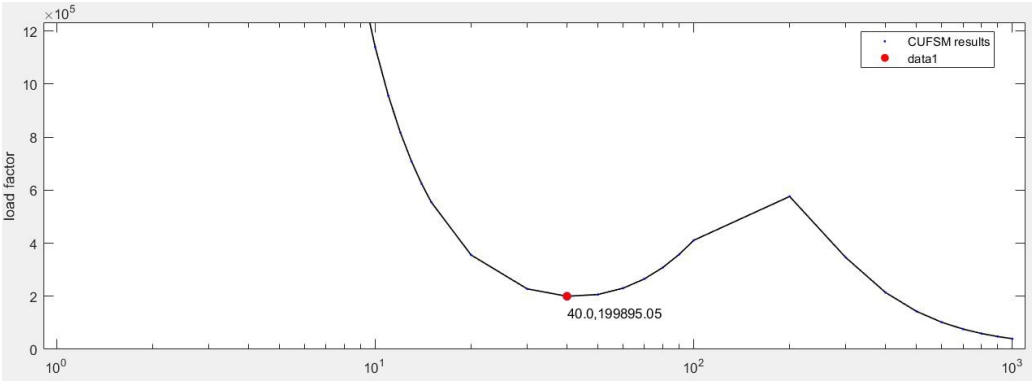


Figure 4.10 Result of elastic buckling analysis of a cross-section of the liner tray subjected to pressure using CUFSM tool

As required in [163], Section 5.5(5), combinations of local and distortional imperfections were investigated to find the most detrimental buckling mode.

Buckling mode shapes are frequently used to define initial imperfections patterns when numerically modelling components made of cold-formed steel [171], [172], [168]. In order to account for imperfections in Abaqus analyses, initially a *Linear Perturbation, Buckle* step was defined, with an output request of 50 eigenvalues. Within this step, an uniform pressure load with a magnitude of 1 N/mm$^2$, was applied on the surface of the liner tray model. The imperfection geometry was recorded into a *.fil file using the *Edit Keywords* option. In the keywords of the buckling model were added the following lines:

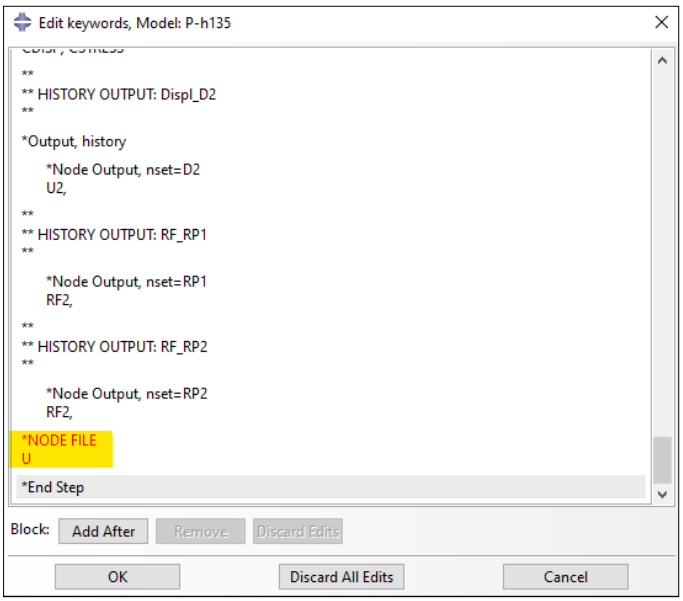


Figure 4.11 Pre-buckling "Edit keywords" option for Pressure model

As a result of buckling analysis, the 1st buckling mode was identified as the most appropriate for an accurate simulation of the global buckling mode (see Figure 4.12), while the 13$^{rd}$ buckling mode complies with distortional buckling interacting with local buckling of the liner tray model (see Figure 4.13).

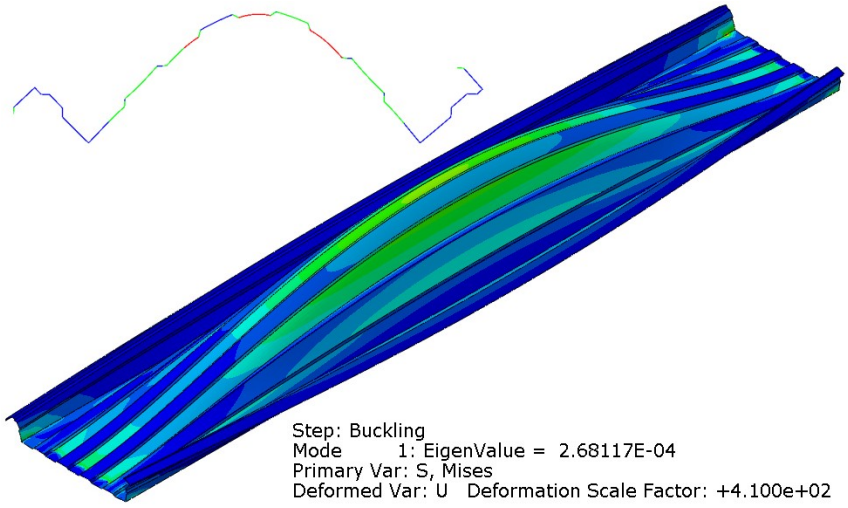


Figure 4.12 The 1st buckling mode, corresponding to the global buckling mode of the model

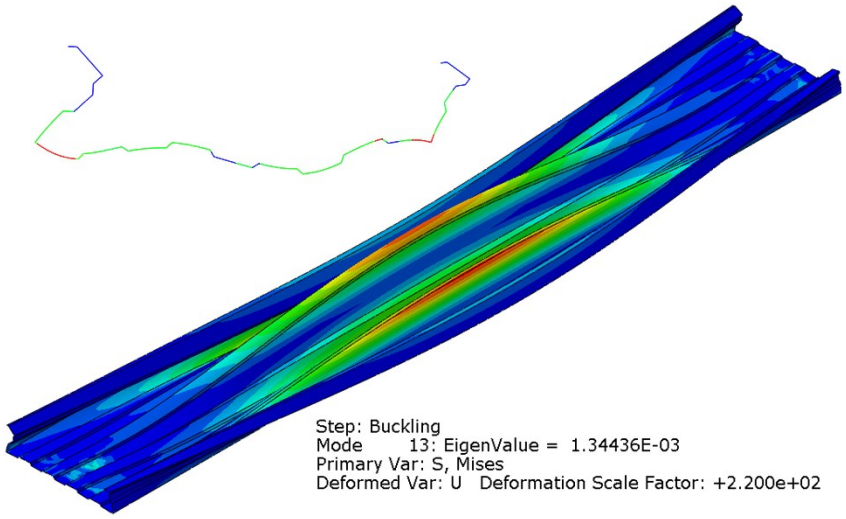


Figure 4.13 The 13rd buckling mode, corresponding to the distortional buckling interacting with local buckling mode

According to [163], when considering combinations of the imperfections for equivalent cross-section imperfections in plated structures, "the leading imperfection should be chosen first, with accompanying imperfections at amplitudes reduced to 70% of the defined value, with the remainder taken as the accompanying imperfections". However, the proposed EN 1993-1-14 was not yet adopted in the European Codification, and, due to a better accuracy of the FE model, the amplitudes of the calculated equivalent geometric imperfections accounted for in the further analysis were determined as follows:

- Determination of the multiplication factors $k_{eq}$:

$$k_{eq,global} = 0.5 \cdot (e_{0,global}/e_{FEM,global}) = 2 \quad (4.6)$$

$$k_{eq,\mathrm{dist+loc}} = 0.25 \cdot \left(\frac{e_{0,\mathrm{dist}}}{e_{FEM,\mathrm{dist}}}\right) + 0.25 \cdot \left(\frac{e_{0,\mathrm{loc}}}{e_{FEM,\mathrm{loc}}}\right) = 0.382 \quad (4.7)$$

- The deformed shape presented in Figure 4.13 shows a strain evolution in the opposite direction to the applied pressure, therefore, this buckling mode was factored into the *Static, Riks* analysis with a negative value corresponding to the calculated equivalent geometric imperfection ($k_{eq,global}$=-2). Furthermore, the 13th buckling mode corresponding to the distortional buckling that interacts with the local buckling of the finite element model was included in the further analysis by multiplying it by $k_{eq,dist\ +\ loc}$ = 0,348.
- For the effects of buckling analysis to be taken into account in *Static, Riks*, importing the *.fil file into the actual model should be done, using the same *Edit Keywords* option, as presented in Figure 4.14.

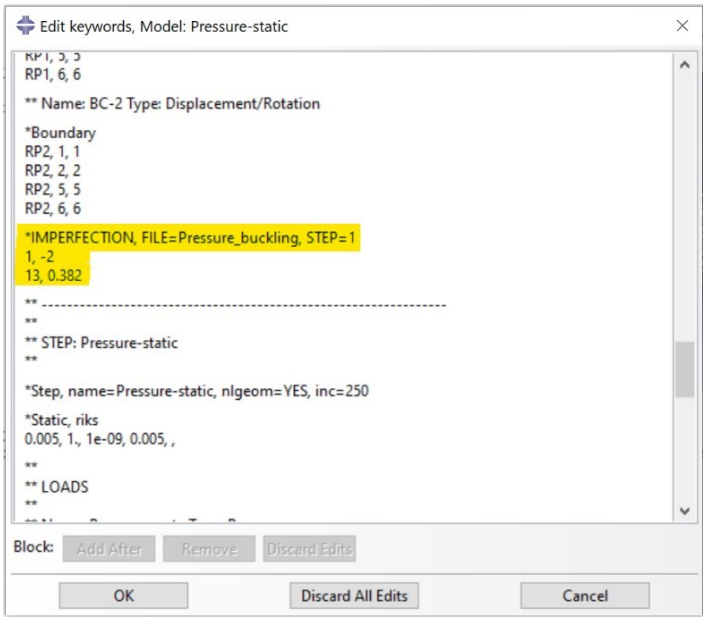


Figure 4.14 Importing imperfection geometry to the actual model using "Edit Keywords" option

As there are two buckling modes to be imported, each of them was specified together with the multiplication factor $k_{eq}$.

### *4.3.1.4 Analysis and validation*

Since the liner tray subjected to such loading conditions undergoes large deformations, the analysis was performed in Abaqus software using General

procedure, Static, Riks solver. The choice of this method at the expense of Static, General solver is justified by the nature of the problem. While both Static, General and Static, Riks steps in the Abaqus/Standard are used to solve linear static problems, they differ in the way they handle the solution process. The general static step is a general-purpose step that uses a standard linear solution algorithm to solve the problem [167]. However, in the case of liner trays, this method proved to be inappropriate because it raised convergence problems. Using the Riks method (a modified Newton-Raphson method) to solve the problem, *Static, Riks* step is useful for problems with large deformations. The Riks method can converge to a solution faster and more robustly than the standard linear solution algorithm in some cases [172], and even than *Dynamic, Implicit* or *Dynamic, Explicit* which runs slow and introduces unwanted dynamic effects. Thus, *Static, Riks* step was considered to be the most appropriate solver for the liner tray model subjected to large deformations and helped to achieve convergence.

Three steps were defined to perform the analysis: Initial, Buckling, Pressure. The boundary conditions and loading features were created in the *Initial step*, and propagated/modified in the *Pressure step*, while imperfections were added and calculated in the *Buckling step*.

As output request, the reaction forces in RP-1 and RP-2 reference points, and the mean mid-span transverse deflection (D2) was set, in order to provide the comparability between experimental and numerical results. For this, the experimental pressure value was transformed into force by multiplying it by the total loaded area of the liner tray.

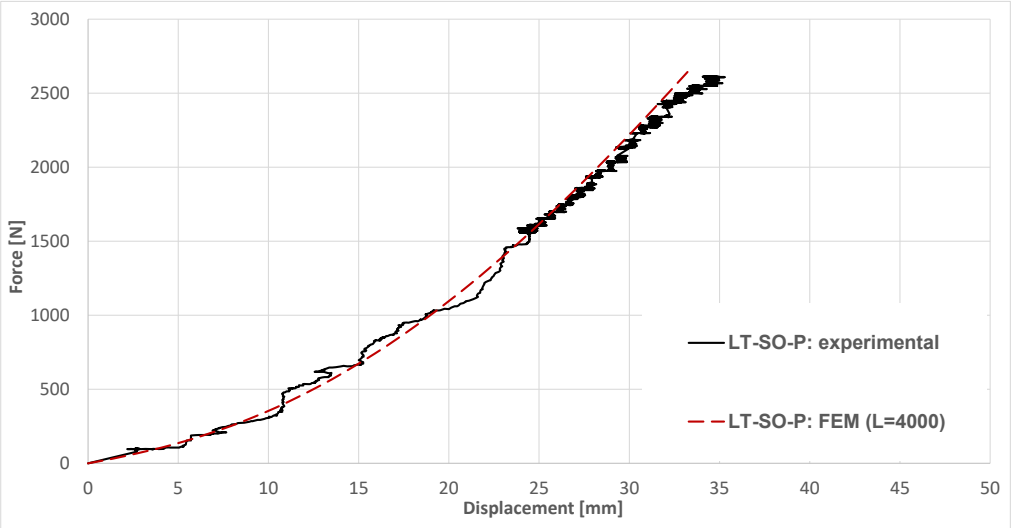


Figure 4.15 Calibration of simple-opened liner tray FEM model subjected to pressure, based on experimental results

On the basis of the described FEM modelling hypotheses, the non-linear analysis, including imperfections in the liner tray subjected to pressure loading, there was plot the numerical result presented in Figure 4.15 in terms of the force-deflection curve. This diagram reveals a strong correlation between numerical and experimental results, both in terms of stiffness and strength. The minor differences at the end of the force-deflection curve can be determined by a decrease in the hardening response at large deformations in real loading conditions, which could not be implemented numerically at this level but are considered for further numerical investigations including damage parameters of the material. However, as a general remark, the FE model of the liner tray was able to capture the experimental behaviour with a high reliability, excluding dynamic effects that occurred during experimental tests.

The finite element model for the liner tray subjected to pressure is considered validated and is presented as a reference model in further parametric investigation.

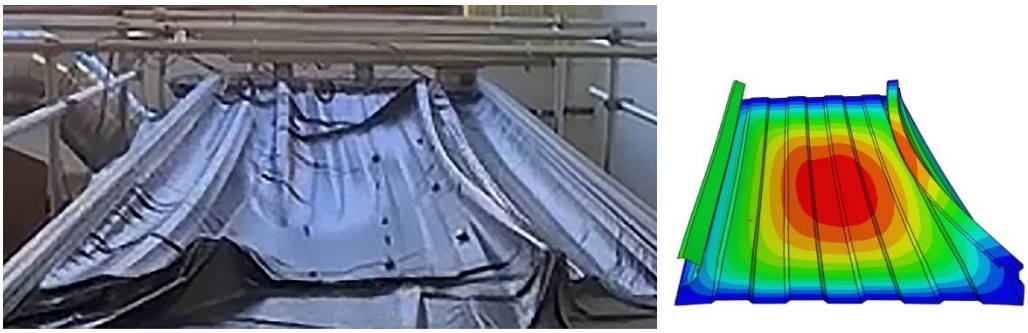

Figure 4.16 LT-SO-P specimen after failure at $P_{max\_exp}$ = 1087.25 Pa (left) and simple-opened liner tray FEM model subjected to pressure at $P_{max\_exp}$ = 1087.25 Pa (right)

### 4.3.2 Parametric study

The parametric study presented herein aims at understanding the influence of different parameters, such as length, sheet thickness, and web height, on the liner trays response under wind pressure. Furthermore, this study allows one to assess the performance of liner trays and to draw out some recommendations with respect to the geometrical features mentioned above. The parametric study assumes conducting several analyses to provide information about the behaviour of different configurations of the liner trays undergoing the same loading and boundary conditions.

It is important to note that the calibrated finite element model thoroughly described in the previous section is labelled as "LT-SO-P: FEM" model and acts as a reference model for this parametric study.

Since in the numerical model, the damage parameters of the material were not defined, the results of the parametric study do not reflect the maximum bearing capacity of the modelled liner tray. Instead, in order to assess the performance of each investigated model, the output force-deflection response curves are presented up to the maximum load value recorded immediately before failure in the

experimental specimen ($P_{max\_exp}$ = 1087.25 Pa which is equivalent to an experimental reaction $F_{max\_exp}$ = 2.61 kN – see Sect. 3.4.1.1).

### *4.3.2.1 Influence of Steel sheet thickness*

The influence of the steel sheet thickness was investigated by changing the thickness of the liner tray FE model for 0.7334 mm (reference), 0.88, 1.0, 1.13, 1.25 and 1.5 mm. All the other parameters were kept constant. The labels chosen for each model indicate the thickness used for the liner trays (e.g., t=1.00 – liner tray with a steel sheet thickness of 1.00 mm). Table 4.2 shows the thickness used for each model analysed. The chosen thickness values represent actual values of the thicknesses of the liner trays that can be found on the market.

Table 4.2 Parametric study input models with different thicknesses

| **Numerical model** | | | | | |
|---|---|---|---|---|---|
| LT-SO-P: FEM | t=0,88 | t=1,00 | t=1,13 | t=1,25 | t=1,50 |
| **Steel sheet thickness (mm)** | | | | | |
| 0,7334 | 0,88 | 1,00 | 1,13 | 1,25 | 1,50 |
|  |  |  |  | 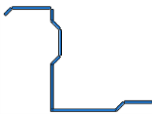 | 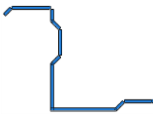 |

Figure 4.17 shows the force–deflection curves for the 4000 mm long liner trays and different thickness configurations. A relevant increase in stiffness could be observed when the thickness of the steel sheet increases.

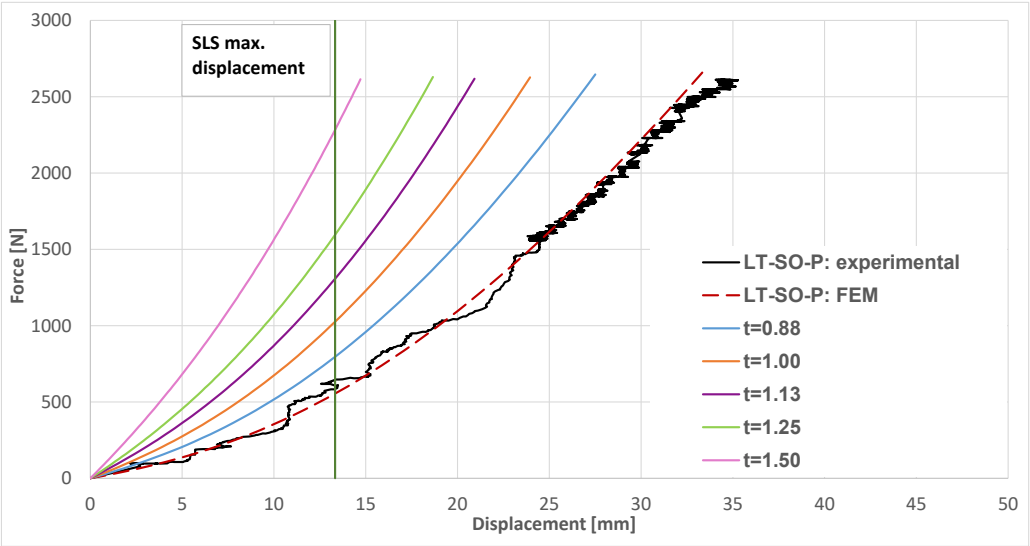


Figure 4.17 Influence of steel sheet thickness on the liner trays subjected to pressure

As can be seen in Table 4.3 the stiffness of the liner trays subjected to pressure (positive bending) increases from 99.91 N/mm for the liner tray with thickness of 0.7334 mm, tested in the experimental investigation, in the vacuum chamber (described in Sect. 3.4.1.1), to stiffnesses up to 185.76 N/mm (for the liner tray with the thickness of 1.5 mm), showing that the stiffness of the liner trays increased with 10-15% each time the next thicker thickness available on the marked was considered in the numerical investigation. Also, in Table 4.3 it is presented the bending moment resistance of the liner trays with the ticknesses analysed in the parametric study, according to the EN 1993-1-3:2007, as well as the associated force load.

From Table 4.3, it can be noted that when considering the allowed SLS maximum deflection of the liner trays with a length of 4000 mm, the force needed to be applied to reach this deflection (L/300 = 13.33 mm) increases from 582.42 N, for LT-SO-P: experimental, to 2301.45 N , for liner trays with a thickness of 1.5 mm. The tests revealed a significant increase in the force needed to apply to reach the deflection of the SLS between t=1.25 and t=1.5, marking a 44% increase in the load needed from one thickness of steel sheet to the next. In addition, it should be noted that the force value at the maximum deflection of SLS in the case of t=1.50 (2.3 kN) is close to the maximum load value for LT-SO-P: experimental (2.6 kN).

Table 4.3 Influence of steel sheet thickness on the liner trays subjected to pressure

| Model | Stiffness [N/mm] | $Mc_{code}$ [kN·m] | $F_{code}$ [N] | F at SLS deformation L/300 [N] | Deflection at $F_{max\_exp}$ [%] |
|---|---|---|---|---|---|
| LT-SO-P: experimental | 99.91 | 1.56 | 3120 | 582.42 | 100 |
| LT-SO-P: FEM | 100.00 | | | 565.5 | 92.79 |
| t = 0.88 | 115.48 | 2.38 | 4760 | 806.93 | 76.54 |
| t = 1.00 | 125.93 | 3.17 | 6340 | 1033.45 | 66.67 |
| t = 1.13 | 140.13 | 3.72 | 7440 | 1308.96 | 58.22 |
| t = 1.25 | 156.52 | 4.04 | 8080 | 1595.69 | 51.93 |
| t = 1.50 | 185.76 | 5.12 | 10240 | 2301.45 | 40.94 |

In terms of deflection at $F_{max\_exp}$ = 2.61kN (equivalent of maximum load value recorded immediately before failure in the experimental investigations for the simple opened liner trays subjected to wind pressure - 1087.25Pa), when reaching the $F_{max\_exp}$ value, the deflection of the liner trays with the wide flange in tension is decreasing from 100% (in the case of LT-SO-P: experimental) to 51.93% (in the case of T = 1.25) and even 40.94%, in the case of liner trays with the thickest steel sheet available on the market, T = 1.50.

### *4.3.2.2 Influence of Web height*

The influence of the web height of the liner trays was investigated by changing the height of the liner tray FE model from 100 mm up to 150 mm. All the other parameters were kept constant. The labels chosen for each model point out the web height used for the liner trays (e.g., h=135 – liner tray with a height of 135 mm). The web heights used for each analysed model are presented in Table 4.4. As in the case of the parametrical study of the thickness of the trays, the values of the web heights chosen to represent the actual values of the heights of the trays that can be found on the market.

Table 4.4 Parametric study input models with different web height

| **Numerical model** | | | | |
|---|---|---|---|---|
| LT-SO-P: FEM | h=115 | h=125 | h=135 | h=150 |
| **Liner tray web height (mm)** | | | | |
| 100 | 115 | 125 | 135 | 150 |
| 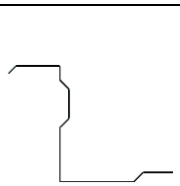 | 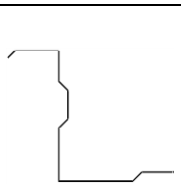 | 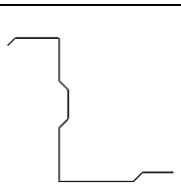 | 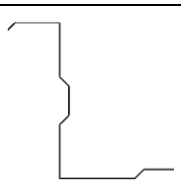 | 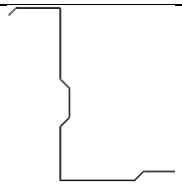 |

As can be seen in the force–deflection diagram shown in Figure 4.18 the variation of the height in the liner trays does not have a considerable impact on the load bearing capacity and the stiffness of the liner trays. A slight increase in stiffness could be observed when the web height of the liner trays rises, but, as also shown in Table 4.5, none of these differences were statistically significant. The stiffness improves by less than 2.5% with increasing web height. The gain in stiffness of LT-SO-P: experimental to h = 150 is less than 5%.

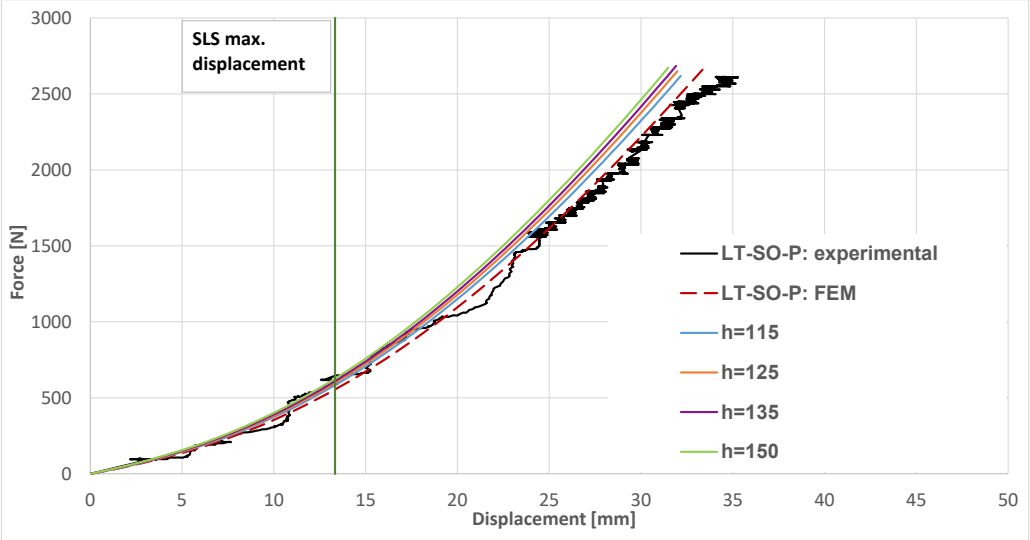


Figure 4.18 Influence of web height on the liner tray subjected to pressure

The minor impact of the increase of the web height of the liner trays is confirmed also by the comparison between the recorded load at the L/300 deflection and between the recorded deflection at $F_{max\_exp}$, presented in Table 4.5. These results indicate a minor difference (0.582 kN compared to 0.647 kN) of the force needed to be applied to reach the SLS deflection 13.33 mm (allowed considered limit for the liner trays with a length of 4000 mm). Table 4.5 shows the bending moment resistance of the liner trays with the web heights analysed in the parametric study, according to EN 1993-1-3:2007, and the associated force load. The results uphold the higher influence of sheet thickness on the behaviour of liner trays subjected to wind loads than the influence of the web height.

Table 4.5 Influence of web height on the liner trays subjected to pressure

| Model | Stiffness [N/mm] | $Mc_{code}$ [kN·m] | $F_{code}$ [N] | F at SLS deflection L/300 [N] | Deflection at $F_{max\_exp}$ [%] |
|---|---|---|---|---|---|
| LT-SO-P: experimental | 99.91 | 1.56 | 3120 | 582.42 | 100 |
| LT-SO-P: FEM | 100.00 | | | 565.5 | 92.79 |
| h = 115 | 101.55 | 1.95 | 3900 | 579.57 | 89.51 |
| h = 125 | 102.15 | 2.20 | 4400 | 603.63 | 88.98 |
| h = 135 | 104.61 | 2.42 | 4860 | 628.56 | 88.78 |
| h = 150 | 104.71 | 2.92 | 5840 | 647.66 | 87.59 |

When reaching the $F_{max\_exp}$ value, the deflection of the liner trays subjected to pressure, with various web hights is decreasing from 100%, in the case of LT-SO-P: experimental, to 87.59%, in the case of h = 150, again emphasising the minor contribution of the web hight in the behaviour of the liner trays with the wide flange in tension.

### *4.3.2.3 Influence of the static scheme / Liner tray length*

The influence of the length of the liner trays was investigated by changing the length of the liner tray FE model from one span of 4000 mm length to two spans of 4000 mm each. The profile was considered as a single continuous sheet for both spans. All other parameters were kept constant. The label chosen for the parametric model indicates the total length of the two spans. The analysed model is presented in Table 4.6.

Table 4.6 Parametric study input models with different length

| **Numerical model** | **Liner tray length (mm)** | |
|---|---|---|
| LT-SO-P: FEM (L=4000) | 4000 | 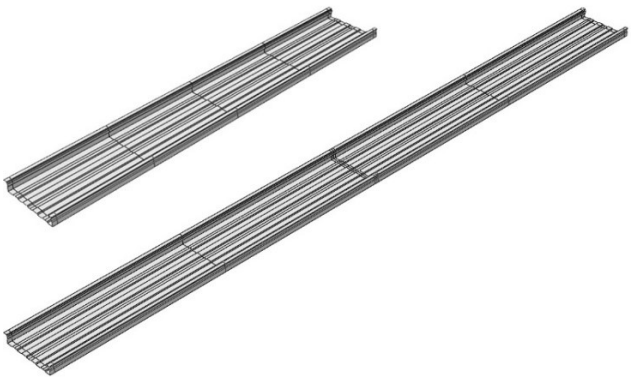 |
| L=4000+4000 | 8000 | |

Figure 4.19 shows the force–deflection diagram of the FE models compared. Variation of the static scheme and lengths in the liner trays has an impact on the load bearing capacity and the stiffness of the liner trays. Both negative and positive values for the bending moment apear in the two-span liner tray. Here, the value for the bending moment relates to the bending moment of the liner tray occured at the mid-span of the two spans of the L=4000+4000 model. An increase in stiffness could be observed when the statical scheme of the liner tray changes from a simply supported beam to a continuous beam with two spans. The gains in stiffness and deflection are shown in Table 4.7: the stiffness improves with around 10% for the continuous beam with two spans when compared to the FE model of the simple supported beam, while the deflection at $F_{max\_exl}$ decreases by 20% at the mid-span.

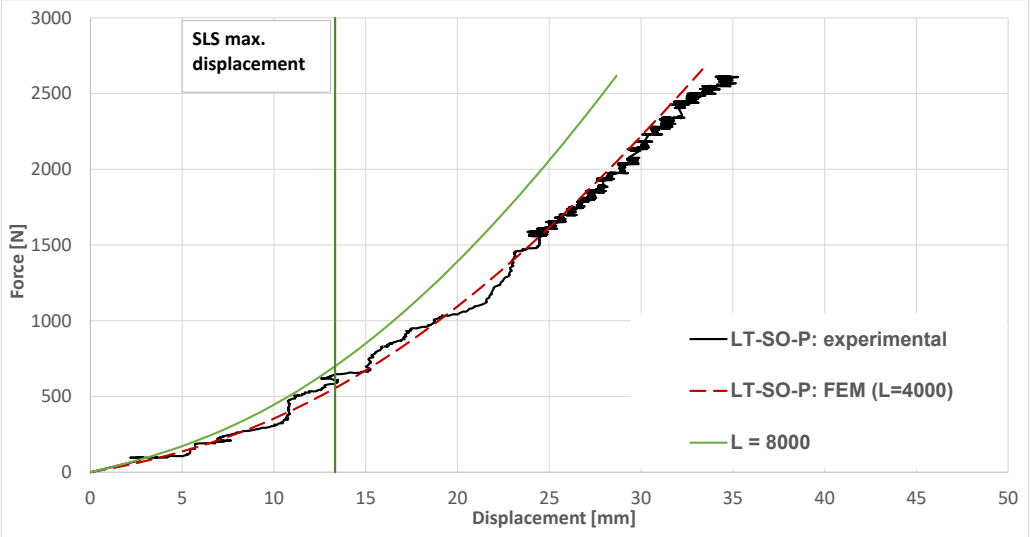


Figure 4.19 Influence of liner tray length on the model subjected to pressure

From Table 4.7, it can be noted that when considering the allowed SLS maximum deflection of the liner trays with the length of 4000 mm, the force needed to be applied to reach this deflection (L/300 = 13.33 mm) increases from 0.582 kN, for LT-SO-P: experimental, to 0.709 kN, for the double-span FE model of the liner trays, meaning a 22% increase in force.

Table 4.7 Influence of span number on the liner trays subjected to pressure

| Model | Stiffness [N/mm] | F at SLS deflection L/300 [N] | Deflection at $F_{max\_experimental}$ [%] |
|---|---|---|---|
| LT-SO-P: experimental | 99.91 | 582.42 | 100 |
| LT-SO-P: FEM | 100.00 | 565.5 | 92.79 |
| L = 4000+4000 | 110.94 | 709.83 | 79.77 |

## 4.4 Finite element analysis of liner trays with wide flange in compression

### 4.4.1 Calibration of the finite model of liner trays

#### *4.4.1.1 Model description*

The numerical model of the suction-subsequent liner tray was created by applying the same algorithm as in the case of models subjected to pressure. The cross-section presented in Figure 4.20 sketch was extruded to a *Shell* part, with the corresponding thickness of 0,7334 mm.

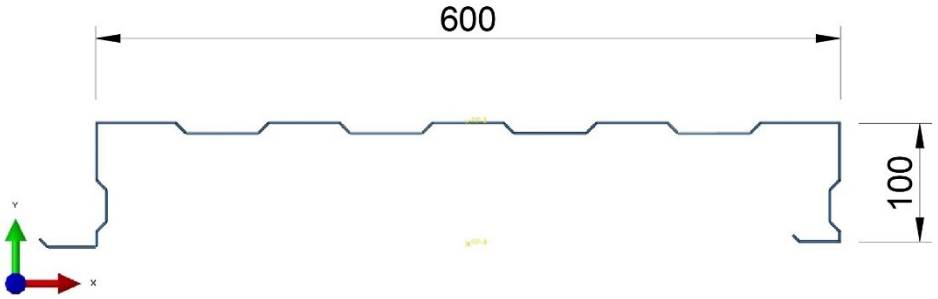


Figure 4.20 Cross-section sketch of the liner tray subjected to suction

The part was assigned a *Homogeneous Shell* section with the following properties: density, elastic properties (Young's modulus, Poisson ratio) and plastic properties (true stress-strain curve of the calibrated material). The material definition procedure is presented in Figure 4.21

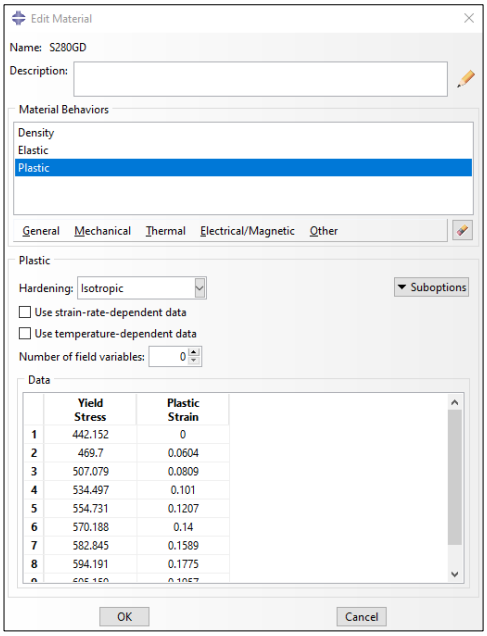


Figure 4.21 Definition of steel material properties in Abaqus

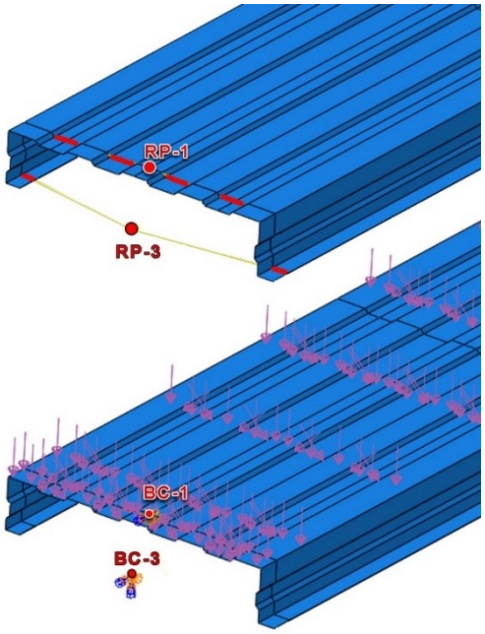


Figure 4.22 Constraints, boundary conditions and loads of the FEM model for liner trays subjected to suction

### *4.4.1.2 Boundary conditions and applied loads*

To reliably simulate experimental boundary conditions, two types of constraints were created (Figure 4.22):

- *Kinematic* couplings with 6 restrained DOF between the bottom stiffeners of the wide flange and *reference points* RP-1 and RP-2, acting as the timber block support of the liner tray;
- *Kinematic* couplings with 5 restrained DOF between the narrow flanges and *reference points* RP-3 and RP-4, meant to reproduce the liner trays support zone located on vacuum chamber.

Certain convergence problems related to overconstraining the liner tray model were avoided by calibrating the boundary conditions. In this way, for each reference point, the following *displacement/rotation* boundary conditions were defined:

Table 4.8 Boundary conditions for suction FEM model

| Reference point | Blocked DOFs | Free DOFs |
|---|---|---|
| RP-1 | U1, U2, U3, UR3 | UR1, UR2 |
| RP-2 | U1, U2, UR3 | U3, UR1, UR2 |
| RP-3 | U1, U2, U3, UR2, UR3 | UR1 |
| RP-4 | U1, U2, UR2, UR3 | U3, UR1 |

The load was applied similarly as in the previous case, as a normal *pressure* load on the wide flange surface, aiming to simulate the experimental load application by means of polyethylene foil, which ensured the needed air pressure within the vacuum chamber. The assumed magnitude of *pressure* loading is 0,001044 N/mm$^2$ (1044 Pa).

### *4.4.1.3 Equivalent geometrical imperfections*

Analytical calculations for equivalent geometrical imperfections of the liner tray subjected to wind suction (apllying uniform load, causing wide flange under compression) were performed in the same manner as for FE analysis of liner trays subjected to wind pressure.

The magnitude of the equivalent geometric imperfection of liner trays with a wide flange under compression when considering local buckling, $e_{o,local}$, and the magnitude for the global equivalent imperfection, $e_{o,global}$, had the same values as in the case of the analysis of FE elements of liner trays with a wide flange in tension: $e_{o,local}$ = 0.8 mm and $e_{o,global}$ = 4 mm.

The magnitude of the equivalent geometric imperfection of liner trays with the wide flange under compression when considering distortional buckling, $e_{o,dist}$, was determined according to Table 5.6, Table 5.7 and eq. (5.17) in [16] as follows:

$$e_{0,dist} = 0.3 \cdot t \cdot \sqrt{\frac{f_{yb}}{\sigma_{cr,d}}} = 0.3 \cdot 0.7334 \cdot \sqrt{\frac{440}{30}} = 0.842 \text{ mm}, \tag{4.8}$$

where:

t: -the thickness of the sheet; $t$ = 0.7334 mm (according to measurements presented in Sect. 3.5.2)

$f_{yb}$: -the basic yield strength according to EN 1993-1-3; $f_{yb}$ = 280 N/mm$^2$

$\sigma_{cr,d}$: -the elastic critical distortional buckling stress; $\sigma_{cr,d}$ = 30 N/mm$^2$ (see Figure 4.10)

The elastic critical distortional buckling stress, $\sigma_{cr,d}$, of a liner tray with wide flange under compression (a liner tray with the cross-section described in 3.2 and Figure 3.1), determined with the use of CUFSM finite strip analysis programme [170] was , $\sigma_{cr,d}$ = 30 N/mm$^2$ (see Figure 4.23).

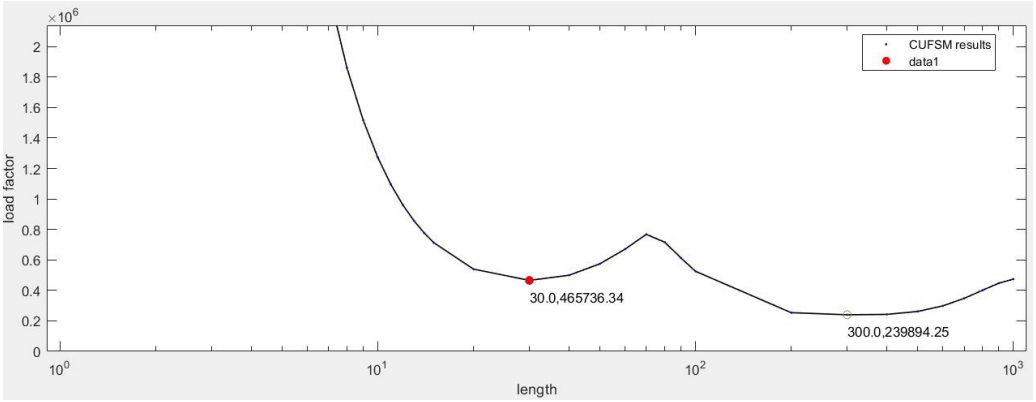


Figure 4.23 Result of elastic buckling analysis of a cross-section of the liner tray subjected to suction using CUFSM software

Similar to the pressure liner tray model, a buckling analysis was performed in a separate step before the actual Static, Riks analysis, in order to identify the most appropriate buckling modes to be imported as imperfections geometry.

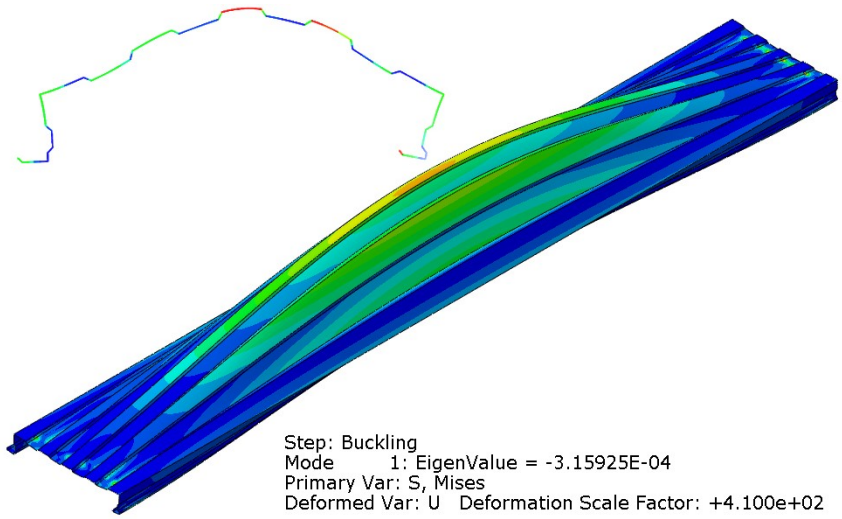


Figure 4.24 The 1st buckling mode, corresponding to the global buckling mode of the model

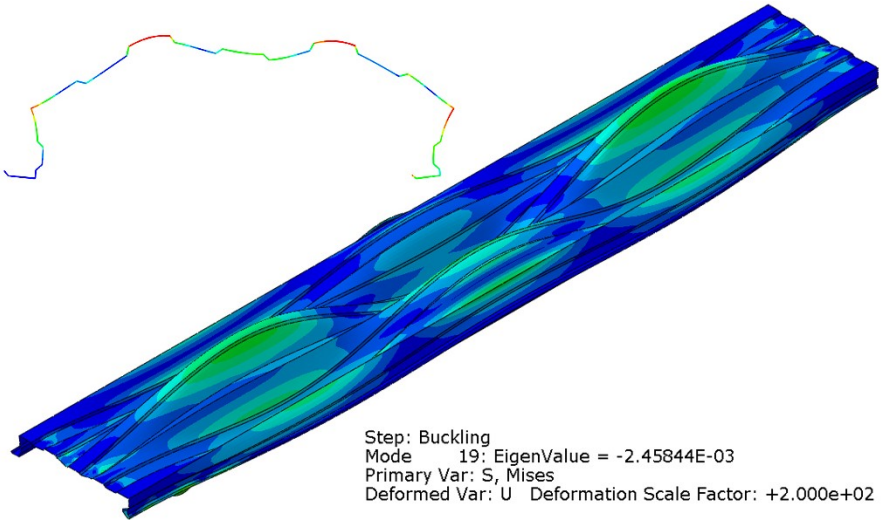


Figure 4.25 The 19th buckling mode, corresponding to the distortional buckling interacting with local buckling mode

As in the pressure liner tray model case, the global buckling mode was weighed as the leading imperfection with accompanying imperfections at amplitudes reduced to 50% of the defined value - see eq. (4.3). The amplitude of the calculated equivalent geometric imperfections, in the case of the suction liner tray model, accounted for the 19th buckling mode (see Figure 4.25) was determined as follows:

$$k_{eq,\mathrm{dist+loc}} = 0.25 \cdot \left(\frac{e_{0,\mathrm{dist}}}{e_{FEM,\mathrm{dist}}}\right) + 0.25 \cdot \left(\frac{e_{0,\mathrm{loc}}}{e_{FEM,\mathrm{loc}}}\right) = 0.410 \tag{4.9}$$

Post-buckling results revealed that the 1st buckling mode has a good agreement with the global buckling of the liner tray, while the 19th mode is associated with the distortional buckling interacting with local buckling of the model. In the same way as described in Sect. 4.3.1.3, the imperfection geometry was imported into the actual analysis by introducing the following lines in the *Edit Keywords* window.

```
*IMPERFECTION, FILE=Suction_bukling-imp, STEP=1
1, -2
19, 0,410
 ** STEP: Suction-static
**
*Step, name=Suction-static, nlgeom=YES
```

#### *4.4.1.4 Analysis and validation*

The finite element analysis of the liner tray model subjected to suction was performed on the basis of 3 steps: Initial, Buckling, Suction. Within *the initial* step the assembly was defined and constraints and boundary conditions were created. The Buckling step involved the assessment of geometric imperfections through the procedure described in previous sub-chapter, while in the Suction step the loading conditions were defined. The analysis was conducted by means of *General* procedure, *Static, Riks* solver, considering the second-order effects computed through *buckle* analysis, as mentioned above. Besides avoiding convergency issues, *Static, Riks* method also significantly reduces computing time.

The reaction forces at the reference points RP-1 and RP-2, as well as the transverse deflection at the mid-span (D2) calculated as the mean deflection of three middle points presented in Figure 4.26, were defined as the analysis output request.

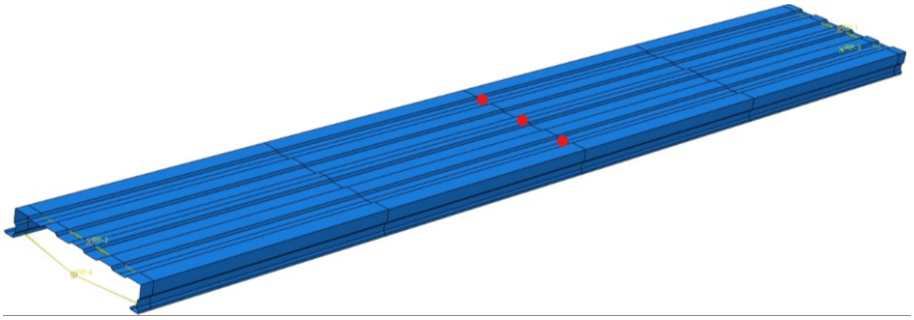

Figure 4.26 Mid-span transverse deflection output points

As presented previously, to ensure the comparability between experimental and numerical results, the comparison between FEM and experimental behaviour was carried out in terms of force, obtained by multiplying the experimental suction value by the loaded area of the liner tray.

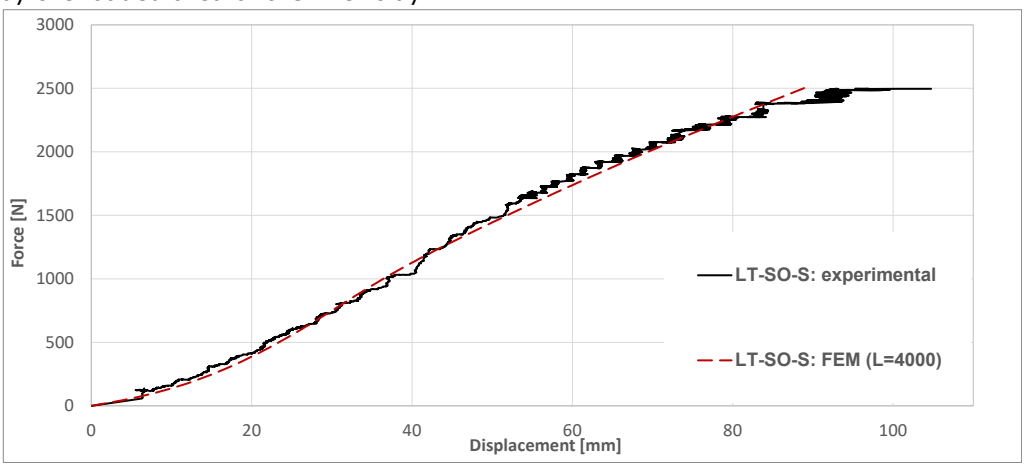


Figure 4.27 Calibration of simple-opened liner tray FEM model subjected to suction, based on experimental results

The post-test numerical processing of the liner tray model subjected to suction generated the response presented in Figure 4.27, in terms of the force-deflection curve. An even better agreement between numerical and experimental results with large deformations was achieved in this case, in comparison with the pressure model. The error between the numerical and experimental results is of maximum 2%. Excluding the real dynamic effects which were not enabled numerically, the FEM results capture the allure of experimental force-deflection curve, faithfully following its slope and the main behaviour parameters such as stiffness, strength, and ductility.

Overall, these results prove the calibration of the FEM element model of the liner tray subjected to suction, providing the reference base for further simulations presented in the following as a parametric study.


Figure 4.28 LT-SO-S specimen after failure at $P_{max\_exp}$ = 1044.27 Pa (left) and simple-opened liner tray FEM model subjected to suction at $P_{max\_exp}$ = 1044.27 Pa (right)

### 4.4.2 Parametric study

The calibrated finite element model, which represents the equivalent of the suction-loaded liner tray, described in the previous subchapter, is labelled "LT-SO-S: FEM", and acts as a reference model for this parametric study.

As in the case of the FE model subjected to pressure loads, in the numerical model the damage parameters of the material were not defined; therefore, the results of the parametric study do not reflect the maximum bearing capacity of the liner tray. Instead, in order to assess the performance of each investigated model, the output force-deflection curves are presented up to the maximum load value recorded immediately before failure in the experimental investigations ($F_{max\_exp}$ = 2.50 kN, equivalent to an applied suction of 1044.27 Pa – see Sect.3.4.2.1).

#### *4.4.2.1 Influence of Steel sheet thickness*

The influence of the thickness of the steel sheet was investigated by changing the thickness of the FE liner tray model from 0.7334 mm to 1.5 mm. All other parameters were kept constant. The labels chosen for each model point out the thickness used for the liner trays, as presented in Table 4.8. The thickness used for each analysed model is the same as in the parametric study of the FE model investigated under pressure loads.

Table 4.9 Parametric study input models with different thicknesses

| **Numerical model** | | | | | |
|---|---|---|---|---|---|
| LT-SO-S: FEM | t=0,88 | t=1,00 | t=1,13 | t=1,25 | t=1,50 |
| **Steel sheet thickness (mm)** | | | | | |
| 0,7334 | 0,88 | 1,00 | 1,13 | 1,25 | 1,50 |
| 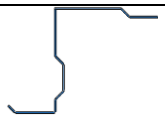 | 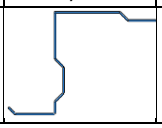 | 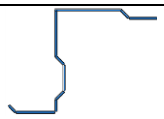 | 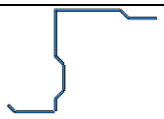 | 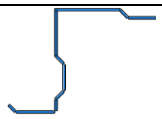 | 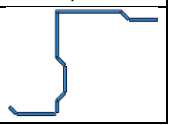 |

Figure 4.29 shows the force–deflection curves for the 4000 mm long liner trays and the different thickness configurations. A proportional increase in stiffness could be observed when the thickness of the steel sheet increases.

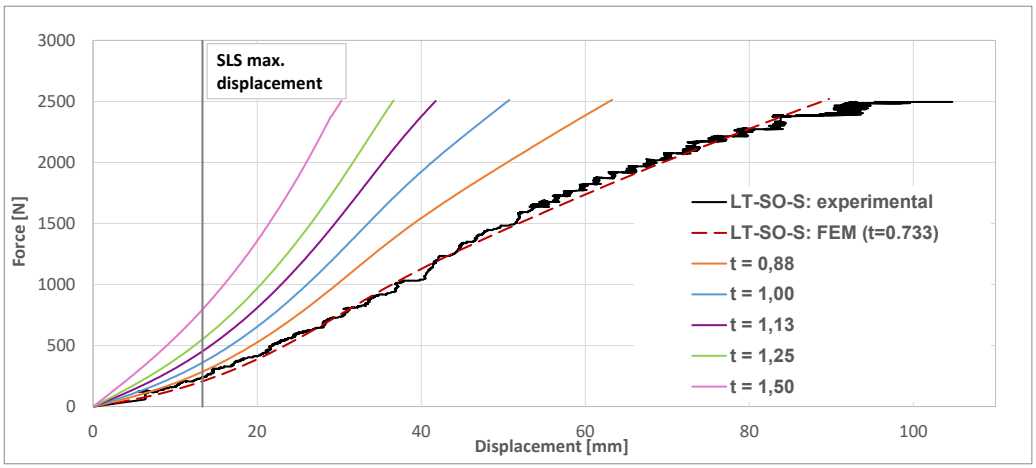


Figure 4.29 Influence of steel sheet thickness on the liner tray subjected to suction

Changing the thickness parameter of the steel sheet had a great influence on the stiffness of the liner trays, as can be observed in Table 4.10. The stiffness of the liner trays subjected to suction loads increases from 36.88 N/mm for the liner tray with the tickness of 0.7334 mm tested in the experimental investigation (presented in Sect. 3.4.2.1), to stiffnesses up to 90.31 N/mm (for the liner tray with a tickness of 1.5 mm), showing an increase of the stiffness of 15-30% for each increment of the tickness considered in the numerical investigation. It is worth mentioning that the stiffness of the FE models subjected to suction loads is 2 to 3 times smaller than in the case of the equivalent FE models subjected to pressure loads (presented in Sect. 4.3.2.1 of the thesis), even though in the experimental investigation the maximum load recorded before failure for both cases (pressure and suction) recorded similar values. This is finally observed by the larger deflection recorded for the suction liner trays.

From Table 4.10, it can be noted that when considering the maximum allowed SLS deflection of the liner trays with a length of 4000 mm, the force that must be applied to reach this deflection (L/300 = 13.33 mm) increases from 237.25 N for LT-SO-S: experimental, to 794.85 N for the FE model with 1.5 mm thickness. These values are again 2 to 3 times lower than in the case of the parametric study of the LT-SO-P model. The tests revealed a significant increase in the force needed to apply to reach the deflection of the SLS between t=1.25 and t=1.5, marking a 44% increase in the load needed from one steel sheet thickness to the next (as happened also in the case of FE models for pressure loads).

Table 4.10 Influence of steel sheet thickness on the liner trays subjected to suction

| Model | Stiffness [N/mm] | $Mc_{code}$ [kN·m] | $F_{code}$ [N] | F at SLS deflection L/300[N] | Deflection at $F_{max\_exp}$ [%] |
|---|---|---|---|---|---|
| LT-SO-S: experimental | 36.88 | 1.53 | 3060 | 237.25 | 100 |
| LT-SO-S: FEM (t=0.73) | 33.99 | | | 216.68 | 86.21 |
| t = 0.88 | 51.04 | 2.08 | 4168 | 290.85 | 60.41 |
| t = 1.00 | 64.51 | 2.58 | 5160 | 363.19 | 48.44 |
| t = 1.13 | 74.20 | 3.17 | 6340 | 448.2 | 39.86 |
| t = 1.25 | 80.52 | 3.77 | 7540 | 552.34 | 34.95 |
| t = 1.50 | 90.31 | 4.91 | 9820 | 794.85 | 28.90 |

Table 4.10 shows the bending moment resistance of the liner trays with the thicknesses analysed in the parametric study, according to EN 1993-1-3:2007, and the associated force load. A significant increase in the bending moment capacity is noticed with the increase of the steel sheet tickness of liner trays, reaching values up to 3.2 times higher when the steel thickness is increased from 0.75mm to 1.5mm.

In terms of deflection at $F_{max}$ = 1044.27Pa = 2609.9 N (maximum load value), when reaching the $F_{max\_exp}$ value, the deflection of the liner trays with the wide flange under compression decreases from 100%, in the case of LT-SO-S: experimental, to 28.90%, in the case of liner trays with the thickest steel sheet available on the market, t = 1.50. A significant difference was found for the increase of the thickness of the steel sheet from the thinnest available on the market to 0.88 mm: this would mean a decrease of the deflection at $F_{max}$ of 40%.

### *4.4.2.2 Influence of the Web height*

The influence of the web height of the liner trays was investigated by changing the height of the liner tray FE model from 100 mm up to 150 mm. All other parameters were kept constant. The labels chosen for each model point out the web height used for the liner trays. Each web height used for the analysed models is presented in Table

4.11. The values represent actual values of the heights of the liner tray that can be found on the market.

Table 4.11 Parametric study input models with different web height

| **Numerical model** | | | | |
|---|---|---|---|---|
| LT-SO-S: FEM | h=115 | h=125 | h=135 | h=150 |
| **Liner tray web height (mm)** | | | | |
| 100 | 115 | 125 | 135 | 150 |
| 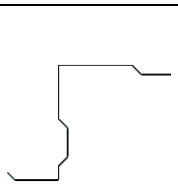 | 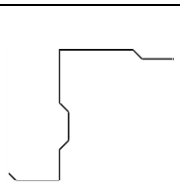 | 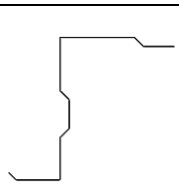 | 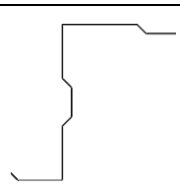 | 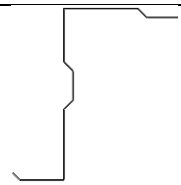 |

As can be seen in the force–deflection diagram shown in Figure 4.30 the variation of the height in the liner trays has a slight impact on the load-bearing capacity and the stiffness of the liner trays when having the wide flange in compression. Nonetheless, the influence of the web height in the case of the FE models subjected to suction is greater than in the case of the FE models subjected to pressure. As shown in Table 4.12, the stiffness improves with up to 42% with increasing web height from *LT-SO-S: experimental* to h = 150.

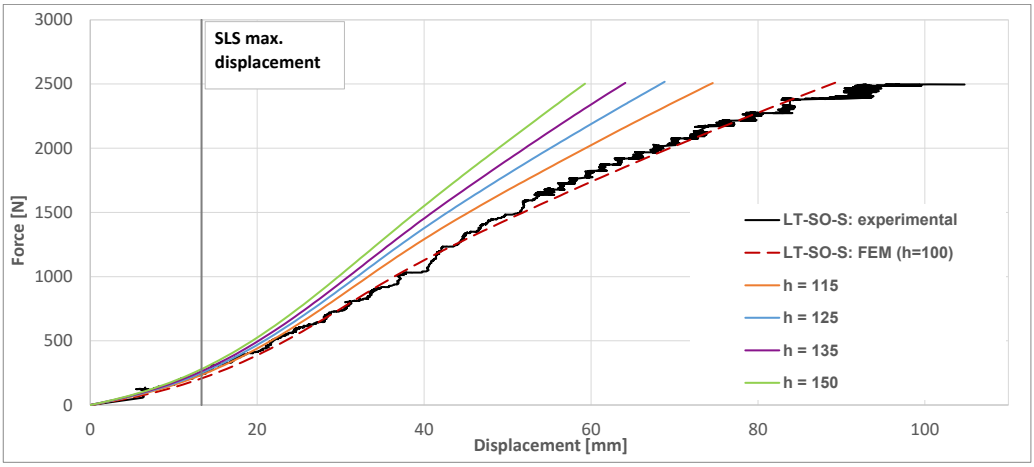


Figure 4.30 Influence of web height on the liner tray subjected to suction

The small impact of the increase in web height of liner trays subjected to suction loads is also confirmed by the comparison between the recorded load at the L/300 deflection between FE models: the force required to reach the maximum SLS deflection of 13.33 mm increases from 0.237 kN (for LT-SO-S: experimental) to 0.287 kN (for h = 150), meaning an increase of 20% of the load.

Table 4.12 Influence of web height on the liner trays subjected to suction

| Model | Stiffness [N/mm] | $Mc_{code}$ [kN·m] | $F_{code}$ [kN] | F at SLS deflection L/300 [N] | Deflection at $F_{max\_exp}$ [%] |
|---|---|---|---|---|---|
| LT-SO-S: experimental | 36.88 | 1.53 | 3060 | 237.25 | 100 |
| LT-SO-S: FEM | 33.99 | | | 216.68 | 86.21 |
| h = 115 | 41.02 | 1.91 | 3820 | 241.51 | 71.19 |
| h = 125 | 45.34 | 2.12 | 4240 | 252.39 | 65.71 |
| h = 135 | 48.55 | 2.33 | 4660 | 266.4 | 61.19 |
| h = 150 | 52.43 | 2.67 | 5340 | 287.21 | 56.58 |

Table 4.12 shows the bending moment resistance of the liner trays with the web heights analysed in the parametric study, according to EN 1993-1-3:2007, and the associated force load. An increase of up to 74% in the bending moment capacity is noticed with the increase of the web heights of liner trays, when comparing the liner trays with a height of 100mm up to liner trays with 150mm height. These results certify, as well as the results of bending moment resistance of liner trays subjected to wind pressure, that steel sheet thickness have a higher influence on the behaviour of liner trays subjected to wind loads than the influence of the web height.

However, when reaching the $F_{max\_exp}$ value, the deflection of the liner trays subjected to suction loads, with various web heights, decreases from 100%, in the case of LT-SO-S: experimental, to 56.58%, in the case of h = 150. These results show a greater contribution of the web hight in the behaviour of the liner trays with the wide flange under compression than in the case of the liner trays with the wide flange in tension, where the deflection at $F_{max\_exp}$ for h = 150 was only 12.41% smaller than in the case of LT-SO-P: experimental.

### *4.4.2.3 Influence of Liner tray length*

The influence of the length of the liner trays was investigated by changing the length of the LT-SO-S:FEM model from a single span to two spans of 4000 mm each. The profile was considered as a single continuous sheet for both spans. All the other parameters were kept constant. The name chosen for the parametric model indicates the total length of the two spans. The analysed model is presented in Table 4.13.

Table 4.13 Parametric study input models with different length

| Numerical model | Liner tray length (mm) | |
|---|---|---|
| LT-SO-S: FEM (L=4000) | 4000 | 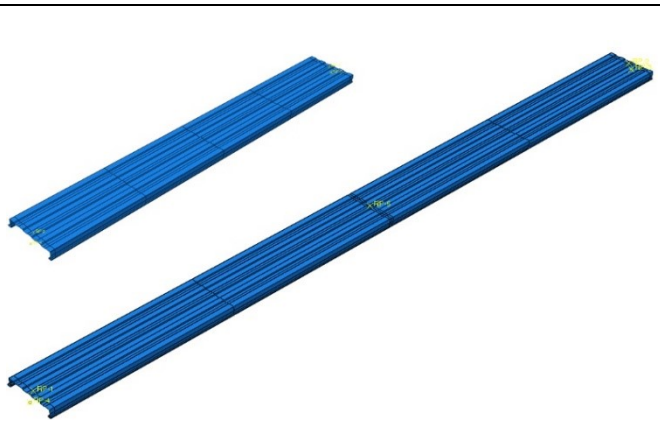 |
| L=4000+4000 | 8000 | |

Figure 4.31 shows the force–deflection diagram of the FE models compared. Variation of the lengths and the static scheme in the liner trays does have a considerable impact on the load bearing capacity and the stiffness of the liner trays. An important increase in stiffness could be observed when the statical scheme of the liner tray changes from simply supported beam to continuous beam with two spans. Important gains in stiffness and decreases in deflection are shown in Table 4.14Table 4.5: the stiffness doubles for the continuous beam with two spans (L = 4000+4000) when compared to the simply supported beam LT-SO-S:experimental.

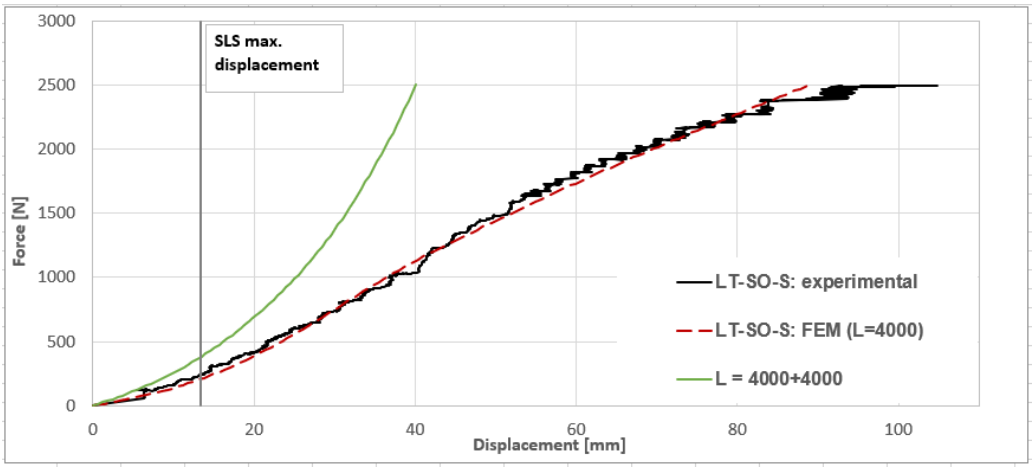


Figure 4.31 Influence of liner tray length on the model subjected to suction

From Table 4.14, it can be observed that when considering the maximum allowed SLS deflection of the liner trays with spans of 4000 mm, the force needed to be applied to reach this deflection (L/300 = 13.33 mm) increases from 0.237 kN, for the LT-SO-S:experimental, to 0.384 kN, for the double-span FE model of the liner trays, meaning a 62% increase in force. This result shows a greater impact on the number of spans of the liner trays with the wide flange under compression than on the case of the liner trays with the wide flange in tension (for which the increase in the force for SLS deflection was 22% from the *LT-SO-P: experimental* specimen to L = 8000 FE model).

Table 4.14 Influence of span number on the liner trays subjected to suction

| Model | Stiffness [N/mm] | F at SLS deflection L/300 [N] | Deflection at $F_{max\_exp}$ [%] |
|---|---|---|---|
| LT-SO-S: experimental | 36.88 | 237.25 | 100 |
| LT-SO-S: FEM | 33.99 | 216.68 | 86.21 |
| L = 4000+4000 | 78.56 | 384.37 | 38.30 |

The parametric study of the length of the liner trays revealed a significant difference between the deflection recorded at $F_{max\_exp}$: while for *LT-SO-S:experimental* specimen the cross section deflection of the liner tray (mid-span transverse deflection) registered at the maximum load value recorded immediately before failure was 104.75 mm, the deflection at the mid-span of the L = 8000 FE model was 40.12 mm. These results show a 61.7% decrease of the deflection at $F_{max\_exp}$ for the FE model resembling a two-span liner tray subjected to wind suction, a considerable influence in comparison with the FE model resembling a two-span liner tray subjected to wind pressure, which recorded a deflection decrease by 20% at the mid-span when reaching $F_{max\_exp}$.

## 4.5 Concluding remarks

To check the efficiency of various options for liner trays subjected to wind loads and to allow the evaluation of certain parameters and influence on liner trays subjected to real loading conditions, numerical investigations were performed.

The FE model used in the numerical simulations was calibrated by applying the results obtained in the experimental tests. Two FE models were calibrated, in order to replicate the experimental behaviour of liner trays in the post-test finite element analysis: a model that simulates the LT-SO-P behaviour and one model that reflects the LT-SO-S behaviour.

Validated numerical models of liner trays subjected to pressure and suction were used in a further parametric study of FE, compiling data on the influence of parameters such as thickness, height and length on the behaviour of the liner trays.

The numerical results of the investigation were categorised into two groups based on the type of wind loading effect, namely liner trays with wide flange in tension (as a result of wind pressure) and trays with wide flange under compression (as a result of wind suction). Within each group, the results of the analysis are described, observing the influence of the parameters. Considering that in the numerical model, the damage parameters of the material were not defined, the results of the parametric study do not reflect the maximum bearing capacity of the liner trays, but, in order to assess the performance of each investigated model, the output force-deflection curves were presented up to the maximum load value recorded immediately before failure in the experimental investigations ($F_{max\_exp}$).

Taking into account the thickness of steel sheet, web height, and liner tray length, the results of the numerical investigation showed that thickness is the parameter that registers the most significant influence on liner trays, followed by the length of the liner trays. Similar conclusions were also shown in the Guidelines and Recommendations for Integrating Specific Profiled Steels sheets in the Eurocodes (GRISPE) [173].

Changing the steel sheet thickness parameter had a greater influence on the stiffness of the liner trays. An increase in stiffness of up to 86%, in the case of liner trays subjected to wind pressure, and up to 250% in the case of liner trays subjected to wind pressure resulted from the numerical investigations. At the same time, when the $F_{max\_exp}$ value is reached, the deflection of the liner trays with the wide flange in tension decreases by up to 59.06%, while the deflection of the liner trays with the wide flange in compression decreases by up to 71.10%.

Changing the length parameter in the liner trays (from one span to two spans, each of 4m length) had a greater influence in the case of liner trays subjected to suction (a deflection at $F_{max\_expl}$ of 38.3% from the original deflection of LT-SO-S specimen in the experimental investigation and double its stiffness) than in the case of liner trays subjected to pressure. Here, at the last mentioned, resulted a deflection at $F_{max\_exp}$ of 79.7% from the original deflection of LT-SO-P specimen and a 10% higher stiffness.

The height of the web proved to be the parameter with the least influence on the liner trays. Although the results of the parametric study of liner trays subjected to pressure indicate a minor difference between the behaviour of the LT-SO-P specimen and the FE models with different web heights, the results of the parametric study of liner trays subjected to suction showed a deflection at $F_{max\_exp}$ of 56.58% from the original deflection of the LT-SO-S specimen and a stiffness that improves with up to 42% with an increase of the web height from LT-SO-S: experimental to h = 150.

The results of the parametric study revealed that the SLS criteria are up to 3-4 times more conservative than the ULS criteria. Moreover, two-span liner trays are preferred to single-span liner trays due to smaler deformations that occur for the

same load value. Additionally, a study of the influence of restrained liner trays will naturally follow to investigate the influence of two-web thickness on the structural behaviour of liner trays subjected to pressure and suction loads. The experimental investigations showed that the restrained liner trays reach more than double load bearing resistances (in both cases – pressure and suction tests), while the stiffness remains roughly the same.

# 5 Environmental impact of buildings with steel-intensive façade systems

The construction industry is witnessing a substantial increase in both energy requirements and environmental impact, particularly in developing countries. A significant share of this energy is consumed during the operational phase of buildings, primarily for indoor heating and cooling [25]. This highlights the urgent need to improve building performance. The building performance is directly related to the construction envelope performance; therefore, the façade system of a building should be chosen rigorously.

At the same time, the environmental impact can be reduced by the three R approaches – reduce, reuse, recycle. There is a pronounced emphasis on reducing the utilization of non-renewable resources and mitigating environmental consequences. The potential for improved environmental efficiency in the reuse of steel structures, as opposed to the recycling of steel, is now a focal point. To understand the factors driving and constraining this process, a methodical investigation of successful instances of reuse is imperative [30].

Thus, the measures implemented in the construction industry to enhance energy and resource efficiency are of crucial significance.

## 5.1 Introduction

The objectives of waste management policies within the European Union are centred on reducing the generation of waste and optimising the utilisation of resources. These policies focus on taking advantage of the full potential of the resources obtained from waste, thereby diminishing the environmental consequences associated with waste. The Waste Framework Directive 98/2008/CE [99] promotes a waste hierarchy that places prevention as the primary focus, succeeded by reuse and recycling, and reserves disposal as the final option.

### 5.1.1 Environmental impact of the façade systems

In light of the concept of sustainable building [174], steel structures that use thin-walled cold-formed techniques emerge as a very inviting approach to the structural system. This approach combines prefabrication, lightweight construction, fast erection, and the potential for reuse or recycling. Steel façade systems align with current construction trends, providing solid and environmentally viable solutions that can meet contemporary demands and ensure adequate thermal comfort in the interior [65].

A liner tray wall system (see Figure 2.14) combines the required thermal resistance by varying the thermal insulation material and its thickness with the required structural demands. In addition, the façade layer (the outer shell of the double-wall shell system) could be formed by different material solutions, therefore

offering the required architectural aspect. The system offers additional benefits based on industrial prefabrication, adaptability, fast installation, and ease of disassembly [65].

### 5.1.2 Reuse of reclaimed steel in construction

In the steel construction sector, a substantial part of the market is comprised of single-storey steel buildings of industrial-hall type. Additionally, structural elements within single-storey steel buildings tend to be characterised by extended spans and relative simplicity. These components are often openly visible and easily accessible at safe working heights. Consequently, single-storey steel buildings present the most significant potential for reuse [31].

The reutilization of steel structures can manifest itself in various manners, taking into account the arrangement (whether identical or different) and the placement (relocation-based or in-situ). Depending on the type of reuse, specific tasks must be executed. For example, in the context of relocation, activities such as dismantling, transport, and reassembly of the structure are prerequisites, unlike in the case of in-situ reuse. These procedures require additional expenses and environmental repercussions, necessitating thorough consideration to determine the feasibility of the reuse process compared to the construction of an entirely new steel-based structure [30].

## 5.2 Environmental impact study case

The purpose of the analysis in this section is to assess the characteristics of single-storey steel-intensive systems using liner trays through environmental impact analyses (using indicators such as climate change in terms of GHG emissions). The assessment includes single-storey steel structures made of completely new materials, as well as structures made of reused elements for the entire structure, for components (elements of the primary structure), or just for some individual members of the structure. The case study is based on a life cycle assessment (LCA) of a single-storey industrial building erected in Timisoara, Romania, and for the cases where reclaimed steel elements were considered, it involved relocation from Germany to Romania. The basis of the analyses, partial results, and the description of these conventional parameters have been presented in two publications by Buzatu et al., 2023 [30] and Hradil et al. [31], in a work within the research project PROGRESS - *Provisions for Greater Reuse of Steel Structures* [109]. With respect to these works, slight modifications and additions have been made. The work presented in [30] and [31] is completed by an environmental impact of the same case scenarios considering a liner tray wall cladding system for the envelope of industrial halls.

### 5.2.1 Assessment scenarios

Six scenarios for single-storey steel structures were selected for the environmental impact assessment:

• Baseline scenario (Case 0) in which the structure is designed as a new structure made with elements from new materials.

• The second scenario (Case 0+) considering a structure made of new elements with new materials, with the structure designed for deconstruction.

• The third scenario (Case 1) referring to a relocated steel structure; the scenario considered the reuse of an existing steel structure that originated in Germany and was reassembled in Romania.

• In the fourth scenario (Case 2) it is weighed a steel structure made with reclaimed elements: existing profiles for beams and columns have been identified in a storage yard in Germany, which are deriving from other deconstructed buildings, and transported to Romania to be reused in a new industrial hall. All other components were made of new steel.

• The fifth scenario (Case 3) is similar to Case 2, considering reclaimed elements such as columns and beams, but also end plates for beams and columns. All other components represent new steel.

• The last scenario (Case 4) considers the reuse of an entire structure relocated from Germany. The percent of steel reused in the superstructure in this scenario is 100%.

The amount of steel consumption and the percent of reused steel, for each case scenario, is presented in Table 5.1:

Table 5.1 Steel consumption (for the load-bearing structure) – total steel vs. reused steel

| Case no. | Total weight [t] | Reused steel [t] | % | Purlins [t] |
|---|---|---|---|---|
| Case 0 | 23.7 | - | - | 2.55 |
| Case 0+ | 24.6 | - | - | 2.55 |
| Case 1 | 24.8 | 17.9 | 72.2 | 2.69 |
| Case 2 | 27.7 | 16.8 | 60.6 | 2.55 |
| Case 3 | 29.1 | 19.9 | 68.3 | 2.55 |
| Case 4 | 27.7 | 27.7 | 100 | 2.55 |

#### *5.2.1.1 Case 0*

The study is built on a single-storey industrial hall located in Romania that has a total length of 30 m, with six identical frames at a bay of 5 m. The span is 17.5 m and the height at the eaves is 6 m. The load bearing structure is made of hot-rolled steel sections (columns - HEA320, beams - IPE300, S355) and the envelope involves steel sandwich panels with mineral wool insulation (120 mm sandwich panels for the roof) and liner tray wall cladding with mineral wool insulation (100/600/0.75 liner trays with 60 mm mineral wool insulation for the walls). All elements of the structure were designed as elements made from new materials. The total weight of steel

consumption was 23682.8 kg + 2550.4 kg + 8280 kg (hot-rolled steel profiles + cold-formed purlins + liner trays & outer steel sheet).

#### *5.2.1.2 Case 0+*

The structure is similar to the previous case, where a 30×17.5 m single-storey industrial hall is made of new steel, but in addition to that case, in Case 0+ the structure is designed and prepared for disassembly (all elements of the structure are demountable), with the aim of maximizing the amount of steel for reuse at the end of life of the building. The total weight of the steel consumption was 24593.4 kg + 2550.4 kg kg + 8280 kg (hot-rolled steel profiles + cold-formed purlins + liner trays & outer steel sheet).

#### *5.2.1.3 Case 1*

The structure was originated in Germany and had (initial dimensions) a span of 17.5 m, a length of 35 m (7 bays of 5 m each), and a height of 6 m at the eaves. The columns were HEA 300 and the beams were IPE 360 steel profiles with variable cross-sections at the beam-to-column connection. Steel grade is S355. To relocate to Romania, the structure had to withstand higher loads than in Germany (characteristic values: snow – 1.5 kN/m$^2$, wind – 0.39 kN/m$^2$). To achieve this condition, it was concluded that only the portal frames of the structure can be reused, either with a smaller bay than the initial or by reinforcing the frames to be able to carry the new loads. Due to the high price of the second option, it was decided to build the structure with a bay of 0.5 m smaller than the original one. In the end, the structure to be rebuilt in Romania has a length of 31.5 m, 7 bays of 4.5 m and a width of 17.5 m (presented in Figure 5.1).

The existing roof, the wall bracing systems, and the longitudinal beams were not strong enough to conform to the seismic requirements, which constrained their manufacture of new steel. In the end, the total weight of the load-bearing steel structure is 24812.7 kg + 2695.1 kg (hot rolled steel profiles + cold formed purlins), of which 17907.1 kg represents reused steel.

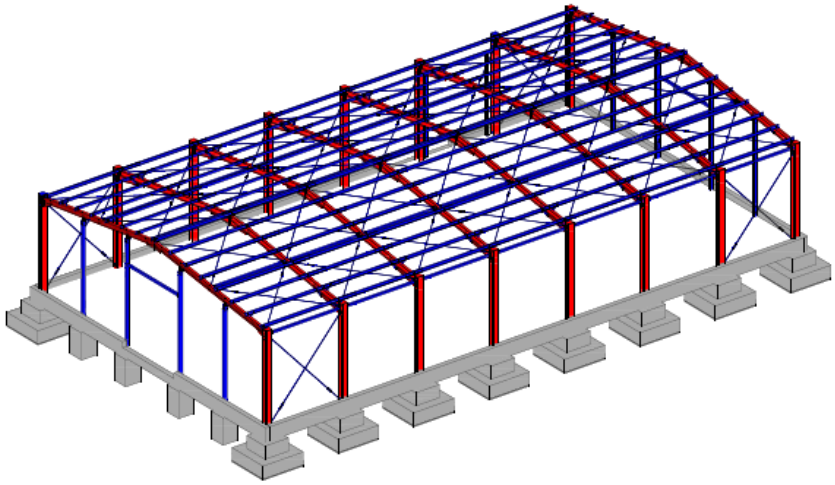

Figure 5.1 The industrial steel structure built in Romania considering the reuse of portal frames (reused steel in red, new steel in blue)

From the existing envelope consisting of a liner tray cladding system, only the liner trays were reused for the structure erected in Romania. Thermal insulation and outer steel sheet (trapezoidal steel sheet) were considered in the investigation as new materials, as well as the sandwich panels used for the roof. In the envelope, 6030 kg represents reused steel resulting from reused liner trays.

#### *5.2.1.4 Case 2*

Existing profiles (as individual members – see Figure 5.2 and Figure 5.3) for beams and columns have been identified in a stockyard in Germany deriving from deconstructed buildings. The beams are IPE 360 steel profiles and the columns are HEA 400. The steel grade is S275. All other components represent new steel. As in Case 0, the structure has a total length of 30 m, with six frames at a 5 m spacing, a span of 17.5 m, and a height at the eaves of 6 m. The weight of the load-bearing steel structure is 27716.3 kg + 2550.4 kg (hot-rolled steel profiles + cold-formed purlins), from which 16795.4 kg represents reused steel.

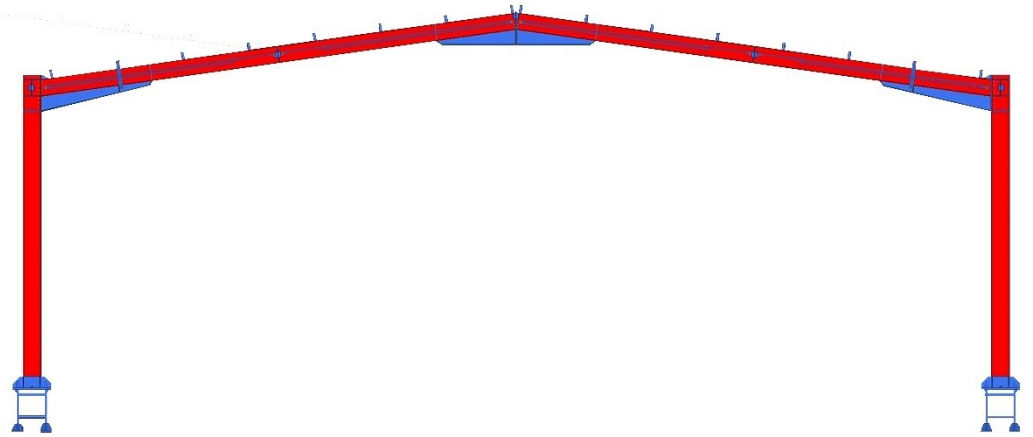

Figure 5.2 Example of portal frame of steel structure considered in Case 2 (individual members without end-plates): reused steel in red, new steel in blue

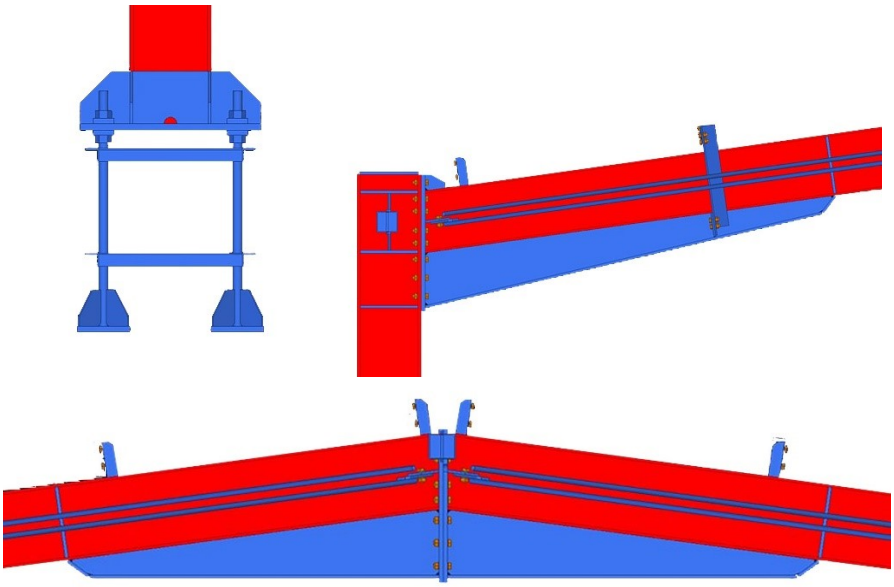

Figure 5.3 Details of individual members used in steel structure considered in Case 2 (reused steel in red, new steel in blue)

The envelope consists, as in Case 1, of 120mm steel sandwich panels with mineral wool insulation (new elements, for the roof) plus the liner trays cladding system in which the thermal insulation and the outer steel sheet were new materials and the liner trays were reused (5400 kg represent reused steel resulting from the reused liner trays).

### *5.2.1.5 Case 3*

Individual members of the steel profiles for beams and columns have been identified in a stockyard in Germany along with end plates for beams and columns (see Figure 5.4). The beams are IPE 360 steel profile, the columns are HEA 400 and the end plates are 30 mm thick. The steel grade is S275. All other components of the steel structure represent new steel.

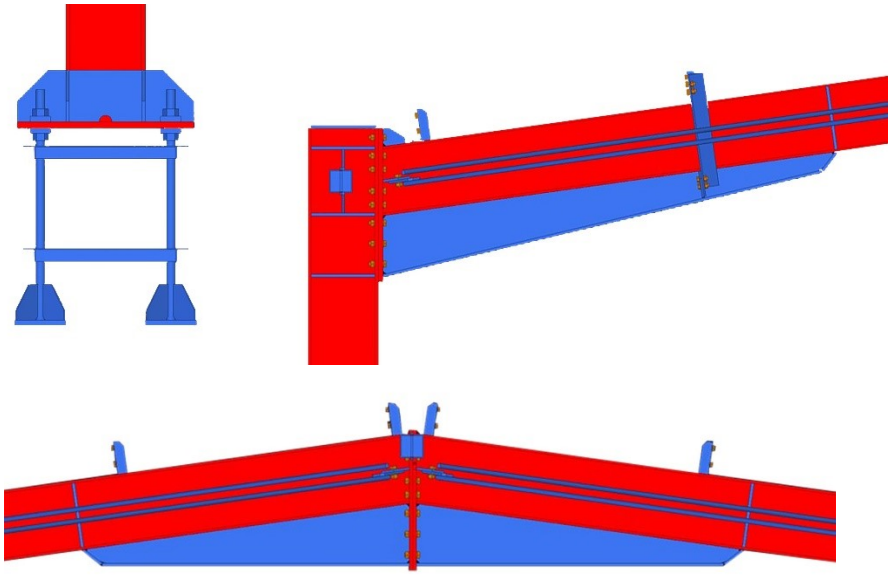

Figure 5.4 The steel profiles for beams and columns (incl. end plates) considered for Case 3 (reused steel in red, new steel in blue)

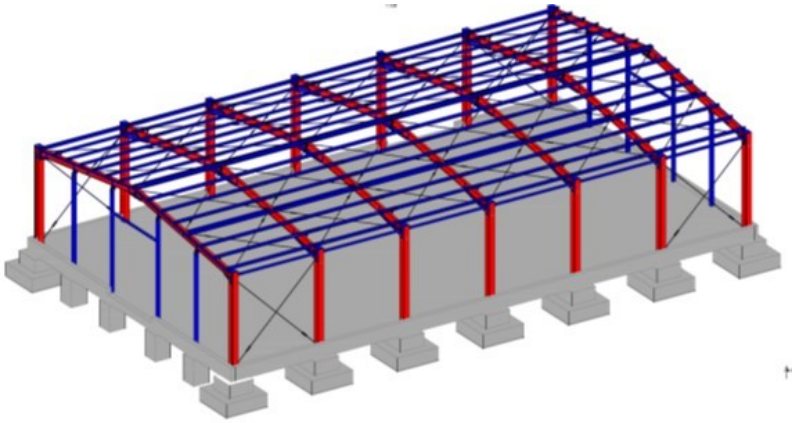

Figure 5.5 The industrial steel structure built in Romania with reclaimed components (reused steel in red, new steel in blue)

The dimensions of the steel structure are the same as in Case 0 and in Case 2. The total weight of the steel structure is 29112.1 kg + 2550.4 kg (hot-rolled steel profiles + cold-formed purlins), from which 19919.7 kg represents reused steel (the steel structure considered for the Case 3 scenario is shown in Figure 5.5).

The envelope has the same stratification as in Case 2: 120mm new mineral wool sandwich panels for the roof + liner tray cladding system (with reused liner trays and new materials for thermal insulation and corrugated steel sheet).

#### *5.2.1.6 Case 4*

The structure originates in Germany and has a total length of 30 m, with six identical frames at 5 m, a span of 17.5 m, and a height at the eaves of 6 m. The total weight of the steel structure is 27716.3 kg + 2550.4 kg (hot-rolled steel profiles + cold-formed purlins), of which all 27716.3 kg represent reused steel. Practically, the entire superstructure was considered to be relocated and reused in this scenario. As in Case 2, the beams are IPE 360 steel profile and the columns are HEA 400. The steel grade is S275. Only the purlins of the steel structure represent new steel in the superstructure. The dimensions of the steel structure are the same as in Case 0 and Case 2. The same solution, as in Case 2, was considered for envelopes.

## 5.3 System boundaries

The environmental assessment considered the following system boundaries for the described case studies:

- The main components of the building are the foundations and the ground floor slab (concrete and steel rebars), the steel load-bearing structure (hot-rolled and cold-formed steel elements), sandwich panels for the roof (steel sandwich panels with mineral wool insulation), liner trays cladding system (a cladding system for walls formed from liner trays + 60 mm thick mineral wool + corrugated steel sheet), triple glazed windows and sectional sliding gates.
- Other materials and components considered in addition to steel:
  - concrete foundations and concrete floor: 185 $m^3$
  - triple-glazed windows: 22.5 $m^2$
  - sectional sliding gates: 48 $m^2$
- The steel rebars were counted as new material, with an input of 73% steel scrap in the manufacturing process and an end-of-life scenario with 95% recycling potential and 5% landfilling or material loss after sorting [175].
- The U-value considered in the assessment is in accordance with the Romanian standard in force [176]:
  - for the external walls - 0.56 $W/m^2 \cdot K$
  - for roof elements - 0.34 $W/m^2 \cdot K$
  - for ground floor slab - 0.76 $W/m^2 \cdot K$
  - for windows and sectional sliding gates - 1.3 $W/m^2 \cdot K$
- The heated floor area of the industrial hall is 525 $m^2$, for Cases 0, 0+, 2, 3 and 4) and 551.25 $m^2$, for Case 1
- The operational lifetime of the building is 25 years.

## 5.4 Environmental assessment

The environmental impact was assessed following the rules described in EN 15804:2012+A2 [54] and EN 15978: 2011 [55]. Life Cycle Assessment includes all stages of life cycle stages ("cradle to cradle") of the steel structure, subdivided into the information module groups A1–A3, A4–A5, B1–B5, B6–B7, C1–C4 and module D [54], shown in Figure 5.6.

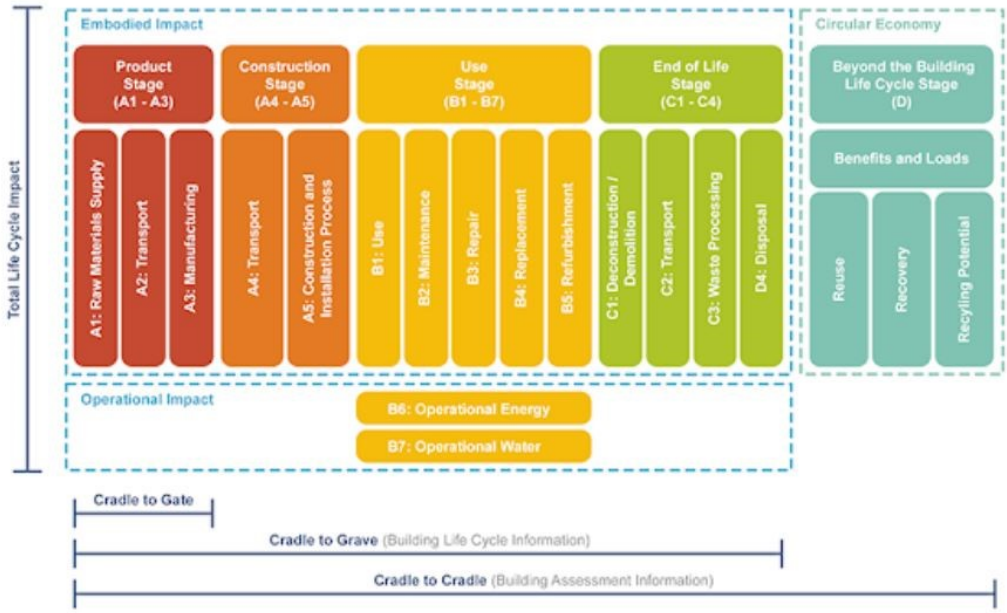


Figure 5.6 Building life cycle, adapted from EN 15978:2011 (figure courtesy of Daniel Overbey, 2023 [177])

### 5.4.1 Methodology

Using the LCA, the environmental impact of secondary products can be evaluated when recycling or reuse is involved. It demands the allocation of environmental impact over different uses, and there are various approaches to reporting this in LCA, which may characterise the process as upstream [178]:

- The cut-off or recycling content approach (100:0) allocates all the environmental impact of reuse or recycling to the product that contains reused or recycled material
- The recyclability or end-of-life approach (0:100) allocates all the environmental impact of reuse or recycling to the product that generates reused or recycled content

• The 50:50 approach allocates half of the environmental impact to the product that generates reused or recycled content and the other half to the product that uses reused or recycled material

• The 100:100 approach allocates the entire environmental impact of reuse or recycling to both products: the one that generates the reused or recycled material and the one that is produced with reused or recycled content.

• The modular approach allocates the benefits separately beyond the system boundary [179].

The approach to accounting for recycling and reuse in LCA, in this thesis, was evaluated using the modular approach, based on the principles of European standards [179], [54].

### 5.4.2 Production stage: Modules $A_1$-$A_3$

This assessment takes into account the manufacture of the load-bearing structure, foundations, floor slab, envelope, windows, and industrial sectional doors. LCA results are calculated for each case scenario considering a "new structure with new materials" and "reused elements" in which different amounts of reused steel were evaluated from the deconstructed industrial building halls. The product stage for reused elements includes blasting and coating (where required) [180].

### 5.4.3 Construction stage: Modules $A_4$-$A_5$

In these modules, the assessment includes the transportation of all construction materials from the manufacturer to the building site, the transportation of equipment, and the erection of the structure. As the location of the building site was considered close to Timisoara city, all the distances from the manufacturers to the building site are between 10 and 70 km.

For the reused steel structure (Case 1) and reused elements (Cases 2, 3, and 4) the distance considered for the transport of reused steel relocated from Germany was 1200 km. Euro 5 articulated truck transport (27t payload capacity) and Euro 4 concrete mixer transport (12-14 t) were assigned to the transport of construction materials from the GaBi database and 65-80% of the payload was considered in the evaluation; also a return journey of empty trucks was taken into account in the evaluation.

Building construction included excavation of soil for the foundation and floor slab, concreting and assembling of the steel structure and envelope using a 10t autocrane, forklifts, man-lifts, wheel loader, bulldozer, excavator, concrete pump, and packaging waste processing [181], [182], [180]. In module A5 the recycling of packaging material at the construction site was also considered, but the recycling potential of the packaging material was neglected and not quantified in module D.

### 5.4.4 Use stage: Modules $B_1$-$B_7$

The use stage refers to the building's lifetime, which starts from the completion of building construction, and it ends when the building is deconstructed or demolished. According to the International Association for Lightweight Metal Building Envelopes in the recommendations for the selection of corrosion protection systems "Experience shows that a service life for industrial buildings of approx. 20 to 25 years is realistic. After that, these buildings are usually replaced due to a change in demand". Therefore, the life expectancy of the industrial hall in each case studied in this assessment is 25 years, with the effect that no maintenance (B2), repair (B3), replacement (B4) of elements, or refurbishment (B5) was considered during this lifetime. The evaluation of operational energy consumption was based on the energy demand for a distribution warehouse [183] and includes energy consumption for heating, cooling, lighting, IT, security, computers, and other systems. In the assessment, neither heat recovery nor mechanical cooling were considered. A similar heat transfer coefficient was targeted for all envelope systems (either consisting of new or reused materials). The envelope systems have been compared using the dedicated online Ubakus software [184]. The external and internal temperature values considered for the evaluation were -5 ° C and 20 ° C, respectively.

Therefore, the use stage was identical for each case scenario (except for Case 1 where the heated floor area is larger 551.25 $m^2$), both new and reused buildings have the same environmental impact during the use stage.

### 5.4.5 End-of-life: Modules $C_1$-$C_4$

In this assessment, the end-of-life scenario for each of the six cases studied involved an instance of 'demolition and recycling' and another one of 'deconstruction and reuse" (Module C1). Deconstruction included dismantling the steel structure and envelope using a 10t auto-crane, forklifts, man-lifts, hydraulic breaker excavator and wheel loader [32], while demolition included working with a 10t auto-crane, bulldozer, hydraulic breaker excavator, hydraulic scrap shear and wheel loader. The energy demand for the demolition of the steel load-bearing structure was assumed to be 0.239 MJ/kg of steel product if the product is recycled and 0.432 MJ/kg of steel product if the product is reused [185]. For cold-formed steel elements, the impacts of deconstruction were modelled based on data from the literature on energy use in demolition, accounting for 0.085 kWh of diesel-powered machinery work per kg of steel deconstructed [186]. For concrete, the environmental impact included the use of diesel in the demolition process [187], while for reinforcement it included the consumption of diesel for the recovery of the reinforcement from crushed concrete [175].

The deconstruction process of the steel structure follows the reverse assembly process, to which additional effort is added to preserve the integrity of the deconstructed components for reuse [53], [107]. Where no other data were available, the supplementary effort was generated in the study as a 1.5 workload multiplier for the amount of elements reused in the end-of-life.

The transportation of residual materials deriving from demolition and deconstruction to the waste processing or the nearest salvage yard is included in the C2 module. Waste processing covered in Module C3 includes handling for reuse, recycling, and disposal. According to the World Steel Association (2017), steel recycling is included in Module A.

### 5.4.6 Benefits and loads beyond the system boundary: Module D

Recovered materials, recovered structures or elements of the structure, steel scrap recycling can result in benefits in the form of $CO_2$ (or other impacts) savings. In this analysis, the data for Module D are based on scenarios that consider current practices and current rates of materials recycling. The calculation model used for the assessment of Module D – Climate Change total [kg $CO_2$eq] is based on an innovative calculation model [29], compatible with the methodology of the EN 15804 standard [179]. The calculated impact involving potential environmental credits or burdens generated by future lifecycles is based on the impacts of reuse and recycling of the materials jointly operated. The calculation is based on the input and output of recycled and reused materials, the impact of virgin material production, and the impact of theoretical pure recycling. The recycling process yield was considered 0.916 t of recycled steel per 1 t of steel scrap (as specified by the World Steel Association, 2017) and the information about Modules A1-3 was based on Environmental Product Declarations (EPD) by Ruukki Construction [188].

### 5.4.7 Assessed Scenarios for the Environmental Impact

Each of the six cases studied covered a view for 'demolition and recycling' and one for 'deconstruction and reuse' in the end-of-life module. In the assessment, it was assumed that when it comes to the reuse of construction materials, both steel and envelopes are reused materials, as described in the following scenarios. For the wall cladding system, in the reuse cases (Cases 1 to 3), only the liner trays were considered to be reused materials, due to the fact that the outer layer of the cladding system in most cases does not meet the reuse requirements. This may be due to aesthetic reasons, such as minor damage (dents, scratches), due to corrosion (after certain years of use, the presence of corrosion is possible) or due to damage induced to the cladding system during disassembly processes [31].

The percentage of steel (see Table 5.2) used in the description below refers to the steel utilised in the load-bearing structure (main and secondary structure) only:

- New steel – demolition and recycling (Case 0): in the assessment it was considered that the external input of steel scrap includes 20% in the manufacturing process (both the blast furnace and the electric arc furnace are used in the fabrication process) [181] and that 90% of the steel is recycled at the structure’s end-of-life

Table 5.2 Assessed scenarios for steel in the load-bearing structure (incl. purlins) – input and output flow of the material

| End-of-life scenario for steel: **Recycle scenario** | In | | | Out | | |
|---|---|---|---|---|---|---|
| | New material | Reused material | Recycled material (scrap) | Waste | Material for reuse | Material for recycling |
| Case 0 | 80% | 0% | 20% | 10% | 0% | 90% |
| Case 1 | 27.92% | 65.10% | 6.98% | 10% | 0% | 90% |
| Case 2 | 35.61% | 55.49% | 8.90% | 10% | 0% | 90% |
| Case 3 | 29.67% | 62.91% | 7.42% | 10% | 0% | 90% |
| Case 4 | 0% | 100% | 0% | 0% | 0% | 100% |
| End-of-life scenario for steel: **Reuse scenario** | In | | | Out | | |
| | New material | Reused material | Recycled material (scrap) | Waste | Material for reuse | Material for recycling |
| Case 0 | 80% | 0% | 20% | 1% | 90% | 9% |
| Case 0+ | 80% | 0% | 20% | 0% | 100% | 0% |
| Case 1 | 27.92% | 65.10% | 6.98% | 3% | 72% | 25% |
| Case 2 | 35.61% | 55.49% | 8.90% | 4.45% | 55.49% | 40.06% |
| Case 3 | 29.67% | 62.91% | 7.42% | 3.71% | 62.91% | 33.40% |
| Case 4 | 0% | 100% | 0% | 0% | 100% | 0% |

• New steel – deconstruction and reuse (Case 0): in the assessment it was considered that the external steel scrap input includes 20% from manufacturing processing, 90% of the steel is reused at the end-of-life of the structure and 90% of the remaining steel is recovered for recycling. Furthermore, 90% of the roof sandwich panels was considered to be reused and 90% of the steel sheets were recovered from the remaining sandwich panels for recycling while 90% of the liner trays of the wall cladding system were reused, and 10% of the liner trays along with 90% of the corrugated steel sheets were recovered for recycling

• New steel – design for deconstruction (Case 0+): the same as Case 0 – new steel, deconstruction, and reuse but with 100% of steel reuse (steel in load-bearing structure) at the structure's end-of-life

• Reused steel structure – demolition and recycling (Case 1): 65.10% of the total steel weight in the load-bearing structure (including purlins) represented reused steel, and the remaining new steel has an external scrap input of 20%. At the end-of-life of the structure, 90% of the steel is recycled (including 90% of the steel sheets of the sandwich panels)

• Reused steel structure – deconstruction and reuse (Case 1): 65.10% of the total steel weight of the load-bearing structure (including purlins) represented reused

steel and the remaining new steel has an external scrap input of 20% from manufacturing processing. At the end-of-life of the structure, 72% of the load-bearing steel structure (representing steel frames only) is reused and 90% of the remaining steel is recovered for recycling (i.e. 25% of the total steel mass). Furthermore, 90% of the roof panels were considered reused and 90% of the steel sheets were recovered from the remaining sandwich panels for recycling. Additionally, 10% of the liner trays along with 90% of the corrugated steel sheets are recovered for recycling, while 90% of the liner trays are reused

- Reused steel elements – demolition and recycling (Case 2): 55.49% of the total steel weight in the load-bearing structure (including purlins) represented reused steel, and the remaining new steel has an external scrap input of 20%. At the end-of-life of the structure, 90% of the steel is recycled, including 90% of the steel sheets in the roof sandwich panels;
- Reused steel elements – deconstruction and reuse (Case 2): 55.49% of the total steel weight of the load-bearing structure (including purlins) represented reused steel, and the remaining new steel has an external scrap input of 20%. At the end-of-life of the structure, 55.49% of the steel load-bearing structure (representing columns and beams only) is reused and 90% of the remaining steel is recovered for recycling (40.06% of the total steel mass of the super-structure). It was considered that 90% of the roof is reused and from the remaining sandwich panels, 90% of the steel sheets are recovered for recycling while from the wall cladding system, 90% from the liner trays are reused and 10% of the liner trays along with 90% of the corrugated steel sheets are recovered for recycling
- Reused steel elements – demolition and recycling (Case 3): 62.91% of the total steel weight of the load-bearing structure (including purlins) represented reused steel, and the remaining new steel has an external scrap input of 20%. At the end-of-life of the structure, it is assumed that 90% of the steel is recycled, including 90% of the steel sheets in roof sandwich panels
- Reused steel elements – deconstruction and reuse (Case 3): 62.91% of the total steel weight of the load-bearing structure represented reused steel and the remaining new steel has an external scrap input of 20%. At the end-of-life of the structure, 62.91% of the steel load-bearing structure, representing only columns and beams, is reused and 90% of the remaining steel is recovered for recycling. For the envelope, it was considered that 90% of the roof is reused and from the remaining sandwich panels 90% of the steel sheets are recovered for recycling while from the wall cladding system 90% from the liner trays are reused, 10% of the liner trays along with 90% of the corrugated steel sheets are recovered for recycling
- Reused structure – demolition and recycling (Case 4): 100% of the total steel weight in the load-bearing structure (including purlins) represented reused steel, only the rebars in the foundations and corrugated steel sheet in wall cladding were considered new steel, with an input scrap of 20%. At the end-of-life of the structure, 100% of the steel is recycled, including 100% of the steel sheets in the sandwich panels, and wall cladding

• Reused structure – deconstruction and reuse (Case 4): 100% of the total steel weight in the superstructure (including purlins and corrugated steel sheets in wall cladding) represented reused steel. At the end-of-life of the structure, all the steel in the load-bearing structure is reused. Regarding the envelope, 100% reuse was considered, excluding the thermal insulation.

## 5.5 Life cycle assessment results

### 5.5.1 Analysis on the entire building

The environmental impact of the assessment was expressed using Total Climate Change as a pointer following the rules described in EN 15804 [54], EN 15978 [55] and ISO 14044 [52].

Figure 5.7 presents the total LCA results of the assessed scenarios of the industrial hall, without showing the use phase in the chart, but which was included in the analysis. The environmental impact related to the use phase is showed in Table 5.3 and Table 5.4; due to the fact that each case scenario has the same environmental impact during the use stage, the use stage environmental impact was not showed in the chart. The LCA savings are reflected as negative values, while positive values define the burdens of material utilization. It can be seen that the benefits and loads beyond the system boundary are not aggregated with the life cycle impacts (Modules A to C), as provided by the CEN/TC 350 methodology.

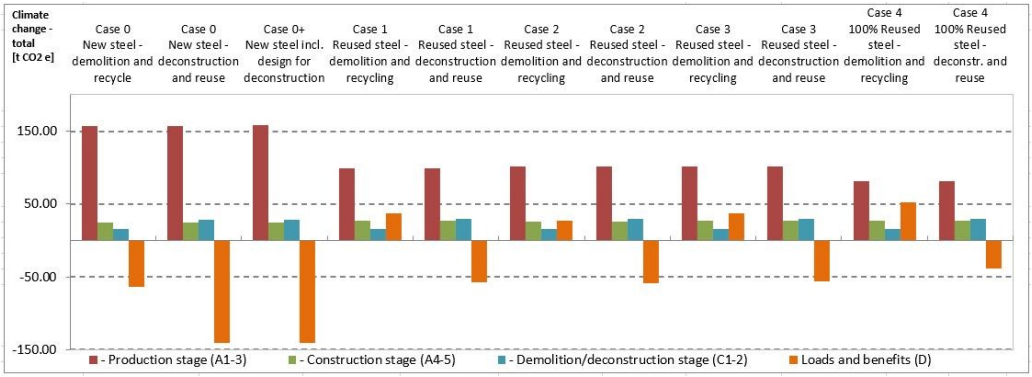


Figure 5.7 LCA results of the scenarios including loads and benefits beyond the system (without showing the use phase in the chart)

Table 5.3 and Table 5.4 outline the greenhouse gas (GHG) emissions for each case study. As the results show, in the production stage (A1-A3), the savings are between 54-58% when reclaimed steel is used in construction (Cases 1 to 3) compared with the case using only new materials (Case 0). Relocating the entire industrial hall superstructure and reusing it as is, including the reuse of the liner trays and outer corrugated steel sheets of the wall cladding system in the envelope (Case

4), involves a significant avoided environmental impact of the materials production process and a decrease in the emissions in the production stage of up to 93% (compared to the baseline scenario - Case 0). The process of including the design for deconstruction in the baseline scenario and the additional amount of steel which this process implies (Case 0+), lifts the emissions in the production stage by 1% compared to the optimal design scenario (Case 0) of the industrial hall.

In the Construction stage (A4-A5), the highest environmental impacts recorded for the reused steel case scenarios (Cases 1 to 4) are caused by the transport of reused steel relocated from Germany to Romania.

Table 5.3 LCA results for Demolition and recycle scenarios

| Scenario | Demolition and recycle [$tCO_2e$] | | | | |
|---|---|---|---|---|---|
| | Case 0 | Case 1 | Case 2 | Case 3 | Case 4 |
| Environmental impacts (A-C) | 1245.22 | 1242.79 | 1191.94 | 1192.54 | 1172.17 |
| Production stage (A1-3) | 157.26 | 99.42 | 101.49 | 101.82 | 81.12 |
| Construction stage (A4-5) | 24.00 | 26.66 | 26.27 | 26.48 | 26.91 |
| Use stage (B) | 1048.83 | 1101.27 | 1048.83 | 1048.83 | 1048.83 |
| Demolition /deconstruction stage (C1-4) | 15.12 | 15.44 | 15.35 | 15.41 | 15.31 |
| Loads and benefits (D) | -63.40 | 37.52 | 26.36 | 37.62 | 51.93 |

As for each case scenario, the lifetime expactancy of the building, the destination, the heat transfer coefficient for elements, and the heated floor area are the same, both new and reused buildings have the same environmental impact during the use stage: 1048.83 t $CO_2$ e. An exception occurred for Case 1, due to its increased heated floor area (551.25 $m^2$) in comparison with the other cases (525 $m^2$), where the Climate Change Total impact was slightly higher than in the other cases. However, the results validate the fact that the use stage is the stage with the highest environmental impact in a life cycle of the buildings, emphasizing the importance of the envelope / façade system in a building.

In the end-of-life stage (C1-C4), when the deconstruction process requires additional workload to preserve the integrity of the deconstructed components for reuse, the savings are acquired by the recycling scenarios. In the *Demolition and Recycle* scenarios, the environmental impacts for modules C1-C4 are almost half in comparison with the *Deconstruction and Reuse* scenarios, despite the waste processing loads acquired after the demolition of the structures.

According to the results (modules A-C), the highest environmental impact is shown by the cases when structures erected with new elements are deconstructed for

the next reuse case (2.39 t $CO_2$ e / $m^2$ – Case 0+) while the lowest emission rate is recorded when structures are built with reused materials and at the end of the structure's life, steel is recovered for recycling (2.23 t $CO_2$ e / $m^2$ – Case 4).

The LCA savings are reflected as negative values in Table 5.3 and Table 5.4. The results in Module D show that, in the scenarios where the structures are built with reused elements and at the end-of-life steel is recovered for recycling, a burden is recorded in the assessment. The highest potential savings (268.07-268.99 kg $CO_2$ e/$m^2$) appear in the scenario where the industrial hall was erected with new elements, which are deconstructed for the next reuse case in the end-of-life.

Table 5.4 LCA results for Deconstruction and reuse scenarios

| Scenario | Deconstruction and reuse [t $CO_2$ e] | | | | | |
|---|---|---|---|---|---|---|
| | Case 0 | Case 0+ | Case 1 | Case 2 | Case 3 | Case 4 |
| Environmental impacts (A-C) | 1258.34 | 1259.37 | 1256.78 | 1206.01 | 1207.0 | 1186.23 |
| Production stage (A1-3) | 157.26 | 158.26 | 99.42 | 101.49 | 101.82 | 11.12 |
| Construction stage (A4-5) | 24.00 | 24.01 | 26.66 | 26.27 | 26.48 | 26.91 |
| Use stage (B) | 1048.83 | 1048.83 | 1101.27 | 1048.83 | 1048.83 | 1048.83 |
| Demol/deconstr stage (C1-4) | 28.24 | 28.27 | 29.43 | 29.42 | 29.87 | 29.37 |
| Loads and benefits (D) | -140.74 | -141.22 | -57.28 | -58.42 | -55.96 | -39.03 |

### 5.5.2 Envelope solutions comparison

In new industrial buildings, the current envelope solutions consisting of sandwich panel systems is already quite high, which may enable future reuse at the end-of-life of the buildings.

In 2022, the European market for sandwich panels used in the construction sector reached a worth value of EUR 3.366 billion, according to *Expert Market Research* [189]. This growth was propelled by increased government investments in infrastructure projects. With prominent industry players channelling more investments into the creation of environmentally friendly sandwich panels, the European market is poised for continued expansion from 2023 to 2028, with an anticipated compounded annual growth rate (CAGR) of 5.2%. The projections indicate

that the value of the European market will increase to EUR 4.568 billion by 2028 (the global size of the sandwich panel market is projected to grow from EUR 9.16 billion in 2023 to EUR 16.13 billion by 2030, at a CAGR of 8.4% [190]).

Based on the fact that the industrial segment is expected to hold a significant market share in the sandwich panels industry (50% of the market, according to [1]), a Life Cycle Assessment of the study cases presented in this chapter was investigated, considering sandwich panels as the only envelope solution. Additionally, a comparison of the LCA results of structures with liner tray cladding envelope and structures with sandwich panels envelope is presented.

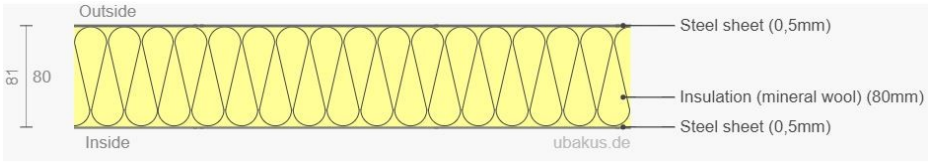


a)

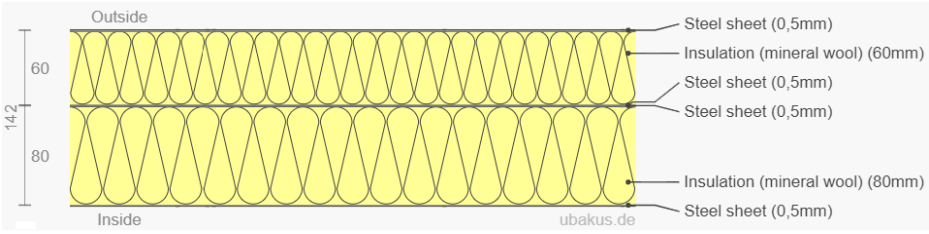


b)

Figure 5.8 Cross-section of envelope solution based on sandwich panels: a) envelope considered for Case 0 and Case 0+ b) envelope considered for cases 1 to 4 (image generated with [184])

For the comparative environmental impact assessment, the system boundary of each case scenario remained the same as in the cases presented in Sect. 5.2 and 5.3, only the envelope changed and involved steel sandwich panels with mineral wool insulation. The thickness of the sandwich panels was chosen in such a wayas to have similar U-values of the elements in both analyses. For Cases 0 and 0+, where the structures were made with new materials, the envelope consisted of 120 mm sandwich panels for the roof and 80 mm sandwich panels for the walls. For Cases 1 to 4, where the analysis involved reused materials, the existing envelope containing 80mm steel sandwich panels with mineral wool insulation was reused, but to comply with the U-values existing in Case 0 and 0+, an additional layer of 60mm sandwich panels (new elements) was added to the entire envelope. The cross-section of the envelope consisting in sandwich panels is presented in Figure 5.8. For the End-of-life assessment, in the *Demolition and Recycle* scenario, it was considered that 90% of the steel sheets from the sandwich panels were recycled, while the mineral wool thermal insulation and 10% of the steel sheets were landfilled. In the *Deconstruction and Reuse* scenario it was considered that 90% of the envelope is reused and from the remaining sandwich panels 90% of the steel sheets are recovered for recycling

(3.45% of the total mass of the sandwich panels). The LCA results of the case studies involving the sandwich panel envelope system are presented in Table 5.5.

Table 5.5 LCA results for case studies with sandwich panels envelope system

| Scenario | Demolition and recycle [$tCO_2e$] | | | | |
|---|---|---|---|---|---|
| | Case 0 | Case 1 | Case 2 | Case 3 | Case 4 |
| Environmental impacts (A-C) | 1230.45 | 1246.79 | 1195.85 | 1196.45 | 1186.46 |
| Production stage (A1-3) | 143.97 | 104.94 | 106.43 | 106.76 | 96.45 |
| Construction stage (A4-5) | 22.46 | 25.00 | 24.79 | 25.00 | 25.43 |
| Use stage (B) | 1048.83 | 1101.27 | 1048.83 | 1048.83 | 1048.83 |
| Demolition /deconstruction stage (C1-4) | 15.20 | 15.59 | 15.80 | 15.85 | 15.75 |
| Scenario | Deconstruction and Reuse [$tCO_2e$] | | | | |
| | Case 0 | Case 1 | Case 2 | Case 3 | Case 4 |
| Environmental impacts (A-C) | 1242.93 | 1260.15 | 1209.00 | 1209.99 | 1199.60 |
| Production stage (A1-3) | 143.97 | 104.94 | 106.43 | 106.76 | 96.45 |
| Construction stage (A4-5) | 22.46 | 25.00 | 24.79 | 25.00 | 25.43 |
| Use stage (B) | 1048.83 | 1101.27 | 1048.83 | 1048.83 | 1048.83 |
| Demolition /deconstruction stage (C1-4) | 27.68 | 28.95 | 28.95 | 29.40 | 28.90 |

The LCA comparison (modules A-C) between cases with liner tray wall cladding and cases with sandwich panels envelope is presented in Figure 5.9.

The results of this comparison show that the *Climate change total* is higher in cases where structures are built with new materials and have liner tray wall cladding envelopes, regardless of the end-of-life scenario. The difference of additional 15-16 t of $CO_2$ e in these cases is mainly correlated with two stages of the life cycle: The highest amount of these additional emissions is recorded in the production stage (A1-A3) due to the higher amount of steel (and the environmental impact related to the steel production process of steel) present in the liner tray built-up wall system than in the sandwich panel envelope system; the rest of the amount of the additional emissions were recorded in the Construction stage (A4-A5) due to the extra workload

required by the installation of the liner tray built-up wall system, as double-shell systems in particular consist of many different individual parts.

However, Figure 5.9 shows a clear trend of decreased rate of emissions in the reused case scenarios (Cases 1 to 4) for the structures with liner tray wall cladding envelope in both *Demolition and Recycle* scenario and *Deconstruction and Reuse* scenario. While close environmental impact results were recorded in modules A4-A5, C1-C4 for identical study cases with liner tray wall cladding envelope and sandwich panel envelope, a difference of 9.52-29.20 kg $CO_2$ e/$m^2$ is registered in the Production stage (A1-A3) when on an existing envelope consisting in sandwich panels is installed an additional layer of sandwich panels.

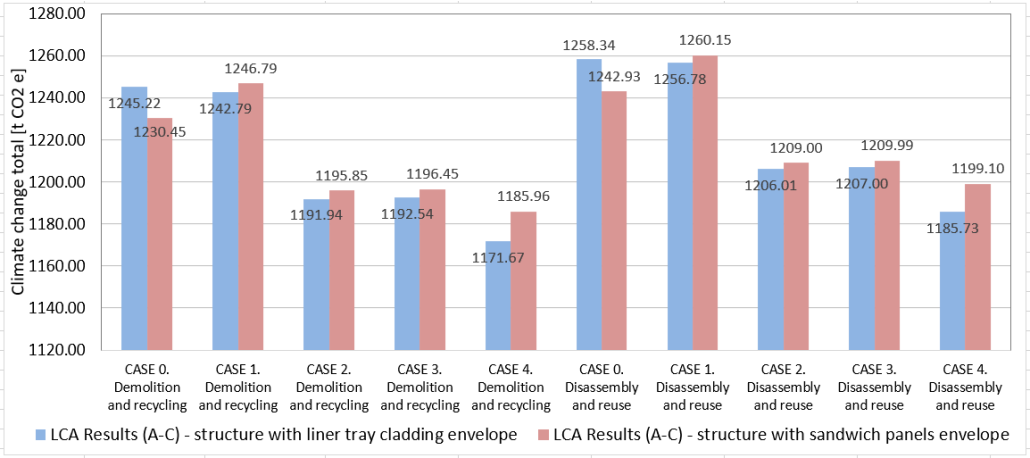


Figure 5.9 LCA comparison (A-C) between structures with liner tray wall cladding envelope and structures with sandwich panels envelope

The smallest environmental impact is shown by the case when the entire structure is built with reclaimed elements and the wall envelope is made of liner tray cladding (1171.67 t $CO_2$ e/$m^2$) while at the end-of-life of the structure the materials are recycled.

In Figure 5.10 is presented a comparison of loads and benefits (impacts computed in Module D) between structures with liner tray wall cladding envelope and structures with sandwich panels envelope. The benefits are reflected in the assessment as negative values.

In all cases the highest potential benefits (negative values) appear for the structures which have a liner tray wall cladding envelope, and the highest loads (positive values) appear for the structures which have sandwich panels envelope system. Differences of 8-25% in the potential benefits and 11-19% in the potential loads are shown between the two envelope solutions.

According to the results, the highest potential benefits appear in Case 0 with a *Demolition and Recycle* scenario in the End-of-life stage for both envelope solutions. In this situation, the maximum potential benefit is recorded for the structures having a liner tray wall cladding envelope (-140.74 t $CO_2$ e/$m^2$).

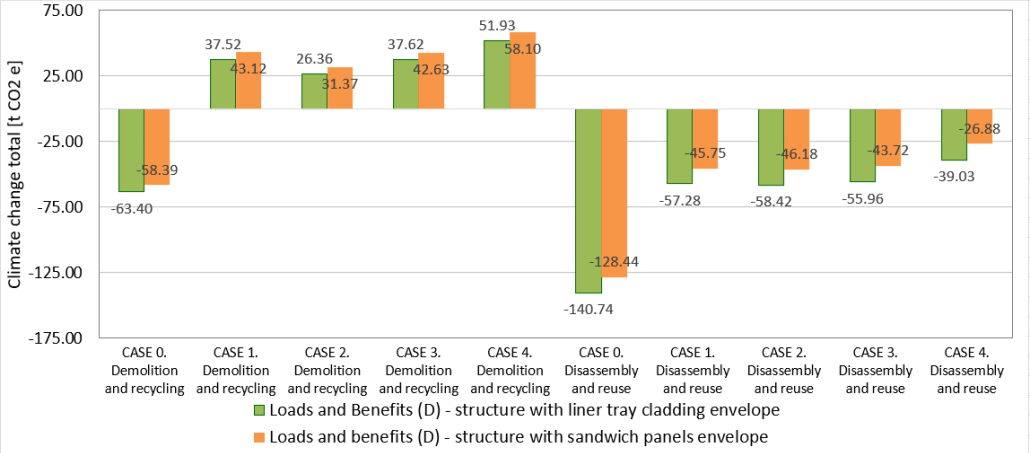


Figure 5.10 Loads and benefits comparison (module D) between structures with liner tray wall cladding envelope and structures with sandwich panels envelope

## 5.6 Concluding remarks

The end-of-life quality of construction products plays an important role in considering the circular economy, as buildings have a long intended lifespan and require a significant amount of material resources. To maintain circularity, these resources have to be kept in service through reuse, reclaim, or recycling. The end-of-life environmental impact of structural materials vary significantly due to their inherent properties; therefore, the reuse of steel is a viable solution to meet the circular economy criteria and reduce its environmental footprint.

Starting from an optimal design case considering a new steel structure with new materials, this chapter presented further design possibilities for the same steel building using reclaimed elements. The case study, based on single-storey industrial halls, compares environmental indicators of the optimal design model in contrast to a structure prepared for disassembly to be reused in the future. Further cases focused on the reuse of an existing steel structure and/or reclaim of various elements based on the same building in a comparative life cycle assessment (LCA). The evaluation stressed the structural feasibility and the environmental benefits of a construction strategy based on the reuse approach.

The results of the Life Cycle Assessment showed that reuse is a strategy that offers superior environmental benefits to recycling (modules A-C), the greatest gain being visible in the production stage (A1-3) where the GHG emissions are between 54-93% lower when the structure is built with reused steel (154.51-193.94 kg of $CO_2$ e/$m^2$ for structures built with reused steel compared to 301.44 kg of $CO_2$ e/$m^2$ for structures built with new steel). Nonetheless, more effort is put in the deconstruction/dismantling phase for the reuse of elements in the future.

The highest environmental impact in a building's life cycle is attained during the Use stage. Therefore, the building envelope is a critical component that plays a significant role in reducing operational energy consumption and environmental

impact. Proper insulation, air tightness, and ventilation of the building envelope can reduce energy consumption. The building envelope's material selection, energy efficiency, and durability can also significantly impact the building's environmental impact. It is essential to consider the building envelope's design and materials carefully to ensure optimal energy efficiency and environmental sustainability.

When considering different envelope solutions, the LCA results reported here confirm that the highest potential benefits (8-25% higher) appear for the structures which have a liner tray wall cladding envelope, and the highest loads (11-19% higher) appear for the structures which have sandwich panels envelope system.

However, due to the large variety of materials and building practices, it is recommended to perform LCA calculations on a case-by-case basis, as the results could differ significantly from the present study.

# 6 Conclusions of PhD study. Contributions of the author. Future research

## 6.1 Conclusions of PhD study

**Chapter 1: Introduction**

An introduction to the research topic was made that shows the scope and objectives of the thesis. The thesis outline was also presented.

**Chapter 2: State of knowledge**

A state-of-the-art of legislative proposals, framework, and principles for international climate action was presented, along with the environmental impact of the construction sector and steel-intensive façade systems.

Amidst environmental concerns and finite resources, the construction industry is bounded to shift toward sustainable methodologies due to its significant role in environmental repercussions. In July 2023, at the European level, a package of legislative proposals named Fit for 55 which aims to diminish the EU's greenhouse gas emissions by at least 55% by 2030 compared to 1990 levels. The legislative package includes new and revised directives, many of them with a direct impact in the construction sector.

The importance of building envelopes and façade systems has grown in the past decades due to the fact that a significant share of the world's energy consumption is attributed to commercial and residential buildings. The concept of a circular economy, centred on waste reduction and improving resource efficiency, needs to be more seriously incorporated into façade design and construction methods. This involves investigating techniques for reusing materials, facilitating recycling, and managing end-of-life processes, as well as valuable life-cycle assessments and life-cycle cost of buildings that would encourage greater consideration for the deconstruction and reuse of construction materials.

From a sustainable perspective, steel-intensive façade systems represent a valuable solution with respect to energy-efficiency performance, energy embodied in building materials, reuse, and high potential for recycling. Liner tray cladding systems are especially valued for the distinct benefits they offer, such as increased load-bearing capacity and stability, speed of installation, reduced maintenance, aesthetic versatility, cost efficiency, and sustainability.

The most critical in the design for structural liner trays with a single span is the bending moment that causes sagging, while vertical shear forces and lateral forces on the supports may be ignored, in most cases. The bending moment resistance becomes particularly critical, especially when the structure is subjected to significant wind loads. Liner trays tested to wind loads in a more natural way of loading but in fully controlled testing conditions should be conducted in order to have a deeper understanding of cladding system behaviour. In this context, the study of liner trays cladding system subjected to wind loads through a vacuum chamber is worthwhile,

contributing to a higher comprehension of the dynamic effect of wind loads on these envelope solutions.

The use of a vacuum chamber to study the wind behaviour of the liner trays presents a novel and innovative approach. By providing a controlled environment, this approach allows a deeper understanding of the dynamic interactions between the wind and the cladding components. The potential to advance the science of wind-resistant building envelopes appears promising through vacuum chamber testing, due to the advantages offered by precise data collection, isolation of wind effects, and generation of innovative design insights.

As research and experimentation in this area continues to evolve, vacuum chamber testing may become standard practice in the evaluation and design of liner trays and other cladding components. This advancement could lead to more resilient and reliable building façades that can withstand the challenges posed by dynamic wind actions.

**Chapter 3: Experimental investigation of liner trays subjected to wind loads**

A vacuum chamber experimental investigation on liner trays with different test configurations subjected to wind loads was presented. To establish the lower limit of the bending moment capacity of the liner trays, tests were performed using simple liner trays without any outer cladding. Furthermore, with regard to getting the direct contribution to the limit of the bending moment capacity of the outer shell in a liner tray wall system, apart from the tests of pure liner trays, the experimental program included tests with outer cladding. As in practice, a liner tray wall system consists of several liner trays used as an inner shell of a double shell wall system, restrained liner trays with and without outer cladding were tested to establish their ultimate moment resistance. The main purpose of the study was a higher comprehension of the dynamic effect of wind loads on these envelope solutions in case of cladding systems under real conditions of service.

The test results were splited into two groups based on the type of wind loading, namely pressure and suction. Within each group, test results were described, observing the location and nature of failure zones. The ultimate load values showed that when subjected to wind pressure, the fasteners in the narrow flanges of the liner trays have a higher role in the load-bearing behaviour of a liner tray double-shell wall system than the cladding. At the same time, in the case of both types of wind loading, the double wall thickness of the restrained liner tray leads to a significantly increased load-bearing limit of the systems.

The results of the experimental specimens were compared to the design values of strength and stiffness obtained following the procedure recommended by EN. The main conclusion that could be drawn is that the norm considers a conservative design approach, having design load values well within the safe range.

**Chapter 4: Numerical investigations on liner trays**

To demonstrate the efficiency of various options for liner trays subjected to wind loads and to allow the evaluation of certain parameters and the influence on

liner trays subjected to real loading conditions, finite element numerical investigations were performed.

Based on the results obtained in the experimental tests two FE models were calibrated for the numerical simulations. The two FE models were calibrated in order to replicate the experimental behaviour of liner trays in the post-test finite element analysis: (i) a model that simulates the behaviour of the LT-SO-P tested specimen and (ii) one model that reflects the behaviour of the LT-SO-S specimen. Validated numerical models of liner trays subjected to pressure and suction were used in a further parametric study of FE, compiling data on the influence of parameters such as thickness, height and length on the behaviour of the liner trays.

The numerical results of the investigation were classified into two groups based on the type of wind loading effect, namely liner trays with wide flange in tension (as a result of wind pressure) and trays with wide flange under compression (as a result of wind suction). Considering that in the numerical model, the damage parameters of the material were not defined, the results of the parametric study reflect the stiffness performance of each investigated model, while the output force-deflection curves were presented up to a maximum load value recorded immediately before failure in the experimental investigations ($F_{max\_exp}$).

Taking into account the thickness of the steel sheet, the height of the web and the length of the liner tray, the results of the parametrical study showed that thickness is the parameter that registers the most significant influence on the liner trays, followed by the length of the liner trays.

Changing the steel sheet thickness parameter also had a greater influence on the stiffness of the liner trays. An increase in stiffness of up to 86%, in the case of liner trays subjected to wind pressure, and up to 250% in the case of liner trays subjected to wind pressure, resulted from the numerical investigations by an increase of thickness form 0,75mm to 1,5mm. At the same time, when the Fmax_exp value is reached, the deflection of the liner trays with the wide flange in tension decreases by up to 59.06%, while the deflection of the liner trays with the wide flange in compression decreases by up to 71.10%.

The change in length and structural system of the liner trays from one span to two spans, each of 4m length leads to a greater influence in the case of liner trays subjected to suction: deflection reduction at $F_{max\_expl}$ of 38.3% from the original deflection of the LT-SO-S specimen in the experimental investigation and double its stiffness than in the case of liner trays subjected to pressure. Here, in the last mentioned, the deflection reduction at $F_{max\_exp}$ is of 79.7% from the original deflection of LT-SO-P specimen accompanied by a 10% higher stiffness.

The height of the web proved to be the parameter with the least influence on the liner trays. Although the results of the parametric study of liner trays subjected to pressure indicate a minor difference between the behaviour of the LT-SO-P specimen and the FE models with different web heights, the results of the parametric study of liner trays subjected to suction showed a deflection at $F_{max\_exp}$ of 56.58% from the original deflection of the LT-SO-S specimen and a stiffness that improves by up to 42% with an increase in web height from LT-SO-S: experimental to h = 150.

**Chapter 5: Environmental impact of buildings with steel-intensive façade systems**

The end-of-life quality of construction products plays an important role in considering the circular economy, as buildings have a long intended lifespan and require a significant amount of material resources. To maintain circularity, these resources have to be kept in service through reuse, reclaim, or recycling. The end-of-life environmental impact of structural materials vary significantly due to their inherent properties; therefore, the reuse of steel is a viable solution to meet the circular economy criteria and reduce the environmental footprint of a structure.

Starting from an optimal design case considering a new steel structure with new materials, in chapter 5 were presented further design possibilities for the same steel building using reclaimed elements. The case study, based on single-storey industrial halls, compares environmental indicators of the optimal design model in contrast to a structure prepared for disassembly to be reused in the future. Further cases focused on the reuse of an existing steel structure and/or reclaim of various elements based on the same building in a comparative life cycle assessment (LCA). The evaluation stressed the structural feasibility and the environmental benefits of a construction strategy based on the reuse approach.

The results of the Life Cycle Assessment showed that reuse is a strategy that offers superior environmental benefits to recycling (modules A-C), the greatest gain being visible in the production stage (A1-3) where the GHG emissions are between 54-93% lower when the structure is built with reused steel: 154.51-193.94 kg of $CO_2$ e/$m^2$ for structures built with reused steel compared to 301.44 kg of $CO_2$ e/$m^2$ for structures built with new steel. Nonetheless, more effort is put into the deconstruction/dismantling phase for the reuse of elements in the future.

The highest environmental impact in a building's life cycle is attained during the Use stage. Therefore, the building envelope is a critical component that plays a significant role in reducing operational energy consumption and environmental impact. Proper insulation, air tightness, and ventilation of the building envelope can reduce energy consumption. Material selection, energy efficiency, and durability of the building envelope can also significantly influence the environmental impact of the building. It is essential to consider the design and materials of the building envelope carefully to ensure optimal energy efficiency and environmental sustainability.

When considering different envelope solutions, the LCA results confirm that the highest potential benefits (8-25% higher) appear for the structures that have a liner tray wall cladding envelope, and the highest loads (11-19% higher) appear for the structures which have sandwich panels envelope system.

## 6.2 Contributions of the author

Based on the experimental, numerical, and environmental impact analysis performed by the author as summarised in Chapter 6.1, the following results are presented as personal contributions to this thesis:

• Synthesis of legislative proposals, frameworks, and principles for climate action that has an impact on the construction sector, the environmental impact of the construction sector, as well as the structural behaviour of the liner trays subjected to wind loads into a comprehensive **state-of-knowledge**.

• Development of **experimental tests** for liner trays. The author was involved in: instrumentation of the experimental setup used for liner trays testing, performing the testing of the liner trays, monitoring the testing of base materials, interpretation of the experimental data, identifying the failure modes of the specimens, determination of the design values of liner trays in wall claddings subjected to horizontal loads following the procedure recommended by EN.

• Analysis of experimental results with regard to design values

• Development of **numerical investigations** of liner trays subjected to pressure and suction. The author was involved in: FE model development, verification, and calibration of the model, numerical simulation performance, parametric study performance, and evaluating the numerical data.

• Evaluation of the **environmental impact** of steel-intensive façade systems. The author was involved in the life cycle assessment of industrial buildings, the life cycle assessment of façade systems, and the evaluation of the assessment data.

It is to be underlined that pioneering experimental tests have been carried out in Romania on structural liner trays subjected to wind loads in a vacuum chamber, showing the dynamic character of the wind loads.

## 6.3 Valorisation of research

Part of the presented results were diseminated within the PROGRESS research project and these findings have been openly accessible through research reports within the project's framework at https://www.steelconstruct.com/wp-content/uploads/PROGRESS-final-report-for-web.pdf.

The research findings and conclusions have been presented and published across various journals and conferences as follows:

*ISI journals*

- **Buzatu R**, Ungureanu V, Ciutina A, Gireadă M, Vitan D, Petran I. Experimental Evaluation of Energy-Efficiency in a Holistically Designed Building. Energies. 2021; 14(16):5061. https://doi.org/10.3390/en14165061
- Belc AL, Ciutina A, **Buzatu R**, Belc F, Costescu C. Environmental Impact Assessment of Different Warm Mix Asphalts. Sustainability. 2021; 13(21):11869. https://doi.org/10.3390/su132111869

*ISI conference proceedings*

- **Buzatu R**, Muntean D, Ciutina A, Ungureanu V, Thermal Performance and Energy Efficiency of Lightweight Steel Buildings: A Case-Study, World Multidisciplinary Civil Engineering - Architecture - Urban Planning Symposium, Prague, 2020. IOP Conf. Ser.: Mater. Sci. Eng. 960 032099, DOI: 10.1088/1757-899X/960/3/032099

- **Buzatu R**, Muntean D, Ungureanu V, Ciutina A, Gireada M, Vitan D, Holistic energy efficient design approach to sustainable building using monitored energy management system, IOP Conf. Series: Earth and Environmental Science 664 (2021) 012037, doi:10.1088/1755-1315/664/1/012037
- **Buzatu R**, Ungureanu V, and Hradil P, Environmental and economic impact of steel industrial buildings made of reclaimed elements, Proceedings of the Eighth International Symposium on Life-Cycle Civil Engineering (IALCCE 2023), 1303-1311, ISBN (Electronic): 978-1-003-32302-0, Milan, Italy: CRC Press, Jul. 2023
- Lukačević I, Rajić A, Ungureanu V, and **Buzatu R**, A comparative life-cycle assessment of structural composite steel-concrete floor systems – A case study, Proceedings of the Eighth International Symposium on Life-Cycle Civil Engineering (IALCCE 2023), 751-758, ISBN (Electronic): 978-1-003-32302-0, Milan, Italy: CRC Press, Jul. 2023

*International conferences*

- Ciutina A, **Buzatu R**, Muntean D.M., Ungureanu V (2019) Heat transfer vs environmental impact of modern façade systems. CLIMA 2019 Bucharest, Romania, in E3S Web of Confereces 111, 03078 (2019) DOI: 10.1051/e3sconf/201911103078
- Ciutina A, Mirea M, Ciopec A, Ungureanu V, **Buzatu R**, Morovan R (2019) Behaviour of wedge foundations under axial compression. CLIMA 2019 Bucharest, Romania, in E3S Web of Confereces 664, 012036 (2019) DOI: 10.1088/1755-1315/664/1/012036

*Others*

- **Legian R**., Ciutina A., Ungureanu V. (2018), Sustainable Design of a Light Steel Structure, Acta Technica Napocensis: Civil Engineering & Architecture, Volume 61, No. 1, (2018) 79-90
- Ciutina A, **Buzatu R**, Muntean DM, Ungureanu V: Sisteme moderne de fatade metalice – Analize termice si de impact asupra mediului. A XVI-a Conferinta Nationala de Constructii Metalice, 13-14 iunie 2019, Timisoara, Romania, ISBN 978-973-638-646-6, Editura Orizonturi Universitare, pp.185-196
- Ciutina A, **Buzatu R**, Muntean DM, Ungureanu V: Sisteme moderne de fatade metalice – Analize termice si de impact asupra mediului. Revista Constructiilor, nr. 166, ianuarie- februarie 2020, pp. 36-38, 40, 42, 43.
- Two presentations were given in the technical committee TC 14 - Sustainability & Eco-Efficiency of Steel Construction of the European Convention for Constructional Steelwork – ECCS:
    - **Buzatu R**, Ungureanu V, Integration of Solar and Wind Energy Supply on an Active House and Extention to Smart Grid System, TC14 Reunion, ECCS, 27 November 2020
    - **Buzatu R**, Ungureanu V, Economic and Environmental Assessment of Reusing Reclaimed Steel: A European case study, TC14 Reunion, ECCS, Coimbra, Portugal, 21-22 November 2019

*Research projects*

- Member in the research team (10.2018-09.2020) in *Smart buildings adaptable to the climate change effects* (CIA_CLIM) project, within PNCDI III, project number PN-III-P1-1.2-PCCDI-2017-0391
- research member (05.2019-05.2020) in *PROvisions for a Greater REuse of Steel Structures* (PROGRESS) project, within Research Fund for Coal and Steel, grant agreement No. 747847
- research member (10.2020-09.2021) in *Structural design tool for cold-formed steel structures* (CFSExpert) project, within PNCDI III, project number PN-III-CEI-EUREKA-2019/ E113493

## 6.4 Future research activities

During the activities fulfilled within this thesis, several needs and opportunities for further research were identified. The main starting points for future research are presented below briefly summarized:

- The results not yet published in this thesis should be refined for publication in peer-reviewed scientific papers. This will ease the distillation of ideas and concepts through direct feedback from reviewers, as well as the strengthening of argumentation. The process of publishing these results in journal articles proves highly effective for disseminating results, offering greater visibility compared to the thesis itself.
- Numerical investigations of simple closed liner trays, restrained opened liner trays and restrained closed liner trays should be furthermore considered. Calibrated numerical models of these experimental tests would contribute to a deeper understanding of the built-up cladding system behavior under wind loads, from a complete cladding structure perspective and from a 'component' perspective.
- Experimental investigations in vacuum chamber of liner trays with different span lengths subjected to wind loads should be further determined to validate the parametric study developed within the numerical investigations.
- Numerical investigations of liner trays validated by experimental tests may be explored in order to extend the study to liner trays with different steel grades. A consistent experimental program will include various steel grades S220, S250, S320, S350 and S550.
- For a more precise evaluation of the operational phase in building life cycle assessments (LCAs), a dynamic methodology should be employed to incorporate dynamic factors such as changes in electricity-mix production, technological progress, climate change (increasing severity of heat waves), variation in occupancy behaviour and changes in climate regulations. By integrating future climate model data and dynamic energy simulations, the approach estimates with higher accuracy the energy consumption in building LCAs while considering anticipated shifts in the regional electricity mix.

- More research is needed for environmental impacts linked to construction activities linked to building construction, building utilisation, maintenance and building deconstruction.

## 6.5 Acknowledgement

Partial research leading to the results related to the environmental assessment of buildings has received founding from the European Commission's Research Fund for Coal and Steel project PROGRESS - *Provisions for Greater Reuse of Steel Structures*, under grant agreement No. 747847, which made possible a research stage of five weeks at VTT Technical Research Centre of Finland, Espoo, Finland.

The partial research leading to the results from chapter 5 has received founding from a grant of the Romanian Ministery of Research and Innovation, CCCDI – UEFISCDI, project number PN-III-P1-1.2-PCCDI-2017-0391 / CIA_CLIM – *Smart buildings adaptable to the climate change effects*, within PNCDI III.

The research conducted in the last 12 months prior the thesis defense received financial support from the project *Network of excellence in applied research and innovation for doctoral and postdoctoral programs* / InoHubDoc", project co-funded by the European Social Fund financing agreement no. POCU/993/6/13/153437.

# 7 Annexes

## 7.1 Annex A1


Figure 7.1 LT-SO-P specimen after experimental test

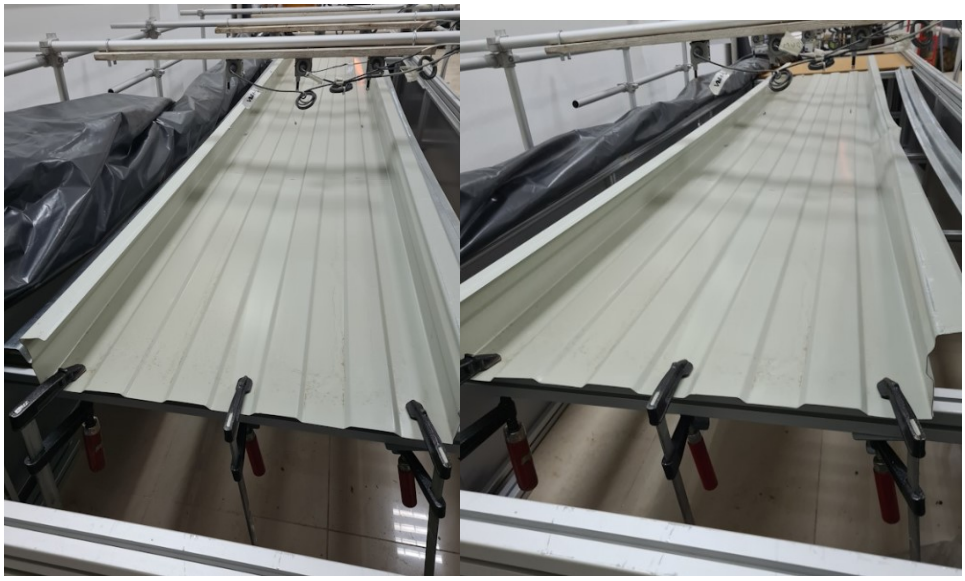

Figure 7.2 LT-SO-P-P specimen before (left) and after (right) experimental test


Figure 7.3 LT-SC-P specimen after the experimental test

Figure 7.4 LT-SC-P specimen after the experimental test – extension to Figure 7.3

Figure 7.5 LT-SC-P specimen after the experimental test – extension to Figure 7.3 and Figure 7.4

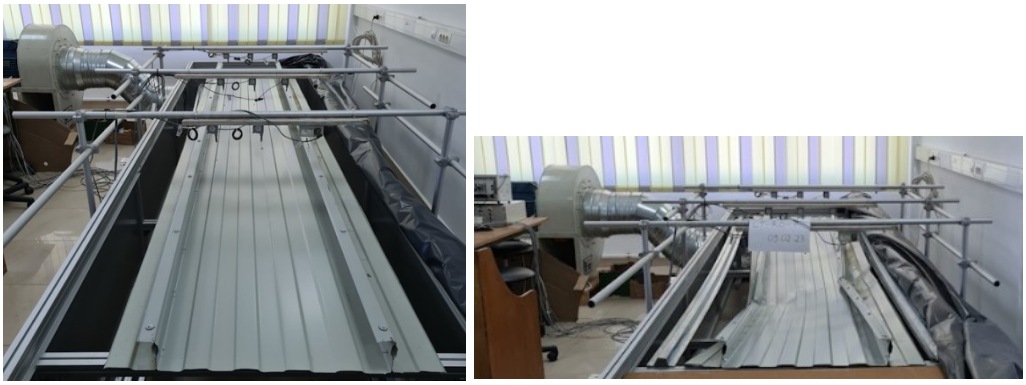

Figure 7.6 LT-RO-P specimen before (left) and after (right) experimental test

Figure 7.7 LT-RO-P specimen after the experimental test - extension to Figure 7.6

Figure 7.8 LT-RC-P specimen after the experimental test

Figure 7.9 LT-SO-S specimen before (up-left) and after (up-right and down) experimental test

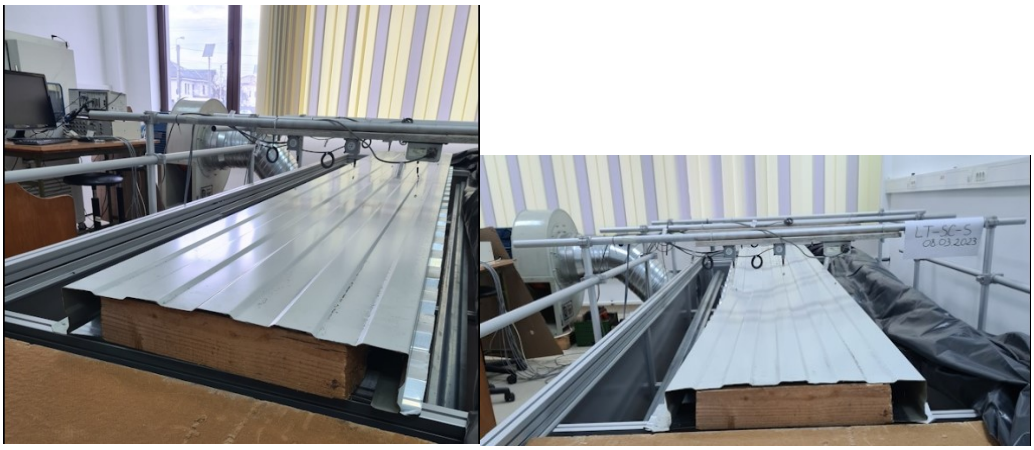

Figure 7.10 LT-SC-S specimen before (left) and after (right) experimental test


Figure 7.11 LT-SC-S specimen after the experimental test – extension to Figure 7.10

Figure 7.12 LT-RO-S specimen after experimental test

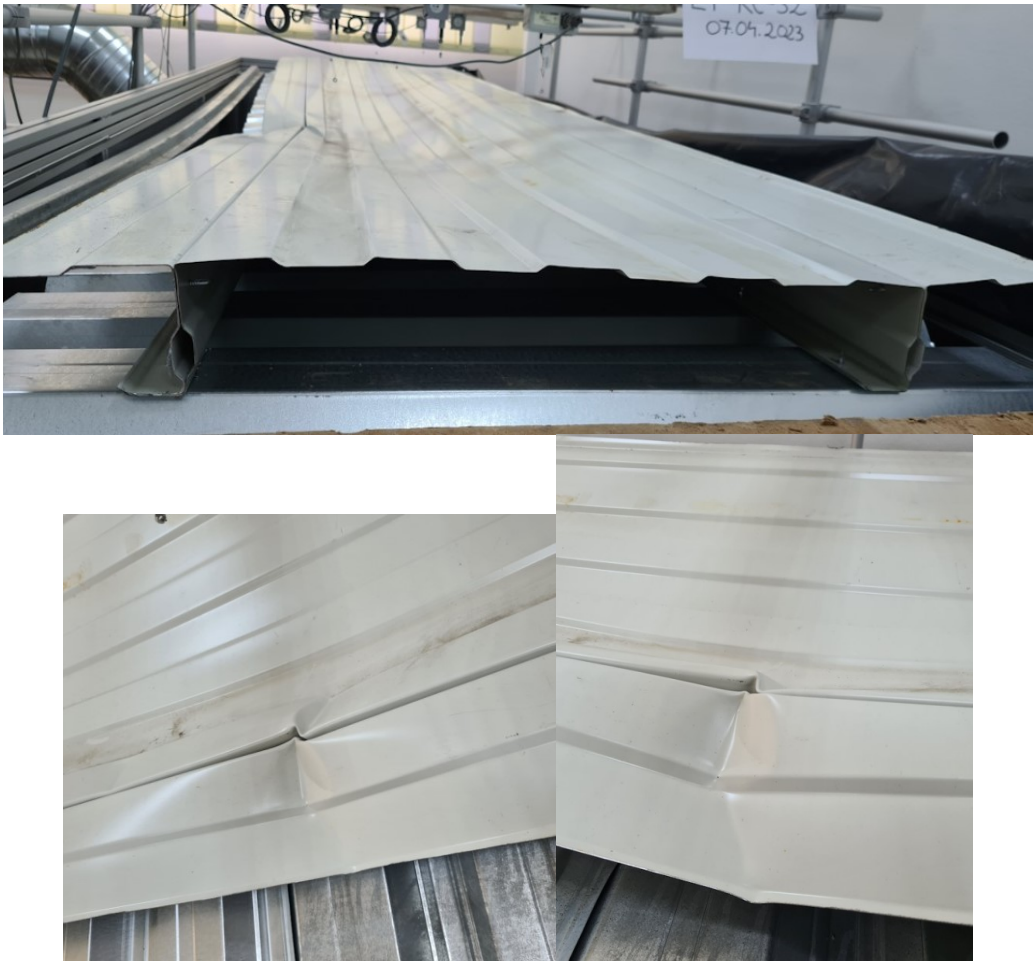


Figure 7.13 LT-RC-S specimen after experimental test

# 8 References


[1] M. J. Roberts, J. M. Davies, and Y. C. Wang, "Modern cladding systems for big sheds: The emerging state of the art," *Thin-Walled Structures*, vol. 175, p. 109264, Jun. 2022, doi: 10.1016/j.tws.2022.109264.

[2] Kingdom Standing Committee on Structural Safety, "Effects of scale." [Online]. Available: https://www.cross-safety.org/uk/safety-information/cross-safety-alert/effects-scale

[3] O. Kaitila, "Web Crippling Of Cold-Formed Thin-Walled Steel Cassettes", [Online]. Available: https://core.ac.uk/download/pdf/80701469.pdf

[4] Environmental Protection Agency, "The National Environmental Policy Act of 1969." [Online]. Available: https://www.energy.gov/nepa/articles/national-environmental-policy-act-1969

[5] Brundtland Commission, "Our Common Future - Report of the World Commission on Environment and Development," United Nations, Oct. 1987.

[6] U. N. Environment, "The Montreal Protocol," *Ozonaction*, Oct. 29, 2018. http://www.unep.org/ozonaction/who-we-are/about-montreal-protocol (accessed Aug. 24, 2023).

[7] U. Nations, "Sustainability," *United Nations*. https://www.un.org/en/academic-impact/sustainability

[8] United Nations, "United Nations Framework Convention on Climate Change." UNITED NATIONS, Jun. 19, 1993. Accessed: Aug. 24, 2023. [Online]. Available: https://treaties.un.org/pages/ViewDetailsIII.aspx?Temp=mtdsg3&chapter=27&clang=_en&mtdsg_no=XXVII-7&src=IND

[9] United Nations, "Kyoto Protocol to the United Nations Framework Convention on Climate Change." Dec. 11, 1997. [Online]. Available: https://unfccc.int/resource/docs/convkp/kpeng.html

[10] United Nations, "Paris Agreement - United Nations Framework Convention on Climate Change," 2015. [Online]. Available: https://unfccc.int/sites/default/files/english_paris_agreement.pdf

[11] Alan Buis (NASA's Global Climate Change), "A Degree of Concern: Why Global Temperatures Matter," *Climate Change: Vital Signs of the Planet*. Accessed: Aug. 24, 2023. [Online]. Available: https://climate.nasa.gov/news/2878/a-degree-of-concern-why-global-temperatures-matter

[12] European Commission, "The European Green Deal." European Commission, Nov. 12, 2019. [Online]. Available: https://ec.europa.eu/info/strategy/priorities-2019-2024/european-green-deal_en

[13] L.-L. Sun, H.-J. Cui, and Q.-S. Ge, "Will China achieve its 2060 carbon neutral commitment from the provincial perspective?," *Advances in Climate Change Research*, vol. 13, no. 2, pp. 169–178, Apr. 2022, doi: 10.1016/j.accre.2022.02.002.

[14] Global Alliance for Buildings and Construction, "Tracking progress | UN environment programme." https://globalabc.org/our-work/tracking-progress-global-status-report

[15] European Commision, "Circular Economy Action Plan For a cleaner and more competitive Europe." EUR-Lex, 2020. [Online]. Available: https://eur-lex.europa.eu/legal-content/EN/TXT/?qid=1583933814386&uri=COM:2020:98:FIN

[16] European Commision, "ETS Directive - Directive 2003/87/EC." EUR-Lex, Oct. 13, 2003. [Online]. Available: http://data.europa.eu/eli/dir/2003/87/oj/eng

[17] European Commision, "The Habitats Directive." https://environment.ec.europa.eu/topics/nature-and-biodiversity/habitats-directive_en (accessed Aug. 25, 2023).
[18] European Commision, "Single-Use Plastics Directive." EUR-Lex. [Online]. Available: https://eur-lex.europa.eu/eli/dir/2019/904/oj
[19] Julian Wettengel - Clean Energy Wire, "Covering the EU's 'Fit for 55' package of climate and energy laws," *Clean Energy Wire*, Jun. 28, 2021. https://www.cleanenergywire.org/factsheets/covering-eus-fit-55-package-climate-and-energy-laws
[20] European Commision, "Effort Sharing Regulation - Decision (EU) 2023/1319 of 28 June 2023 amending Implementing Decision (EU) 2020/2126 to revise Member States' annual emission allocations for the period from 2023 to 2030." EUR-Lex, Jun. 28, 2023. [Online]. Available: http://data.europa.eu/eli/dec_impl/2023/1319/oj/eng
[21] European Commision, "Effort sharing 2021-2030: targets and flexibilities." https://climate.ec.europa.eu/eu-action/effort-sharing-member-states-emission-targets/effort-sharing-2021-2030-targets-and-flexibilities_en (accessed Aug. 25, 2023).
[22] International Energy Agency, "Global Status Report for Buildings and Construction 2019 – Analysis." [Online]. Available: https://www.iea.org/reports/global-status-report-for-buildings-and-construction-2019
[23] Climate Action Tracker (2022), "Decarbonising Buildings - Achieving zero carbon heating and cooling", [Online]. Available: https://climateactiontracker.org/publications/decarbonising-buildings-achieving-net-zero-carbon-heating-and-cooling/
[24] United Nations Environment Programme, "2022 Global Status Report for Buildings and Construction," Nov. 2022. [Online]. Available: http://www.unep.org/resources/publication/2022-global-status-report-buildings-and-construction
[25] R. Buzatu, V. Ungureanu, A. Ciutina, M. Gireadă, D. Vitan, and I. Petran, "Experimental Evaluation of Energy-Efficiency in a Holistically Designed Building," *Energies*, vol. 14, no. 16, Art. no. 16, Jan. 2021, doi: 10.3390/en14165061.
[26] R. Buzatu, D. Muntean, V. Ungureanu, A. Ciutina, M. Gireadă, and D. Vitan, "Holistic energy efficient design approach to sustainable building using monitored energy management system," *IOP Conf. Ser.: Earth Environ. Sci.*, vol. 664, no. 1, p. 012037, May 2021, doi: 10.1088/1755-1315/664/1/012037.
[27] G. Limpens, H. Jeanmart, and F. Maréchal, "Belgian Energy Transition: What Are the Options?," *Energies*, vol. 13, no. 1, Art. no. 1, Jan. 2020, doi: 10.3390/en13010261.
[28] Kristin Musulin, "5 key ways to reduce GHG emissions in building construction," *Smart Cities Dive*. [Online]. Available: https://www.smartcitiesdive.com/news/5-key-ways-to-reduce-ghg-emissions-in-building-construction/564707/
[29] P. Hradil, L. Fülöp, and V. Ungureanu, "Reusability of components from single-storey steel-framed buildings," *Steel Construction: Design and Research*, vol. 12, no. 2, pp. 91–97, May 2019, doi: 10.1002/stco.201800032.
[30] R. Buzatu, V. Ungureanu, and P. Hradil, "Environmental and economic impact of steel industrial buildings made of reclaimed elements," in *Proceedings of the Eighth International Symposium on Life-Cycle Civil Engineering (IALCCE 2023)*, Milan, Italy: CRC Press, Jul. 2023, pp. 1303–1311.

[31] P. Hradil *et al.*, "Provisions for a Greater Reuse of Steel Structures (PROGRESS) - Final Report," European Commission, Research Fund for Coal and Steel, 2020.
[32] S. Vares, P. Hradil, M. Sansom, and V. Ungureanu, "Economic potential and environmental impacts of reused steel structures," *Structure and Infrastructure Engineering*, vol. 16, pp. 1–12, Sep. 2019, doi: 10.1080/15732479.2019.1662064.
[33] "Greenhouse gas emissions trends and projections under the scope of the Effort Sharing legislation, EU-27 — European Environment Agency." https://www.eea.europa.eu/data-and-maps/figures/eu-27-ghg-emission-trends-1
[34] Brütting Jan, Camille Vandervaeren, Gennaro Senatore, Niels De Temmerman, and Corentin Fivet, "Environmental impact minimization of reticular structures made of reused and new elements through Life Cycle Assessment and Mixed-Integer Linear Programming," *Energy and Buildings*, vol. 215, p. 109827, May 2020, doi: 10.1016/j.enbuild.2020.109827.
[35] C. Piccardo and L. Gustavsson, "Deep energy retrofits using different retrofit materials under different scenarios: Life cycle cost and primary energy implications," *Energy*, vol. 281, p. 128131, Oct. 2023, doi: 10.1016/j.energy.2023.128131.
[36] C. Rodrigues and F. Freire, "Environmental impacts and costs of residential building retrofits – What matters?," *Sustainable Cities and Society*, vol. 67, p. 102733, Apr. 2021, doi: 10.1016/j.scs.2021.102733.
[37] V. Hasik, E. Escott, R. Bates, S. Carlisle, B. Faircloth, and M. M. Bilec, "Comparative whole-building life cycle assessment of renovation and new construction," *Building and Environment*, vol. 161, p. 106218, Aug. 2019, doi: 10.1016/j.buildenv.2019.106218.
[38] R. Buzatu, D. Muntean, A. Ciutina, and V. Ungureanu, "Thermal Performance and Energy Efficiency of Lightweight Steel Buildings: a Case-Study," *IOP Conf. Ser.: Mater. Sci. Eng.*, vol. 960, p. 032099, Dec. 2020, doi: 10.1088/1757-899X/960/3/032099.
[39] UN environment programme, "CO2 emissions from buildings and construction hit new high, leaving sector off track to decarbonize by 2050," *UN Environment*, Nov. 09, 2022. http://www.unep.org/news-and-stories/press-release/co2-emissions-buildings-and-construction-hit-new-high-leaving-sector
[40] M. Kong, C. Ji, T. Hong, and H. Kang, "Impact of the use of recycled materials on the energy conservation and energy transition of buildings using life cycle assessment: A case study in South Korea," *Renewable and Sustainable Energy Reviews*, vol. 155, p. 111891, Mar. 2022, doi: 10.1016/j.rser.2021.111891.
[41] European Academies Science Advisory Council and Secretariat, *Decarbonisation of buildings: for climate, health and jobs*. 2021. Accessed: Jun. 15, 2021. [Online]. Available: http://nbn-resolving.org/urn:nbn:de:gbv:3:2-137698
[42] P. Kamrath, M. Kuhnhenne, D. Pyschny, and K. Janczyk, "Deconstruction, recycling and reuse of lightweight metal constructions," in *Life Cycle Analysis and Assessment in Civil Engineering: Towards an Integrated Vision*, CRC Press, 2018.
[43] J. L. Hao *et al.*, "Carbon emission reduction in prefabrication construction during materialization stage: A BIM-based life-cycle assessment approach," *Science of The Total Environment*, vol. 723, p. 137870, Jun. 2020, doi: 10.1016/j.scitotenv.2020.137870.

[44] O. Iuorio, L. Napolano, L. Fiorino, and R. Landolfo, "The environmental impacts of an innovative modular lightweight steel system: The Elissa case," *Journal of Cleaner Production*, vol. 238, p. 117905, Nov. 2019, doi: 10.1016/j.jclepro.2019.117905.
[45] European Council, "Fit for 55: making buildings in the EU greener," Jun. 02, 2023. https://www.consilium.europa.eu/en/infographics/fit-for-55-making-buildings-in-the-eu-greener/
[46] EU Commission, "Directive 2010/31/EU of the European Parliament and of the Council of 19 May 2010 on the energy performance of buildings." 2010.
[47] G. Erbach, L. Jensen, S. Chahri, and E. Claros, "Fit for 55 package - Briefing," EPRS | European Parliamentary Research Service.
[48] European Council, "Fit for 55: how the EU will become more energy-efficient," Jul. 26, 2023. https://www.consilium.europa.eu/en/infographics/fit-for-55-how-the-eu-will-become-more-energy-efficient/
[49] I. Zabalza Bribián, A. Aranda Usón, and S. Scarpellini, "Life cycle assessment in buildings: State-of-the-art and simplified LCA methodology as a complement for building certification," *Building and Environment*, vol. 44, no. 12, pp. 2510–2520, Dec. 2009, doi: 10.1016/j.buildenv.2009.05.001.
[50] M. S. Sandanayake, "Environmental Impacts of Construction in Building Industry—A Review of Knowledge Advances, Gaps and Future Directions," *Knowledge*, vol. 2, no. 1, Art. no. 1, Mar. 2022, doi: 10.3390/knowledge2010008.
[51] 14:00-17:00, "ISO 14040:2006 Environmental management — Life cycle assessment — Principles and framework." Aug. 12, 2014. [Online]. Available: https://www.iso.org/standard/37456.html
[52] International Organization for Standardization, "ISO 14044:2006/Amd 2:2020 Environmental management — Life cycle assessment — Requirements and guidelines — Amendment 2." Geneva, Switzerland, 2020.
[53] CEN, "EN 15643:2021 - Sustainability of construction works - Framework for assessment of buildings and civil engineering works." 2021.
[54] CEN, "EN 15804:2012+A2:2019 - Sustainability of construction works - Environmental product declarations - Core rules for the product category of construction products." 2019.
[55] CEN, "EN 15978:2011 - Sustainability of construction works. Assessment of environmental performance of buildings. Calculation method." 2011.
[56] N. Soares, P. Santos, H. Gervásio, J. J. Costa, and L. Simões da Silva, "Energy efficiency and thermal performance of lightweight steel-framed (LSF) construction: A review," *Renewable and Sustainable Energy Reviews*, vol. 78, pp. 194–209, Oct. 2017, doi: 10.1016/j.rser.2017.04.066.
[57] H. Gervásio, P. Santos, R. Martins, and L. Simões da Silva, "A macro-component approach for the assessment of building sustainability in early stages of design," *Building and Environment*, vol. 73, pp. 256–270, 2014, doi: 10.1016/j.buildenv.2013.12.015.
[58] M. M. Khasreen, P. F. G. Banfill, and G. F. Menzies, "Life-Cycle Assessment and the Environmental Impact of Buildings: A Review," *Sustainability*, vol. 1, no. 3, Art. no. 3, Sep. 2009, doi: 10.3390/su1030674.
[59] A. Hussien *et al.*, "A statistical analysis of life cycle assessment for buildings and buildings' refurbishment research," *Ain Shams Engineering Journal*, vol. 14, no. 10, p. 102143, Oct. 2023, doi: 10.1016/j.asej.2023.102143.
[60] S. Abu Dabous, T. Ibrahim, S. Shareef, E. Mushtaha, and I. Alsyouf, "Sustainable façade cladding selection for buildings in hot climates based on

thermal performance and energy consumption," *Results in Engineering*, vol. 16, p. 100643, Dec. 2022, doi: 10.1016/j.rineng.2022.100643.
[61] G. Manioğlu and Z. Yılmaz, "Economic evaluation of the building envelope and operation period of heating system in terms of thermal comfort," *Energy and Buildings*, vol. 38, no. 3, pp. 266–272, Mar. 2006, doi: 10.1016/j.enbuild.2005.06.009.
[62] Z. S. Moussavi Nadoushani, A. Akbarnezhad, J. Ferre Jornet, and J. Xiao, "Multi-criteria selection of façade systems based on sustainability criteria," *Building and Environment*, vol. 121, pp. 67–78, Aug. 2017, doi: 10.1016/j.buildenv.2017.05.016.
[63] N. Singhaputtangkul, S. P. Low, A. L. Teo, and B.-G. Hwang, "Criteria for Architects and Engineers to Achieve Sustainability and Buildability in Building Envelope Designs," *Journal of Management in Engineering*, vol. 30, no. 2, pp. 236–245, Mar. 2014, doi: 10.1061/(ASCE)ME.1943-5479.0000198.
[64] J. E. Martabid and C. Mourgues, "Criteria Used for Selecting Envelope Wall Systems in Chilean Residential Projects," *Journal of Construction Engineering and Management*, vol. 141, no. 12, 2015, doi: 10.1061/(ASCE)CO.1943-7862.0001025.
[65] A. Ciutina, R. Buzatu, D. M. Muntean, and V. Ungureanu, "Heat transfer vs environmental impact of modern façade systems," *E3S Web Conf.*, vol. 111, p. 03078, 2019, doi: 10.1051/e3sconf/201911103078.
[66] C. Paech, "Structural Membranes Used in Modern Building Facades," *Procedia Engineering*, vol. 155, pp. 61–70, Jan. 2016, doi: 10.1016/j.proeng.2016.08.007.
[67] V. M. Taborianski and R. T. A. Prado, "Methodology of CO 2 emission evaluation in the life cycle of office building façades," *Environmental Impact Assessment Review*, vol. 33, no. 1, pp. 41–47, 2012, doi: 10.1016/j.eiar.2011.10.004.
[68] K.-H. Kim, "A comparative life cycle assessment of a transparent composite façade system and a glass curtain wall system," *Energy and Buildings*, vol. 43, no. 12, pp. 3436–3445, 2011, doi: 10.1016/j.enbuild.2011.09.006.
[69] M. Ottelé, K. Perini, A. L. A. Fraaij, E. M. Haas, and R. Raiteri, "Comparative life cycle analysis for green façades and living wall systems," *Energy and Buildings*, vol. 43, no. 12, pp. 3419–3429, 2011, doi: 10.1016/j.enbuild.2011.09.010.
[70] B. Han, R. Wang, L. Yao, H. Liu, and Z. Wang, "Life cycle assessment of ceramic façade material and its comparative analysis with three other common façade materials," *Journal of Cleaner Production*, vol. 99, pp. 86–93, 2015, doi: 10.1016/j.jclepro.2015.03.032.
[71] R. Azari, "Integrated energy and environmental life cycle assessment of office building envelopes," *Energy and Buildings*, vol. 82, pp. 156–162, 2014, doi: 10.1016/j.enbuild.2014.06.041.
[72] A. Jasiolek, "Paper-based building envelopes – Environmental and performance assessment of original and literature-based designs," *Building and Environment*, p. 110755, Aug. 2023, doi: 10.1016/j.buildenv.2023.110755.
[73] A. Aslani and C. Hachem-Vermette, "Energy and environmental assessment of high-performance building envelope in cold climate," *Energy and Buildings*, vol. 260, p. 111924, Apr. 2022, doi: 10.1016/j.enbuild.2022.111924.
[74] R. Azari and R. Palomera-Arias, "Building envelopes: A comparison of impacts on environment," presented at the AEI 2015: Birth and Life of the Integrated Building - Proceedings of the AEI Conference 2015, 2015, pp. 230–236. doi: 10.1061/9780784479070.021.

[75] R. M. Pulselli, E. Simoncini, and N. Marchettini, "Energy and emergy based cost-benefit evaluation of building envelopes relative to geographical location and climate," *Building and Environment*, vol. 44, no. 5, pp. 920–928, 2009, doi: 10.1016/j.buildenv.2008.06.009.
[76] R. Kahhat *et al.*, "Environmental impacts over the life cycle of residential buildings using different exterior wall systems," *Journal of Infrastructure Systems*, vol. 15, no. 3, pp. 211–221, 2009, doi: 10.1061/(ASCE)1076-0342(2009)15:3(211).
[77] M. Pfundstein, R. Gellert, M. Spitzner, and A. Rudolphi, *Insulating Materials: Principles, Materials, Applications*, 1st edition. Basel : Munich: Birkhäuser Architecture, 2008.
[78] R. Baetens, B. P. Jelle, and A. Gustavsen, "Aerogel insulation for building applications: A state-of-the-art review," *Energy and Buildings*, vol. 43, no. 4, pp. 761–769, 2011, doi: 10.1016/j.enbuild.2010.12.012.
[79] E. Cuce, P. M. Cuce, C. J. Wood, and S. B. Riffat, "Toward aerogel based thermal superinsulation in buildings: A comprehensive review," *Renewable and Sustainable Energy Reviews*, vol. 34, pp. 273–299, 2014, doi: 10.1016/j.rser.2014.03.017.
[80] M. Alam, H. Singh, and M. C. Limbachiya, "Vacuum insulation panels (vips) for building construction industry - a review of the contemporary developments and future directions," *Applied Energy*, vol. 88, no. 11, pp. 3592–3602, 2011, doi: 10.1016/j.apenergy.2011.04.040.
[81] F. Isaia, S. Fantucci, A. Capozzoli, and M. Perino, "Vacuum insulation panels: Thermal bridging effects and energy performance in real building applications," presented at the Energy Procedia, 2015, pp. 269–278. doi: 10.1016/j.egypro.2015.12.181.
[82] L. Cozzarini, L. Marsich, A. Ferluga, and C. Schmid, "Life cycle analysis of a novel thermal insulator obtained from recycled glass waste," *Developments in the Built Environment*, vol. 3, p. 100014, Aug. 2020, doi: 10.1016/j.dibe.2020.100014.
[83] P. Ricciardi, E. Belloni, and F. Cotana, "Innovative panels with recycled materials: Thermal and acoustic performance and Life Cycle Assessment," *Applied Energy*, vol. 134, pp. 150–162, 2014, doi: 10.1016/j.apenergy.2014.07.112.
[84] F. Asdrubali *et al.*, "Experimental and numerical characterization of innovative cardboard based panels: Thermal and acoustic performance analysis and life cycle assessment," *Building and Environment*, vol. 95, pp. 145–159, 2016, doi: 10.1016/j.buildenv.2015.09.003.
[85] M. Sinka, P. Van den Heede, N. De Belie, D. Bajare, G. Sahmenko, and A. Korjakins, "Comparative life cycle assessment of magnesium binders as an alternative for hemp concrete," *Resources, Conservation and Recycling*, vol. 133, pp. 288–299, 2018, doi: 10.1016/j.resconrec.2018.02.024.
[86] A. Arrigoni, R. Pelosato, P. Melià, G. Ruggieri, S. Sabbadini, and G. Dotelli, "Life cycle assessment of natural building materials: the role of carbonation, mixture components and transport in the environmental impacts of hempcrete blocks," *Journal of Cleaner Production*, vol. 149, pp. 1051–1061, 2017, doi: 10.1016/j.jclepro.2017.02.161.
[87] L. Zampori, G. Dotelli, and V. Vernelli, "Life cycle assessment of hemp cultivation and use of hemp-based thermal insulator materials in buildings," *Environmental Science and Technology*, vol. 47, no. 13, pp. 7413–7420, 2013, doi: 10.1021/es401326a.

[88] H. Gervásio, P. Santos, L. S. Da Silva, and A. M. G. Lopes, "Influence of thermal insulation on the energy balance for cold-formed buildings," *Advanced Steel Construction*, vol. 6, no. 2, pp. 742–766, 2010.
[89] S. Füchsl, F. Rheude, and H. Röder, "Life cycle assessment (LCA) of thermal insulation materials: A critical review," *Cleaner Materials*, vol. 5, p. 100119, Sep. 2022, doi: 10.1016/j.clema.2022.100119.
[90] P. Linhares, V. Hermo, and C. Meire, "Environmental design guidelines for residential NZEBs with liner tray construction," *Journal of Building Engineering*, vol. 42, p. 102580, Oct. 2021, doi: 10.1016/j.jobe.2021.102580.
[91] J. Gosling, P. Sassi, M. Naim, and R. Lark, "Adaptable buildings: A systems approach," *Sustainable Cities and Society*, vol. 7, pp. 44–51, 2013, doi: 10.1016/j.scs.2012.11.002.
[92] T. O'Grady, R. Minunno, H.-Y. Chong, and G. M. Morrison, "Design for disassembly, deconstruction and resilience: A circular economy index for the built environment," *Resources, Conservation and Recycling*, vol. 175, p. 105847, Dec. 2021, doi: 10.1016/j.resconrec.2021.105847.
[93] P. Santos, M. Gonçalves, C. Martins, N. Soares, and J. J. Costa, "Thermal transmittance of lightweight steel framed walls: Experimental versus numerical and analytical approaches," *Journal of Building Engineering*, vol. 25, 2019, doi: 10.1016/j.jobe.2019.100776.
[94] D. Don, S. Navaratnam, P. Rajeev, and J. Sanjayan, "Study of Technological Advancement and Challenges of Façade System for Sustainable Building: Current Design Practice," In Review, preprint, Jul. 2023. doi: 10.21203/rs.3.rs-3179925/v1.
[95] V. Ungureanu, L. Marsavina, P. Negrea, N. Muntean, and C. Croitoru, "Smart buildings adaptable to the effects of climate change - final report - 30PCCDI," Timisoara, Romania, 30PCCDI/2018, 2021. [Online]. Available: https://www.icer.ro/images/Raport_Final_2021_30PCCDI_VU-merged.pdf
[96] D. Ramon, K. Allacker, D. Trigaux, H. Wouters, and N. P. M. van Lipzig, "Dynamic modelling of operational energy use in a building LCA: A case study of a Belgian office building," *Energy and Buildings*, vol. 278, p. 112634, Jan. 2023, doi: 10.1016/j.enbuild.2022.112634.
[97] S. Su, X. Li, Y. Zhu, and B. Lin, "Dynamic LCA framework for environmental impact assessment of buildings," *Energy and Buildings*, vol. 149, pp. 310–320, 2017, doi: 10.1016/j.enbuild.2017.05.042.
[98] I. Yitmen, A. Al-Musaed, and F. Yücelgazi, "ANP model for evaluating the performance of adaptive façade systems in complex commercial buildings," *Engineering, Construction and Architectural Management*, vol. 29, no. 1, pp. 431–455, Jan. 2021, doi: 10.1108/ECAM-07-2020-0559.
[99] DIRECTIVE 2008/98/EC OF THE EUROPEAN PARLIAMENT, *Directive 2008/98/EC of the European Parliament and of the Council of 19 November 2008 on waste and repealing certain Directives (Text with EEA relevance)*, vol. 312. 2008. Accessed: Nov. 19, 2022. [Online]. Available: http://data.europa.eu/eli/dir/2008/98/oj/eng
[100] "Waste Framework Directive." https://environment.ec.europa.eu/topics/waste-and-recycling/waste-framework-directive_en (accessed Aug. 27, 2023).
[101] Eurostat, "Generation of waste by waste category, hazardousness and NACE Rev. 2 activity," 2022. https://ec.europa.eu/eurostat/databrowser/view/env_wasgen/default/table?lang=en (accessed Nov. 20, 2022).

[102] World Steel Association, "Steel in the Circular Economy - A life cycle perspective," 2015. [Online]. Available: https://worldsteel.org/wp-content/uploads/Steel-in-the-circular-economy-infographic.pdf
[103] O. Yilmaz, A. Anctil, and T. Karanfil, "LCA as a decision support tool for evaluation of best available techniques (BATs) for cleaner production of iron casting," *Journal of Cleaner Production*, vol. 105, pp. 337–347, 2015, doi: 10.1016/j.jclepro.2014.02.022.
[104] European Topic Centre on Waste and Materials in a Green Economy, "Contribution of remanufacturing to Circular Economy," ETC/WMGE 2021/10, 2021. [Online]. Available: file:///C:/Users/Raluca/Downloads/Remanufacturing_for%20website.pdf
[105] A. Di Maria, J. Eyckmans, and K. Van Acker, "Downcycling versus recycling of construction and demolition waste: Combining LCA and LCC to support sustainable policy making," *Waste Management*, vol. 75, pp. 3–21, 2018, doi: 10.1016/j.wasman.2018.01.028.
[106] C. Llatas, N. Bizcocho, B. Soust-Verdaguer, M. V. Montes, and R. Quiñones, "An LCA-based model for assessing prevention versus non-prevention of construction waste in buildings," *Waste Management*, vol. 126, pp. 608–622, 2021, doi: 10.1016/j.wasman.2021.03.047.
[107] A. M. G. Coelho, R. Pimentel, V. Ungureanu, P. Hradil, and J. Kesti, "European Recommendations for Reuse of Steel Products in Single-Storey Buildings," p. 234, 2020.
[108] "Building envelopes - Steel constructions," *steelconstruction.info*. https://steelconstruction.info/Building_envelopes
[109] European Convention for Constructional Steelwork (ECCS), "PROGRESS," *European Convention for Constructional Steelwork*. https://www.steelconstruct.com/eu-projects/progress/
[110] M. Buyle, W. Galle, W. Debacker, and A. Audenaert, "Sustainability assessment of circular building alternatives: Consequential LCA and LCC for internal wall assemblies as a case study in a Belgian context," *Journal of Cleaner Production*, vol. 218, pp. 141–156, 2019, doi: 10.1016/j.jclepro.2019.01.306.
[111] V. Hartkopf, A. Aziz, and V. Loftness, "Facades and Enclosures: Building for Sustainability," 2020, pp. 295–325. doi: 10.1007/978-1-0716-0684-1_873.
[112] A. Tzempelikos and A. K. Athienitis, "SIMULATION FOR FAÇADE OPTIONS AND IMPACT ON HVAC SYSTEM DESIGN".
[113] S. Moghtadernejad, S. Mirza, and L. Chouinard, "Façade Design Stages: Issues and Considerations," *Journal of Architectural Engineering*, vol. 25, p. 04018033, Mar. 2019, doi: 10.1061/(ASCE)AE.1943-5568.0000335.
[114] S. Hassanli, K. Kwok, and D. Fletcher, "Utilizing cavity flow within double skin façade for wind energy harvesting in buildings," *Journal of Wind Engineering and Industrial Aerodynamics*, vol. 167, pp. 114–127, Aug. 2017, doi: 10.1016/j.jweia.2017.04.019.
[115] M. Bayoumi, "Impacts of window opening grade on improving the energy efficiency of a façade in hot climates," *Building and Environment*, vol. 119, Apr. 2017, doi: 10.1016/j.buildenv.2017.04.008.
[116] A. Aflaki, N. Mahyuddin, Z. Alcheikh Mahmoud, and mohamad rizal Baharum, "A review on natural ventilation applications through building façade components and ventilation openings in tropical climates," *Energy and Buildings*, vol. 101, Apr. 2015, doi: 10.1016/j.enbuild.2015.04.033.

[117] Y. K. Yi, "Building facade multi-objective optimization for daylight and aesthetical perception," *Building and Environment*, vol. 156, pp. 178–190, Jun. 2019, doi: 10.1016/j.buildenv.2019.04.002.
[118] I. Turan, A. Chegut, D. Fink, and C. Reinhart, "The value of daylight in office spaces," *Building and Environment*, vol. 168, p. 106503, 2020.
[119] M. W. Akram, M. Hasanuzzaman, E. Cuce, and P. M. Cuce, "Global technological advancement and challenges of glazed window, facade system and vertical greenery-based energy savings in buildings: A comprehensive review," *Energy and Built Environment*, vol. 4, Nov. 2021, doi: 10.1016/j.enbenv.2021.11.003.
[120] A. M. Nugroho, "The Impact of Living Wall on Building Passive Cooling: A Systematic Review and Initial Test," *IOP Conf. Ser.: Earth Environ. Sci.*, vol. 448, no. 1, p. 012120, Mar. 2020, doi: 10.1088/1755-1315/448/1/012120.
[121] R. Loonen, M. Trcka, D. Cóstola, and J. Hensen, "Climate adaptive building shells: State-of-the-art and future challenges," *Renewable and Sustainable Energy Reviews*, vol. 25, pp. 483–493, Sep. 2013, doi: 10.1016/j.rser.2013.04.016.
[122] S. Attia, S. Bilir Mahcicek, T. Safy, C. Struck, R. Loonen, and F. Goia, "Current Trends and Future Challenges in the Performance Assessment of Adaptive Façade Systems," *Energy and Buildings*, vol. 179, Sep. 2018, doi: 10.1016/j.enbuild.2018.09.017.
[123] A. Prieto, U. Knaack, T. Auer, and T. Klein, "COOLFACADE: State-of-the-art review and evaluation of solar cooling technologies on their potential for façade integration," *Renewable and Sustainable Energy Reviews*, vol. 101, pp. 395–414, Mar. 2019, doi: 10.1016/j.rser.2018.11.015.
[124] S. Attia, R. Lioure, and Q. Declaude, "Future trends and main concepts of adaptive facade systems," *Energy Science and Engineering*, vol. 1, pp. 1–18, May 2020, doi: 10.1002/ese3.725.
[125] "KME Company - Copper and copper-alloy products." https://www.kme.com/en/copperdivision/architecture/installation
[126] "Bemo - Façades solutions," *Bemo*. https://bemo.com/en/aluminium-composite-panels-facade
[127] "Trimo - Façade claddings," *Cantori Architectural Skins*. https://www.cantorialluminio.it/en/tetris-systems/trimo/
[128] "Built-up Systems. Roofing and Cladding. Architectural Profiles. Curved Roof & Walls. Firewall Systems. Acoustic Systems. Sustainable Systems - PDF Free Download." https://docplayer.net/57646757-Built-up-systems-roofing-and-cladding-architectural-profiles-curved-roof-walls-firewall-systems-acoustic-systems-sustainable-systems.html (accessed Jul. 24, 2023).
[129] J. Rondal and D. Dubina, *Light Gauge Metal Structures Recent Advances*. Springer Science & Business Media, 2007.
[130] M. Georgescu, V. Ungureanu, A. Gruin, and A. Floricel, "Building Cladding using Liner Trays: Experimental and Numerical Approach," *IOP Conference Series: Materials Science and Engineering*, vol. 603, p. 022051, Sep. 2019, doi: 10.1088/1757-899X/603/2/022051.
[131] CEN, "SR EN 1993-1-3:2007 - Eurocod 3: Design of steel structures - Part 1-3: General rules - Supplementary rules for cold-formed members and sheeting (In Romanian)." 2007.
[132] CEN, "EN 10346:2015 - Continuously hot-dip coated steel flat products for cold forming - Technical delivery conditions." 2015.

[133] D. Dubina, V. Ungureanu, and R. Landolfo, "Design of Cold-formed Steel Structures: Eurocode 3: Design of Steel Structures. Part 1-3 Design of cold-formed Steel Structures | Wiley," in *Design of Cold-formed Steel Structures*, Berlin: Ernst & Sohn, A Wiley Company, pp. 437–462.
[134] J. M. Davies, "Light gauge steel cassette wall construction — theory and practice," *Journal of Constructional Steel Research*, vol. 62, no. 11, pp. 1077–1086, Nov. 2006, doi: 10.1016/j.jcsr.2006.06.028.
[135] R. Baehre and J. Buca, "Die wirksame Breite des Zuggurtes von biegebeanspruchten Kassetten," *Stahlbau*, vol. 55, no. 9, pp. 276–285, 1986.
[136] R. Baehre, "Longitudinal Shear Effects and Dimensioning of Waffle Structures.," *Stahlbau*, vol. 56, no. 7, pp. 197–202, 1987.
[137] R. Baehre, J. Buca, and R. Egner, "Empfehlungen zur Bemessung von Kassettenprofilen, R. Schardt Festschrift," University of Darmstadt, 1990.
[138] R. Baehre and J. Buca, "Der Einfluss der Schubfteifigkeit der Aussenschale auf das Traguerhalten von zweischaliger Dünnblech-Fassadenkonstruktionen," *Bauingenieur*, vol. 68, no. 1, pp. 27–34, 1993.
[139] J. M. Davies and D. W. Dewhust, "The shear behavior of thin-walled cassette sections infilled with rigid insulation," in *Proceedings of International Conference on Experimental Model Research and Testing of Thin-Walled Structures*, Prague, Czech Republic, 1997.
[140] J. M. Davies and A. S. Fragos, "The local shear buckling of thin-walled cassettes infilled by rigid insulations – 1. Tests," in *proceedings of 3th European Conference on Steel Structures – Eurosteel 2002*, Coimbra, Portugal, Sep. 2002.
[141] J. M. Davies, "- Cassette wall construction: Current research and practice," in *Advances in Steel Structures (ICASS '02)*, S. L. Chan, J. G. Teng, and K. F. Chung, Eds., Oxford: Elsevier, 2002, pp. 57–68. doi: 10.1016/B978-008044017-0/50008-1.
[142] P. A. Voutay and J. M. Davies, "Analysis of Cassette Sections in compression, Current Research and Practice," in *Advances in Steel Structures (ICASS '02)*, S. L. Chan, J. G. Teng, and K. F. Chung, Eds., Oxford: Elsevier Science Ltd., 2002, pp. 401–408.
[143] European Commission, "Guidelines and Recommendations for Integrating Specific Profiled Steel Sheets in the Eurocodes (GRISPE) - Final Report," European Community's Research Fund for Coal and Steel (RFCS) - GRISPE PLUS Project, 2017. [Online]. Available: http://www.grispeplus.eu/wp-content/uploads/2017/09/Liner-trays-English-V2.pdf
[144] Markus KUHNHENNE, Dominik PYSCHNY, and Lisa KRAMER, "Design Manual for Liner Trays - Deliverable 3.1," European Community's Research Fund for Coal and Steel (RFCS) - GRISPE PLUS Project, 2018. [Online]. Available: http://www.grispeplus.eu/wp-content/uploads/2017/09/Liner-trays-English-V2.pdf
[145] "Grispe Plus | Valorisation of knowledge for specific profiled steel sheets," *Grispe Plus*. http://www.grispeplus.eu/
[146] CEN/TC 250, "FprEN 1993-1-3 - Eurocod 3: Design of steel structures - Part 1-3: Cold-formed members and sheeting." 2023.
[147] M. Georgescu, V. Ungureanu, and A. Gruin, "Local collapse of liner trays: experimental and theoretical approach," in *Eighth International Conference on ADVANCES IN STEEL STRUCTURES*, Lisabon, Portugal, 2015.
[148] M. Georgescu, V. Ungureanu, A. Gruin, and A. Floricel, "Experimental and theoretical investigation on the local collapse of liner trays," *ce/papers*, vol. 1, no. 2–3, pp. 1736–1745, 2017, doi: 10.1002/cepa.217.

[149] M. Georgescu, V. Ungureanu, A. Gruin, and A. Floricel, "Collapse Modes of Liner Trays: Experimental and Numerical Approach," in *Eighth International Conference on THIN-WALLED STRUCTURES - ICTWS 2018*, Lisabon, Portugal, 2018.
[150] T. Misiek and S. Käpplein, "Tragverhalten von Stahlkassettenprofilen mit direkt oder indirekt befestigter Außenschale," *Stahlbau*, vol. 84, no. 11, pp. 875–889, 2015, doi: 10.1002/stab.201510328.
[151] P.-A. Voutay, "Stability of Cassette Walls in Compression," University of Manchester, 2005.
[152] A. Wiegand, "Zur Sanierung von Kassettenprofilfassaden mit einer neuen Außenschale aus Sandwichelementen," Technische Universität Dortmund, Dortmund, 2021.
[153] Dubina D., Ungureanu V. and Landolfo R., *Design of Cold-formed Steel Structures*. Ernst & Sohn, 2012.
[154] "Profile Galvanizate," *Profile Galvanizate*. https://www.profilegalvanizate.ro/ (accessed Jul. 25, 2023).
[155] "Mathcad: Math Software for Engineering Calculations | Mathcad." [Online]. Available: https://www.mathcad.com/en
[156] Autodesk, "AutoCAD Software." [Online]. Available: https://www.autodesk.com/products/autocad/overview
[157] CEN, "SR EN 1993-1-5:2007 - Eurocod 3: Design of steel structures - Part 1-5: Plated structural elements (in Romanian)." 2007.
[158] CEN, "SR EN ISO 6892-1:2019: Metallic materials — Tensile testing — Part 1: Method of test at room temperature (in Romanian)." 2019.
[159] "Research Institute for Renewable Energies." https://www.icer.ro/en/ (accessed Jul. 12, 2023).
[160] "SODECA. Producător de ventilatoare şi extractoare industriale." https://www.sodeca.com/ro (accessed Aug. 01, 2023).
[161] "Sentera.eu - Pressure transmitter, 0-4000 Pa." https://www.sentera.eu/en/productdetails/pressure-transmitter--display--0-4000-pa--24-vdc/124871 (accessed Aug. 01, 2023).
[162] "Centrul de Cercetare pentru Mecanica Materialelor şi Siguranța Construcțiilor." https://www.ct.upt.ro/centre/cemsig/index.htm (accessed Jul. 12, 2023).
[163] CEN, "prEN 1993-1-14; Eurocode 3: Design of steel structures - Part 1-14: Design assisted by finite element analysis. CEN/TC 250/SC 3 N 3723." 2022.
[164] Dassault Systèmes Simulia Corp., "Abaqus 2000." Providence, RI.
[165] P. Arasaratnam, K. S. Sivakumaran, and M. J. Tait, "True Stress-True Strain Models for Structural Steel Elements," *ISRN Civil Engineering*, vol. 2011, p. 656401, Aug. 2011, doi: 10.5402/2011/656401.
[166] A. Ene and A. Stratan, "Monotonic and Cyclic Modelling of Structural Steel for Finite Element Analysis," presented at the The 13th International Conference "Innovative Technologies for Joining Advanced Materials" (TIMA 22), Timisoara, Romania: (accepted for publication), Nov. 2022.
[167] Dassault, "Abaqus 2020 – Abaqus Analysis User's Manual." Dassault Systemes Simulia Corp., 2020.
[168] V. M. Zeinoddini and B. W. Schafer, "Simulation of geometric imperfections in cold-formed steel members using spectral representation approach," *Thin-Walled Structures*, vol. 60, pp. 105–117, Nov. 2012, doi: 10.1016/j.tws.2012.07.001.
[169] B. W. Schafer and T. Peköz, "Computational modeling of cold-formed steel: characterizing geometric imperfections and residual stresses," *Journal of*

*Constructional Steel Research*, vol. 47, no. 3, pp. 193–210, Sep. 1998, doi: 10.1016/S0143-974X(98)00007-8.
[170] Autodesk, "CUFSM Software." Johns Hopkins Whiting School of Engineering. [Online]. Available: https://www.ce.jhu.edu/cufsm/downloads/
[171] J.-H. Zhang and B. Young, "Finite element analysis and design of cold-formed steel built-up closed section columns with web stiffeners," *Thin-Walled Structures*, vol. 131, pp. 223–237, Oct. 2018, doi: 10.1016/j.tws.2018.06.008.
[172] B. W. Schafer, Z. Li, and C. D. Moen, "Computational modeling of cold-formed steel," *Thin-Walled Structures*, vol. 48, no. 10–11, pp. 752–762, Oct. 2010, doi: 10.1016/j.tws.2010.04.008.
[173] C. Fauth, "Guidelines and Recommendations for Integrating Specific Profiled Steels sheets in the Euro-codes (GRISPE) - Deliverable 2.3," 2016.
[174] M. R. C. Doughty and G. P. Hammond, "Sustainability and the built environment at and beyond the city scale," *Building and Environment*, vol. 39, no. 10, pp. 1223–1233, Oct. 2004, doi: 10.1016/j.buildenv.2004.03.008.
[175] S. A. Celsa Steel, "EPD - Steel reinforcement products for concrete." The International EPD® System, Aug. 19, 2020.
[176] "C 107-2:2005 + A1:2017 Normativ privind calculul termotehnic al elementelor de constructie ale cladirilor: Ordinul nr. 2641/2017 privind modificarea şi completarea reglementării tehnice 'Metodologie de calcul al performanţei energetice a clădirilor', aprobată prin Ordinul ministrului transporturilor, construcţiilor şi turismului nr. 157/2007."
[177] D. Overbey, "LCA Stages Matter When Tracking Embodied Carbon | 2021-01-29 | Building Enclosure." https://www.buildingenclosureonline.com/blogs/14-the-be-blog/post/89547-lca-stages-matter-when-tracking-embodied-carbon (accessed Aug. 18, 2023).
[178] K. Allacker, F. Mathieux, D. Pennington, and R. Pant, "The search for an appropriate end-of-life formula for the purpose of the European Commission Environmental Footprint initiative," *Int J Life Cycle Assess*, vol. 22, no. 9, pp. 1441–1458, Sep. 2017, doi: 10.1007/s11367-016-1244-0.
[179] CEN, "EN 15804:2012+A1:2013 - Sustainability of construction works - Environmental product declarations - Core rules for the product category of construction products." 2013.
[180] JSC Litana ir Ko, "EPD - Primed and painted steel structures." 2021.
[181] Sphera Solutions GmbH, "GaBi: Product Sustainability Software." 2021.
[182] European Association for Panels and and Profiles, "EPD - Double skin steel faced sandwich panels." 2018.
[183] L. Konrad, M. Kłodawski, and P. Gepner, "Energy Consumption in a Distributional Warehouse: A Practical Case Study for Different Warehouse Technologies," *Energies*, vol. 14, no. 9, p. 2709, 2021, doi: https://doi.org/10.3390/en14092709.
[184] "U-value calculator | ubakus.de." https://www.ubakus.de/u-wert-rechner/
[185] M. Gordon Engineering, *Demolition Energy Analysis off Office Building Structural Systems*. The Athena Sustainable Materials Institute, 1997.
[186] Europrofil AB, "EPD - Light gauge steel profiles and components." 2020.
[187] S. A. B. M. Interbeton, "EPD - Environmental Product Declaration for Ready Mixed Concrete C25/30 XC3, S2." 2021.
[188] Ruukki Construction Oy, "EPD - Hot-dip galvanised building products." 2020.
[189] "Europe Sandwich Panels Market Report and Forecast 2023-2028." https://www.expertmarketresearch.com/reports/europe-sandwich-panels-market (accessed Aug. 23, 2023).

[190] "Sandwich Panel Market Size, Share | Industry Growth [2030]." https://www.fortunebusinessinsights.com/sandwich-panel-market-107786 (accessed Aug. 23, 2023).